DISSERTATION | DOCTORAL THESIS

Titel | Title

Pathway-specific regulation of macrophage antimicrobial responses by Mediator kinase

verfasst von | submitted by

Dott. mag. Maurizio Forte

angestrebter akademischer Grad | in partial fulfilment of the requirements for the degree of

Doctor of Philosophy (PhD)

Wien | Vienna, 2025

Studienkennzahl lt. Studienblatt | Degree programme code as it appears on the student record sheet:	UA 794 620 490
Dissertationsgebiet lt. Studienblatt | Field of study as it appears on the student record sheet:	Molekulare Biologie
Betreut von | Supervisor:	Univ.-Prof. Mag. Dr. Pavel Kovarik

Aknowledgements

I would like to thank my supervisor, Pavel Kovarik, for giving me the chance to carry out my PhD studies in his lab and for entrusting me with this difficult but intriguing project. Thank you for your supervision and for your valuable insights and perspective on research.

Everyone knows a PhD is tough, so you better embark on this adventure with the right companions.
Thank you to the Kokonuts, who made the lab such a pleasant environment with their excitement for science and genuine joy for life. It has truly been one of the most positive workplaces I've ever been part of. Thanks to my deskmates Jeanne and Christina who made every day a little bit lighter, even when I was just trying to focus in the middle of your goofy conversations, which happened quite often in these past months xD. Thank you, Jeanne (Genie!), for being the best gym rat buddy, mice-shaker, and otaku I could share my everyday life with (arigatō!). Thank you, Christina, for your rational thinking that helped us progress on this troublesome project, and for all the spontaneous and genuine laughs along the way. Thank you, Nora, for your positive and open-hearted attitude and for the many efforts you put into the Mediator kinase project in the past. Thank you, Ronit, for the hours spent analysing (and re-analysing!) countless RNA-seq datasets without a single complaint and always with a big smile (just the occasional "Kurwa!"). Thank you, Juli, for your kind presence and inspiring care for both people and the planet, combined with your motivated attitude toward science. Thank you, Fiona, for our Italian conversations together. And thank you, Annika, for being such a precious resource in the lab, your broad knowledge and genuine, sometimes intense, passion for science have been invaluable. A bunch of geeks that couldn't be more different from one another yet somehow sharing core values that make the group a real unity.

Thank you to the army of students that tried to solve the Mediator kinase puzzle, the four L paladins: Luisa, Lisa, Liuba, Lynn. A special thank you to my 2x student Zarghun, for your straightforward and critique attitude toward science, I am glad to have been part of your scientific growth and very thankful for your help in shaping the project during critical times.
Thank you to former lab members: Anita, Kevin E., Kevin D. and Marti, for your insights and valuable suggestions.

Thank you to the 4th floor members, and to the Versteeg, Baccarini, and Decker labs for sharing methods, information, and reagents. You have all been important in my growth, and I'm grateful for the friendships formed along the way. Thank you to Aarathy, Katrin and Ursi for their precious help with the Pro-seq experiments, one of the most time- and brain-intensive parts of my PhD journey.

Thank you to the entire SMICH community, and especially Theresa, for always being so kind and willing to help, or simply to listen to a poor PhD student's complaints (especially in these last months!).

Thank you to the Staber/Pabinger labs at Anna-Spiegel, especially Lukas, Pegah, and Simone, for welcoming me during difficult times and helping me redeem myself and rediscover my worth.

Thank you to my university friends from Pavia, who are now spread across the world.
Thank you to my lab mates from Lab 500 at CNR. Thank you to my Master's thesis supervisors, Giovanni Maga and Laura Bavagnoli, for being so instrumental in my academic journey. I will always keep you in my memory, Prof. Maga.
Thank you to the Roslin Institute and Paul Digard for giving me my first research experience abroad.

Thank you to Roberto Puglisi, my first scientific "crush" back in high school, for sparking in me the flame for the exciting yet tough world of research.

Thank you to Claudia, the first person I met in Vienna, for making sure I never felt alone in a new city, and indeed I never did since then.

Thank you to my Stars Fitness gym buddies for helping me release stress and recharge my energy, even on the cloudiest days.

Thank you to my Italian (almost) crew - Adrian(O), Ale, Ana, Brank(it)o, Dani, Samu, and Sara. There's a word limit to this thesis that won't let me write about each of you in detail, but I hope (actually, I'm sure) you know how much you all mean to me.

Thank you to my life-long friends - Anto, Benni, Chiara, Jessi, Miglio, Sele, Silvia, and all the others - for always being there whenever I come home, ready to catch up on the past and present.

Thank you to my grandparents, the most wonderful elders a grandson could ask for, whose excitement for life and the world around us continues to inspire me.
Thank you to the rest of my beautiful, noisy family for your love and support from afar, you've never stopped caring about me.

Thank you, Mum, for your unconditional love and for shaping me into someone I can now be proud of when I look in the mirror.

Last but not least, thank you, Lau, for being my partner. I don't think I ever understood what love truly meant until I met you. This achievement would not have been possible without you. I once believed that being with someone in the same field would be impossible, but boy, was I wrong!
You complement me and make me a better person every single day.

This work is also thanks to you all who helped pave this path.

The research presented in this thesis was conducted at the Max Perutz Labs.
For the main results section, I performed nearly all experimental work. I was also actively involved in writing of the manuscript and was responsible for figure preparation and data visualization. Details about author contribution can be found in the results section.
In the second part of the thesis, I co-designed, carried out, and analyzed dot-blot experiments to assess the global RNA-binding activity of a TTP mutant lacking its nuclear localization signal (NLS). During the writing of this thesis, AI-based tools were used exclusively to refine and polish the text of the Introduction and Discussion sections.

Table of Contents

Abstract

The innate immune system is tightly regulated at multiple levels to ensure a rapid yet balanced response to external cues. This thesis investigates the regulation by transcriptional and to a lesser extent also by post-transcriptional mechanisms, focusing on macrophages as key effector cells in innate immunity.

The first part of this thesis centres on Mediator kinase, a core regulatory component of the transcriptional machinery composed of the paralogous cyclin-dependent kinases CDK8 and CDK19. As part of the Mediator complex, Mediator kinase modulates signal-induced transcription, acting as either an activator or a repressor. We investigated how Mediator kinase activity shapes macrophage responses to diverse immune stimuli, focusing on Toll-like receptor (TLR) and JAK-STAT signaling.

Using selective small-molecule inhibitors, we conducted a comprehensive series of experiments combining transcriptomic profiling, transcription factor activity inference, and functional infection assays in macrophages. Pharmacological inhibition revealed a robust dependency on Mediator kinase activity in primary macrophages, in contrast to immortalized cell lines. Mediator kinase promoted JAK–STAT-dependent transcription in responses to cytokines, including interferons (IFNs), but repressed TLR-induced gene expression. Many interferon-stimulated genes (ISGs) showed increased induction upon TLR stimulation in the absence of Mediator kinase activity. Motif enrichment analysis identified the interferon-stimulated response element (ISRE) as a key regulatory motif, suggesting that TLR signaling represses ISRE-driven transcription in a stimulus-specific manner. Mediator kinase inhibition relieved this repression, enhancing clearance of *Listeria monocytogenes*, which engages both TLR and JAK–STAT pathways.

The second project of this thesis explores the hierarchy of target recognition by the mRNA-destabilizing protein tristetraprolin (TTP), showing that mRNA fate can be predetermined through nuclear engagement.

Zusammenfassung

Das angeborene Immunsystem wird auf mehreren Ebenen streng reguliert, um eine schnelle und dennoch ausgewogene Reaktion auf externe Reize zu gewährleisten. Diese Arbeit untersucht die Regulation durch transkriptionelle und teilweise auch durch posttranskriptionelle Mechanismen, wobei der Schwerpunkt auf Makrophagen als wichtige Effektorzellen der angeborenen Immunität liegt.

Der erste Teil dieser Arbeit beschreibt das Hauprojekt, dass sich auf die Mediator-Kinase konzentriert, die eine zentrale regulatorische Komponente des Transkriptionsapparats darstellt. Die enzymatisch aktiven Untereinheiten der Mediator-Kinase sind die paraloge Proteine CDK8 und CDK19. Als Teil des Mediator-Komplexes moduliert die Mediator-Kinase die signalinduzierte Transkription und wirkt dabei entweder als Aktivator oder als Repressor. Die Dissertation untersucht, wie die Mediator-Kinase die Reaktionen von Makrophagen auf verschiedene Immunreize beeinflusst, wobei der Fokus auf Toll-like-Rezeptoren (TLR)- und JAK-STAT-Signalwegen liegt.

Unter Verwendung selektiver niedermolekularer Inhibitoren von Mediator-Kinase in Kombination mit Transkriptom-Profiling, Transkriptionsfaktor-Aktivitätsinferenz und funktionellen Infektionsassays konnte eine starke Regulation von primären Makrophagen durch Mediator-Kinase nachgewiesen werden. Im Gegensatz dazu war die Abhängigkeit in immortalisierten Zelllinien nur schwach ausgeprägt. Die Mediator-Kinase steigerte die JAK-STAT-abhängige Transkription nach Stimulation mit Zytokinen, einschließlich Interferonen (IFNs), unterdrückte jedoch die TLR-induzierte Genexpression. Viele IFN-stimulierte Gene (ISGs) zeigten bei einer Inhibition der Mediator-Kinase eine erhöhte Induktion nach TLR-Stimulation. Motif-Anreicherungsanalysen identifizierten das IFN-stimulierte Response-Element (ISRE) als ein wichtiges regulatorisches Motiv. Dieses Ergebnis deutete darauf hin, dass die TLR-Signalübertragung die ISRE-gesteuerte Transkription auf eine stimulus-spezifische Weise unterdrückt. Die Hemmung der Mediator-Kinase hob diese Unterdrückung auf und verstärkte die Clearance von Listeria monocytogenes, das sowohl den TLR- als auch den JAK-STAT-Signalweg aktiviert.

Das zweite Projekt dieser Arbeit untersucht die Hierarchie der Zielerkennung durch das mRNA-destabilisierende Protein Tristetraprolin (TTP) und zeigt, dass das Schicksal der mRNA durch die Bindung im Zellkern vorbestimmt werden kann.

Introduction

Immunity

The term ‘‘immunity’’ comes from the Latin word ‘‘immunis,’’ meaning ‘‘exempt’’, which at the organismal level, refers to protection from further infection. The immune system is conventionally divided into two arms: the innate and the adaptive immune systems.

Innate immunity is a protective defense system that is present from the onset of an organism life. It does not rely on genetic rearrangements and remains constant throughout the course of an infection. In stark contrast, adaptive immunity is mediated by specialized immune cells known as lymphocytes, which undergo genetic rearrangements to adapt and fight against external cues. This dissertation will focus on the innate immune system.

Immune cells: the players of immunity

The innate immune system comprises a diverse array of cell types that serve as the first line of defense against pathogens. These include myeloid-derived cells such as macrophages, monocytes, neutrophils, dendritic cells (DCs), basophils, eosinophils, and mast cells, all of which contribute to pathogen recognition, phagocytosis, and the initiation of inflammation. Macrophages and neutrophils are particularly important for engulfing and clearing microbes (professional phagocytes), while DCs bridge innate and adaptive immunity by presenting antigens to lymphocytes.

In addition to myeloid cells, several lymphoid-derived cell types contribute to innate immune responses. Natural killer (NK) cells play a critical role in detecting and eliminating virally infected or transformed cells without prior antigen sensitization. Other innate lymphoid cells (ILCs), including ILC1s, ILC2s, and ILC3s, mirror the effector functions of adaptive T helper (Th) cell but lack antigen-specific receptors. Instead, ILCs respond rapidly to environmental cues, particularly at mucosal and barrier sites. Importantly, conventional T cells, including $CD4^+$ Th cells and $CD8^+$ cytotoxic T cells, are part of the adaptive immune system. They are characterized by the expression of antigen-specific T cell receptors (TCRs) generated through somatic recombination. Although they do not belong to the innate immune system, their activation and function are often shaped by signals derived from innate immune cells, highlighting the dynamic interplay between these two arms of immunity.

The Macrophage cell type

Macrophages are key players of the innate immune system, residing in virtually all tissues where they perform essential roles in host defense, tissue maintenance, and repair.[1] While many macrophages originate from circulating monocytes, tissue-resident macrophages, such as Kupffer cells in the liver, peritoneal macrophages in the peritoneal cavity and alveolar macrophages in the lungs, arise during embryonic development and self-renew throughout life.[2] The process by which macrophages adopt different functional programs in response to environmental cues is called macrophage polarization. Traditionally, macrophage polarization has been described in terms of two functional subtypes based on their activation state *in vitro*: M1

(classically activated) and M2 (alternatively activated) macrophages.[3] However, it is now widely recognized that this classification is an oversimplification, as macrophage activation *in vivo* provides a spectrum of many intermediate and partially overlapping phenotypes.[4-5] To account for this complexity, current nomenclature often refers to these populations as M1-like and M2-like macrophages, emphasizing the spectrum of activation states. M1-like macrophages are typically induced by stimuli such as interferon-gamma (IFNγ) and microbial products (e.g., lipopolysaccharide, LPS), resulting in a pro-inflammatory phenotype characterized by the production of cytokines like TNF-α and IL-12. These macrophages are effective at killing pathogens and promoting inflammation. In contrast, M2-like macrophages are activated by cytokines such as IL-4 and IL-13 and are primarily involved in resolving inflammation, promoting tissue repair, and regulating immune responses through the secretion of anti-inflammatory cytokines like IL-10 and TGF-β. This remarkable plasticity allows macrophages to orchestrate a wide range of immune and tissue homeostatic functions, positioning them as central players in protective immunity and the pathogenesis of various diseases, including chronic inflammation, fibrosis, and cancer.[1]

Macrophage effector functions

Macrophages are central effectors of the innate immune system, equipped with a diverse array of mechanisms that maintain tissue integrity and defend the host against infection. A hallmark of their function is phagocytosis, the process by which macrophages internalize and degrade pathogens, apoptotic cells, and cellular debris. Phagocytosis is mediated through a coordinated network of pattern recognition receptors (PRRs), Fc receptors, complement receptors, and scavenger receptors.[6] Apart from engulfment, macrophages exert potent microbicidal activities within phagolysosomes, including the generation of reactive oxygen species (ROS), reactive nitrogen species (RNS), and the delivery of hydrolytic enzymes that efficiently kill internalized microbes.[7] In addition to direct antimicrobial functions, macrophages play a pivotal role in orchestrating immune responses by secreting a broad spectrum of cytokines and chemokines. These mediators recruit and activate other leukocytes, modulate inflammation, and support tissue repair.[8] Acting as antigen-presenting cells (APCs), macrophages also process and present peptides via MHC class II molecules, thereby activating T cells and initiating adaptive immunity.[9] Finally, macrophages contribute to resolution of inflammation and tissue remodelling through efferocytosis, the clearance of apoptotic cells, and the production of growth factors that facilitate wound healing and angiogenesis. Through these diversified roles, macrophages function as both sentinels and regulators of immune responses, allowing a rapid and effective response to infection yet preserving tissue homeostasis.

Innate immune recognition

The rise of the field of innate immunity can be historically identified with the groundbreaking theories of Charles A. Janeway, who in 1989 suggested the existence of sentinel receptors expressed by immune cells, which he defined as “pattern recognition receptors” (PRRs).[10] These receptors recognize “pathogen-associated

molecular patterns" (PAMPs), conserved microbial molecules that are broadly expressed in pathogens but absent in host cells. Before Janeway's theory, various recognition molecules (later considered as PRRs) had already been identified, including CD14, which senses LPS, and the mannose-binding lectin, which functions upstream of the complement cascade.[11-12] However, it is now widely accepted that PRRs can recognize molecules that are present in both pathogenic and non-pathogenic microorganisms. For this reason, the term microbial-associated molecular patterns (MAMPs) is often used. Moreover, increasing evidence indicates that PRRs can also detect host-derived molecules released upon cellular stress or damage.[13] These endogenous danger signals are collectively referred to as damage- or danger-associated molecular patterns (DAMPs), a broad term that includes proteins, lipids, nucleic acids, and even metabolites. This represents a revolutionary deviation from the classical paradigm based on which the immune system exists entirely to discriminate ‘‘self’’ from ‘‘non-self’’. Instead, it highlights a broader role for immunity in sensing perturbed homeostasis, with profound implications for understanding the pathogenesis of autoimmune and inflammatory diseases.

The first experimental validation of Janeway´s theories came in 1996, when the Hoffman´s group discovered the "Toll" receptor in *Drosophila melanogaster*. Flies strains carrying a genetic mutation in the Toll gene exhibited increased susceptibility to fungal infections caused by a defective antifungal response.[14] Janeway and Medhiztov subsequently identified the mammalian homolog of Toll, initially termed hToll and now known as Toll-like receptor 4 (TLR4).[15] Subsequent work from different laboratories has identified several of such similar Toll-like receptors (TLRs) each recognizing a wide range of PAMPs.

TLRs

TLRs comprise type I transmembrane proteins, composed of: 1) an ectodomain with leucine-rich repeats (LRRs) responsible for PAMP recognition; 2) a transmembrane domain; 3) a cytoplasmic Toll/interleukin (IL)-1 receptor (TIR) domain, which mediates downstream signaling.[16] To date, 10 TLRs in humans and 12 in mice have been identified. TLRs are broadly categorized into cell surface and endosomal subfamilies based on their subcellular localization and ligand specificity. Cell surface TLRs (TLR1, TLR2, TLR4, and TLR5) recognize lipid and protein components of microbes, whereas endosomal TLRs (TLR3, TLR7, TLR8, TLR9, and TLR13) detect nucleic acids. Upon recognition of their cognate PAMP, TLRs recruit adaptor proteins carrying TIR domains, most notably myeloid differentiation primary response 88 (MYD88) and TIR domain-containing adaptor inducing IFN-β (TRIF). These adaptors trigger different downstream signaling cascades that ultimately result in the production of inflammatory cytokines, chemokines and type I interferons (IFNs), respectively.

Cell surface TLRs

Cell surface TLRs are sentinel receptors of the innate immune system that primarily recognize microbial membrane components such as lipids, proteins, and

glycoproteins. These receptors are crucial for detecting extracellular pathogens and initiating immune responses.

TLR4 was the first TLR identified and remains the most extensively studied. It recognizes lipopolysaccharide (LPS), a major component of the outer membrane of Gram-negative bacteria. However, TLR4 binding to LPS is relatively weak and requires its interaction with co-receptors and accessory proteins, including MD-2, LPS-binding protein (LBP) and the glycosylphosphatidylinositol (GPI)- anchored LRR-containing protein CD14.[17-20] Structural studies have shown that five of the six lipid chains in lipid A, a critical component of LPS, bind the hydrophobic pocket of MD-2, while the remaining acyl chain interacts directly with TLR4.[17] The TLR4-MD2 interaction seems to be critical, as TLR4 response is completely abolished in MD2-deficient mice but not CD14- and LBP-deficient mice.[21] The essential role of TLR4 *in vivo* is exemplified by LPS hyporesponsiveness in mice carrying a loss-of-function mutation in the *Tlr4* gene.[22-23] While LPS is its preferential ligand, TLR4 can also recognize a variety of other PAMPs and DAMPs, including: lipoteichoic acid (LTA),[24] fibrinogen,[25] β-glucans,[26] fungal mannans, such as glucuronoxylomannan (GXM), Der p 2, a major allergen from dust mite (HDM), and heat shock proteins (HSPs).[27-29]

TLR2 exhibits a broad ligand specificity and senses various lipid-containing microbial components, including peptidoglycan (PGN) and lipoteichoic acid (LTA), as well as glycolipids, lipopeptides, and GPI anchors.[30-32] TLR2 forms heterodimers with either TLR1 or TLR6 to achieve specificity: TLR2-TLR1 recognizes triacylated lipoproteins, while TLR2-TLR6 binds diacylated lipoproteins.[33-34] Structural studies show that in the TLR2-TLR1 complex, two lipid chains of the synthetic ligand Pam3CSK4 bind TLR2, while a third inserts into the hydrophobic channel of TLR1.[35] Two key features distinguish TLR1 from TLR6: TLR6 has two bulky phenylalanines that block triacylated ligand binding, and the larger hydrophobic dimer interface of TLR2-TLR6 stabilizes diacylated ligand binding.[36]

TLR5 recognizes flagellin, the major structural component of bacteria flagella.[37-39] Its expression is spatially restricted to the crypts of the small intestine, where it co-localizes with Paneth cell markers, suggesting a role in gut mucosal defense.[40]

TLR11, a murine homolog related to TLR5, is highly expressed in the kidney and bladder. TLR11-deficient mice exhibit increased susceptibility to uropathogenic bacterial infections, suggesting a role in the urinary tract immunity.[40] TLR11 forms a heterodimer with TLR12 to recognize profilin, a protein derived from the protozoan parasite Toxoplasma gondii.[41-42]

Endosomal TLRs

Endosomal TLRs are critical components of the innate immune system, specialized in detecting nucleic acid signatures derived from viruses, bacteria, and damaged host cells. These receptors are localized to intracellular compartments such as endosomes, where they recognize PAMPs in a context that minimizes recognition of self-nucleic acids.

TLR3 was the first TLR identified to recognize double-stranded RNA (dsRNA), a molecular found in the genomes of many RNA viruses and produced as an

intermediate during viral replication. Its best-characterized ligand is polyinosinic-polycytidylic acid (Poly(I:C)), a synthetic analog of dsRNA.[43] Physiological ligands of TLR3 include different RNA viruses, such as Zika virus[44], as well as dsRNA intermediates generated during replication of DNA viruses like mouse cytomegalovirus and herpes simplex virus type 1 (HSV-1).[45]

TLR7 and TLR8 recognize single-stranded RNA (ssRNA) derived from viruses and bacteria.[46-47] These receptors are involved in host defense against RNA viruses, including influenza A virus (IAV)[48], HIV[49], vesicular stomatitis virus (VSV)[46], and severe acute respiratory syndrome coronavirus 2 (SARS-CoV-2)[50].

TLR9 detects unmethylated CpG motifs commonly found in bacterial and viral DNA, as well as in synthetic oligodeoxynucleotides (ODNs).[51-52] TLR9 not only contributes to antiviral responses but also plays an anti-inflammatory role; for example, lung interstitial macrophages produce the anti-inflammatory cytokine IL-10 in response to CpG DNA via TLR9, preventing airway allergy.[53]

TLR13, which is restricted to mice, recognizes highly conserved sequences in bacterial 23S ribosomal RNA (rRNA).[54-55]

TLR10, found in humans, is the least characterized member among the TLR family. While some studies suggest it may respond to dsRNA and viral proteins from IAV and HIV[56-58], its physiological ligands and precise immune function remain unclear.

TLR signaling

Signaling by mammalian TLRs induces a diverse range of intracellular responses that converge into the production of inflammatory cytokines, chemokines, antimicrobial peptides, and the antiviral cytokines IFN-α and IFN-β, both members of the type I IFN family. PAMP-induced dimerization of two TLR ectodomains brings their cytoplasmic TIR domains together, allowing their interaction with the TIR domains of cytoplasmic adaptor molecules that initiate downstream signaling. To date, four such adaptor proteins have been identified in mammals: Myd88, MAL (also known as TIRAP), TRIF and TRAM.

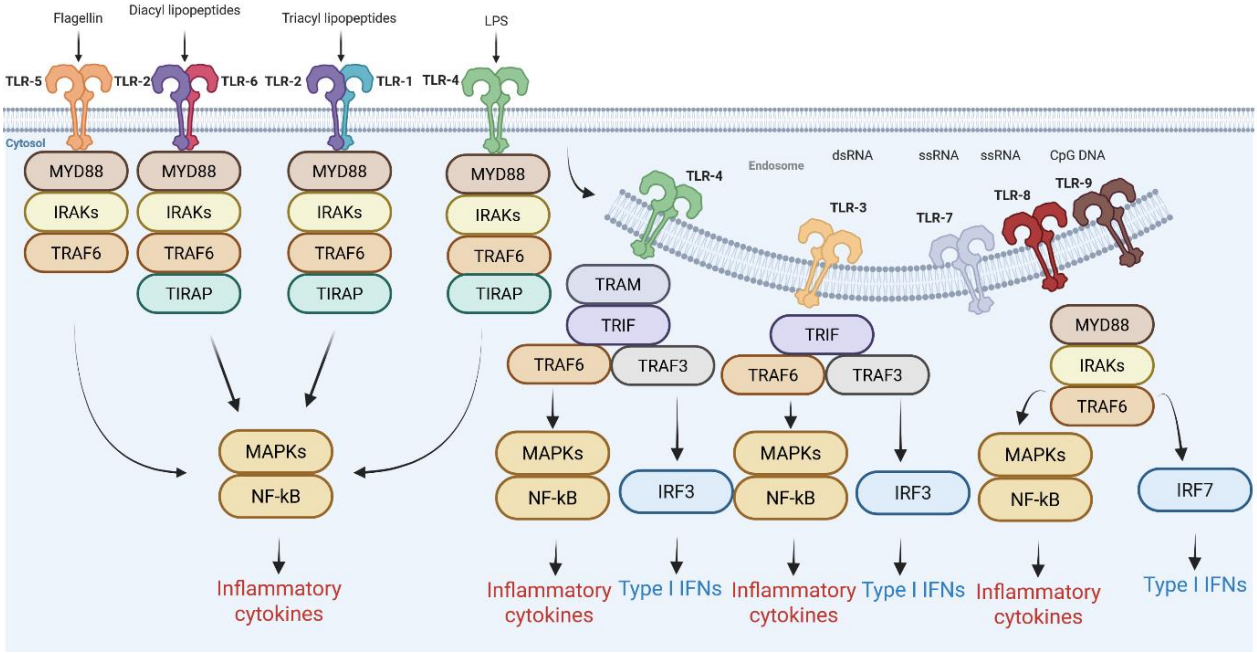

Figure 1. Overview of TLR signaling pathways. Cell surface TLRs (TLR1, 2, 4, 5, 6) recognize bacterial components such as lipoproteins and lipopolysaccharide (LPS), recruiting the adaptor protein MYD88, IRAKs, TRAF6, and sometimes TIRAP to activate MAP kinases (MAPKs) and NF-κB, leading to production of inflammatory cytokines. Endosomal TLRs (TLR3, 7, 8, 9) recognize viral and bacterial nucleic acids (double-stranded RNA, single-stranded RNA, CpG DNA) and utilize TRIF or MYD88 pathways. TLR3 signals via TRIF to activate TRAF3 and IRF3 for type I IFN production, while TLR7, TLR8 and TLR9 activate IRF3 through TRAF6 for type I IFNs, alongside NF-κB/MAPKs-mediated inflammatory cytokines expression. Notably, TLR4 is unique among the cell surface TLRs because it triggers both inflammatory cytokine production and type I IFN induction. Created with Biorender.

Most TLRs signal exclusively through Myd88. Upon ligand engagement, MAL/TIRAP senses the dimerized TIR domain and stimulates the assembly of supramolecular organizing centres (SMOCs). The concept of SMOCs have been first introduced by Kagan et al as location-specific higher-order signaling platforms in which increased local concentrations of signaling components promote allosteric interactions that are required for enzyme activation.[59-61] SMOCs are now recognized as critical sites of innate immune signal transduction. In the context of TLR signaling, two major SMOCs have been described: the Myddosome, seeded by TIRAP/MAL and the putative Triffosome, potentially seeded by TRAM.[62] The Myddosome consists of multiple copies of Myd88 and members of the IL-1 receptor associated kinase (IRAK) family of serine-threonine kinases. Structurally, Myd88 contains a C-terminal TIR domain, which interacts with the TIR domains of TLRs and MAL/TRAP, and a N-terminal death domain (DD), which mediates interaction with the DD of IRAKs. *In vitro*, the Myddosome assembles with a stoichiometry of approximately 6-8 molecules of Myd88 with 4 molecules each of IRAK4 and IRAK2, although the precise *in vivo* stoichiometry remains unclear.[61] IRAK1 is believed to participate in Myddosome formation, although its relative importance compared to IRAK2 varies between humans and mice, as

suggested by RNAi-based screens.[63] Activated IRAKs autophosphorylate and recruit the E3 ubiquitin ligase TRAF6, which functions as both a scaffold and signaling hub. TRAF6 performs two main functions: 1) it activates the kinase TAK1, which in turn stimulates the IKK complex and the mitogen-associated protein kinase (MAPK) pathways, leading to the activation of the transcription factors NF-κB and AP-1; 2) it recruits the IKK-related kinase TBK1, which rapidly induces AKT-dependent glycolysis via induction of the hexokinase, a master regulator of glycolytic metabolism.[64] TAK1 phosphorylates and activates the IkB kinase (IKK) complex, composed of IKKα, IKKβ and IKKγ (also known as NEMO). TAK1 phosphorylates and activates IKKβ, which in turn phosphorylates IkB, an inhibitor that sequesters the transcription factor NFkB in the cytoplasm. Phosphorylation of IkB triggers its ubiquitination and proteasomal degradation, allowing NFkB nuclear translocation.[65] Nuclear NFkB drives transcription of pro-inflammatory cytokines such as TNF-a, IL1β and IL-6. Genetic deficiencies in Myd88 or other myddosome components abolish signaling downstream of all TLRs except TLR3 and TLR4, which can activate Myd88-independent pathways. One of such responses to fist be identified was the induction of type I IFNs and interferon-stimulated genes (ISGs), a response mediated by TRAM, TRIF, and TRAF3.[66-68] In the case of TLR4, this Myd88-independent signaling is initiated after receptor endocytosis. Once internalized into the endosome, TLR4 dimers interact with TRAM, which recruits TRIF to propagate downstream signaling.[69] TRIF then promotes TRAF3-dependent activation of TBK1, culminating in the production of type I IFNs and ISGs expression (Figure 1).[70-72]

Interferons discovery: a road to the JAK-STAT pathway

In 1957, Isaacs & Lindenmann reported a phenomenon of “virus interference” in Influenza virus-infected chick embryo cells. The cells released a material, that did not seem to be part of the original virus, likely a secreted small protein, which they named “interferon”.[73] Today, IFNs are well recognized as key regulators of antiviral and antimicrobial defences programs. The story of the Janus kinase (JAK)-signal transducer and activator of transcription (STAT) pathway is closely linked to that of IFNs. In the early 1990s, efforts by the Stark, Darnell and Kerr laboratories to understand how cells respond to IFNs led the identification of the JAK-STAT signaling cascade. By generating cDNA libraries from mRNAs induced by IFN-treatment, these groups were able to identify several IFN-stimulated genes (ISGs).[74] Subsequent studies revealed the promoters and regulatory elements of these ISGs.

To dissect the signaling pathway, researchers designed a system using an ISG promoter to drive the expression of a lethal marker, enabling the isolation of IFN-unresponsive mutant cells. Genetic complementation of one such mutant revealed that the inactivated gene was TYK2, a member of the newly identified family of tyrosine kinases known as Janus kinases.[75] At the time, their substrates were unknown. The Wilks lab then identified two additional family members, JAK1 and JAK2, named after the two-faced Roman god Janus, reflecting their dual domain architecture.[76]

Further studies showed that the IFN signal was transduced by cytoplasmic factors that translocated to the nucleus upon stimulation. The Darnell lab subsequently purified

the first members of the STAT family of transcription factors, STAT1, STAT2, with the cofactor interferon regulatory factor 9 (IRF9). The acronym STAT reflects their rapid response (echoing the medical term "*stat"* for immediate action).[77] IFNs belong to the class II cytokines, which also include IL10-related cytokines.[78] Today IFNs are classified into three groups, type I, type II and type III, based on their structural homology, chromosomal location and the transmembrane receptors they engage.

Type I IFNs can be produced by virtually all nucleated cells upon encountering viruses or bacteria. However, they are mainly produced by cells of the hematopoietic system and act in a paracrine manner to coordinate immune responses. Type I IFNs are secreted by infected cells and they serve three major functions: (1) they induce cell-intrinsic antimicrobial states in both infected and bystander cells, limiting spreading of pathogens; (2) they modulate innate immune responses by promoting antigen presentation and NK cells functions; (3) they activate the adaptive immune system by supporting antigen-specific T and B cell responses and the establishment of immunological memory. While type I IFNs are well established as protective against viral infections, their roles in bacterial infections and autoimmune diseases is under debate.[79] Indeed, mice lacking the type I IFN receptor (IFNAR) show increased susceptibility towards viral infections[80] but their responses to bacterial infections can be either beneficial or detrimental.[81-83] The type I IFN family includes IFNα, IFNβ, IFNε, IFNκ and IFNω. Among these, IFNα, encoded by more than a dozen genes, and IFNβ, encoded by a single gene family, are the most represented members. The other type I IFN subtypes remain poorly characterized because of restricted tissue expression or redundant function with IFNα/β.[84] Type I IFNs bind to the heterodimeric transmembrane receptor IFNAR, which consists of the two chains IFNAR1 and IFNAR2. Upon IFNAR receptor engagement, JAK1 and TYK2 kinases are recruited and trans-phosphorylated. Activated JAKs subsequently cause the recruitment of STAT1-STAT2 heterodimers and STAT1-STAT1 homodimers and cause their phosphorylation on Y701 and Y690 (STAT2). Activated STAT1-STAT2 heterodimers translocate into the nucleus, where they bind to the IRF9 to form the trimolecular complex called IFN- stimulated gene factor 3 (ISGF3) complex. The ISGF3 complex binds to the interferon-stimulated response elements (ISRE; consensus sequence TTTCNNTTTC) motifs on target DNA sequences.[85-86] The tyrosine phosphorylated STAT1 homodimer, also called gamma-interferon activated factor (GAF), binds to gamma-interferon activated sites (GAS) to induce the expression of ISG.[87] Type I IFNs are unique among all cytokines in that they can activate all seven known STAT family members. However, the activation of these STATs is not essential for induction of canonical type I IFN-induced genes. Among the hundreds of known ISGs, some contain only ISRE or only GAS elements in their promoters, while others harbor both.[88] As a result, optimal transcriptional activation of specific genes may require distinct combinations of STAT-containing complexes tailored to the promoter architecture. Even though predominantly activating STAT1 homodimers, also IFNγ, described below, can under certain conditions cause non-canonical activation of ISGF3 complexes.[89-91]

IFNγ is the only member of type II IFNs. In stark contrast with type I IFNs, IFNγ is only expressed by a limited number of cells, mainly innate-like lymphocyte populations (NK cells and ILCs) or adaptive immune cells (T-cells). Type II IFN receptor knockout mice show defects in resistance to bacterial and viral infections.[92] IFNγ binds to IFNGR, which is made of IFNGR1 and IFNGR2 subunits, and their associated JAK1 and JAK2. In analogy with type I IFNs, STAT1 homodimer (GAF) is activated by Y701 phosphorylation, resulting in its nuclear translocation. In the nucleus, GAF binds to GAS motifs in the promoters of ISGs and crucial serine phosphorylation of chromatin-bound GAF is achieved.

Type III interferons (IFNs), represented by the IFNλ family, are the most recently discovered class of IFNs. While they retain antiviral properties like type I IFNs, they are structurally distinct from both type I and type II IFNs. IFNλ signals through a unique heterodimeric receptor composed of IL-28Rα and IL-10Rβ subunits. Despite engaging a different receptor, IFNλ induces a similar downstream signaling cascade, leading to the formation of the ISGF3 complex and the activation of interferon-stimulated genes (ISGs). Expression of type III IFNs is largely restricted to epithelial barrier tissues, particularly in the lung and gut, where they play a critical role in mucosal antiviral defense.[93]

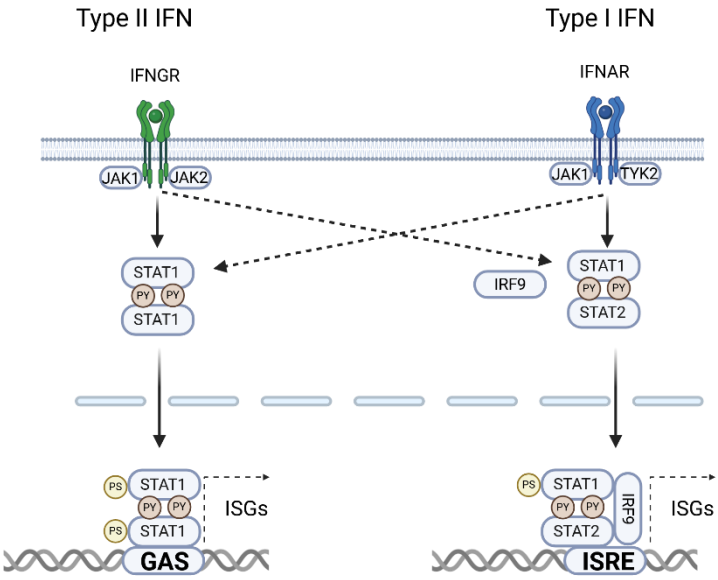

Figure 2. JAK-STAT signaling pathways leading to GAS and ISRE-mediated transcriptional activation. The left panel illustrates type II interferon (IFN-γ) signaling, where IFN-γ binding to INFGR receptor activates associated kinases JAK1 and JAK2. This results in tyrosine phosphorylation and dimerization of STAT1, which translocates to the nucleus and binds GAS elements to regulate gene expression. The right panel depicts type I interferon (IFN-α/β) signaling, where IFN binding to IFNAR receptor activates JAK1 and TYK2, leading to tyrosine phosphorylation of STAT1 and STAT2. Together with IRF9, these form the ISGF3 complex that binds ISREs in target gene promoters, driving transcriptional activation of ISGs. Type II IFNs can induce STAT1 homodimers and type II IFNs can induce ISGF3 complexes. Nuclear serine 727 phosphorylation allows full transcriptional activation in both pathways. Created with Biorender.

JAK-STAT pathway structure and logic

There are four mammalian JAKs (JAK1, JAK2, JAK3 and TYK2) and seven STATs (STAT1, STAT2, STAT3, STAT4, STAT5A, STAT5B, STAT6). STATs are grouped in three genomic clusters that are reminiscent of ancestral gene duplications.[94] Nearly 60 cytokines including many interleukins, colony-stimulating factors (CSFs), hormone-like cytokines, and growth factors hijack the JAK-STAT pathway to produce ligand-, tissue- and context-dependent responses.

Mammalian JAK family share a four domains structure: 1) The FERM domain, 2) the SH2-like domain, 3) the pseudokinase domain and 4) the kinase domain. The FERM domain mediates interaction with upstream receptors and promotes kinase function. The SH2-like domain also mediates interaction with upstream receptors. The pseudokinase (JH2) domain is a regulatory domain, which limits unwarranted kinase activity. The kinase domain (JH1) carries the tyrosine residues necessary for trans-activation of JAKs, and the catalytic elements required for the tyrosine-phosphorylation of receptors. All four members of the JAK family associate with the membrane-proximal regions of cytokine receptor intracellular domains through two distinct conserved motifs in the receptor: a proline-rich segment termed “Box1” and a hydrophobic segment called “Box2”.[95] Crystal structures of full-length JAKs were remarkably difficult to be obtained. Nevertheless, recent cryo-electron microscopy (cryo-EM) structure of full-length JAK1 complexed with the intracellular domain of the interferon λ receptor 1 (IFNλR1) has been obtained.[96]

Mammalian STATs share a similar structure that is composed of seven domains. The N-terminal domain (NTD) is involved in protein-protein interactions. The coiled-coil domain (CCD) is also involved in protein-protein interactions and contains the nuclear localization signal (NLS) for nuclear translocation. The DNA-binding domain (DBD) is important to bind to bind target DNA sequences and contains nuclear import and export signals. The linker domain is structurally important and promotes transcriptional activity. The SH2 domain serves two functions, it binds phosphorylated tyrosines on cytokine receptors and allows dimerization of cognate STATs through interaction between their tyrosine-phosphorylated sites. Due to its crucial functions, the SH2 domain is the most conserved domain among the STAT family. In contrast, the C-termini of STATs, which harbours the transactivation domain (TAD), is the least conserved part. However, in the C-terminal domain a conserved serine residue within a P(M)SP motif (between aminoacids 720 and 730) is also found and in the majority of cases its mutation to alanine alters STAT transcriptional activity.[97]

Cytokine receptor ligation activates JAKs, leading to JAK auto/transphosphorylation, activation and phosphorylation of tyrosine residues in the receptor tails. Receptor phosphorylation creates docking sites for cytoplasmic STATs dimer, which are recruited to the receptor complex via tyrosine-phosphate biding SH2 domains. The activated tyrosine-phosphorylated STATs (pSTATs) homo or heterodimerize via intermolecular SH2-phosphotyrosine interactions. Upon dimerization, STATs translocate into the nucleus and bind DNA regulatory elements to alter chromatin accessibility and induce gene expression (Figure 2). Once in the nucleus, STAT members can bind to either gamma interferon-activated site (GAS) or

interferon-stimulated response elements (ISRE) depending on the nature of the complex in which they reside. In some cases, tetramer formation is essential for the complete transcriptional activity of STATs. This is exemplified by STAT1 in response to type II IFNs[98] and by STAT3 in response to the pro-inflammatory cytokine IL-6.[99]

Canonical and non-canonical JAK-STAT pathway: U-STATs and p-STATs

Tyrosine phosphorylation is considered a prerequisite for STAT activity. However, increasing evidence suggests that unphosphorylated STATs (U-STATs) also serve important cellular functions, shedding light towards a non-canonical JAK-STAT pathway. Studies have demonstrated that U-STAT3 can prolong IL-6–driven gene transcription by forming complexes with unphosphorylated NF-κB (U-NF-κB).[100] In these complexes STAT3 is responsible for nuclear shuttling, while NF-κB provides the DNA-binding and transactivation domains. Furthermore, prolonged exposure to IFN-β or overexpression of components of the ISGF3 complex (STAT1-STAT2-IRF9) supports a role for U-STAT1 in sustaining the expression of ISGs that confer resistance against viruses and DNA damage.[101-102] More recently, Platanitis et al. described a model in which basal ISG expression is initially maintained by unphosphorylated complexes such as U-ISGF3 and STAT2-IRF9, which are later replaced by fully assembled, tyrosine-phosphorylated ISGF3 complexes during interferon signaling.[89] This molecular switch suggests a layered regulatory mechanism in which phosphorylated and unphosphorylated STAT complexes contribute to temporal control of the interferon response.

Beyond their canonical roles as transcription factors, U-STATs also perform functions in chromatin regulation. In *Drosophila* U-STAT92E, the solely STAT member, promotes heterochromatin stability through its interaction with heterochromatin protein 1 (HP1).[103] In mammals, U-STAT5A acts as a tumor suppressor by binding to HP1α, stabilizing heterochromatin, and repressing multiple oncogenes.[104]

In addition to nuclear roles, U-STATs also exert organelle-specific functions. For instance, U-STAT3 localizes to mitochondria, where it supports glycolysis and oxidative phosphorylation, thereby facilitating RAS-dependent oncogenic transformation.[105]

Together, these findings underscore that U-STATs are versatile regulators of gene expression, chromatin architecture, and cellular metabolism, with critical implications for immunity, oncogenesis, and cellular homeostasis.

Negative feedback of the JAK-STAT pathway

Rapid induction of the JAK-STAT pathway is essential for mounting effective antimicrobial and cytokine. However, prolonged activation can be detrimental to host tissues, necessitating tight regulation of both pathway activation and termination to maintain immune homeostasis. While upstream activation steps have been discussed above, this section focuses on negative feedback that fine-tune JAK-STAT pathway.

The Suppressor of Cytokine Signaling (SOCS) proteins are the best-characterized inhibitors of this pathway. The SOCS family consists of 8 members, CIS and SOCS1-7, .[106] all sharing a central SH2 domain, a variable N-terminal region, and a C-terminal SOCS box.[107] SOCS1, SOCS2, SOCS3 and CIS, are expressed at low

levels in unstimulated cells but are rapidly induced by cytokines, establishing a negative feedback loop. The SH2 domain of SOCS1 can bind tyrosine phosphorylated JAKs, thereby directly inhibiting JAK activity.[108] On the other hand, SOCS3 inhibition of JAKs requires binding to the activated cytokine-receptor.[109-110] In contrast, CIS seems to act rather by competing with STATs for binding to the activated cytokine-receptor.[111] SOCS proteins were reported to interact with Elongins B and C, components of the ubiquitin E3 ligase complex, implicating them in proteasomal degradation of signaling proteins.[112-113]

The importance of SOCS proteins is indicated by knockout models: *Socs1* -/- mice, die shortly after birth, mainly due to dysregulated IFN-γ responses[114-115], while *Socs3* -/- mice exhibit embryonic lethality likely due to placental defects and erythrocytosis.[116-117]

Other key negative regulators include protein tyrosine phosphatases (PTPs) such as SHP1, SHP2, CD45, PTPRD, PTPRT, TCPTP, PTP1B and DUSP2, which dephosphorylate tyrosine residues on either JAKs, STATs or cytokine receptors.[118]

The ubiquitin-proteasome pathway has been also implicated in regulating JAK-STAT signaling. For instance, STAT1 can be targeted by at least three different E3 ligases.[119-121]

The protein inhibitor of activated STAT (PIAS) family, PIAS1, PIAS3, PIASX and PIASY, also inhibits STAT function. PIAS proteins share a common central RING-finger-like zinc-binding domain (RLD), a putative N-terminal SAP (scaffold attachment factor A and B (SAF-A/B), acinus and PIAS) and a highly acidic region (AD).[122] The SAP domain is responsible for subcellular localization, anchoring to the nuclear matrix, whereas the RLD domain shows is homologous to a small ubiquitin-like modifier (SUMO) E3 ligase in yeast. All PIAS family members have been shown to inhibit STAT-mediated gene activation.

PIAS1 and PIAS3 directly inhibit STAT1 and STAT3 DNA-binding[123-124], respectively, while PIASX and PIASY inhibit STAT4- and STAT1-driven transcription without affecting DNA-binding.[125-126] Within the AD, a putative small ubiquitin-related modifier 1 (SUMO1) interaction motif (SIM) is present. SUMO conjugation to target proteins (sumoylation), in analogy to ubiquitylation, has been described to modulate subcellular function, protein-protein interaction, and transcriptional activity.[127] STAT1 was reported to be sumoylated by PIAS proteins via their SUMO E3 ligase activity.[128] Interestingly, PIAS proteins have been reported to regulate the activity of other transcription factors.[122]

Post-translational modifications of STATs

STATs can be subjected to different post-translational modifications (PTM), including phosphorylation, methylation, acetylation, ubiquitylation, ISGylation and sumoylation. Among these, phosphorylation of conserved tyrosine residues is the most critical for conical JAK-STAT signaling. For example, phosphorylation of STAT1 at tyrosine 701 is essential for IFN signaling and occurs upon receptor engagement. This modification induces STAT1 binding to importin-alpha5, allowing its nuclear translocation.[129]

All STATs except for STAT2 and STAT6 are known to be subjected to phosphorylation at a canonical serine residue within a conserved P(M)SP motif, representing a non-canonical modification that can occur independently of tyrosine phosphorylation.[97] Both type I and type II IFNs induce phosphorylation of STAT1 at serine 727 within its TAD, although this modification is dispensable for type I IFN responses. Complementation studies in STAT1-deficient U3A cells (lacking STAT1) showed that the ISGF3 complex remains functional with either STAT1β isoform lacking the C-terminus or a S727A mutant.[130-131] Notably, S727 phosphorylation occurs only on chromatin-bound STAT1 molecules[132]. Furthermore S727 phosphorylation of STAT1 and STAT3 has been shown to be required for maximal transcriptional activation of a GAS-containing luciferase reporter constructs in response to IFNs or IL-6, respectively.[133] However, subsequent studies revealed that this requirement is highly gene-specific, suggesting that S727 phosphorylation may fine-tune transcriptional output in a context-dependent manner. This was further supported by in vivo studies using S727A knock-in mice. For STAT1, S727 phosphorylation was shown to be critical for full IFN-γ–mediated innate immune responses and protection against *Listeria monocytogenes* infection.[131] Similarly, mice lacking STAT3 S727 phosphorylation exhibited severe postnatal growth defects and impaired expression of a subset of IL-6-responsive genes.[132] Recent work from our lab identified cyclin-dependent kinase 8 (CDK8), but not its paralog CDK19, as the kinase responsible for STAT1 S727 phosphorylation during IFN responses.[134-135]

Beyond IFN signaling, non-canonical S727 phosphorylation of STATs also occurs in other cellular contexts. Stress-activated MAPK such as p38 and JNK, as well as the growth factor-regulated ERK 1/2, have been implicated in this modification.[97] Another serine residue of STAT1, S708, is targeted by IKKε in response to type I IFNs.[136] This modification inhibits STAT1 homodimerization without affecting ISGF3 formation, thus providing a distinct mechanism for regulation of type I and type II IFN responses.[137] This phosphorylation depends on prior tyrosine dephosphorylation and induces expression of the antiviral gene *Ifit2*, conferring resistance to West Nile virus.[138]

Methylation of STATs has also been reported. For examples, arginine 31 (R31) methylation of STAT1 by protein-arginine methyltransferase 1 (PRMT1) is thought to occur constitutively, independently of phosphorylation, and may influence DNA-binding. Although difficult to be replicated consistently,[139-140] a recent study linked STAT3 methylation by PRMT2 to leptin-mediated regulation of energy balance through modulation of STAT3 tyrosine phosphorylation. [141]

Acetylation of STAT3 on K685 by the acetyltransferase p300 was reported to be essential for its cytokine-stimulated function[142], even though the study had controverses. Several studies have shown that this acetylation, which is independent from tyrosine phosphorylation, is important for distinct functions of STAT3.[143-145]

Other PTMs of STATs, including poly-ubiquitylation, SUMOylation, ISGylation, and others, have also been reported, further expanding the regulatory complexity of these transcription factors.[77]

TLR and JAK-STAT synergism

Under steady state, cells integrate multiple signals, which in turn activate several signalling pathways. One of the most classical examples in immunity is TLR signaling combined with a cytokine signal (e.g. IFNγ), which activates NF-κB (and AP-1/CREB) and JAK-STAT pathway, respectively.[146] Therefore, many groups have made different observations regarding the cooperativity between STATs and other TFs. In macrophages, NF-κB and the ISGF3 complex cooperate to promote the expression of the Nitric oxide synthase (iNOS) gene (*Nos2)* gene.[147] Recent work using BMDMs has demonstrated that stress-induced p38 MAPK signaling promotes ISG transcription through the cooperative binding of CREB and c-Jun (as part of the AP-1 complex), likely in concert with STATs at ISG promoters.[90] IL-4 is a well-established cytokine that drives macrophage polarization toward an alternatively activated (M2-like) phenotype, typically associated with anti-inflammatory functions. Interestingly, IL-4–polarized macrophages acquire an expanded and synergistic transcriptional response, which enables a hyperinflammatory gene expression program upon subsequent stimulation with TLR ligands.[148] Mechanistically, this priming effect appears to result from enhanced recruitment of inflammatory transcription factors, such as NF-κB and AP-1. Importantly, the magnitude and nature of this synergistic response are not uniform but are influenced by genetic background. Macrophages from different mouse strains exhibit distinct transcriptional and epigenetic responses to IL-4, which in turn shape their capacity to induce inflammatory genes upon TLR stimulation.[149-150]

Listeria monocytogenes: an intracellular pathogen model of infection

Listeria monocytogenes is a well-established Gram-positive intracellular pathogen, which is commonly used to study host-pathogen interactions, with a particular focus on host transcriptional responses to infection. The first evidence of *L. monocytogenes* intracellular replication came from its direct detection in mononuclear cells in 1926. In the late 90s, *L. monocytogenes* was recognized as food-borne pathogen and the etiological agent of listeriosis. In most individuals, listeriosis rate is quite low and is characterized by mild to severe gastroenteritis. In contrast, listeriosis shows high severity symptoms in children, elderly people, immunocompromised individuals and in pregnant women, where it can lead to bacterial sepsis and complications_during pregnancy.[151]

L. monocytogenes can be internalized in both phagocytic and non-phagocytic cells, and bacterial entry is one of the most characterized steps in its infection cycle. In non-phagocytic cells, members of the internalin (Inl) protein family, mainly InlA and InlB, mediate bacterial entry by binding of a plethora of cell receptors, such as E-cadherin and Met, thereby promoting receptor-mediated endocytosis.[152] In phagocytic cells, like macrophages, bacterial uptake typically occurs through phagocytosis following opsonization, a process in which oponins, such as IgG antibodies or complement proteins, coat the pathogen to facilitate its recognition and ingestion by phagocytes. However, a recent screen of approximately 350 human ISGs during *L. monocytogenes* infection identified the affinity immunoglobulin receptor FCGR1A (also known as CD64)

as a unique phagocytic receptor that can mediate bacterial uptake independently of opsonins.[153]

Once inside the vacuole, *Listeria monocytogenes* virulence factors listeriolysin O (LLO) and the phospholipases PlcA and PlcB mediate vacuolar rupture, allowing bacterial escape into the cytosol. LLO is a critical virulence factor that forms pores in the phagosomal membrane, facilitating bacterial escape. However, emerging evidence suggests that LLO may also function at earlier stages of infection, prior to bacterial entry, as well as after internalization.[154] In addition to its role in membrane disruption, LLO has been shown to induce profound alterations in the morphology and function of various host organelles, potentially benefiting the pathogen.[155-157]

Upon infection, *L. monocytogenes* can reprogram host cell transcription and induce epigenetic modifications. A recently described class of bacterial virulence factors, known as nucleomodulins, are secreted effectors that enter the host cell cytoplasm and translocate to the nucleus, where they modulate host gene expression.[158] In *Listeria monocytogenes*, the nuclear-targeted protein LntA was the first identified nucleomodulin. LntA interacts with the chromatin-silencing complex BAHD1, preventing its recruitment to the promoters of a subset of interferon-stimulated genes (ISGs), thereby enhancing their expression.[159] Notably, infection of *BAHD1*$^{+/-}$ mice with wild-type *Listeria*, or with strains that constitutively express *lntA*, resulted in attenuated disease severity. These findings suggest that the LntA–BAHD1 interaction, while modulating host responses, may paradoxically impair bacterial virulence by promoting a more robust immune response.

L. monocytogenes releases a variety of PAMPs that activate innate immune sensing. Upon entry into the host cytosol, *L. monocytogenes* is detected by several innate immune sensors.[151] One key PAMP is cyclic di-AMP, a bacterial second messenger secreted by the pathogen and detected by the host cytosolic receptor stimulator of interferon genes (STING). Bacterial lysis within the cytosol leads to the release of DNA, which is sensed by cyclic GMP-AMP synthase (cGAS). This enzyme catalyzes the production of cyclic GMP-AMP (cGAMP), a potent secondary messenger that also activates STING. Additionally, *Listeria* releases 5´-triphosphate RNA, which is recognized by the RNA sensor retinoic acid-inducible gene I (RIGI). These pathways converge on the STING-IRF3 axis, ultimately promoting the induction of type I IFNs and the expression of ISGs.[160-163] In parallel, TLR1, TLR2 and the nucleotide-binding oligomerization domain-containing protein 1 (NOD1) are activated upon encounter of *L. monocytogenes* PAMPs. These PRRs synergize in the activation of NF-kB signaling and stress-activated kinases, mounting antibacterial response (Figure 3).

Macrophages are central effectors in the host defense against *L. monocytogenes*, employing a multifaceted arsenal of bactericidal mechanisms to restrict and eliminate intracellular bacteria. Upon phagocytosis, macrophages expose L. monocytogenes to a hostile environment within the phagolysosome, characterized by acidification, hydrolytic enzymes, and the generation of reactive oxygen species (ROS) and reactive nitrogen species (RNS), such as nitric oxide (NO), which are potent antimicrobial agents.[7]

Upon phagosomal escape, *L. monocytogenes* becomes susceptible to additional cell-autonomous defenses. In the cytosol, macrophages can activate inflammasome pathways, particularly the AIM2 and NLRP3 inflammasomes, in response to bacterial DNA and other PAMPs.[164-165] Inflammasome activation leads to the cleavage of pro-caspase-1, resulting in the maturation and secretion of pro-inflammatory cytokines IL-1β and IL-18, as well as the induction of pyroptosis, a lytic, inflammatory form of programmed cell death that eliminates the intracellular niche for bacterial replication and alerts neighboring immune cells.[166] In addition, type I IFN responses, triggered by cytosolic sensing of *Listeria*-derived nucleic acids, can sensitize infected macrophages to apoptosis via upregulation of pro-apoptotic factors.[167-169] Autophagy also contributes to bacterial clearance by targeting cytosolic *L. monocytogenes* for lysosomal degradation.[170-171]

Collectively, these bactericidal and cell death mechanisms act in concert to limit *L. monocytogenes* replication, promote pathogen clearance, and orchestrate a robust inflammatory response that is essential for host protection.

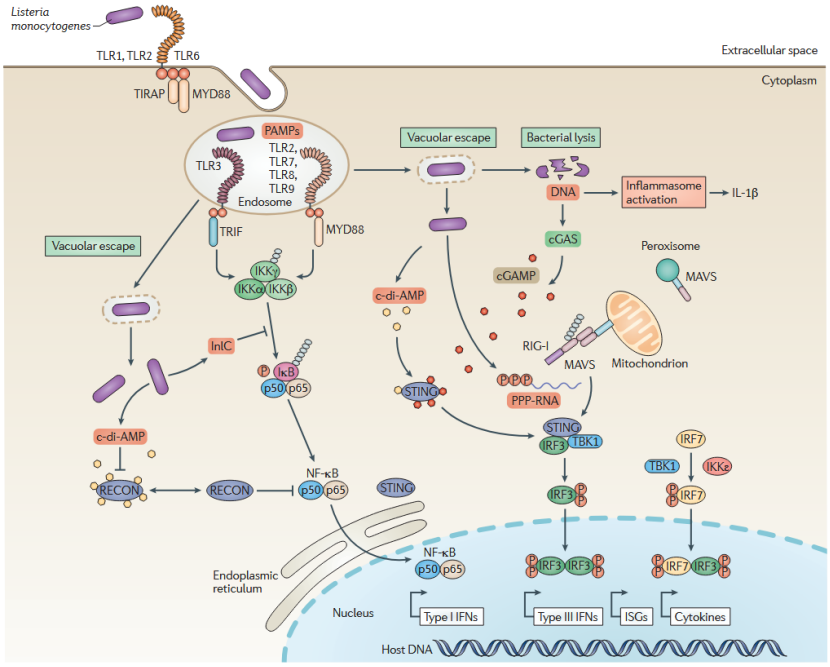

Figure 3. Innate immune sensing during *Listeria monocytogenes* infection (Radoshevich & Cossart, 2018). Surface and endosomal TLRs engage MyD88 or TRIF to induce NF-κB activation and proinflammatory cytokine production. Cytosolic bacterial cyclic-di-AMP activates STING-dependent NF-κB and type I IFN responses. Bacterial lysis releases DNA, sensed by cGAS to produce cGAMP, further engaging STING and IRF3. Bacterial RNA can be detected by RIG-I, signaling through MAVS to promote IRF3 and IRF7 activation. These parallel pathways converge to induce expression of type I and III IFNs, ISGs, and proinflammatory cytokines. Inflammasome activation by bacterial components promotes IL-1β release, adding another layer of immune defense.

Transcriptional control in eukaryotes

Eukaryotic genes are transcribed by three different types of RNA polymerases (RNA pol). RNA Pol I transcribes multiple copies of ribosomal RNAs (rRNAs) except for the 5S rRNA. RNA Pol III is required for the transcription of tRNA, 5S rRNA and small

nuclear RNAs (snRNA), such as the splicing component U6 snRNA. Finally, RNA pol II is crucial for the transcription of all protein-coding genes, as well as some snRNAs and microRNAs. RNA polymerases consist of 12 to 17 different subunits, with all three polymerases containing a ten-subunit core that carries the catalytic activity at its center.[172]

RNA polymerase II CTD code

RNA pol II is made of 12 subunits, among which the largest one is RBP1. The carboxy-terminal domain (CTD) of the RBP1 subunit represents a unique region consisting of heptapeptide repeats with the consensus sequence Tyr1-Ser2-Pro3-Thr4-Ser5-Pro6-Ser7 (YSPTSPS). The number of repeats is highly variable, ranging from 26 in budding yeast to 52 in mammals. Of the 52 repeats that constitute mammalian CTD, the first 26 are highly conserved. Each residue within the CTD can be subjected to different PTMs, constituting the so called “CTD code”.

In yeast, the entire CTD code was shown to not be essential for the function of Pol II, as only eight repeats of the full-length CTD are required for budding yeast survival.[173] However, a reduced number of heptapeptide repeats within the CTD has also been associated with higher DNA instability, indicating the importance of CTD integrity for optimal cellular functions.[174] Recently, the Cramer lab demonstrated that CTD shortening can alter Pol II proximal-pausing and enhancer activation in human cells.[175] Additionally, the CTD was shown to form non-covalent interactions that are connected with liquid-liquid phase separation, suggesting that this could be another mechanism employed by the CTD to regulate transcription.[176-177] The CTD can regulate each step in the transcription process, from initiation to termination. Moreover, it is important for regulating several co-transcriptional processes, including splicing and chromatin modification. The unmodified CTD of Pol II is responsible for its recruitment to promoters[178] and the assembly of the pre-initiation complex (PIC) via its strong affinity for the Mediator complex.[179] In both budding yeast and humans, each of the heptapeptide residue (except for the Proline residues) is phosphorylated at some point during the transcription cycle. The phosphorylation state of the CTD follows a precise spatial and temporal dynamic (Figure 4). The first modifications reported were phosphorylation of Ser5 and Ser2. Phosphorylated Ser5 (Ser5P) levels peak around the transcriptional start site (TSS) of genes, whereas Ser2P levels tend to increase across gene bodies, then drastically decrease after the polyadenylation site (PAS).[180-181] This phosphorylation pattern is conserved across multiple species, including mammals.

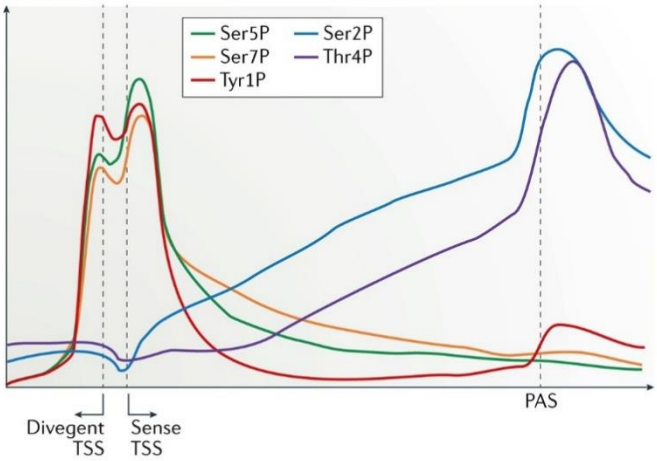

Figure 4. Pattern of Pol II CTD modifications across the gene (Harlen & Churchman, 2017).
Chromatin immunoprecipitation (ChIP) average peak distribution for distinct Pol II CTD phospho-forms across protein-coding genes in humans. Occupancy of Pol Ser5P and Ser2P peaks at the transcriptional start site (TSS) to decrease across the gene body. Conversely, Ser5P and Thr1P increase towards the gene body and peak in proximity of the poly-adenylation site (PAS). Tyr1P peaks only the PAS.

Conversely, Tyr1P has different effects in budding yeast and in metazoans. In yeast, Tyr1P has a similar phosphorylation profile to that of Ser2P and seems to be involved in transcription termination.[182] In contrast, in metazoans, increased Tyr1P levels are detected near promoters and are correlated with paused Pol II complexes in sense and antisense orientations.[183-184] Ser7 phosphorylation (Ser7P) peaks at promoters of all Pol II-transcribed genes and remains constant throughout the gene body. Mutation of Ser7 to alanine showed defects in 3´processing at snRNA genes in mammals, although its exact role at coding genes remains to be understood.[185-186] Thr4 phosphorylation (Thr4P) remains the least characterized; however, Thr4P levels peak downstream of the PAS and seems to be involved in 3´end processing of both coding and non-coding transcripts.[187-188] Beside phosphorylation, residues of the CTD can be subjected to various PTMs, including proline isomerization and O-GlcNAcylation, which further expand its regulatory potential.[189]

Together, these dynamic and site-specific CTD modifications coordinate the recruitment of transcription and RNA processing factors, underscoring the CTD's central role as an integrative platform in the regulation of eukaryotic gene expression.

RNA pol II cycle

Pol II regulation is a mechanism underlying different cellular processes, including differentiation, maintenance of cell identity, and responses to environmental cues. It can occur at different stages of the transcription cycle, which require the cooperation and subsequent recruitment of several factors (Figure 5). The importance of Mediator and the Mediator kinase module on these different stages of transcription will be further discussed in the Mediator complex paragraph.

Transcriptional initiation and promoter clearance

Initiation of transcription requires the coordinated recruitment of several factors, known as general transcription factors (GTFs), which constitute the pre-initiation complex (PIC). Historically, biochemical studies have identified a set of six GTFs: TFIIA, TFIIB, TFIID, TFIIE, TFIIF and TFIIH[190], which together with Pol II and Mediator constitute the PIC. PIC assembly occurs upon recognition of specific motifs present within core promoters, short sequences which extend ~50 bp upstream and downstream of the TSS. The most well-known of such motifs, the TATA-box motif, is located ~ 30 bp upstream of the TSS and is conserved from yeast to humans. Nevertheless, the TATA-box is found in only a minority of core promoters and many other core-promoter motifs were characterized.[191] The TATA-box is recognized by the TATA-box binding protein (TBP), a component of the TFIID complex, which initiates PIC nucleation.[192-193] Upon binding of TBP to promoters, TFIIA further stabilizes TBP-promoter interactions via direct contacts with TBP and the upstream DNA backbone.[194] TFIIB subsequently binds to TBP, also making contact with DNA sequences located upstream and downstream of the TATA box.[195] This resulting assembly is then able to recruit RNA pol II through TFIIF.[196] A fully function PIC is allowed by recruitment of TFIIE and TFIIH.[197-198] The ATP-dependent activity of XBP translocase, one of the subunits of TFIIH, allows DNA melting, which is essential for formation of the open complex, initiating transcription of nascent RNA.[199]

A different subunit of TFIIH, cyclin-dependent kinase 7 (CDK7, also known as Kin28 in *S. cerevisiae*), along with its regulatory subunit cyclin H, phosphorylates the Pol II CTD at Ser5 and Ser7 residues, allowing transition from transcriptional initiation to elongation in a process known as promoter clearance.[200-201] Ser5 phosphorylation (Ser5P) influences mRNA capping by recruiting the mRNA capping complex, which methylates the N7 position of guanine on the nascent transcript.[180] This capping process stabilizes the primary mRNA (pre-mRNA) and protects it from degradation by nucleases.

As a result of promoter clearance, early elongating Pol II complexes are formed; however, these complexes are generally short-lived and subject to further regulation. The fate of these early elongating Pol II complexes is determined by additional regulatory mechanisms, including promoter-proximal pausing, which serves as a critical checkpoint in the control of gene expression.

RNA Pol II proximal pausing and release

The phenomenon of promoter-proximal Pol II pausing was first described in the mid-80s by John Lis in pioneering studies of the *Drosophila* heat-shock protein (hsp) genes.[202-203] In these studies, Pol II was found to be preloaded at hsp promoters prior to heat stress. Surprisingly, Pol II stalled shortly downstream within the transcribed region, remaining tightly associated with short nascent transcripts. Upon heat shock, this paused Pol II was rapidly released into productive elongating complexes. Simultaneously, promoter-proximal pausing has been observed at several mammalian

loci, including the β-globin gene cluster, c-myc and Fos genes, underscoring its role as a key regulatory checkpoint during early transcription elongation.[204-206]

The advent of genome-wide techniques for monitoring Pol II occupancy and kinetic in metazoan cells has advanced our understanding of Pol II pausing. Chromatin immunoprecipitation on chip (ChIP-chip) experiments revealed prominent Pol II peaks near many promoters[207-208], indicating that Pol II might undergo this additional rate-limiting step in proximity of the TSS. Subsequent experiments in *Drosophila* have revealed that most active genes show Pol II promoter-proximal occupancy, suggesting that pausing is a wide-spread phenomenon.[209-210]

At the molecular level, promoter-proximal pausing is primarily established by two factors: the negative elongation factor (NELF) and the DRB sensitivity-inducing factor (DSIF). DSIF is a heterodimer composed of the Spt4 and Spt5 subunits, with Spt5 being the subunit that directly contacts Pol II.[211-212] Spt5 association with Pol II occurs after promoter escape, once Pol II has synthetized an RNA transcript of approximately 18-20 nucleotides. Spt5 binding promotes recruitment of the capping enzyme, enabling prompt and efficient RNA capping.[213-214] In addition, Spt5 recruits NELF to the Pol II elongation complex.[215]

The NELF complex is composed of the four subunits, NELF-A, B, C/D and NELF-E. NELF-A anchors the complex to Pol II[216], while NELF-B contributes to the recruitment of the NELF complex to promoters.[217] NELF-E carries RNA recognition motifs that allow interaction with the nascent transcript.[218] NELF ablation is lethal in mammals[219], and its depletion in cells leads to a drastic reduction in promoter-proximal paused Pol II. Promoter-proximal pausing is prominent at innate immune genes, where it facilitates rapid and robust transcriptional responses to inflammatory stimuli.[220] Studies have demonstrated that NELF plays a critical role in regulating inflammatory gene expression in macrophages, highlighting its broader significance in immune responses.[221] Notably, a recent study using auxin-inducible degron systems suggest that NELF may function in processed beyond canonical pause-release transition.[222] Acute NELF depletion caused premature Pol II termination, possibly because of impaired interaction with the cap-binding complex. DSIF depletion similarly results in reduced Pol II pausing and is accompanied by defects in elongation.[223] Interestingly, in contrast to NELF, DSIF can act as either an activator or a repressor of transcription, indicating that the role of DSIF might depend on interacting factors.[224]

To achieve productive elongation, paused Pol II complexes need to be released by the positive transcription elongation factor (P-TEFb).[225] P-TEFb comprises the CDK9 kinase and its regulatory subunit Cyclin T1. CDK9 phosphorylates both NELF and DSIF, resulting in the release of the NELF complex, while DSIF is converted into a positive elongation factor that remains stably associated with the Pol II machinery during elongation. Importantly, P-TEFb is also required for phosphorylation of Pol II CTD at Ser2 residues (Ser2P), which is a marker for productive elongation. Although P-TEFb carries out this initial step, the majority of Ser2P is believed to derive from the activity of the CDK12 and CDK13 kinases.[226-227] Short-term inhibition of P-TEFb activity using compounds such as DRB or flavopiridol (FP), traps Pol II in the early elongation step at nearly every protein-coding gene.[228-229] Given the crucial role of P-

TEFb in regulating pause release, it is not surprising that its biological availability is tightly controlled. In cycling cells, 50%-90% of P-TEFb is normally sequestered in an inactive state within the larger complex 7SK snRNP.[225] Only upon regulated dissociation from the 7SK snRNP complex is P-TEFb released and able to exert its activity. Many signaling pathways which are triggered by cellular stress can release and activate P-TEFb function.[230] Several factors are known to contribute to P-TEFb release from 7SK complexes, including the HIV Tat protein and the bromodomain-containing protein BRD4.[231-232] The most active form of P-TEFb is associated with the super elongation complex (SEC).[233] Excluding p-TEFb, SEC consist of the eleven-nineteen Lys-rich leukaemia (ELL) proteins (ELL1, 2 and 3), the MLL translocation partners AF4/FMR2 family member 1 (AFF1), AFF4, eleven-nineteen leukaemia (ENL) and ALL1-fused gene from chromosome 9 (AF9). The SEC plays a pivotal role in promoting rapid transcriptional elongation at genes that require robust activation, such as immediate-early genes (IEG) and those involved in development and disease, by coordinating paused Pol II release and enhancing productive elongation.

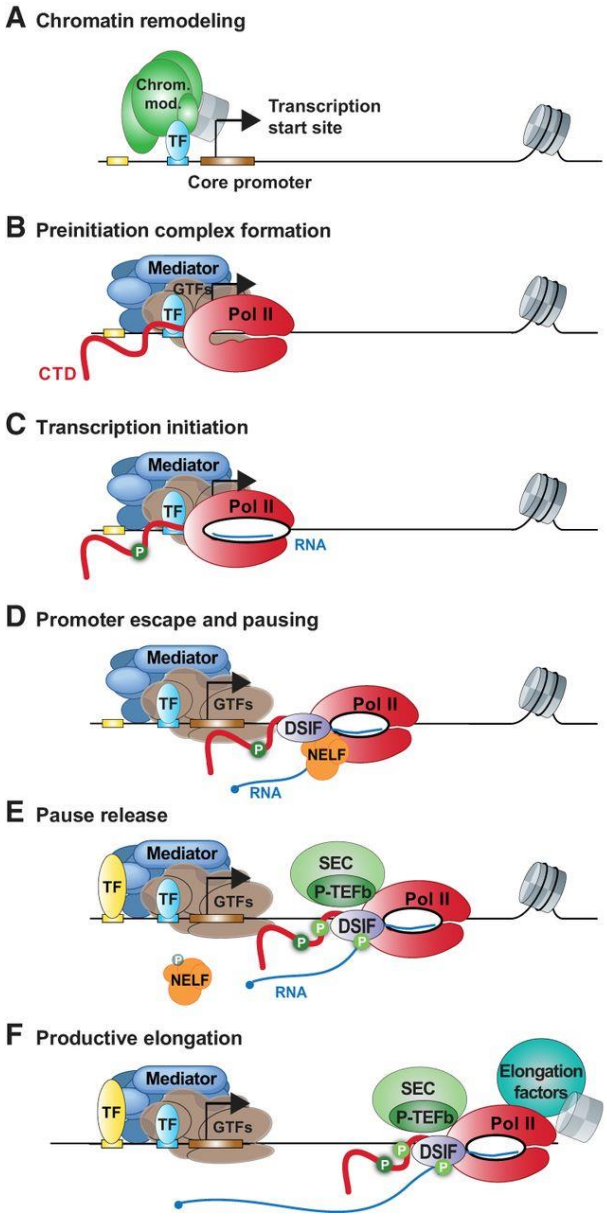

Figure 5. Early steps of Pol II cycle (Core & Adelman, 2019).
A) Chromatin remodelers are recruited by transcription factors (TFs) to expose the transcription start site through removal of nucleosomes. B) TFs, general transcription factors (GTFs), Mediator and RNA polymerase II (Pol II) assemble at the core promoter resulting in the formation of the pre-initiation complex (PIC). C) Phosphorylation of the serine 5 residue of Pol II C-terminal domain (CTD) initiates RNA synthesis. D) Pol II escapes the promoter and proximally pauses downstream. Pol II promoter-proximal pausing is regulated by negative elongation factors NELF and DSIF. E) Positive transcription elongation factor b (P-TEFb) phosphorylates NELF, DSIF, and Pol II CTD at serine 2 residue, promoting transition into productive elongation. F) Pol II proceeds with transcription elongation, assisted by elongation factors and the super elongation complex (SEC). A second round of transcription can now occur through recruitment of new Pol II molecules.

Transcriptional elongation

Productive elongation by Pol II requires extensive chromatin remodelling achieved through nucleosome turnover and co-transcriptional histone and DNA modifications. The dynamic replacement of nucleosomes during elongation is primarily driven by chromatin remodelers and histone chaperones. One of such factors is the facilitates chromatin transcription (FACT), which travels with Pol II, interacts with the histone H2A-H2B dimer, and regulates nucleosome disassembly and reassembly.[234-236]

Histone PTMs are tightly associated with specific stages of the transcription cycle. Active promoters are marked by high levels of H3K4me3 and multiple acetylation marks on histone H3 and H4 Lysin residues. In contrast, gene bodies of actively transcribed genes are enriched with mono-ubiquitylated H2B (H2Bbub), H3K36me3, H3K79me2/3.[208-237-238]

The Histone- lysine N- methyltransferase SETD2 associates with the phosphorylated Pol II CTD and deposits H3K36me3 along gene bodies, influencing RNA splicing and suppressing cryptic transcription. This regulation likely involves additional factors recruitment such as histone deacetylases and nucleosome remodellers.[239-240]

Furthermore, enhancer-promoter contacts, poly ADP-ribosylases (PARPs) and topoisomerases also contribute to assure a productive elongation, although their precise role remain incompletely understood.[241]

Transcriptional termination

After Pol II successful elongation, the elongated transcript acquires a polyadenylation signal (PAS), which most commonly consist in the AAUAAAA sequence. Upon pre-mRNA polyadenylation, transcriptional termination occurs. At the 3´ends of genes, pre-mRNAs undergo mRNA processing: nucleolytic cleavage and polyadenylation to produce a fully mature transcript.[242] Processing is tightly coupled to termination; if cleavage occurs prematurely, the result of transcription will be a truncated gene product. This transcriptional coupling is enabled by physical interactions between the RNA processing machinery and the Pol II CTD.[243] Consequently, these processes most be under rigid control.

The 3′ end processing machinery includes the cleavage and polyadenylation specificity factor (CPSF) complex, a large multiprotein assembly in mammals. CPSF recognizes the PAS and activates its endonuclease subunit, CPSF73, to cleave the nascent transcript downstream of the PAS.[244] Subsequently, the poly(A) polymerase (PAP) adds a poly(A) tail to the new 3´end of the transcript.

Currently, two models for transcription termination have been proposed: the allosteric (or anti-terminator) model and the torpedo model, which are not mutually exclusive.[245-246]

In the allosteric model, transcription of the PAS modifies Pol II, promoting transcription termination. This may occur via the PP1 phosphatase and its regulatory subunits PNUTS, which co-purify with 3´end processing complexes.[247] PP1 dephosphorylates the SPT5 subunit of DSIF, slowing down Pol II downstream of the PAS and enabling its termination via the XRN2 torpedo exonuclease.[248] The Integrator

complex also contributes to termination, particularly during premature transcriptional termination.[249] At Integrator-containing promoters, the PP2A phosphatase decreases Pol II elongation by dephosphorylating Pol II CTD and SPT5, leading to termination.[250]

In the torpedo model, cleavage of the PAS exposes the 5´end of the nascent RNA to XRN2, a 5´-3´exonuclease. XRN2 degrades the RNA and dissociates Pol II from the DNA template.[251]

The two models are likely complementary: following PAS transcription, the 3′ end processing machinery assembles on the transcript, activating endonucleases and phosphatases. This results in Pol II CTD dephosphorylation and transcript cleavage, after which XRN2 degrades the remaining RNA, ultimately triggering termination.

The Mediator complex

Mediator of RNA polymerase II transcription (Mediator) was first identified in yeast approximately 30 years ago as a crucial regulatory factor in transcription.[252] Since then, it has been recognized as an evolutionarily conserved multisubunit complex that acts on the basal transcriptional machinery by bridging the action of general transcription factors (GTFs) and Pol II, thereby promoting PIC assembly at target promoters.[253]

Although conserved, the structure and subunit composition of Mediator have evolved considerably. Yeast Mediator incudes 21 subunits and is approximately 0.8 MDa in size, whereas human Mediator includes 26 subunits and is approximately 1.4 MDa in size. Interestingly, mouse and human Mediator complexes are highly conserved, and contain the same number of subunits, which are tightly associated. In yeast, deletion of 10 out of the 25 Mediator subunits is lethal. Similarly, in mammals, knockout of several Mediator subunits leads to embryonic lethality, underscoring its essential role in transcriptional regulation.

Structurally, yeast Mediator is organized into three distinct modules: the head, middle and tail, all of which can be biochemically reconstituted. The Human Mediator complex mirrors this organization. The head and middle modules bind to Pol II, while the tail module serves regulatory functions, including interactions with transcriptional activators. Noteworthy, MED14 and MED17 subunits form critical contacts that connect the head, middle and tail modules, providing support to the complex.[254-256] Additionally, a four-subunit kinase module, also known as the Mediator kinase module, MKM, or CDK module can reversibly associate with Mediator. This module can exist independently of Mediator. Indeed, MKM purified from Hela cells was shown to be stable on its own.[257] Notably, MED26 is mutually exclusive with the Mediator kinase module (MKM); structural and biochemical studies indicate that MED26-containing Mediator complexes do not simultaneously incorporate the MKM but co-purify with Pol II.[258-259]

Recent high-resolution structures of Mediator and TFIID had shown how the two factors cooperate to position TFIIH within the PIC via several contact sites.[254] Specifically, Mediator is responsible for the positioning of CDK7-Cyclin H within the PIC. This interaction, mediated via the head and hook domains of Mediator, ensures proper orientation of CDK7 for phosphorylation of Pol II CTD.[254-255] In addition to its critical role in PIC assembly, Mediator also facilitates transcriptional reinitiation, acting

as a scaffold that supports multiple rounds of transcription from a single promoter. Recent studies indicate that Mediator remains associated with the promoter after the first round of transcription, enabling efficient reassembly of the transcription machinery and sustained gene expression.[253-260]

As previously discussed, p-TEFb and the SEC complexes are important establishers of productive transcription elongation. In addition, The Little Elongation Complex (LEC) is a specialized transcription elongation complex that functions primarily at small nuclear RNA (snRNA) gene.[261] The MED26 subunit plays a pivotal role in recruiting SEC or LEC to target genes.[262-263] MED26 has also been shown to interact with TFIID[262], or the TATA-binding protein (TBP)-associated factor 7[263], suggesting that MED26 acts as a molecular switch to promote the transition from Pol II initiation to elongation. Interestingly, MED26-mediated recruitment of LEC has also been implicated in promoting Pol II termination and 3´end processing of snRNAs and replication-dependent histone mRNAs.[264] A very recent study reported that a similar process also occurs for polyadenylated transcripts; in this case, the MED23 subunit was found to be critical for the interaction with termination factors as well as with 3′ mRNA.[265] In addition to its structural and regulatory roles, Mediator also functions as a metabolic hub; recent findings have shown that Mediator-bound 2-ketoacid dehydrogenases locally produce acetyl-CoA to fuel de novo histone acetylation, a process regulated by nitric oxide signaling.[266]

The Mediator kinase module

In yeast, the MKM is composed of four different subunits: the Cyclin-dependent kinase 8 (CDK8), cyclin C (CCNC), MED12 and MED13. Nevertheless, in Vertebrates three out of four subunits have evolved paralogs, respectively called CDK19, MED12L and MED13L, providing additional functional layers which have remained enigmatic.

CDK8 and CDK19 belong to the family of cyclin-dependent kinases (CDKs), serine/threonine kinases whose activity depends on a regulatory subunit known as cyclin.[267] CDKs are divided into cell-cycle regulating CDKs or transcriptional CDKs, the latter including (CDK7, CDK8/CDK19, CDK9, CDK12 and CDK13). Notably, CDK8 and CDK19 are unique among CDKs in that they lack a canonical threonine phosphorylation site in the activation (T-) loop, which is instead substituted by an aspartate residue, conferring constitutive activation in the presence of their cyclin partner.[268]

The Tsai lab has determined the cryo-EM structure of *Saccharomyces cerevisae* MKM.[269] The authors concluded that the N-terminal region of Med12 contacts the Cdk8-Ccnc dimer and triggers the kinase activity of Cdk8. This occurs via stabilization of its otherwise disordered T-loop, allowing the substrate to access the active site. Conversely, the C-terminal region of Med12 interacts with Med13 and ultimately contacts Ccnc. In a recent paper, the Tsai lab has also provided the first high-resolution cryoEM structures of human core Mediator (cMED), the MKM and cMED bound by the MED13 IDR.[270] They reported that MED12 HEAT repeats and MED13 IDR contact different cMED surfaces, especially in the “hook” domain. Importantly, the MED13 IDR inhibits the interaction of RNA pol II and MED26 with cMED, thereby repressing

transcription of cMED-dependent genes. These findings are corroborated by a cross-linking-mass spectrometry analysis performed by the Cramer lab using yeast CDK-Mediator.[271]

Beyond its regulatory role in the MKM, CCNC can also associate with CDK3, promoting the transition from G0 to G1 phase of the cell cycle.[272] Mutations in MED12 are implicated in a broad spectrum of human diseases, most notably in tumorigenesis and neurodevelopmental disorders.[273-274] As for MED13, although alterations have been observed in various tumors, its precise role in cancer development remains unclear.[273]

CDK8 and CDK19 mechanistic insights

Early *in vitro* biochemical studies, implicated CDK8 as a negative regulator of transcription. In yeast, CDK8 homolog (also known as Srb10) represses gene expression programs through phosphorylation of TFs, which decreases their stability.[275-276] In higher eukaryotes, CDK8 was found to repress transcription by phosphorylating cyclin H of TFIIH, blocking PIC formation[277], and by sterically preventing Mediator-Pol II interaction.[278-281] The dynamic regulatory role of CDK8 was highlighted when it was shown to serve as a molecular switch, modulated by signal-induced remodelling of the Mediator complex.[282-285] In mammals, CDK8 also phosphorylates stimuli-induced transcription factors (STFs) such as Notch ICD[286], Smads[287], STATs[134]. However, the outcome of this phosphorylation is to promote transcriptional activation of such STFs, potentiating their activity and/or increasing their turnover, indicating CDK8 has other functions beyond repression. The observation that binding of CDK8 at a subset of p53 responsive genes correlated with transcriptional coactivation provided the first direct evidence of its positive role in stimulus-specific transcription.[288]

Two seminal studies from the Epinosa lab, using cancer cells, provided compelling evidence that CDK8 promotes Pol II elongation. First, CDK8 depletion at IEGs slowed down elongation complexes by impairing CDK8-mediated recruitment of P-TEFb. Notably, this depletion led to decreased levels of Ser2P and Ser5P at IEGs and reduced recruitment of CDK7 and CDK9, suggesting the observed effects might not be direct.[289] Second, CDK8 was shown to be required for the recruitment of SEC at HIF1A-regulated genes.[290]

While these studies provided important insights into CDK8 function, they also had notable limitations: (1) they did not address the role of CDK19; (2) they could not distinguish between kinase-dependent and kinase-independent functions; 3) they relied on HCT116 colorectal cancer cells, which have specific genetic dependencies. The development of potent and selective small-molecule inhibitors targeting CDK8/CDK19, in combination with genetic depletion approaches and analog-sensitive CDK8 mutants[291], has helped to address these gaps. The first inhibitor, Senexin A (SnxA), had an IC_{50} in the micromolar range.[292] Subsequently the highly selective and potent inhibitor Cortistatin A (CA), with an IC_{50} in the nanomolar range, was used in a seminal study in acute myeloid leukemia (AML) cells. Super-enhancers (SE) are expansive clusters of transcriptional enhancers that cooperate to drive robust

expression of genes involved in diverse cellular processes, including development, cell identity, and disease.[293] Interestingly, inhibition of CDK8/19 kinase activity using CA led to hyperactivation of SE-associated tumor-suppressor genes in AML cells.[294] Similarly, the Serrano lab has recently showed that CDK8/19 inhibition in embryonic stem cells causes SE hyperactivation, stabilizing the naive pluripotent state by upregulating key pluripotency genes and preventing differentiation.[295]

A comprehensive phosphoproteomic study in unstimulated HCT116 cells provided the first global view of CDK8/19 kinase substrates, identifying 78 high-confidence phosphosites across 84 proteins, preferentially within the conserved PX(S/T)P motif.[134-287] These targets included TFs, chromatin regulators, Pol II regulating factors and proteins involved in DNA replication, repair and ubiquitination, suggesting that CDK8/19 functions extend beyond transcription.[296] Notably, long-term inhibition of CDK8/19 increases the stability of Mediator complex subunits, thereby linking kinase function to control of protein abundance.[297]

In metazoans, CDK8 and CDK19 evolved as two distinct and mutually exclusive paralogs within the Mediator kinase module. Although they were initially thought to function redundantly, recent studies from our group and others have revealed functional divergence.[135-291-298-299] For instance, in IFNγ-stimulated CDK8 and CDK19 mouse embryonic fibroblasts (MEFs), CDK8 retains kinase activity while CDK19 acts as a scaffold.[135] Importantly, differences in CDK8 and CDK19 expression levels across cell types could contribute to these mechanistic distinctions. In contrast, the Firestein lab reported functional redundancy in regulating intestinal epithelium homeostasis via the SWI/SNF chromatin remodelling complex.[300-301] Likewise, the Roninson group demonstrated that CDK8 and CDK19 share overlapping substrates in 293T cells, indicating redundancy at the level of their kinase activity.[297]

Together, these findings illustrate that CDK8 and CDK19 are versatile regulators of signal-induced transcription, with roles that go beyond simple repression or activation. Their functions encompass the regulation of transcriptional machinery, STFs, chromatin remodelling and epigenetic changes. Whether their activities are redundant or distinct appears to depend on the cellular context and signaling environment, highlighting the complexity and adaptability of Mediator kinase module in metazoan gene regulation (Figure 6).

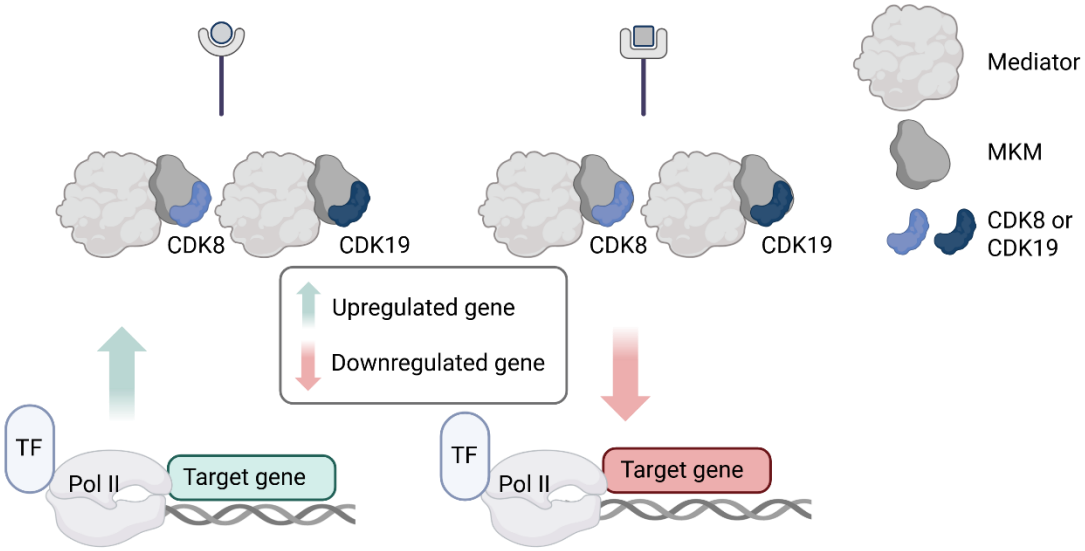

Figure 6. Differential gene regulation by Mediator kinase module (MKM) complexes containing CDK8 or CDK19 in response to distinct signals.
Two distinct signaling inputs (left and right) converge on the Mediator-MKM complexes. The downstream transcriptional outcomes diverge: on the left, MKM promotes transcriptional activation (green), while on the right, it mediates transcriptional repression (red). The functional outcome of MKM activity is determined by stimulus-specific transcription factors and/or regulation of the RNA Pol II transcription cycle. CDK8 and CDK19 can act redundantly or exert distinct roles depending on the cellular context.

Mediator kinase role in inflammation: cell type and context specificity

Numerous studies have shown that CDK8 is a driver in various cancers, including colorectal, breast, melanoma and leukemia, by enhancing the activity of key TFs such as β-catenin, STAT1, and p53, thereby promoting tumor growth, invasion, and metastasis. Notably, Mediator kinase has also been shown to potentiate NFκB-dependent transcriptional programs, further supporting their role in oncogenic and inflammatory signaling.[302] However, the effects of the Mediator kinase are highly context-dependent, and in certain tissue types, it may also exhibit tumor-suppressive functions.[294]

The central role of the Mediator kinase in oncogenic transcriptional regulation has prompted the development of several selective inhibitors, enabling both clinical and experimental applications.[303] Although many studies have investigated Mediator kinase function in cancer cell lines with defined genetic dependencies, its role in the immune system remains poorly understood. Our lab has shown that CDK8 phosphorylates STAT1 and other STAT family members at their conserved Ser727 residue, modulating the IFN response and fine-tuning the expression of ISGs.[134-135] Importantly, recent studies have demonstrated that Mediator kinase inhibition can suppress hyperactive IFN signaling in pathological contexts such as Down syndrome.[304] Since hyperactive IFN signaling is a hallmark of many interferonopathies

and immune-related disorders, Mediator kinase inhibition may offer an important therapeutic intervention.

Beyond the context of IFN signaling, recent chemical biology studies have expanded our understanding of the immunomodulatory functions of Mediator kinase in the myeloid compartment. Selective inhibition of CDK8/19 has been shown to modulate cytokine production in myeloid cells, most notably by increasing the expression of the anti-inflammatory cytokine IL-10 and a subset of immune-related genes.[305] Consistent with these findings, Mediator kinase inhibition increases the expression of arginase-1, a key enzyme involved in anti-inflammatory and tissue-repair functions in macrophages, through activation of STAT6 and p38 MAPK.[306] Notably, recent work has demonstrated that novel Mediator kinase inhibitors can exert potent anti-inflammatory effects *in vivo* by promoting IL-10 production.[307]

Beyond innate immune cells, emerging evidence have revealed critical roles for Mediator kinase in adaptive immune cells function. In contrast to its effects in other immune contexts, CDK8 fine-tunes IL-6-mediated transcriptional response in primary human Th1 cells by restricting STAT3-dependent gene expression upon IL-6 stimulation.[308] Inhibition of Mediator kinase has been shown to promote the conversion of antigen-specific effector and memory T cells into Foxp3$^+$ regulatory T cells (Tregs), thereby enhancing immune tolerance.[309] This pro-tolerogenic effect is further supported by studies demonstrating that Mediator kinase inhibition suppresses autoimmune diseases by enhancing Treg cell development.[310] Likewise, targeting the Mediator kinase module can also enhance effector T cell activity, leading to improved antitumor immunity, as recently demonstrated in preclinical models.[311]

Collectively, these findings underscore the complex and context-dependent roles of Mediator kinase in modulating both pro-and anti-inflammatory pathways, highlighting its potential as a therapeutic target to fine-tune immune responses in cancer and autoimmune diseases.

While a few studies have begun to explore the role of Mediator kinase in host defence against infectious agents, primarily focusing on viral infections[312-314], its role in bacterial infection models remains largely unexplored. The research presented in this thesis addresses this gap by elucidating the function of Mediator kinase in regulating host immune responses during bacterial infections, offering insights into its role in bacterial pathogenesis.

Post-transcriptional control of gene expression

While transcriptional regulation establishes the initial framework of gene expression, the level, timing, and specificity of protein production are ultimately shaped by post-transcriptional mechanisms. These processes, including RNA splicing, nuclear export, mRNA stability, and translational efficiency, allow for rapid and reversible control of gene expression and are especially important in dynamic environments such as inflammation.

Once fully processed mRNAs have been exported into the cytoplasm, their fate is determined by RNA-binding proteins (RBPs), which modulate mRNA stability and

translation output.[315] Canonical mRNA decay typically proceeds through poly(A) tail shortening (deadenylation) followed by removal of the 7-methylguanosine cap (decapping), ultimately leading to exonucleolytic degradation.[316]

Tristetraprolin (TTP): a key regulator of inflammatory mRNA decay

Among the many RBPs that regulate mRNA fates, tristetraprolin (TTP) is a key regulator of decay of mRNAs encoding inflammatory mediators including cytokines and chemokines.

In mammals, TTP (encoded by Zfp36) is a member of the Zfp36 protein family, which also includes the paralogs Zfp36l1, Zfp36l2, and (in mice) Zfp36l3. The importance of the Zfp36 family in immune regulation is underscored by genetic mouse models lacking individual family members. Deletion of Zfp36l1 and zfp36l2 is associated with embryonic or early postnatal lethality, respectively.[317-318] In contrast, TTP knockout mice do not exhibit developmental abnormalities but instead develop the so called “TTP deficiency syndrome” characterized by systemic, spontaneous inflammation due to the stabilization of mRNAs encoding *Tnf*[319-320], and multiple other cytokines and chemokines[321-324].

Unlike some RBPs, which possess intrinsic endonuclease activity, TTP promotes mRNA decay by recruiting the CCR4-NOT deadenlyase and the DCP1/DCP2 decapping complexes to its target mRNAs.[325-327] Following decapping and deadenylation, the mRNA is degraded by the 5´- 3´exonuclease Xrn1 or the 3´-5´exonuclease activity within the exosome.[328]

All TTP family members contain a tandem zinc finger (TZF) domain composed of two C3H1 (Cys-Cys-Cys-His) motifs, which are essential for binding AU-rich elements (AREs) in the 3´untranslated region (3´UTR) of target mRNAs. Mutations in the TZF domain have been shown to disrupt RNA binding[325] or to phenocopy the TTP knockout phenotype *in vivo*[329], proving that TTP RNA-binding activity is critical for TTP-mediated mRNA decay.

Genome-wide mapping of TTP target AREs was performed by several crosslinking immunoprecipitation-high-throughput sequencing (CLIP-seq) approaches in different immune cells, proving that TTP preferentially binds to the UAUUUAU sequence.[330-333] However, TTP binding was not restricted to 3′UTRs; it also occurred in 5′UTRs, coding sequences, and introns, suggesting that TTP may engage its targets within the nucleus. The biological significance of TTP binding on intronic sequences remains unclear, as no consistent effects on splicing or stability have been observed.[330] Interestingly, TTP binding to 3´UTRs does not always lead to mRNA destabilization, possibly due to unknown co-factors specific PTMs that influence TTP activity. Notably, the 3´UTR of TTP mRNA contains AREs, allowing TTP to autoregulate its own expression through a negative feedback loop.[334]

TTP function is tightly controlled at multiple levels, enabling timely and selective mRNA decay. As an IEG, TTP is expressed at low levels under steady state conditions but is rapidly induced in response to inflammatory stimuli such as TNFα, IL-4, IL-10 and IFNγ, and bacterial products such as LPS.[319-334-337] The mouse and human Zfp36 promoter contains a STAT1 GAS element, which is likely employed by other signal-

induced STATs to activate transcription.[337] In addition, NF-κB has been shown to directly promote Zfp36 transcription in response to LPS or TNFα in macrophages.[338] A key aspect of TTP regulation is control of its protein stability, which is closely linked to its phosphorylation state. TTP is extensively phosphorylated, with more than 30 reported phosphorylation sites, though the functional significance of most remains unclear.[339] The best characterized phospho-sites in murine TTP are Serine 52 (S52) and Serine 178 (S178), which are phosphorylated by MK2 kinase, downstream of the p38 MAPK pathway.[334-340] Phosphorylation at these residues enhances TTP protein stability[339-341-342] but reduces its RNA-binding activity[343-345]. This has been validated in mouse models harboring alanine substitutions at these positions (S52A/S178A), where TTP displays increased mRNA decay activity despite being highly unstable.[346] Recently, the E3 ubiquitin ligase HUWE1 was identified as a key regulator of TTP degradation. HUWE1 promotes TTP degradation in a phosphorylation-dependent manner, independent of S52/S178, and likely acts through modulation of phosphatase activity.[347] These findings support a model in which, during the early phase of inflammation, MAPK-mediated phosphorylation stabilizes TTP in an inactive form, while later dephosphorylation activates TTP, albeit at the expense of its stability, thus promoting the resolution phase of inflammation.

In summary, TTP is a key regulator of inflammation, tightly controlled at the transcriptional, post-transcriptional, and post-translational level. However, how its RNA-binding activity, phosphorylation state, and subcellular localization are coordinated remains incompletely understood. Further elucidation of these regulatory processes may uncover new strategies to modulate TTP function in inflammatory diseases.

Preamble

The innate immune system relies on precisely regulated transcriptional and post-transcriptional mechanisms to mount rapid, context-specific responses to pathogens and inflammatory stimuli. These regulatory layers shape both the magnitude and timing of immune activation, ensuring that responses are effective yet controlled. A central challenge in immunology is to understand how these processes are dynamically integrated and tailored to specific cellular contexts. This dissertation addresses two key regulatory mechanisms that govern inflammatory gene expression in macrophages: (1) the context-dependent function of the Mediator kinase module during innate immune signaling, and (2) the spatial regulation of mRNA decay by the RBP tristetraprolin (TTP).

Aims

Project 1

Mediator kinase is an essential transcriptional coordinator that positively or negatively modulates stimulus-induced transcription. The effect on the transcriptional output is gene- and pathway-dependent and remains mechanistically poorly understood. The limited knowledge results in part from the lack of studies that systematically investigate Mediator kinase effects in different pathways in one cell system. The project aims to fill this knowledge gap by investigating Mediator kinase function in major pathways that activate the anti-viral and anti-bacterial responses of macrophages. Macrophages are key sentinel cells that convert inflammatory cues, including bacterial products and danger signals, into rapid gene expression changes driving various effector functions. How Mediator kinase regulates macrophage responses to the diverse signals has so far not been addressed.

Aims of Project 1:

1. Define the transcriptional impact of Mediator kinase in macrophage responses to JAK-STAT-triggering cytokines and TLR ligands.
2. Systematically analyze the pathway- and gene-specific effects of Mediator kinase and identify the regulatory logic.
3. Determine Mediator kinase function in macrophage antimicrobial activity.

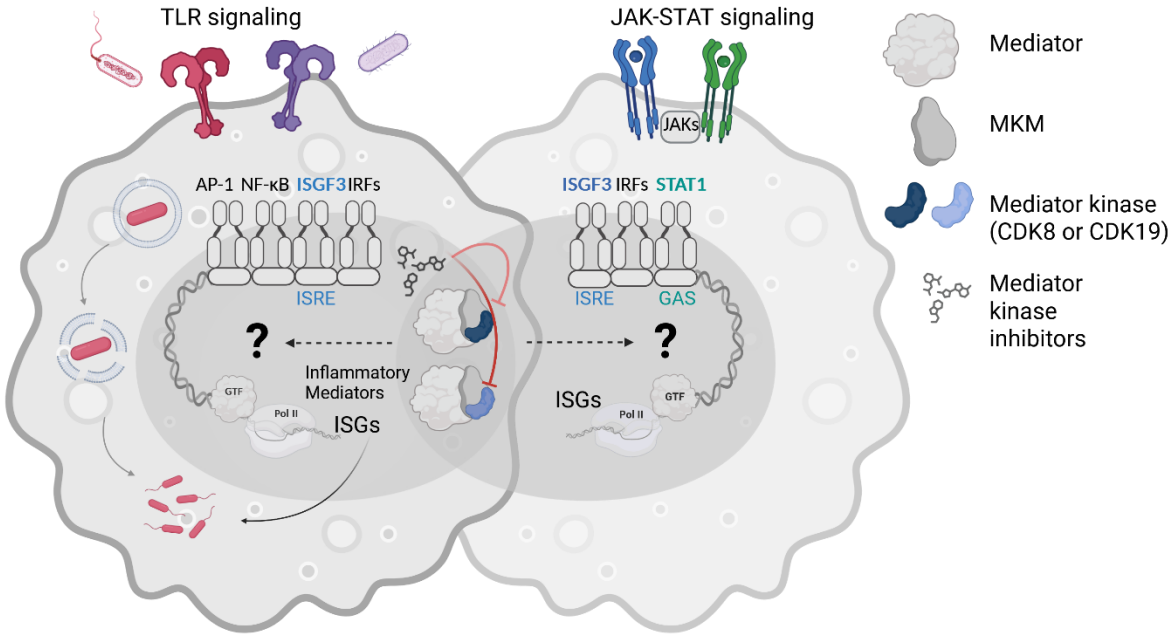

Figure 7. Model of pathway- and gene-specific regulation of macrophage transcription by Mediator kinase.
Macrophages detect microbial ligands (e.g., bacterial products via TLRs) and cytokines (e.g., IFN-β, IFN-γ via JAK-STAT receptors), triggering distinct transcriptional programs. Left: TLR activation induces inflammatory mediator and ISG transcription via AP-1, NF-κB, IRFs, and ISGF3 complexes binding to ISRE-containing promoters. Right: Cytokine stimulation activates STAT1 and ISGF3 via JAKs, leading to ISG transcription through ISRE and GAS promoter elements. Mediator kinase (CDK8/19, blue subunits of the Mediator complex) acts as a key transcriptional regulator at target promoters in both contexts. The regulatory mechanisms and gene-specific effects remain incompletely understood. Red arrows indicate experimental inhibition of Mediator kinase, which modulates transcriptional outcomes in both pathways. This model illustrates the working hypothesis of this thesis: that Mediator kinase exerts stimulus- and gene-specific transcriptional control in macrophage antibacterial and antiviral responses. Created with Biorender.

Project 2

Post-transcriptional regulation of gene expression allows cells to rapidly and precisely adjust protein output in response to environmental cues. In the context of inflammation, where transcriptional changes alone are insufficient for a prompt control, RBPs serve as critical regulators of mRNA stability and translation. Among these, TTP, encoded by *Zfp36*, is a well-established mediator of mRNA decay, particularly of mRNAs encoding inflammatory mediators. TTP promotes degradation by binding AREs in the 3′UTRs of target mRNAs and recruiting deadenylation and decapping complexes. Despite this well-characterized role, emerging evidence suggests that TTP function is not exclusively cytoplasmic and that its RNA-binding activity and subcellular localization are tightly regulated. However, the precise spatiotemporal determinants that govern TTP-mediated mRNA decay remain incompletely understood.

Aims of project 2:

1. Determine the spatial and temporal hierarchy of TTP-driven mRNA destabilization.
2. Define the role of the TTP-driven mRNA decay hierarchy in the control of the cellular immune response.

Results

TLR signaling switches Mediator kinase from activator to repressor of interferon-stimulated genes to dampen macrophage activation

Maurizio Forte, Nora Bischoff, Ronit Chakraborty, Jeanne Fesselet, Thomas Decker, and Pavel Kovarik

Submitted to *Science Immunology* as of December 4, 2025
(Receipt of submission: aee4775)

In this study, we explored the context-dependent role of Mediator kinase activity in regulating macrophage responses to innate immune stimuli. Using systematic RNA-seq and a bacterial infection model, we revealed that Mediator kinase acts as a molecular switch coordinating opposing transcriptional programs during macrophage activation. Specifically, inhibition of Mediator kinase enhances ISG expression and bactericidal functions downstream of TLR signaling, while repressing ISG induction mediated by IFNs and IL-10 via JAK-STAT pathways. These findings reveal an underappreciated role for Mediator kinase in shaping macrophage antimicrobial responses and provide mechanistic insight into its dual regulatory function in innate immunity.

Contribution:
In this study, I conceptualized the project together with Pavel Kovarik (PK) and co-designed all the experiments. I carried out nearly all the experimental work except for sample preparation of RAW 264.7 for Quantseq (Nora Bischoff) and isolation of peritoneal macrophages (Jeanne Fesselet). Ronit Chakraborty took care of the analysis of RNA-seq data. I was also actively involved in writing of the manuscript and was responsible for figure preparation and data visualization.

Successful Submission of a Manuscript to Science Immunology (aee4775)

From sciimmunoleditors@aaas.org on 04.12.2025 10:17
Manuscript Title: TLR signaling switches Mediator kinase from activator to repressor of interferon-stimulated genes to dampen macrophage activation
Author: Forte
Manuscript Number: aee4775

Dear Dr. Forte
You are listed as a coauthor on the above manuscript, which has recently been submitted to Science Immunology. According to Science Immunology policy, all authors must have seen and approved the submission of their manuscript. Please click on the following link to register your account and confirm your authorship on this manuscript (note: your username is the email at which you received this correspondence). The link also allows you to complete your demographic information, and to update your subject-area expertise and institutions. If you have never logged into our portal before or have forgotten your password, you may (re)set it here: https://cts.sciencemag.org/scc/#/forgot-password. You must login before you can verify authorship.
https://cts.sciencemag.org/scc/#/action/account/c7b27d79-d0ef-11f0-bab3-0ad102f82f1d/reset-password?token=1513afd5-d0f2-11f0-bab3-0ad102f82f1d&autoLogin=true&redirect=https://cts.sciencemag.org/scc/#/action/article/e6942c0b-a8cd-4939-942c-0ba8cd593958/author/5675676/verifyAuthorship?email=maurizio.forte@univie.ac.at&token=15105474-d0f2-11f0-bab3-0ad102f82f1d
If you have not read this paper or do not approve its submission to Science Immunology, please let us know as soon as possible. Please refer to the manuscript number listed above in any correspondence (you can just reply to this message).
Once you register your account using the link above, you can see the status of your manuscript at any time by logging into your account at the Science Journals Content Tracking System at https://cts.sciencemag.org.
We also encourage you to link your account to your ORCID ID, an identifier that facilitates the correct attribution of your publications to you. To learn more about ORCID or to obtain an ORCID ID, visit their site at: http://orcid.org.
Your manuscript is now undergoing an initial screening to determine whether it will be sent for in-depth review.
Sincerely,
The Editors
Science Immunology

TLR signaling switches Mediator kinase from activator to repressor of interferon-stimulated genes to dampen macrophage activation

Maurizio Forte[1,2,3], Nora Bischoff[1,2], Ronit Chakraborty[1,2,3], Jeanne Fesselet [1,2,3], Thomas Decker[1,2], Pavel Kovarik[1,2*]

[1] Max Perutz Labs, Vienna Biocenter Campus (VBC), Dr.-Bohr-Gasse 9, 1030 Vienna, Austria.
[2] University of Vienna, Max Perutz Labs, Department of Microbiology, Immunobiology and Genetics, Dr.-Bohr-Gasse 9, 1030 Vienna, Austria.
[3] Vienna Biocenter PhD Program, a Doctoral School of the University of Vienna and Medical University of Vienna, 1030 Vienna, Austria.
* correspondence pavel.kovarik@univie.ac.at

ABSTRACT

Mediator kinase is an essential transcriptional coordinator that can either enhance or repress stimulus-induced gene expression, with its effects varying unpredictably depending on a poorly characterized context. Here, we employed a multilayered, systematic approach—combining transcriptomics, transcription factor binding inference, cellular defense to viral and bacterial infections, and pharmacological inhibition—to elucidate how Mediator kinase regulates pathways driving antimicrobial macrophage activation.

We used primary mouse macrophages, which displayed an unprecedentedly strong requirement for Mediator kinase activity in contrast to cell lines including immortalized macrophages. Mediator kinase activated responses to JAK-STAT pathway agonists, including interferons, with the predominant regulatory motif being the interferon-stimulated response element (ISRE). Remarkably, the activating role of Mediator kinase was reversed into a repressive one upon TLR ligation. Consistently, Mediator kinase inhibition abrogated the ISRE repression, enhanced TLR responses, and boosted cell-autonomous immunity to *Listeria monocytogenes*.

This study identifies the contextual determinants that govern the positive versus negative regulation of JAK–STAT pathways by Mediator kinase in macrophages and suggests that acute Mediator kinase inhibition might be beneficial in the management of bacterial infections.

INTRODUCTION

Successful defense against infections requires precisely balanced immune responses at cellular and organismal levels. Failures in mechanisms that activate or dampen immune responses increase the risk of infectious disease or severe tissue damage, respectively. The fundamental importance of faithful orchestration of immune reactions is underlined by the multitude of transcriptional, post-transcriptional and post-translational mechanisms that act in concert to safeguard the fidelity of the defense pathways (*1-6*). A critical process in these control mechanisms is negative feedback, at various levels, which prevents overshooting inflammation.

Host defense is in general initiated by pathways triggered by pathogen-sensing receptors among which the toll-like receptors (TLRs) cover the broadest spectrum of microbes (*7*). TLRs elicit signaling pathways that culminate in the activation of the transcription factors (TF) NF-κB and AP-1. Several TLRs additionally stimulate the TRIF- and TBK-dependent pathway that causes activation of the TF IRF3. The protein products of genes induced by these TFs participate directly or indirectly in defense (*8*). Exaggerated activation of defense products following TLR stimulation is efficiently prevented by negative feedback mechanisms such as induction of the NF-κB inhibitor IκB or the RNA-binding proteins Zfp36 and Regnase which promote the degradation of cytokine mRNAs (*8-11*).

Cytokines induced upon TLR ligation such as IL-1α/IL-1β and TNF trigger TLR-like signaling thereby causing NF-κB and AP-1 activation. This feed-forward loop amplifies the response and extends it to cells beyond the typical sentinels like macrophages. In addition, a subset of TLRs induce IFNβ, a cytokine from the type I interferon (IFN-I) family, which triggers the JAK-STAT pathway (*8*). The pathway is in general induced upon binding of cytokines such as IFN-I, IFN-II (i.e. IFNγ), IL-10, or IL-12 to their cognate receptors and subsequent activation of the STAT family of TFs by JAK tyrosine kinases (*12*). Depending on the cytokine, different STATs and combinations of them are activated, e.g. immediate IFN-I signaling generates predominantly the ISGF3, composed of STAT1, STAT2 and IRF9, while IFNγ activates predominantly STAT1 homodimers (*12*). Similar to the TLR pathways, uncontrolled JAK-STAT-induced gene expression can be detrimental to the host. A powerful negative feedback mechanism controlling JAK-STAT pathways is the induction of the SOCS proteins which inhibit JAK kinases thereby abolishing STAT activation (*13*). Another negative feedback mechanism ensures that the promoter occupancy of STAT1, STAT2 and STAT3 decreases once processive transcription has commenced (*14*).

Transcription induced by TLR or JAK-STAT pathways is subject to general transcription regulation which includes TF-driven assembly of the pre-initiation complex, RNA polymerase

II (RNA Pol II) recruitment and/or pause release, and chromatin remodelling (*2, 15, 16*). Mediator kinase, a reversibly associated module of the Mediator complex, is an important component of these regulatory steps (*17*). The enzymatic activity of Mediator kinase is brought about by either CDK8 or its paralog CDK19 which bind to Mediator kinase in mutually exclusive ways. Other components are MED12 and MED13, or the paralogs MED12L and MED13L, and the cyclin subunit CCNC (*17*). Most of the Mediator kinase subunits are essential for mammalian development (*18-20*). Mediator kinase has remarkably versatile functions in transcription regulation. Upon association with the Mediator complex, it prevents the recruitment of TFIIH thereby disabling transcription initiation (*21-23*). Inhibitory function has also been reported for genes associated with super-enhancers in acute myeloid leukaemia (AML) cells (*24*). On the other hand, Mediator kinase can regulate transcription positively by promoting RNA Pol II pause release, as demonstrated for IFNγ-stimulated transcription (*25*). The complexity is further increased by Mediator kinase phosphorylation of diverse domains of TFs, including the activation domains of STAT1 and STAT3, and the ubiquitin ligase recognition domains of SMAD1 and SMAD3 (*26, 27*). Despite this broad knowledge, it has been difficult to reconcile the transcriptional impact of Mediator kinase with its biological effects observed upon the use of selective Mediator kinase inhibitors: While Mediator kinase inhibition promoted specifically regulatory T cell (T_{reg}) differentiation independent of TGFβ (*28*), it also enhanced Th-17 differentiation under Th-17 polarizing conditions (*29*) and induced anti-leukemic differentiation of AML cells (*24*). On the other hand, it enabled sustainable expansion of primary T cells, including CAR T cells in vitro (*30*), and maintained naïve pluripotency of embryonic stem cells (*31*). These findings indicate that Mediator kinase can drive diverse - and even opposing - cellular programs such as promotion or suppression of cell differentiation. The mechanisms underlying the Mediator kinase versatility remain to be elucidated.

To disentangle the functional diversity of Mediator kinase, we systematically investigated how it regulates transcriptional responses in pathways triggered during anti-microbial activation of macrophages. Comparative benchmarking of transcriptional responses upon pharmacological Mediator kinase inhibition revealed that primary mouse macrophages, but not immortalized macrophage cell lines, represent a superior model for studying Mediator kinase function: Both bone marrow-derived macrophages and tissue-resident peritoneal macrophages showed a robust regulation by Mediator kinase, while an immortalized macrophage cell line was modestly dependent on Mediator kinase and resembled other immortalized cell lines. This notable finding was critical for subsequent transcriptome-wide analyses which established that Mediator kinase largely negatively regulates TLR responses but enhances JAK-STAT-dependent responses in macrophages. Unexpectedly, the activating

effect of Mediator kinase on JAK-STAT-dependent responses was converted into a repressive one by TLR signalling and converged on ISREs in interferon-stimulated genes. Mediator kinase inhibition released the ISRE repression and boosted clearance of *Listeria monocytogenes* that depends on both TLR and IFN signaling. The study exemplifies how the cell signaling context can switch Mediator kinase from transcriptional activator to a repressor and suggests ways for therapeutic exploitation of Mediator kinase inhibition in bacterial infections.

RESULTS

Mediator kinase robustly regulates gene expression in primary macrophages but not in immortalized cells

To systematically investigate pathway- and stimulus-specific functions of Mediator kinase, we selected macrophages – a sentinel cell type known for its dynamic responses to a variety of cues including cytokines, bacterial products, and live pathogens (*32*). We initially benchmarked three different macrophage types according to their requirement for Mediator kinase in responses to IFNγ, a cytokine previously used for Mediator kinase studies in other cells (*25, 26, 33*): Mouse peritoneal macrophages (PMs) and bone marrow-derived macrophages (BMDMs) representing tissue-resident and in vitro-differentiated primary macrophages, respectively, and the mouse leukemic macrophage cell line RAW 264.7 as an example of immortalized cells (*34*). The ground state gene expression profiles were similar in these three macrophage types, with the Pearson coefficient ranging between 0.91 and 0.93 (**Figure 1A**). For comparison, gene expression profiles of macrophages and mouse alveolar epithelial cells were less similar (Pearson coefficient between 0.78 and 0.81) (**Figure S1A**).

All three macrophage types were treated with the Mediator kinase inhibitor Senexin B (SnxB) (*33*) for 30 min followed by stimulation with IFNγ for 4 h. Subsequent RNA-seq and differential expression analyses revealed that primary macrophages, both PMs and BMDMs, were robustly regulated by Mediator kinase whereas the immortalized macrophage cell line RAW 246.7 displayed only modest regulation: 3,285 and 1,563 differentially expressed genes (DEGs) were found in PMs and BMDMs, respectively, but only 203 in RAW 264.7 cells (**Figure 1B, Data file S1**). The activation of STAT1, assessed by tyrosine 701 phosphorylation, was comparable in all three macrophage types (**Figure S1B**). As expected, this JAK1- and JAK2-mediated phosphorylation was not affected by SnxB (**Figure S1B**). The minor Mediator kinase effects on gene expression in the RAW 264.7 cell line as compared to primary macrophages

(PMs and BMDMs) prompted us to revisit the Mediator kinase impact in other IFNγ-treated immortal cell lines studied earlier. Strikingly, the DEG counts were low in these cell lines: 45 DEGs in mouse embryo fibroblasts (MEFs) (*25*) and 7 DEGs in the human HEK293 cells (*33*) (**Figure 1C**).

Collectively, primary macrophages exhibited unprecedently robust dependence on Mediator kinase during IFNγ responses. In contrast, immortalized cells of various types and origin, including a macrophage cell line, showed a minor requirement for Mediator kinase. Consequently, we selected primary macrophages for detailed Mediator kinase studies.

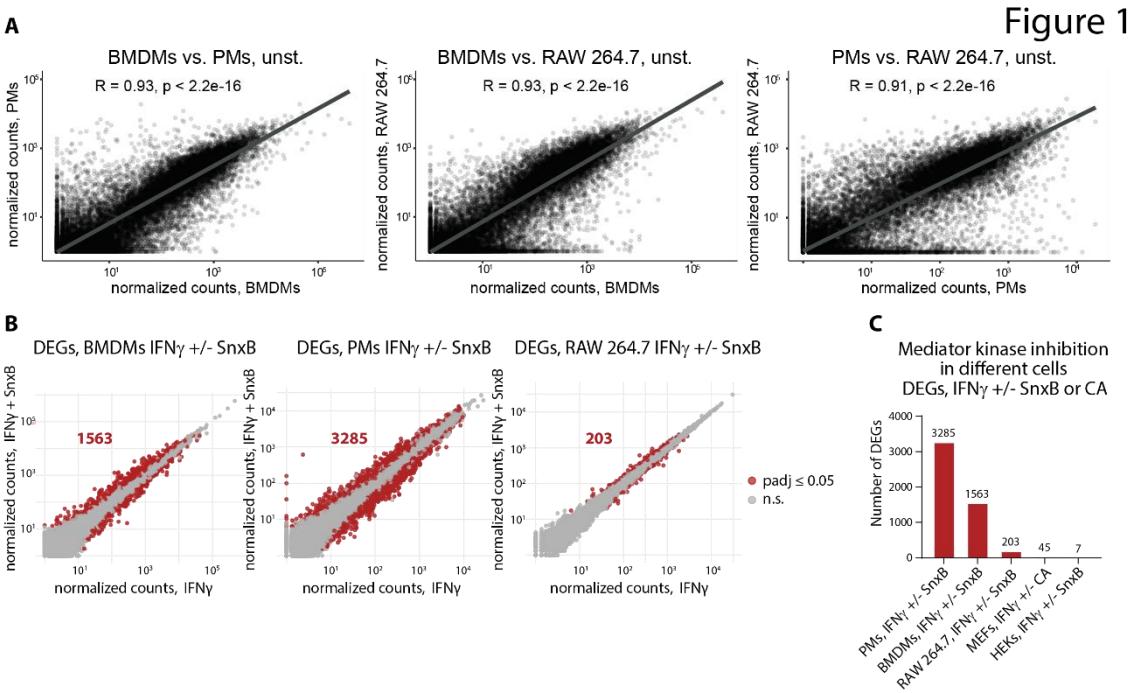

Figure 1. Primary macrophages but not immortalized cells exhibit strong regulation by Mediator kinase

(A) Correlation analysis of gene expression data from unstimulated BMDMs, PMs and the RAW 264.7 macrophage cell line. Mean DESeq2-normalized RNA-seq counts of BMDMs and PMs from littermate mice (n=3 each) and RAW 264.7 cells (n=3) were plotted against each other in all combinations and Pearson correlation coefficients (R) with *p*-values were calculated.

(**B**) Effects of Mediator kinase inhibition on gene expression in IFNγ-stimulated BMDMs, PMs and RAW 264.7 cells. Cells were pretreated with SnxB (2.5 μM) for 30 min and IFNγ (10 ng/mL) was subsequently added for 4 h. Mean DESeq2-normalized RNA-seq counts of SnxB-treated samples (n=3) were plotted against controls. Differentially expressed genes (DEGs; padj ≤ 0.05) are highlighted in red; n.s. (non-significant) in grey. Total numbers of DEGs are indicated.

(**C**) Comparison of Mediator kinase inhibition effects in different cells stimulated with IFNγ. DEGs (padj ≤ 0.05) are indicated. Data for PMs, BMDMs and RAW 264.7 cells are from (B). Data for MEFs (1 h pretreatment with 0.1 μM CA followed by 6 h IFNγ) are from (*25*) and for HEK293 cells (1 h pretreatment with 1 μM SnxB followed by 4 h IFNγ) are from (*33*).

Macrophage Mediator kinase promotes the establishment of tonic IFN signaling signature and unprimed antiviral defense

To address the transcriptional activator versus repressor functions of Mediator kinase in macrophages we determined genes that were up- or down-regulated upon SnxB treatment in unstimulated and IFNγ-stimulated BMDMs and PMs. Unstimulated cells were treated with SnxB for the same time as stimulated cells, i.e. 4 h 30 min. Mediator kinase inhibition caused up- or down-regulation of many genes in both BMDMs and PMs (**Figures 2A and S2A**, **Data file S1**). We mostly used BMDMs in subsequent experiments. Gene set enrichment analysis (GSEA) revealed that SnxB treatment caused significant down-regulation of the IFN pathway signature in unstimulated and IFNγ-stimulated BMDMs (**Figure 2B, Data file S2**).

The finding that SnxB down-regulated IFN pathways also in unstimulated macrophages suggested a critical role of Mediator kinase in the ability of cells to launch efficient antiviral defense which is dependent on tonic IFN signaling (*35*). To test this, we infected BMDMs with vesicular stomatitis virus (VSV) without priming the antiviral programs by IFN-I pretreatment. The viral loads and the infection rate were significantly higher in BMDMs treated with SnxB as compared to controls, indicating inefficient antiviral defense upon Mediator kinase inhibition (**Figures 2C and S2C**). The cell death rate in infected BMDMs was not changed upon SnxB treatment (**Figure S2C and S2D**). The poor protection of SnxB-treated BMDMs against VSV was accompanied by low expression of the antiviral ISGs *Mx2* and *Ifit2* (**Figure 2D**), both of which were affected by SnxB also in uninfected cells (**Figure S2E**).

Taken together, Mediator kinase inhibition causes broad gene expression changes in unstimulated as well as in IFNγ-stimulated primary macrophages. Mediator kinase inhibition reduces the IFN signaling signature in IFNγ-stimulated macrophages, consistent with previous studies using other cells (*25, 26, 36*), but also in unstimulated BMDMs revealing a key role of Mediator kinase in tonic IFN signaling, as supported by defense assays against VSV infection.

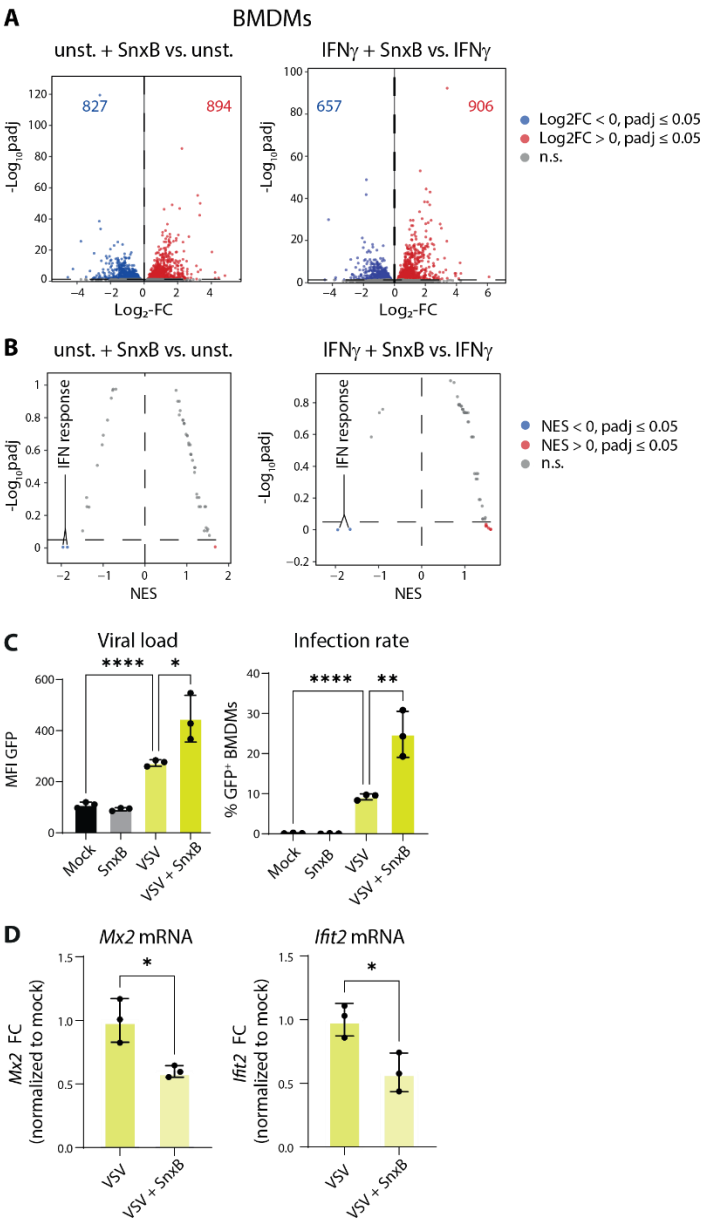

Figure 2. Mediator kinase promotes tonic IFN signaling signature and unprimed antiviral defense in BMDMs

(**A**) Mediator kinase inhibition causes up- or down-regulation of gene expression in unstimulated and IFNγ-stimulated BMDMs. Unstimulated cells were pretreated with SnxB (2.5 µM) or vehicle for 4 h 30 min. IFNγ-stimulated samples are described in Figure 1B. Down-regulated genes (Log2-FC < 0; padj ≤ 0.05) shown in blue, up-regulated genes (Log2-FC > 0; padj ≤ 0.05) shown in red and non-significant genes (n.s.) in grey.

(**B**) Hallmark gene set enrichment analysis (GSEA) of SnxB-treated BMDMs under unstimulated or IFNγ-stimulated conditions. Down-regulated (normalized enrichment score, NES < 0; padj ≤ 0.05) and up-regulated (NES > 0; padj ≤ 0.05) Hallmark gene sets are shown in blue and red, respectively; n.s., not significant. IFN response gene sets are depicted.

(**C**) Impairment of defense against VSV infection upon Mediator kinase inhibition. BMDMs pretreated with SnxB (2.5 µM, 30 min) or vehicle and subsequently infected with GFP-

expressing VSV (MOI = 5, 24 h). Mean fluorescence intensity (MFI, left) and percentage of GFP-positive BMDMs (right) are shown. Mean of biological replicates ± SD; n = 3; unpaired Student´s t-test, *p < 0.05, **p < 0.01, ****p < 0.0001.
(**D**) *Mx2* and *Ifit2* expression in VSV-infected BMDMs. BMDMs were pretreated with SnxB (2.5 µM, 30 min) or vehicle and subsequently infected with VSV (MOI = 5, 4 h). *Mx2* and *Ifit2* expression was quantitated by RT-qPCR. Relative values to *Hprt* expression are shown. Fold changes (FC) between SnxB versus vehicle treated samples are shown. Mean of biological replicates ± SD; n = 3; unpaired Student´s t-test, *p < 0.05.

Transcription induced by JAK-STAT pathway ligands is positively regulated by Mediator kinase

Cells maintain the expression of IFN signaling components, including STATs, at operational levels through basal IFN signaling that is driven by low-level production of IFN-Is at steady state (*37*). Down-regulation of the baseline IFN response, i.e. without IFNγ stimulation, in SnxB-treated BMDMs (**Figure 2B**) therefore implied that Mediator kinase is required for IFN-I response, in addition to the previously reported requirement in the IFNγ response (*25*). Furthermore, since IFN-I and IFNγ responses employ distinct JAK-STAT pathways, the data suggested that Mediator kinase positively regulates responses involving JAK-STAT signaling more broadly. To test this, we compared the effect of Mediator kinase inhibition on responses of BMDMs to IFNγ, IFNβ, and IL-10 which are predominantly driven by STAT1 homodimers, ISGF3 (STAT1-STAT2-IRF9 complex), and STAT3 homodimers, respectively (*38*). We found 288 IFNγ-induced genes which were Mediator kinase-dependent (i.e. SnxB-sensitive); the majority (165 genes) of them were less induced upon SnxB treatment (**Figure 3A**, **Data file S3**). The SnxB effects were caused by changes in transcription, as confirmed by pre-mRNA analysis for *Gbp4* and *Cxcl9* (**Figure 3B**). The responses to IFNβ were regulated by Mediator kinase in similar ways: Out of 271 IFNβ-stimulated and Mediator kinase-dependent genes, 192 genes were less induced upon SnxB treatment (**Figures 3C and S3A**, **Data file S3**). Similar to IFNγ, *Gbp4* and *Cxcl9* pre-mRNA analysis verified that the SnxB-dependent gene expression changes resulted from transcriptional effects (**Figure 3D**). As expected, SnxB treatment inhibited S727 but not Y701 phosphorylation of STAT1 (**Figure S3B**). The response to IL-10 was also in general repressed by SnxB (**Figures 3E, 3F and S3C**). IL-10-induced phosphorylation of STAT3 at S727 was inhibited by SnxB treatment whereas Y705 phosphorylation remained unaffected (**Figure S3D**), consistent with previous studies (*26*). In summary, these results indicate that Mediator kinase enhances responses to cytokines that trigger JAK-STAT pathways.

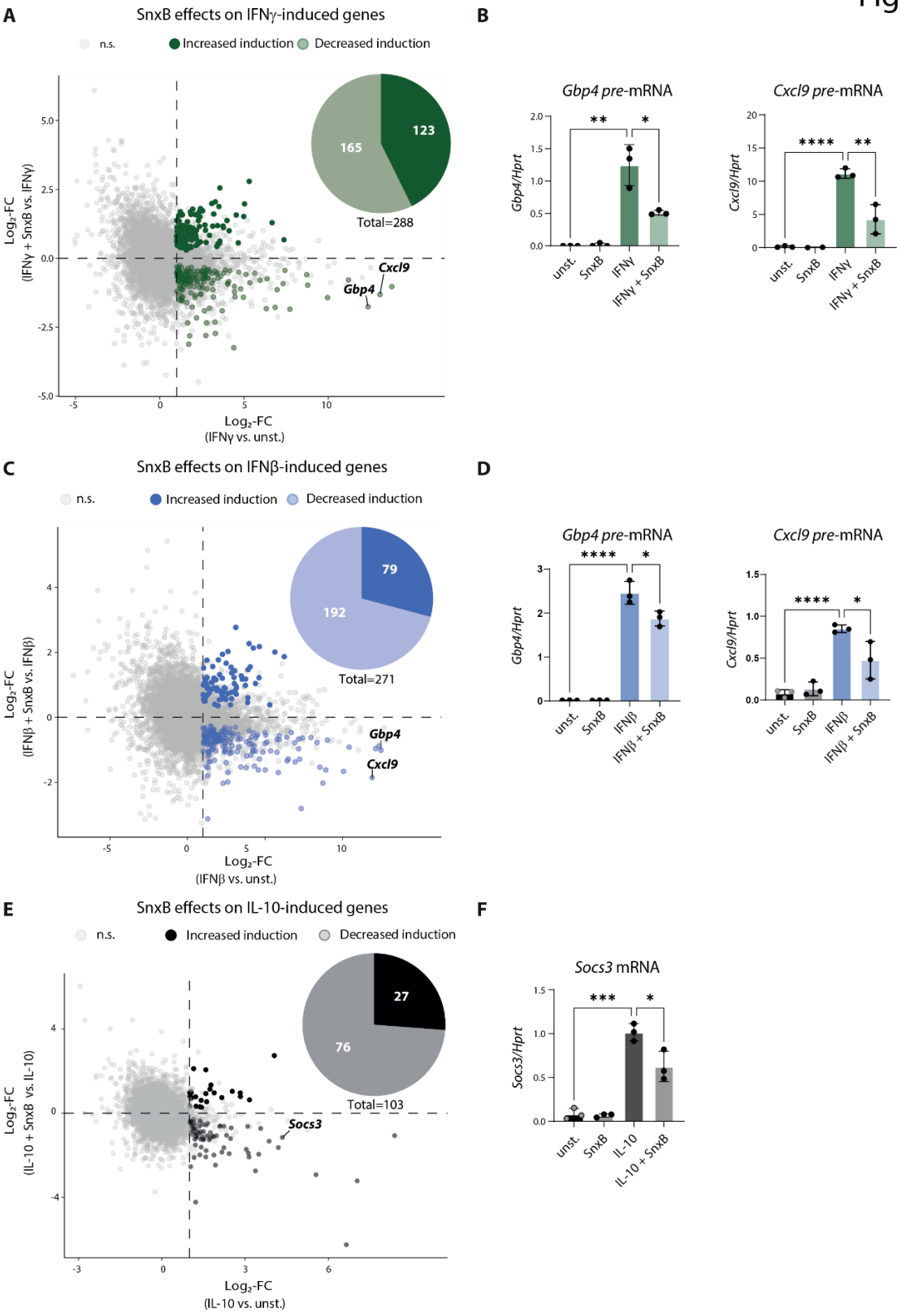

Figure 3. Mediator kinase regulates JAK-STAT responses positively

(**A**) Effects of Mediator kinase inhibition on IFNγ-induced genes in BMDM samples described in Figures 1B and 2A. Genes induced more than 2-fold by IFNγ (Log2-FC > 1, padj ≤ 0.05)

showing higher induction upon SnxB treatment (Log2-FC > 0, padj ≤ 0.05) are in dark green; genes showing decreased induction (Log2-FC < 0, padj ≤ 0.05) are in light green. Grey, not significant. Pie chart summarizes the scatterplot results.
(**B**) *Gbp4* and *Cxcl9* pre-mRNA expression in BMDMs treated as in (A). pre-mRNA expression was quantitated using RT-qPCR. Relative values to *Hprt* expression are shown. Mean of biological replicates ± SD; n= 3; unpaired Student´s t-test, **p* < 0.05, ***p* < 0.01, ****p < 0.0001.
(**C**) Effects of Mediator kinase inhibition on IFNβ-induced genes. BMDMs were pretreated with SnxB (2.5 μM, 30 min) or vehicle, stimulated with IFNβ (250 IU/mL, 4 h) and analyzed by RNA-seq. Genes induced more than 2-fold by IFNβ (Log2-FC > 1, padj ≤ 0.05) showing higher induction upon SnxB treatment (Log2-FC > 0, padj ≤ 0.05) are in dark blue; genes showing decreased induction (Log2-FC < 0, padj ≤ 0.05) are in light blue. Grey, not significant. Pie chart summarizes the scatterplot results.
(**D**) *Gbp4* and *Cxcl9* pre-mRNA expression in BMDMs stimulated as described in (C) and quantitated as described in (B). Mean of biological replicates ± SD; n= 3; unpaired Student´s t-test, *p < 0.05, ****p < 0.0001.
(**E**) Effects of Mediator kinase inhibition on IL-10-induced genes. BMDMs were pretreated with SnxB (2.5 μM, 30 min) or vehicle, stimulated with IL-10 (10 ng/mL, 4h) and analyzed by RNA-seq. Genes induced more than 2-fold by IL-10 (Log2-FC > 1, padj ≤ 0.05) showing higher induction upon SnxB treatment (Log2-FC > 0, padj ≤ 0.05) are in black; genes showing decreased induction (Log2-FC < 0, padj ≤ 0.05) are dark grey. Grey, not significant. Pie chart summarizes the scatterplot results.
(**F**) *Socs3* mRNA expression in BMDMs treated as in (E) and quantitated as in (B). Mean of biological replicates ± SD; n= 3; unpaired Student´s t-test, *p < 0.05, ***p < 0.001.

Transcriptional responses to TLR ligands are largely repressed by Mediator kinase

To complete the comparative analysis of Mediator kinase functions in stimulus-induced transcription, we included the TLR4 response as another key antimicrobial pathway in macrophages, next to JAK-STAT signaling. BMDMs and PMs were stimulated with the TLR4 ligand lipopolysaccharide (LPS) for 4 h after a 30-min pretreatment with SnxB or a vehicle control followed by RNA-seq. In addition, we used cortistatin A (CA) as a Mediator kinase inhibitor unrelated to SnxB (*24*) in BMDMs. The sample replicate clustering indicated that LPS induced a major re-programming of the transcriptome both in BMDMs and PMs and that SnxB and CA caused similar effects (**Figure S4A**). Comparison of unstimulated versus stimulated BMDMs revealed that Mediator kinase inhibition promoted the TLR4 response: Out of 523 LPS-stimulated and SnxB-sensitive genes the majority (373 genes) were more highly induced in SnxB-treated BMDMs (**Figure 4A**, **Data file S3**). The results were verified for *Il10*, *Ccl7*, *Ccl2* and *Il1a* mRNAs using RT-qPCR (**Figure S4B**). Mediator kinase inhibition enhanced the TLR4 response also in PMs (**Figures S4C and S4D**). Importantly, the SnxB effects were

caused by changes in transcription, as confirmed by pre-mRNA analysis for *Il10* and *Ccl7* (**Figure 4B**). The changes caused by SnxB at the level of mRNA expression were observed also at the protein level, as confirmed for the cytokines and chemokines IL-10, CCL7, CCL2 and IL-1α (**Figure 4C**), suggesting that they were biologically significant.

To validate that the enhancement of the TLR responses was caused by selective inhibition of Mediator kinase, we profiled the activation of key kinases and TFs in BMDMs stimulated with LPS for up to 45 min in the presence of SnxB or CA. We included also IFNγ-stimulation as a well-studied pathway in context of Mediator kinase (*25, 26*). The activity of the MAP kinases p38, JNK and ERK was not affected upon Mediator kinase inhibition (**Figure 4D**). Moreover, the activating NF-κB phosphorylation at Ser536 and the degradation of IκB in LPS-stimulated cells proceeded normally in SnxB- or CA-treated BMDMs (**Figure 4D**). As expected, SnxB and CA inhibited STAT1 phosphorylation at Ser727 in IFNγ- but not in LPS-stimulated BMDMs (**Figure 4D**), since Mediator kinase phosphorylates this residue in the IFN response whereas the p38 MAP kinase does it in the LPS response (*26, 39*). Although STAT1 Ser727 phosphorylation is marker for Mediator kinase activity in JAK-STAT pathways (*26, 29, 30*), STAT1-driven transcription is regulated by Mediator kinase mostly independently of this modification (*25*). We further validated that the activating phosphorylation of the TFs CREB at Ser 133 and c-Jun at Ser63 as well as the inhibitory phosphorylation of c-Jun at Ser243 (pS243), which is constitutive in resting cells (*40*), remained unchanged upon Mediator kinase inhibition (**Figure S4E**).

Given that TLR4 signaling activates also IFN-I signaling (IFNβ induction) in addition to the canonical TLR/MyD88 pathway, we wondered whether ISGs indirectly induced by LPS were less well induced upon Mediator kinase inhibition, as observed in direct responses to IFNs (**Figure 3**). We thus conducted GSEA for SnxB effects on LPS-induced genes. The analysis revealed that, opposite to direct stimulation with IFN, the IFN pathway terms were up-regulated by SnxB in cells stimulated with LPS (**Figure 4E, Data file S2**).

We then examined BMDMs stimulated with the TLR2 ligand Pam3CSK4 to more broadly define the role of Mediator kinase in TLR signaling pathways. TLR4 and TLR2 pathways differ in the spectrum of activated TFs: NF-κB and AP-1 are activated by both receptors while IRF3 is activated only by TLR4 ligation (*8*). Since IRF3 is driver of *Ifnb1* gene expression, TLR4 but not TLR2 pathway stimulates production of IFNβ. In agreement, LPS, but not Pam3CSK4, caused induction of *Ifnb1* mRNA and induced Y701 phosphorylation of STAT1 in BMDMs (**Figures S5A and S5B**). Stimulation of BMDMs with Pam3CSK4 for 4 h following a 30-min pretreatment with SnxB showed that, analogous to TLR4, Mediator kinase

inhibition transcriptionally enhanced the TLR2 response: 129 genes were more highly induced while 46 genes were less induced upon SnxB treatment (**Figures 5C - 5E**, **Data file S3**).

In summary, the data show that Mediator kinase acts predominantly as repressor of responses involving TLR4 and TLR2 pathways thereby contrasting its function in JAK-STAT pathways. Remarkably, Mediator kinase regulates the IFN signaling signature in opposite ways in TLR4 versus IFN responses.

Figure 4

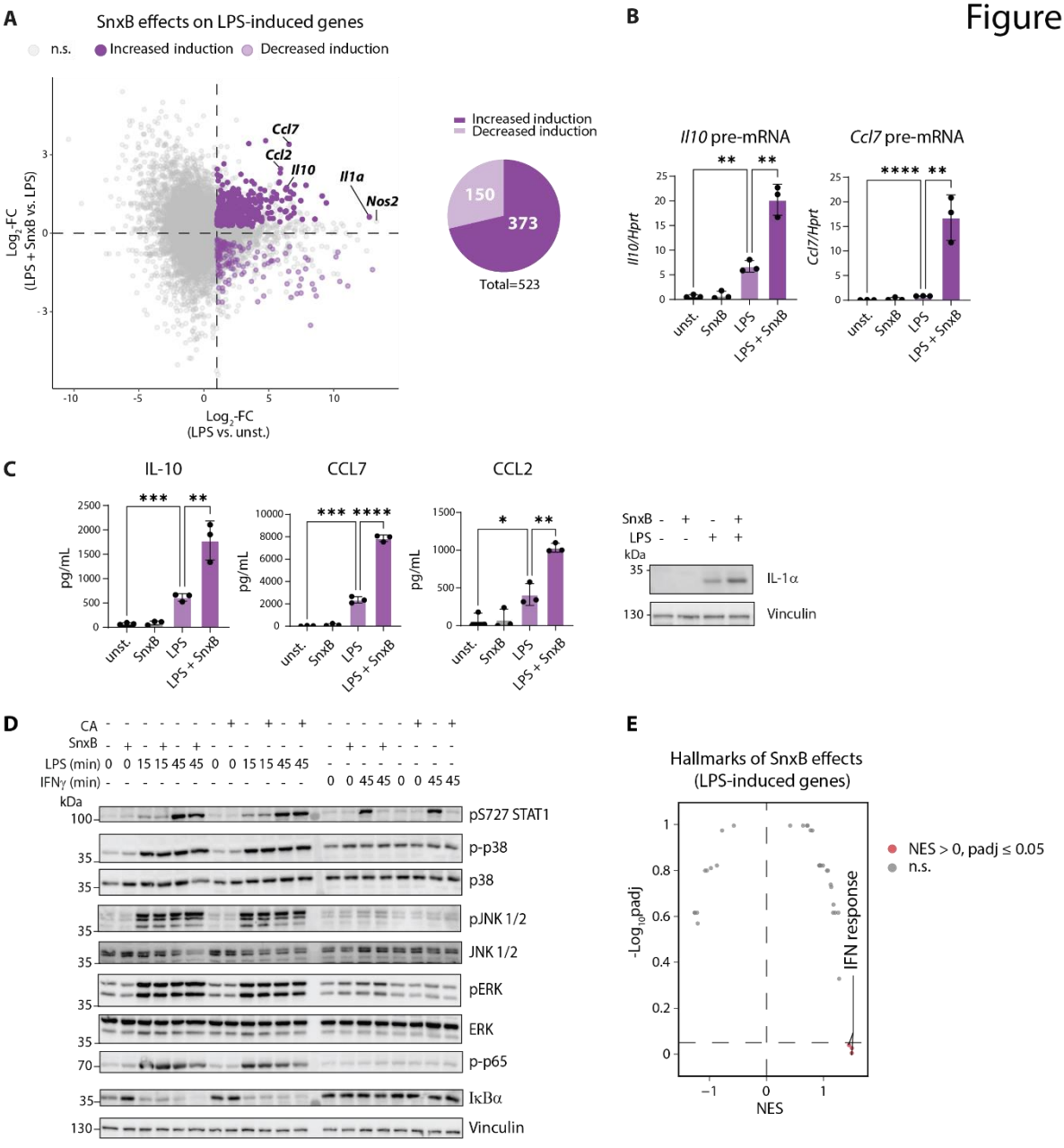

Figure 4. Mediator kinase regulates TLR responses negatively

(**A**) Effects of Mediator kinase inhibition on LPS-induced genes. BMDMs were pretreated with SnxB (2.5 µM, 30 min) or vehicle, stimulated with LPS (10 ng/mL, 4 h) and analyzed by RNA-

seq. Genes induced more than 2-fold by LPS (Log2-FC > 1, padj ≤ 0.05) showing higher induction upon SnxB treatment (Log2-FC > 0, padj ≤ 0.05) are in dark purple; genes showing decreased induction (Log2-FC < 0, padj ≤ 0.05) are in light purple. Grey, not significant. Pie chart summarizes the scatterplot results.
(**B**) *Il10* and *Ccl7* pre-mRNA expression in BMDMs treated as in (A). pre-mRNA expression was quantitated using RT-qPCR. Relative values to *Hprt* expression are shown. Mean of biological replicates ± SD; n= 3; unpaired Student´s t-test, **p < 0.01, ****p < 0.0001.
(**C**) Effects of SnxB on IL-10, CCL7, CCL2 and IL-1α protein amounts in LPS-stimulated BMDMs. Cells were treated as in (A), and IL-10, CCL7 and CCL2 were quantitated in the supernatants using ELISA. IL-1α was quantitated in whole cell extracts using western blotting; loading control Vinculin. Mean of biological replicates ± SD; n= 3; unpaired Student´s t-test, *p < 0.05, **p < 0.001; ***p < 0.001, ****p < 0.0001.
(**D**) Phosphorylation and total protein levels of components of LPS and IFNγ pathways. BMDMs were pretreated with SnxB (2.5 μM, 30 min) or CA (0.1 μM, 30 min) or vehicle and stimulated with LPS (10 ng/mL) or IFNγ (10 ng/mL). Whole cell extracts were analyzed by western blotting using the indicated antibodies; Vinculin, loading control.
(**E**) Hallmark GSEA for SnxB-sensitive LPS-induced genes in RNA-seq samples from (A). Up-regulated (NES > 0; padj ≤ 0.05) Hallmark gene sets are shown in red; no down-regulated gene sets were found; n.s., not significant. IFN response gene sets are depicted.

TLR ligation switches Mediator kinase at ISRE regulatory motifs from activator into repressor

Having shown opposite regulation of JAK-STAT versus TLR responses by Mediator kinase, we asked whether the different Mediator kinase functions are associated with distinct gene regulatory motifs. To this end, we carried out HOMER (Hypergeometric Optimization of Motif EnRichment (*41*)) analysis. In unstimulated BMDMs, the leading regulatory motif associated with genes down-regulated by SnxB is ISRE (**Figure 5A**), which represents the canonical binding sequence for ISGF3 and IRFs (*42*). All top five motifs in the ranked list were ISREs (**Data file S4**). In contrast, motifs enriched in genes up-regulated by SnxB under these conditions were heterogenous and distinct from ISREs (**Figure 5A, Data file S4**). The association of ISRE with genes down-regulated by SnxB in unstimulated BMDMs provided a rationale for the negative enrichment of IFN gene sets in GSEA (**Figure 2B**). Next, we used HOMER for the analysis of SnxB-sensitive genes in BMDMs stimulated with IFNβ, IFNγ or LPS. The analysis was carried out using genes which were both induced by individual stimulations and sensitive to SnxB (**Data file S3**). The leading motif associated with genes showing lower induction upon SnxB treatment was ISRE in both IFNβ- or IFNγ-stimulated

BMDMs (**Figure 5A, Data file S4**), in line with the critical role of several IRFs, particularly IRF1 and ISGF3/IRF9, in IFN responses (*42*). In contrast, the analysis of genes more highly induced upon SnxB treatment was not informative: No enriched motif was identified in IFNβ-stimulated BMDMs, and one motif was found in IFNγ-stimulated cells (**Figure 5A, Data file S4**). Surprisingly, HOMER results for LPS-induced genes showed opposite motif enrichment: No motif was enriched in genes less induced upon SnxB treatment, while all top-ranked motifs in more highly induced genes after SnxB treatment were ISREs (**Figure 5A, Data file S4**). Together, these results indicated that Mediator kinase negatively regulated ISGs if they were induced during the LPS response but positively regulated them during direct stimulation with IFNs or in unstimulated cells. We then asked whether the reversed regulation of ISGs by Mediator kinase during LPS response was still dependent on JAK-STAT signaling. To this end, we added the JAK1 and JAK2 inhibitor ruxolitinib to SnxB-treated BMDMs 3 hours after LPS stimulation and continued the cultivation for 2 more hours. The 2-hour presence of ruxolitinib was sufficient to abrogate the LPS-dependent STAT1 Y701 phosphorylation (**Figure S6A**). Subsequent analysis of *Gbp4* and *Cxcl9* pre-mRNA levels revealed that JAK-STAT inhibition by ruxolitinib abolished both the SnxB-dependent increase in LPS-induced ISG transcription and the induction of these genes by LPS (**Figure 5B**). This experiment corroborated the HOMER analysis showing that the SnxB-imposed increase in induction of ISGs during LPS response was associated with ISREs (**Figure 5A**).

To quantitate the opposite effects of Mediator kinase on ISG expression in IFN- vs. LPS-stimulated BMDMs, we first defined the IFNβ- and IFNγ-stimulated gene sets (padj ≤ 0.05 and Log2-FC > 1) as IFNβ-ISGs and IFNγ-ISGs (**Figures S6B and S6C, Data file S5**). Subsequently, SnxB effects on individual IFNβ-ISGs and IFNγ-ISGs were plotted as fold-changes and the means were calculated for unstimulated, and IFNβ-, IFNγ- and LPS-stimulated conditions (**Figures 5C and 5D, Data file S5**). This analysis showed that SnxB effects on ISG induction were significantly different in each condition: SnxB enhanced ISG induction in LPS-stimulated BMDMs but inhibited it in unstimulated as well as in IFNβ- and IFNγ-stimulated cells. Importantly, non-ISGs were not regulated by SnxB in these ways as demonstrated by comparing SnxB-imposed fold-changes in non-ISGs and ISGs in each condition (**Figures S6D and S6E, Data file S5**). Although SnxB overall increased ISG induction in LPS-stimulated BMDMs it remained unclear how the SnxB effect was distributed across the ISGs, for example whether the ISG expression level mattered. To this end, we plotted normalized counts of IFNβ- or IFNγ-ISGs and non-ISGs in LPS-stimulated samples against those in SnxB-treated LPS-stimulated samples (**Figures 5E and 5F**). The regression curve intercept was significantly higher for ISGs than non-ISGs (0.58 vs. 0.20, respectively)

while the slopes were comparable, indicating that SnxB enhanced ISGs independently of their expression levels.

In contrast to TLR4 stimulation by LPS, TLR2 stimulation by Pam3CSK4 does not cause IFN production and JAK-STAT activation. Nevertheless, BMDMs express ISGs also during the TLR2 response owing to the low-level production IFNβ that drives basal ISG expression in unstimulated cells (*35*). The baseline ISG expression is positively regulated by Mediator kinase, as revealed by SnxB treatment of unstimulated BMDMs (**Figure 2B**). To test whether TLR2 signaling reverts the Mediator kinase function in ISG regulation like TLR4, we analyzed Pam3CSK4 stimulation in the same way as we did for LPS, i.e. by visualizing SnxB effects on fold-changes in induction and on normalized counts (**Figures S6F and S6G, Data file S5**). The analysis revealed that SnxB enhanced ISG induction in Pam3CSK4-stimulated BMDMs but inhibited it in unstimulated and IFNβ-stimulated cells, and that the SnxB effect was independent of the ISG expression levels, thereby yielding qualitatively similar results as in the LPS response.

Collectively, these analyses provide evidence that Mediator kinase acts in general as activator of ISRE-driven ISG expression in unstimulated and IFN-stimulated BMDMs. However, this activating function is reversed into a repressive one in the context of bacterial cell wall-triggered TLR signaling, regardless of whether the bacterial product induces IFNβ. Both activating and repressive functions of Mediator kinase in ISG regulation are associated with the presence of ISREs in the gene promoters and require JAK-STAT signaling.

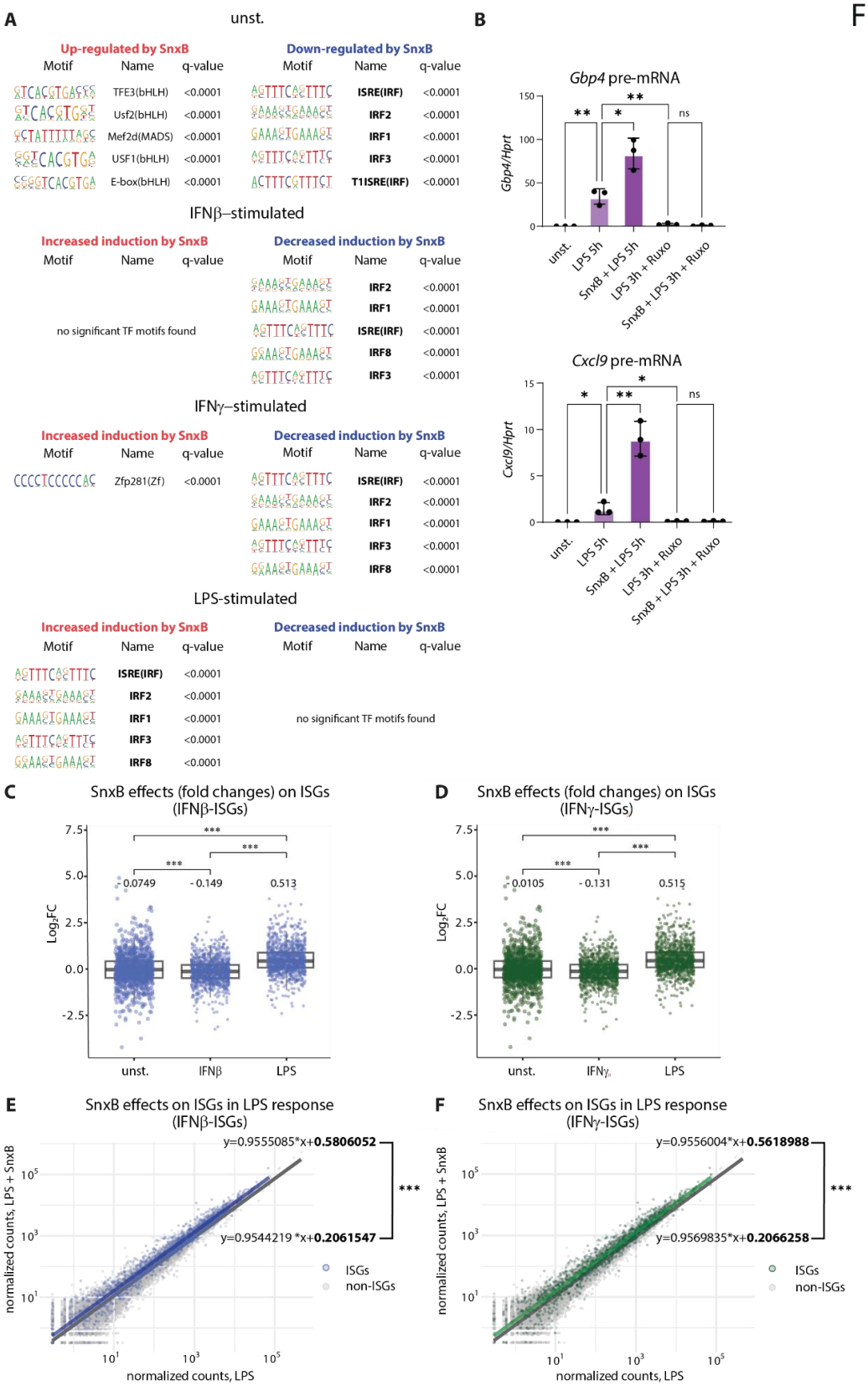

Figure 5. LPS signaling reverts Mediator kinase at ISREs from activator to repressor

(**A**) Enrichment of TF binding motifs in SnxB-sensitive genes revealed using HOMER analysis. Positive and negative effects of SnxB on gene expression was assessed in unstimulated, IFNγ-

, IFNβ- and LPS-stimulated BMDMs. For stimulated samples, SnxB-sensitive genes were pre-filtered for those induced by the stimulus (Log2-FC > 1, padj ≤ 0.05). Promoter regions spanning −1,000 to +500 bp relative to the transcription start site (TSS) were subject to HOMER. Up to five top-ranked motifs are shown for each condition; only significant motifs (*q* ≤ 0.05) are shown.
(**B**) Effects of ruxolitinib on transcription regulation by Mediator kinase. *Gbp4* and *Cxcl9* pre-mRNA expression in BMDMs stimulated with LPS (10 ng/mL, 5 h), BMDMs pretreated with SnxB (2.5 µM, 30 min) followed by LPS stimulation (5 h), BMDMs stimulated with LPS (5 h) in the presence of ruxolitinib (Ruxo) in the last 2 h, and BMDMs pretreated with SnxB (30 min) followed by LPS stimulation (5 h) in presence of Ruxo in the last 2 h. pre-mRNA expression was quantitated using RT-qPCR. Relative values to *Hprt* expression are shown. Mean of biological replicates ± SD; n = 3; unpaired Student´s t-test, *p < 0.05, **p < 0.01. ns, not significant.
(**C, D**) SnxB-dependent effects (Log_2-FC) on IFNβ-ISGs (n = 1679) under unstimulated, IFNβ- or LPS-stimulated conditions (**C**), and on IFNγ-ISGs (n = 1353) under unstimulated, IFNγ - or LPS-stimulated conditions (**D**). RNA-seq data are from Figures 3A and 3C; ISGs are defined in Figures S6B and 6SC. Mean changes across ISGs are shown. The mean changes are negative under unstimulated and IFN-stimulated conditions but positive under LPS-stimulated conditions. RNA-seq data were from Figures 3 and 4. Unpaired Student´s *t*-test, ***p ≤ 0.001.
(**E, F**) Comparison of normalized RNA-seq counts for ISGs and non-ISGs in SnxB-treated and LPS-stimulated BMDMs versus LPS-stimulated BMDMs. Means of normalized counts were plotted, and linear regression slopes and intercepts were calculated for IFNγ-ISGs (Log2-FC > 1, padj ≤ 0.05) (**E),** IFNβ-ISGs (Log2-FC > 1, padj ≤ 0.05,) (**F**) and for non-ISGs (both panels). Non-ISGs are defined in Figures S6B and S6C as genes not fulfilling filter for IFN induction (Log2-FC > 1, padj ≤ 0.05). Significance of regression intercept differences between ISGs and non-ISGs: unpaired Student's *t*-test, ***p ≤ 0.001.

Mediator kinase inhibition boosts antimicrobial self-defense of BMDMs

TLR and IFN signaling pathways act simultaneously to orchestrate the macrophage antimicrobial defense in multiple ways (*43*). We thus asked whether the effects of Mediator kinase on TLR and IFN responses (**Figures 3 - 5**) impact the antimicrobial response of BMDMs against *Listeria monocytogenes* (*Lm*). *Lm* is a gram-positive intracellular pathogen that triggers TLRs, most significantly TLR2, and the cGAS-STING pathway which stimulates IFN-I production leading to JAK-STAT activation and ISG induction (*44*). We infected BMDMs at the multiplicity of infection (MOI) 1 or 10 in the presence or absence of SnxB and assessed clearance of intracellular bacteria up to 24 h post infection (p.i.). SnxB treatment did not affect the viability of BMDMs during this period (**Figures S7A**). SnxB reduced the counts of live intracellular *Lm* 8 h p.i. at both MOIs (**Figure 6A**); the effect was observed also at 12 h p.i and vanished 24 h p.i. when only few live bacteria were detected regardless of SnxB treatment (**Figure S7B**). Since SnxB treatment did not impair phagocytosis in BMDMs and was not toxic

to *Lm* (**Figures 6B and S7C**), we concluded that Mediator kinase inhibition enhanced the bactericidal activity of BMDMs.

Cell-autonomous immunity of macrophages against intracellular bacteria is determined by multiple mechanisms, including processes driven by the Gbp family of ISGs (*45*). Upon Mediator kinase inhibition by SnxB, Gbp genes expressed in BMDMs are more strongly induced by LPS but less induced by IFNβ (**Figures 6C and S7D**), similar to most other ISGs (**Figure 5**). Strikingly, we found that *Gbp10*, a Gbp family member required for macrophage protection against *Lm* infection (*45*), was more strongly induced by *Lm* in SnxB-treated BMDMs as compared to controls (**Figure 6D**). Gbp proteins are ISGs that promote microbial killing in several ways, for example by preventing evasion of degradative organelles by the pathogen or by enhancing the NADPH-dependent production of reactive oxygen species (ROS) (*46*). In agreement, SnxB treatment increased ROS levels in *Lm*-infected BMDMs (**Figure 6E**). Mitochondrial ROS production was not affected by SnxB treatment (**Figure S7E**) suggesting that the SnxB-dependent increase in total ROS levels resulted from the NADPH-mediated process. Reactive species produced by *Lm*-infected macrophages include also nitric oxide – a molecule with ambiguous functions in defense against *Lm* (*47, 48*). Nitric oxide is generated in macrophages largely by the inducible nitric oxide synthase iNos encoded by *Nos2* that is synergistically stimulated by IFN and TLR pathways (*49*). Consistent with *Nos2* being an ISG, we found that its expression was enhanced by SnxB in *Lm*-infected BMDMs (**Figures S7F and S7G**).

Together, Mediator kinase inhibition augments cell-autonomous defense of BMDMs against *Lm* infection demonstrating that the increased responses of BMDMs to TLR2 and TLR4 ligands following SnxB treatment (**Figure 4**) are functionally important. Moreover, the SnxB-mediated up-regulation of the ISG signature in BMDMs stimulated by bacterial products (**Figure 5**) occurs also upon challenge with live bacteria.

Figure 6

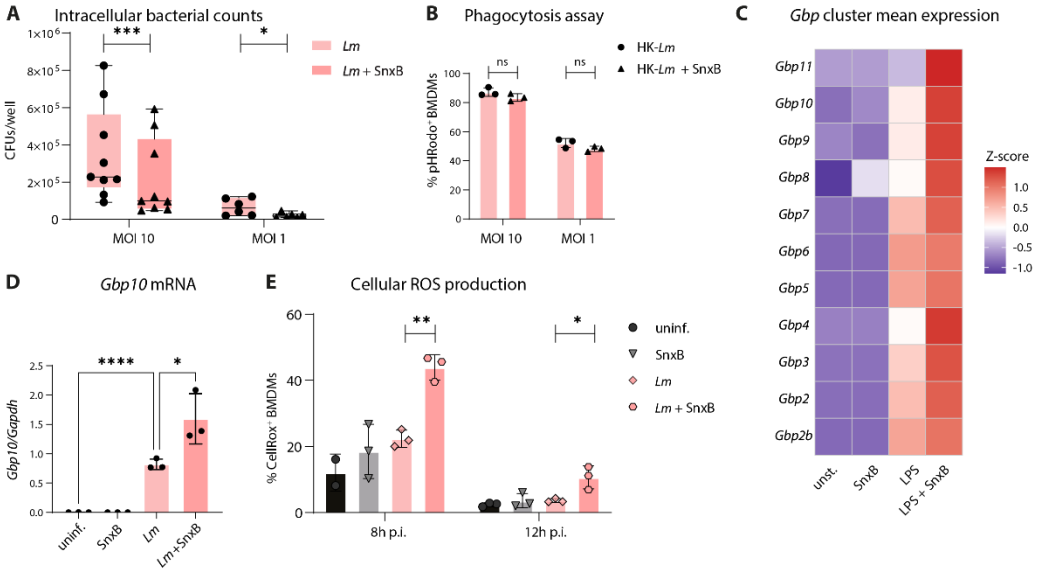

Figure 6. Mediator kinase inhibition boosts cell-autonomous immunity of BMDMs against *Lm*

(**A**) Mediator kinase inhibition effect on intracellular bacterial counts. BMDMs were pretreated with SnxB (2.5 µM, 30 min) or vehicle and infected with *Listeria monocytogenes* (*Lm)* at an MOI of 10 or 1 for 8 h. Bacterial loads are shown as colony-forming units (CFU); Tukey boxplot; n = 9 for MOI 10, n = 6 for MOI 1; means of independent biological replicates ± SD; paired t-test, *p < 0.05, ***p < 0.001.

(**B**) Phagocytosis assessment upon Mediator kinase inhibition. BMDMs were pretreated with SnxB (2.5 µM, 30 min) or vehicle and incubated with pHrodo-labeled heat-killed *Lm* (MOI 10 or 1) for 8 h. Phagocytosis was assessed using flow cytometry. Percentages of pHrodo$^+$ BMDMs are shown. Unpaired Student´s t-test; ns, not significant.

(**C**) Regulation of *Gbp* genes by Mediator kinase in LPS-stimulated BMDMs. Heatmap showing Z-scores of normalized RNA-seq counts for the *Gbp* gene family in LPS-stimulated BMDMs pretreated with SnxB or vehicle. RNA-seq data are from Figure 4A.

(**D**) *Gbp10* mRNA expression in BMDMs infected with *Lm* as in (A). mRNA expression was quantitated using RT-qPCR. Relative values to *Gapdh* expression are shown. Mean of biological replicates ± SD; n= 3; unpaired Student´s t-test, *p < 0.05, ****p < 0.0001.

(**E**) Mediator kinase regulation of cellular ROS production during *Lm* infection. BMDMs were infected with *Lm* (MOI 10) for 8 or 12 h following pretreatment with SnxB (2.5 µM, 30 min). ROS production was determined by flow cytometry and is shown as percentage of CellRox green$^+$ cells. Two-way ANOVA with Dunett's multiple comparison test, *p < 0.05, **p < 0.01.

DISCUSSION

It has been speculated that the enigmatic Mediator kinase ability to regulate transcription positively or negatively results from integration of context-dependent processes, such as cell type-defined transcriptome ground state, with stimulus-specific signaling pathways. In this

study, we provide the first evidence that the positive transcriptional regulation of a cellular response by Mediator kinase can be converted into a negative one if a second signaling pathway is activated in parallel. We reveal this functional switch by studying the IFN-stimulated JAK-STAT and microbial products-triggered TLR pathways in primary macrophages. In the ground state, the Mediator kinase acts largely as a transcriptional activator in the JAK-STAT pathway. The additional stimulation of TLR pathways overrules the ground state and converts Mediator kinase into a JAK-STAT pathway repressor.

A critical aspect of our study is the careful selection of the cell system for the systematic Mediator kinase analysis. Although macrophages are physiological targets for cytokines and microbial products (*50*), our benchmarking revealed that Mediator kinase robustly regulates responses only in primary macrophages but not in the immortalized macrophage cell line RAW 264.7. The modest Mediator kinase effects in RAW 264.7 resemble data from other immortalized cells such as MEFs or HEK293 cells (*25, 33*). Although the molecular explanation for the minor impact of Mediator kinase on stimulus-dependent transcription in immortalized cells is currently unknown, our results indicate that Mediator kinase should be preferentially studied in primary cells in which signaling pathways and transcriptional networks are unperturbed by immortalization. The substantial and immunologically relevant impact of Mediator kinase inhibition in primary T cells subsets supports this notion (*28-30*).

The previously reported enhancing role of Mediator kinase in the IFNγ response (*25*) is extended in this study to IFNβ, an IFN-I type, and IL-10 responses. IFNβ, IFNγ and IL-10 activate distinct JAK-STAT pathways, and the transcriptional responses to them are driven by different transcription factors, most significantly by the trimeric ISGF3 complex, STAT1 dimers, and STAT3 dimers, respectively (*12*). The broad JAK-STAT representation indicates that Mediator kinase is a broad positive regulator of JAK-STAT pathways and that the Mediator kinase-facilitated RNA Pol II pause release enhancing the IFNγ response (*25*) might be involved also in other JAK-STAT pathways. It should be noted that the impact of Mediator kinase on the IFNγ response is largely independent of its role as STAT1 S727 kinase (*25, 26, 51*). Over 75% of genes, including many ISGs, are paused in resting macrophages (*52, 53*), implying a potentially widespread role of Mediator kinase in RNA Pol II pause release following macrophage stimulation. Although we noticed that ISGs are dependent on Mediator kinase also in unstimulated macrophages, the underlying mechanism is likely the same as during stimulation, owing to endogenous IFNβ production. Moreover, ISRE motifs were enriched in genes positively regulated by Mediator kinase in both unstimulated and IFN-stimulated macrophages. Nevertheless, the effect on ISGs under steady state conditions is remarkable since Mediator kinase is especially important for rapid gene expression changes during cell

reprogramming by external cues including differentiation signals (*18, 25, 54, 55*). The biological significance of the Mediator kinase regulation of ISGs during steady state is evidenced by our data showing impaired macrophage protection against VSV infection upon Mediator kinase inhibition as this natural immunity requires baseline ISG expression (*35*). Another line of evidence for the steady state regulation of ISGs is provided by studies on the Down syndrome-linked interferonopathy. The hyperactivated steady state IFN signaling associated with trisomy chromosome 21, which is caused in part by the higher number of chromosome 21-located IFN receptor genes, is sensitive to Mediator kinase inhibition (*36*).

Contrasting the JAK-STAT pathways, bacterial products-triggered TLR responses were negatively regulated by Mediator kinase implying mechanistically distinct modes of Mediator kinase engagement in these two key macrophage activation routes. Mediator kinase has been reported to promote the inhibitory c-Jun phosphorylation pS243 and this correlated with Il10 gene repression following TLR7/TLR8 stimulation using the synthetic agonist R848 (*56*). However, this still poorly characterized c-Jun modification (*40*) remained unaffected by Mediator kinase inhibition during the LPS response, excluding pS243 as a mechanism of transcriptional repression in our study. Differences between LPS/TLR4 versus R848-activated TLR7/TLR8 pathways such as the exclusive endosomal origin of TLR7/TLR8 signals as compared to TLR4 which signals from both the cell membrane and the endosome (*7*) might account for the disparate results in the studies. Transcriptional repression might be caused by the ability of Mediator kinase to negatively regulate TFIIH and interactions between Mediator and RNA Pol II (*57*) (*58-60*). However, the biological significance of these inhibitory effects on the general transcription machinery remains to be elucidated. Another mechanism of Mediator kinase-dependent transcriptional repression is via phosphorylation and the subsequent degradation of TFs as reported for the yeast Ste12 (*61*). Since we did not detect altered levels and phosphorylation states of relevant TFs (i.e. AP1, CREB, and NF-κB) or other components of the TLR pathway, the protein degradation mechanism was not accountable for our findings. In fact, a Mediator kinase-dependent phosphorylation and subsequent degradation of TFs may promote rather than inhibit transcription in that it facilitates the TF turnover at the promoter as shown for SMAD1 (*27*).

Given that the negative regulation of LPS- or Pam3CSK4-elicted TLR responses most significantly affects ISGs, we propose that microbial signals convert Mediator kinase from an ISG activator in direct IFN responses to a repressor. This repressive mode still operates via IFN/JAK-STAT signaling as it is sensitive to ruxolitinib and targets ISRE-driven genes, i.e. the IRF bindings sites. IRFs often act in concert with activated STATs to drive the second wave ISGs such as the Gbp genes (*62, 63*). Our data therefore suggest that, following TLR

stimulation, Mediator kinase interferes with the second wave ISGs. Future studies on mechanisms underlying Mediator kinase-dependent negative regulation of ISGs in TLR responses should therefore focus on IRFs.

The TLR-imposed switch of Mediator kinase activity from activator to repressor of JAK-STAT may provide a model for a broad understanding of the versatility of Mediator kinase. For example, the therapeutically promising conversion of antigen-specific effector T cells into Treg cells via Mediator kinase inhibition (*64*) might be driven by similar mechanisms. This conversion involves JAK-STAT signaling although TCR ligation does not directly activate STATs (*28*). Instead, TCR induces several pathways, including PI3 kinase and MAPK signaling, leading to IL-2 production which in turn triggers the JAK-STAT pathway (*65*), thereby resembling the LPS response comprising LPS-induced IFNβ in macrophages. The T cell-specific wiring of signaling networks may in general provide a context in which Mediator kinase acts as a repressor of JAK-STAT pathways, as evidenced also by studies on CAR T cells or IL-6 responses of Th1 cells (*29, 30*).

Mediator kinase inhibition is becoming increasingly attractive as a prospective drug in diverse settings including autoimmune diseases, cancer and stem cell generation (*30, 31, 64, 66, 67*). The therapeutic potential is extended by our finding that the cell-autonomous immunity of macrophages to *Lm* infection is augmented upon Mediator kinase inhibition. Although the mechanism of the boosted macrophage defense against *Lm* remains to be elucidated, the increased expression of Gbp genes in Mediator kinase-inhibited macrophages suggests future avenues of research, as several Gbps, including *Gbp10*, can prevent *Lm* phagosome escape (*46*). The general enhancement of TLR responses upon Mediator kinase inhibition, including chemokine production, suggests options also in systemic antimicrobial defense. The challenge for advancing the therapeutic exploitation of Mediator kinase inhibitors is the identification of the suitable cellular and disease context. Our findings showing conversion of Mediator kinase function from activator to repressor may help precisely identifying appropriate conditions for intervention.

METHODS

Mice

Peritoneal macrophages and bone marrow were isolated from C57BL/6 mice of both sexes. Animals were bred and housed under specific pathogen-free conditions with controlled temperature and humidity, a 12-hour light–dark cycle, and ad libitum access to food and water.

Mice were used in accordance with the Austrian law for animal experiments under the animal license number BMWF-V/3b/ 2020-0.175.109 issued by the Austrian Ministry of Science.

Cell cultures

All cells were grown at 37°C and 5% CO_2. BMDMs were differentiated from bone marrow isolated from femurs and tibias of 8 to 12 weeks old mice. Mice were of both sexes and cells were grown separately for each experiment. Femur and tibia were isolated and cut bones were centrifuged at 3000g for 1.5 min to retrieve the bone marrow. Bone marrow cells were cultured for 9 - 10 days in DMEM (Sigma-Aldrich, catalog #D6429) supplemented with 10% of fetal bovine serum (FBS; Sigma-Aldrich) and either 30% L-cell-conditioned medium as a source of colony-stimulating factor 1 (CSF-1) or human recombinant macrophage colony-stimulating factor (M-CSF) (500 ng/mL; a gift from L. Ziegler-Heitbrock, Helmholtz Center, Munich, Germany), penicillin (100 U/mL), and streptomycin (100 ng/mL) (Pen/Strep, both Sigma-Aldrich).

Peritoneal macrophages (PMs) were isolated from euthanized mice by peritoneal lavage using Phosphate Buffered Saline (PBS) supplemented with 3% FBS. Cells were resuspended in DMEM supplemented with 10% FBS, and Pen/Strep, and seeded in either 3.5 or 6 cm tissue culture (TC) dishes. Cells were incubated at 37°C and 5% CO_2 for 3 hours to allow PM adhesion. Thereafter, cells were washed twice with PBS, medium was exchanged, and treatments were performed as specified.

RAW 264.7 cells (ATCC TIB-71) were cultured in DMEM supplemented with 10% FBS and Pen/Strep. Cells tested negatively for mycoplasma contamination.

Stimulation reagents and inhibitors

Murine IFNγ (Gibco, catalog #PMC4031) was used at a concentration of 10 ng/mL, murine IFN-β (PBL Assay Science, catalog #12400-1) at 250 IU/mL, murine IL-10 (Invitrogen, catalog #RMIL105) at 10 ng/mL, LPS (Sigma-Aldrich, catalog #L2637) at 10 ng/mL and Pam3CSK4 (Invivogen, catalog #tlrl-pms) at 10 ng/mL were used for cell stimulations.

Senexin B (Cayman Chemical, catalog #Cay28459-5) was applied at a concentration of 2.5 µM 30 minutes before stimulation, and Cortistatin A (kindly provided by Dylan Taatjes, University of Colorado, Boulder) was applied at a concentration of 100 nM 30 minutes before stimulation. Ruxolitinib (INCB18424; MedChemExpress catalog #HY-50856) was applied at a concentration of 1.5 µM either 1 hour before LPS stimulation or at the indicated incubation times after stimulation. The iNOS inhibitor 1400W (Cayman Chemical, catalog #214358-33-5) was applied at a concentration of 10 µM 30 minutes before *Lm* infection.

Cell lysis and western blotting

BMDMs (2 × 10^6 cells) or RAW 264.7 (1 × 10^6 cells) were seeded in 2 mL DMEM (with 10% FBS and Pen/Strep) in one well of a 6-well plate and stimulated the next day as indicated. For PMs, the peritoneal lavage of 2 mice was pooled for each condition and plated on a 6 cm TC dish. PMs were stimulated immediately after 3 h incubation for adhesion. Cells were washed with ice-cold PBS and lysed in Frackelton buffer (10 mM Tris-HCl pH8, 30 mM $Na_4P_2O_7$, 50 mM NaCl, 50 mM NaF, 1% Triton X-100 1 mM sodium orthovanadate and 1x cOmplete protease inhibitor cocktail (Roche, 11836145001) for 5 min on ice. Lysates were cleared by centrifugation at 1600g for 5 min at 4°C and protein concentration was measured using Pierce BCA Protein Assay kit (Thermo-Fisher Scientific, Cat #23225). After concentration adjustment, cell lysates were mixed at a ratio of 4:1 with SDS loading dye and heated for 5 min at 95°C. 20 µg of each sample were loaded onto an SDS polyacrylamide gel for separation. Samples were loaded twice to detect the phosphorylated and total protein separately. The gels were blotted on nitrocellulose membrane (GE Healthcare) in carbonate transfer buffer (3 mM Na_2CO_3, 10 mM $NaHCO_3$, and 20% ethanol) for 16 h at 200 mA and additional 2 h at 400 mA at 4°C. Membranes were blocked in either 5% non-fat dry milk powder or 10% BSA in TBS-T (20 mM Tris, 150 mM NaCl, 0.5% Tween 20, pH 8.0) for 1 h at room temperature (RT). After washing three times with TBS-T, primary antibody was added, and membranes were incubated overnight at 4 °C while shaking. Membranes were then washed three times with TBS-T and incubated with HRP-conjugated secondary antibody in 1:2500 dilution for 1 h at RT. After another three washing steps with TBS-T, membranes were incubated with either SuperSignal West Pico PLUS (Thermo Scientific, #34580) or ECL Prime Western Blotting Detection Reagent (Amersham, #RPN2236) and developed using the ChemiDoc Touch Imaging system (Bio-Rad). Antibodies and dilutions are listed in Table S1.

RNA-isolation, reverse transcription and qPCR

BMDMs (2 × 10^6) were seeded in 2 mL of DMEM supplemented with 10% FBS and Pen/Strep in one well of a 6-well plate and treated the next day as indicated. RNA was isolated using the NucleoSpin RNA II Kit (Macherey-Nagel, catalog#740955) following manufacturer's instructions. The complementary DNA (cDNA) synthesis was performed by reverse transcription of 400 ng of total RNA using oligo$(dT)_{18}$ primers for mRNA, or Random Hexamer Primer for pre-mRNA, and a recombinant M-MuLV reverse transcriptase (RevertAid, Thermo Fischer Scientific) according to the manufacturer`s instructions. Real-time qPCR (RT-qPCR) was run on CFX Touch qPCR cyclers (Bio-Rad), paired with CFX Maestro Analysis software,

using the Luna Universal qPCR Master Mix (NEB, catalog#M3003). Relative expression levels were calculated by applying a two-fold standard dilution series from cDNA derived from samples. Primers are listed in Table S6.

Quantseq

For PMs, cells were prepared as described above. PMs from one mouse were used for one RNA-seq sample. RNA isolation was performed with High Performance RNA Isolation kit (Vienna, VBC Molecular Tools Shop, RNAisomag) and a KingFisher Flex robot (Thermo Fisher Scientific), according to manufacturer's instructions. For BMDMs, $2x10^6$ cells were seeded and the next day treated as indicated followed by total RNA isolation using either QIAzol Lysis Reagent (QIAGEN) and chloroform extraction or NucleoSpin RNA II Kit (Macherey-Nagel, catalog#740955) according to the manufacturer's instructions. In the case of QIAzol lysis, total RNA was subsequently precipitated with a 1:10 mixture of isopropanol and 5 M NaCl at pH 7. For RAW 264.7, $1x10^6$ cells were seeded in DMEM supplemented with 10% FBS and Pen/Strep in a 6-cm dish. Total RNA was isolated using QIAzol, followed by chloroform extraction. Subsequently, the RNA was precipitated with a 1:10 mixture of isopropanol and 5 M NaCl at pH 7. Library preparation (Quantseq 3´mRNA, Lexogen), quality control and Solexa sequencing were performed by the NGS Facility at Vienna BioCenter Core Facilities (VBCF) (https://www.viennabiocenter.org/facilities). All samples were analyzed on an Illumina NovaSeq 6000, except for IFNγ- and LPS-stimulated PM samples, which were analyzed on an Illumina NovaSeq X. Sequencing was performed using either single-end 100 bp (SR100) or paired-end 150 bp (PE150) reads.

Quantseq Data Analysis

Raw reads were demultiplexed, following which Unique Molecular Identifiers (UMI) were extracted from the reads and appended to the header using UMI-tools version 1.1.6 (*68*). This was followed by the trimming of adapters, PolyA and low-quality reads using Trim Galore version: 0.6.10 (https://www.bioinformatics.babraham.ac.uk/projects/trim_galore). Quality control of the reads after UMI extraction and during trimming was performed using FastQC version: 0.12.1 (https://www.bioinformatics.babraham.ac.uk/projects/fastqc). PolyG and PolyX trimming on the reads was implemented using fastp version: 0.24.3 (*69*). The trimmed reads had the headers renamed to keep the UMI as the header end. The trimmed reads were then mapped to GRCm39/mm39 mouse genome assembly using STAR version 2.7.11b (*70*). The percentage of Uniquely Mapped Reads was around 79 – 85% for BMDMs and PMs and around 85 – 90% for RAWs. Sorting and Indexing of the aligned reads, along with the conversion to

BAM was performed using Samtools version 1.21-1.23 (*71*). The deduplication of the aligned reads was achieved using UMI-tools version 1.1.6 (*68*). Read count for each gene was achieved by implementing HT-Seq version 2.0.9-3.13.3 (*72*). Differential Expression Analysis (DEA) was performed on Read counts using DESeq2 Package version 1.44.0 (*73*). Gene Set Enrichment Analysis (GSEA) was performed using clusterProfiler Package version 4.12.6 (*74*). Genes that were down- or up-regulated (padj ≤ 0.05) were used for the analysis. As a background all other genes were used. Results for DEA and GSA were visualized using ggplot2 package for R version.

Transcription factor binding motif discovery

Known motif analysis was performed with the *findMotifsGenome* function of the HOMER software (*75*). The analysis was conducted on genomic regions spanning -1000 to +500 bp relative to TSS of differentially expressed genes. All other genes were used as the background set.

BMDM infection with Vesicular stomatitis virus (VSV)

GFP-expressing VSV was grown on L929 cells for 36 hours, after which supernatants were clarified and titrated on L929 cells by plaque assay as previously described (*76*). BMDMs were infected at MOI of 5 for 4 h for RT-qPCR and for 24 h for flow cytometry analysis of GFP expression. For flow cytometry, BMDMs were harvested by incubation for 5 min in citric saline (135 mM potassium chloride and 15 mM sodium citrate), collected by centrifugation together with the culture medium to include cells in suspension, and then washed twice in PBS. Cell pellets were resuspended in FACS buffer (1x PBS + 2% BSA), and GFP expression was analyzed using a LSRFortessa Cell Analyzer (BD Biosciences) at the Max Perutz Labs FACS facility. Propidium iodide (PI, Thermo Fisher Scientific) was used to assess cell death at a final concentration of 1 µg/ml immediately before flow cytometry to avoid false positive staining. Percentage of GFP- or PI-positive cells and GFP mean florescence intensity (MFI) was performed with FlowJo. 50.000 cells were acquired for each dot plot. Unstained uninfected or infected cells were used as negative controls. One part of cells killed by incubation at 95°C was mixed to one part of live cells as positive control. Doublets were excluded based on SSC-H/SSC-A and FSCH/FSC-A.

ELISA

For cytokine measurements, $2x10^6$ BMDMs were seeded in 2 mL of DMEM supplemented with 10% FBS and Pen/Strep in one well of a 6-well plate. The culture supernatant was collected

and spun for 5 min at 300g to remove debris. ELISAs were performed according to the manufacturer's protocols. ELISAs kits used: Mouse IL-10 Uncoated ELISA, (Invitrogen, catalog #88-7105), Mouse Ccl7 ELISA Development Kit (ABTS) (PeproTech, Invitrogen catalog #900-K123K) and Mouse Ccl2 Uncoated ELISA Kit (Invitrogen, catalog #88-7391-22).

Culture and preparation of *Listeria monocytogenes*

The stock of *Lm* LO28 strain was yearly revived following mice infection. In brief, L028 strain was grown in Brain-heart-infusion (BHI) media for 16 hours. Stationary phase cultures were then diluted to an optical density $(OD)_{600}$ of 0.1 and incubated at 37°C until reaching OD_{600} = 1. A C57BL/6N mouse was infected intraperitoneally with 10^6 bacteria. After 24 hours, spleen was collected and homogenized in 1 mL of ice-cold PBS on ice. Four 10-fold serial dilutions were then plated on Listeria Selective Agar (Thermo Scientific, catalog #PO5026A) and incubated for 16 h at 37°C and 5% CO_2. Next day, 1 single colony was picked, grown in BHI media for 16 h and then mixed in a 1:1 ratio of bacteria with 100% glycerol. Aliquots were stored at -80°C before use. Heat-killed *Lm* was obtained by incubation at 70°C for 20 minutes. The absence of live bacteria was confirmed by plating on BHI agar plates.

BMDM infection with *Lm*

Lm was grown overnight in BHI medium at 37°C with continuous shaking. Upon reaching stationary phase, bacterial density was estimated by measuring OD_{600} (1 OD = 1 × 10^9 viable bacteria). The appropriate culture volume was centrifuged, and the bacterial pellet was washed twice with PBS and resuspended in DMEM supplemented with 10% FBS. BMDMs were seeded in DMEM supplemented with 10% FBS and M-CSF (500 ng/ml) and infected with MOI of 10 or 1 for the indicated period. After 1 hour, the medium was replaced with DMEM supplemented with 10% FBS and gentamicin (50 µg/ml, MP Biomedicals). One hour later, the medium was replaced with DMEM supplemented with 10% FBS and gentamicin (10 µg/ml), which was kept until the end of the experiment.

Colony forming unit (CFU) assay

For in vitro CFU assays, 0.5 × 10^5 BMDMs were seeded in 200 µl of DMEM supplemented with 10% FBS and M-CSF (500 ng/ml) in 96-well plates and infected with *Lm* at different time points, as indicated in the figure legends. After each time point, cells were washed twice with PBS and lysed in 50 µl of sterile nuclease-free water twice for 5 min at 37°C. For quantifying bacterial loads, four 1:10 serial dilutions of these lysates were plated on plates containing BHI medium and incubated for 1 day at 37°C. For SnxB toxicity assay, 2x10^7 bacteria were

incubated in one well of a 6-well plate at 37°C for the indicated periods. Four 1:10 serial dilutions were plated on plates containing BHI medium and incubated for 1 day at 37°C to calculate the initial number of CFUs/mL.

PI staining to measure macrophage death

To assess cell death, 2 × 10^6 BMDMs were seeded in 2 ml of DMEM supplemented with 10% FBS and M-CSF (500 ng/ml) in one well of a 6-well plate. Cells were infected with *L. monocytogenes* for the indicated time points. For flow cytometry, BMDMs were incubated for 5 min in pre-warmed citric saline solution (135 mM potassium chloride and 15 mM sodium citrate) at 37°C. Adherent cells were then harvested together with culture supernatant to collect suspension cells and collected by centrifugation in cold PBS. Cell pellets were washed and resuspended in 300 µL of FACS buffer and stained with PI at a final concentration of 1 µg/ml immediately before flow cytometry to avoid false positive staining. Unstained uninfected or infected cells were used as negative controls. One part of cells killed at 95°C was mixed to one part of live cells as positive control. Flow cytometry was carried out with a LSR Fortessa II (BD Biosciences) operated with FACS-Diva at the Max Perutz Labs FACS facility (www.maxperutzlabs.ac.at/ research/facilities/biooptics-facs). Analysis of the percentage of PI-positive cells was performed with FlowJo and 50,000 events were acquired for each dot plot. Doublets were excluded based on SSC-H/SSC-A and FSCH/FSC-A.

In vitro phagocytosis assay

Heat-killed *Lm* were stained with the pH-sensitive dye pHrodo Red (Invitrogen catalog # P35372; 25 µM) according to the manufacturer protocol (0.8x10^7 bacteria in 1 mL total volume). BMDMs (0.3 x 10^6 cells) were seeded in 1 mL DMEM supplemented with 10% FBS and Pen/Strep in one well of an uncoated 12-well plate. After the addition of heat-killed *Lm* at a MOI of 10 or 1, plates were first spun for 5 minutes at 500g and then incubated at 37°C for 1 hour. As negative control, cells in a different plate were incubated for 1 hour at 4°C prior and after the addition of heat-killed *Lm*. BMDMs were then incubated for 5 min in pre-warmed citric saline solution (135 mM potassium chloride and 15 mM sodium citrate) at 37°C, and adherent cells were harvested and collected by centrifugation in cold PBS. Cell pellets were washed and resuspended in 200 µL of FACS buffer. Data were acquired using LSR Fortessa II (BD Biosciences) operated with FACS-Diva and analyzed with FlowJo software. Doublets were excluded based on SSC-H/SSC-A and FSCH/FSC-A. pHrodo fluorescence was acquired under the PE channel.

Measurement of NO production

To assess nitric oxide (NO) production, 1 × 10^6 BMDMs were seeded in 500 µl of DMEM supplemented with 10% FBS and M-CSF (500 ng/ml) in a well of a 24-well plate. After 12 hours of *Lm* infection (MOI 10), NO levels were indirectly quantitated by measuring the concentration of nitrite in the culture medium using the Griess assay. For each sample, 100 µL of culture supernatant was mixed in technical triplicate with 100 µL of 1% sulfanilamide in 5% phosphoric acid and 100 µL of 0.1% N-(1 naphthyl)ethylenediamine dihydrochloride (NEDD) in double-distilled water in a 96-well plate. Absorbance was immediately measured at 545 nm using a microplate reader. Sodium nitrite ($NaNO_2$) standards were serially diluted to generate a standard curve for nitrite quantification.

Measurement of ROS production

For measurement of reactive oxygen species (ROS) production, 1 × 10^6 BMDMs were seeded in 1 mL of DMEM supplemented with 10% FBS and M-CSF (500 ng/ml) in one well of a 12-well plate. After 8 or 12 hours of *L. monocytogenes* infection (MOI of 10), BMDMs were then incubated for 5 min in pre-warmed citric saline solution at 37°C. All subsequent steps were performed at room temperature. Adherent cells were then harvested together with culture supernatant to collect suspension cells and collected by centrifugation in PBS. Cell pellets were washed once with PBS and then stained. For cellular ROS detection, CellROX green (Thermo Fischer Scientific, catalog #C10444) was used at the concentration of 5 µM and cells were stained in complete medium for 30 min at 37°C according to manufacturer's protocol. For mitochondrial specific ROS quantification, MitoSOX red (Thermo Fischer Scientific, catalog# M36008) was used at the concentration of 5 µM and cells were stained in PBS for 15 min at 37°C according to manufacturer's protocol. Data were acquired using LSR Fortessa II (BD Biosciences) operated with FACS-Diva and analyzed with FlowJo software. Doublets were excluded based on SSC-H/SSC-A and FSCH/FSC-A. CellROX and MitoSOX fluorescence was acquired respectively under the FITC or the PE channel.

Quantification and statistical analysis

All visualizations and statistical analysis were performed using GraphPad Prism v.10.3.1 software or the R project. Statistical significances were calculated using a two-tailed unpaired Student's *t* test, one-way analysis of variance (ANOVA) with Tukey´s multiple comparison test, two-way ANOVA with Šídák's multiple comparisons test, linear regression model, or Pearson's correlation tests, as indicated in the figure legends. Results were considered to be significant with *$p < 0.05$, **$p < 0.01$, ***$p < 0.001$ or ****$p < 0.0001$.

DATA DEPOSITION

RNA-seq data have been deposited at Gene Expression Omnibus and are accessible through GEO accession numbers GSE310562 (private token sfcjweakzfunzon), GSE310563 (private token elyjyecsvfmnlur), GSE310565 (private token upspioimtdidfwt), GSE310566 (private token wxqbycigzbypdkl), GSE310567 (private token mzqjsikeljoxdid).

ACKNOWLEDGEMENTS

We are grateful to Christina Zeiler for valuable discussions. We thank Gijs Versteeg for GFP-expressing VSV and Laura Boccuni for advice on *Lm* infection. The VBCF NGS Facility and Max Perutz Labs BioOptics Facility are acknowledged for services. The Life Science Compute Cluster (LiSC) of the University of Vienna is appreciated for providing computing environment for data analyses. The study was supported by the Austrian Science Fund grants W1261, P35852 and PAT1837425 to PK and the Max Perutz PhD fellowship to JF.

AUTHOR CONTRIBUTIONS

M.F. and P.K. conceived the study and designed experiments. M.F. performed all experiments except RNA-seq of RAW 264.7 cells. N.B. performed sample preparation for RNA-seq of RAW 264.7. J.F. performed isolation of peritoneal macrophages. R.C. analyzed RNA-seq datasets. T.D. provided expertise for infection experiments. M.F. and P.K. wrote the manuscript. All authors read and approved the manuscript.

DECLARATION OF INTERESTS

The authors declare no competing interests.

REFERENCES

1. S. Carpenter, E. P. Ricci, B. C. Mercier, M. J. Moore, K. A. Fitzgerald, Post-transcriptional regulation of gene expression in innate immunity. *Nature reviews* **14**, 361-376 (2014).

2. C. K. Glass, G. Natoli, Molecular control of activation and priming in macrophages. *Nat Immunol* **17**, 26-33 (2016).

3. T. D. Troutman, E. Kofman, C. K. Glass, Exploiting dynamic enhancer landscapes to decode macrophage and microglia phenotypes in health and disease. *Mol Cell* **81**, 3888-3903 (2021).

4. M. Turner, M. D. Diaz-Munoz, RNA-binding proteins control gene expression and cell fate in the immune system. *Nat Immunol* **19**, 120-129 (2018).

5. P. Broz, V. M. Dixit, Inflammasomes: mechanism of assembly, regulation and signalling. *Nature reviews* **16**, 407-420 (2016).

6. C. C. Lee, A. M. Avalos, H. L. Ploegh, Accessory molecules for Toll-like receptors and their function. *Nature reviews* **12**, 168-179 (2012).

7. T. Kawai, S. Akira, The role of pattern-recognition receptors in innate immunity: update on Toll-like receptors. *Nat Immunol* **11**, 373-384 (2010).

8. T. Kawai, M. Ikegawa, D. Ori, S. Akira, Decoding Toll-like receptors: Recent insights and perspectives in innate immunity. *Immunity* **57**, 649-673 (2024).

9. A. Bestehorn *et al.*, Cytoplasmic mRNA decay controlling inflammatory gene expression is determined by pre-mRNA fate decision. *Mol Cell* **85**, 742-755 e749 (2025).

10. V. Sedlyarov *et al.*, The Bicarbonate Transporter SLC4A7 Plays a Key Role in Macrophage Phagosome Acidification. *Cell host & microbe* **23**, 766-774 e765 (2018).

11. T. Uehata, O. Takeuchi, Regnase-1 Is an Endoribonuclease Essential for the Maintenance of Immune Homeostasis. *J Interferon Cytokine Res* **37**, 220-229 (2017).

12. G. R. Stark, J. E. Darnell, Jr., The JAK-STAT pathway at twenty. *Immunity* **36**, 503-514 (2012).

13. A. Yoshimura, M. Ito, S. Chikuma, T. Akanuma, H. Nakatsukasa, Negative Regulation of Cytokine Signaling in Immunity. *Cold Spring Harb Perspect Biol* **10**, (2018).

14. I. Wiesauer, C. Gaumannmuller, I. Steinparzer, B. Strobl, P. Kovarik, Promoter Occupancy of STAT1 in Interferon Responses Is Regulated by Processive Transcription. *Mol Cell Biol* **35**, 716-727 (2015).

15. G. Natoli, S. Ghisletti, I. Barozzi, The genomic landscapes of inflammation. *Genes Dev* **25**, 101-106 (2011).

16. O. Babadei, B. Strobl, M. Muller, T. Decker, Transcriptional control of interferon-stimulated genes. *J Biol Chem* **300**, 107771 (2024).

17. O. Luyties, D. J. Taatjes, The Mediator kinase module: an interface between cell signaling and transcription. *Trends in biochemical sciences* **47**, 314-327 (2022).

18. A. Postlmayr, C. E. Dumeau, A. Wutz, Cdk8 is required for establishment of H3K27me3 and gene repression by Xist and mouse development. *Development* **147**, (2020).

19. P. P. Rocha, M. Scholze, W. Bleiss, H. Schrewe, Med12 is essential for early mouse development and for canonical Wnt and Wnt/PCP signaling. *Development* **137**, 2723-2731 (2010).

20. N. Li *et al.*, Cyclin C is a haploinsufficient tumour suppressor. *Nat Cell Biol* **16**, 1080-1091 (2014).

21. R. Abdella *et al.*, Structure of the human Mediator-bound transcription preinitiation complex. *Science* **372**, 52-56 (2021).

22. X. Chen *et al.*, Structures of the human Mediator and Mediator-bound preinitiation complex. *Science* **372**, (2021).

23. S. Rengachari, S. Schilbach, S. Aibara, C. Dienemann, P. Cramer, Structure of the human Mediator-RNA polymerase II pre-initiation complex. *Nature* **594**, 129-133 (2021).

24. H. E. Pelish *et al.*, Mediator kinase inhibition further activates super-enhancer-associated genes in AML. *Nature* **526**, 273-276 (2015).

25. I. Steinparzer *et al.*, Transcriptional Responses to IFN-gamma Require Mediator Kinase-Dependent Pause Release and Mechanistically Distinct CDK8 and CDK19 Functions. *Mol Cell* **76**, 485-499 e488 (2019).

26. J. Bancerek *et al.*, CDK8 kinase phosphorylates transcription factor STAT1 to selectively regulate the interferon response. *Immunity* **38**, 250-262 (2013).

27. C. Alarcon *et al.*, Nuclear CDKs drive Smad transcriptional activation and turnover in BMP and TGF-beta pathways. *Cell* **139**, 757-769 (2009).

28. M. Akamatsu *et al.*, Conversion of antigen-specific effector/memory T cells into Foxp3-expressing Treg cells by inhibition of CDK8/19. *Sci Immunol* **4**, (2019).

29. J. Martinez-Fabregas *et al.*, CDK8 Fine-Tunes IL-6 Transcriptional Activities by Limiting STAT3 Resident Time at the Gene Loci. *Cell reports* **33**, 108545 (2020).

30. K. A. Freitas *et al.*, Enhanced T cell effector activity by targeting the Mediator kinase module. *Science* **378**, eabn5647 (2022).

31. C. J. Lynch *et al.*, Global hyperactivation of enhancers stabilizes human and mouse naive pluripotency through inhibition of CDK8/19 Mediator kinases. *Nat Cell Biol* **22**, 1223-1238 (2020).

32. P. J. Murray, Macrophage Polarization. *Annual review of physiology* **79**, 541-566 (2017).

33. M. Chen *et al.*, CDK8 and CDK19: positive regulators of signal-induced transcription and negative regulators of Mediator complex proteins. *Nucleic Acids Res*, (2023).

34. W. C. Raschke, S. Baird, P. Ralph, I. Nakoinz, Functional macrophage cell lines transformed by Abelson leukemia virus. *Cell* **15**, 261-267 (1978).

35. D. J. Gough, N. L. Messina, C. J. Clarke, R. W. Johnstone, D. E. Levy, Constitutive type I interferon modulates homeostatic balance through tonic signaling. *Immunity* **36**, 166-174 (2012).

36. K. A. Cozzolino *et al.*, Mediator kinase inhibition suppresses hyperactive interferon signaling in Down syndrome. *eLife* **13**, (2025).

37. N. Fortelny *et al.*, JAK-STAT signaling maintains homeostasis in T cells and macrophages. *Nat Immunol* **25**, 847-859 (2024).

38. C. Schindler, D. E. Levy, T. Decker, JAK-STAT signaling: from interferons to cytokines. *J Biol Chem* **282**, 20059-20063 (2007).

39. P. Kovarik *et al.*, Stress-induced phosphorylation of STAT1 at Ser727 requires p38 mitogen-activated protein kinase whereas IFN-gamma uses a different signaling pathway. *Proc Natl Acad Sci U S A* **96**, 13956-13961 (1999).

40. W. J. Boyle *et al.*, Activation of protein kinase C decreases phosphorylation of c-Jun at sites that negatively regulate its DNA-binding activity. *Cell* **64**, 573-584 (1991).

41. S. H. Duttke, M. W. Chang, S. Heinz, C. Benner, Identification and dynamic quantification of regulatory elements using total RNA. *Genome research* **29**, 1836-1846 (2019).

42. T. Tamura, H. Yanai, D. Savitsky, T. Taniguchi, The IRF family transcription factors in immunity and oncogenesis. *Annual review of immunology* **26**, 535-584 (2008).

43. X. Hu, S. D. Chakravarty, L. B. Ivashkiv, Regulation of interferon and Toll-like receptor signaling during macrophage activation by opposing feedforward and feedback inhibition mechanisms. *Immunol Rev* **226**, 41-56 (2008).

44. K. Hansen *et al.*, Listeria monocytogenes induces IFNbeta expression through an IFI16-, cGAS- and STING-dependent pathway. *Embo J* **33**, 1654-1666 (2014).

45. B. H. Kim *et al.*, A family of IFN-gamma-inducible 65-kD GTPases protects against bacterial infection. *Science* **332**, 717-721 (2011).

46. J. D. MacMicking, Interferon-inducible effector mechanisms in cell-autonomous immunity. *Nature reviews* **12**, 367-382 (2012).

47. J. D. MacMicking *et al.*, Altered responses to bacterial infection and endotoxic shock in mice lacking inducible nitric oxide synthase. *Cell* **81**, 641-650 (1995).

48. H. Zwaferink, S. Stockinger, S. Reipert, T. Decker, Stimulation of inducible nitric oxide synthase expression by beta interferon increases necrotic death of macrophages upon Listeria monocytogenes infection. *Infect Immun* **76**, 1649-1656 (2008).

49. M. Farlik *et al.*, Nonconventional initiation complex assembly by STAT and NF-kappaB transcription factors regulates nitric oxide synthase expression. *Immunity* **33**, 25-34 (2010).

50. F. Ginhoux, J. L. Schultze, P. J. Murray, J. Ochando, S. K. Biswas, New insights into the multidimensional concept of macrophage ontogeny, activation and function. *Nat Immunol* **17**, 34-40 (2016).

51. I. Sadzak *et al.*, Recruitment of Stat1 to chromatin is required for interferon-induced serine phosphorylation of Stat1 transactivation domain. *Proc Natl Acad Sci U S A* **105**, 8944-8949 (2008).

52. L. Yu *et al.*, Negative elongation factor complex enables macrophage inflammatory responses by controlling anti-inflammatory gene expression. *Nat Commun* **11**, 2286 (2020).

53. A. Ravi Sundar Jose Geetha *et al.*, Dynamic control of gene expression by ISGF3 and IRF1 during IFNbeta and IFNgamma signaling. *EMBO J* **43**, 2233-2263 (2024).

54. M. D. Galbraith *et al.*, HIF1A employs CDK8-mediator to stimulate RNAPII elongation in response to hypoxia. *Cell* **153**, 1327-1339 (2013).

55. M. Chen *et al.*, CDK8/19 Mediator kinases potentiate induction of transcription by NFkappaB. *Proc Natl Acad Sci U S A* **114**, 10208-10213 (2017).

56. L. Johannessen *et al.*, Small-molecule studies identify CDK8 as a regulator of IL-10 in myeloid cells. *Nat Chem Biol* **13**, 1102-1108 (2017).

57. M. T. Knuesel, K. D. Meyer, C. Bernecky, D. J. Taatjes, The human CDK8 subcomplex is a molecular switch that controls Mediator coactivator function. *Genes Dev* **23**, 439-451 (2009).

58. H. Elmlund *et al.*, The cyclin-dependent kinase 8 module sterically blocks Mediator interactions with RNA polymerase II. *Proc Natl Acad Sci U S A* **103**, 15788-15793 (2006).

59. K. L. Tsai *et al.*, A conserved Mediator-CDK8 kinase module association regulates Mediator-RNA polymerase II interaction. *Nat Struct Mol Biol* **20**, 611-619 (2013).

60. S. Akoulitchev, S. Chuikov, D. Reinberg, TFIIH is negatively regulated by cdk8-containing mediator complexes. *Nature* **407**, 102-106 (2000).

61. C. Nelson, S. Goto, K. Lund, W. Hung, I. Sadowski, Srb10/Cdk8 regulates yeast filamentous growth by phosphorylating the transcription factor Ste12. *Nature* **421**, 187-190 (2003).

62. K. Honda, A. Takaoka, T. Taniguchi, Type I interferon [corrected] gene induction by the interferon regulatory factor family of transcription factors. *Immunity* **25**, 349-360 (2006).

63. J. D. MacMicking, IFN-inducible GTPases and immunity to intracellular pathogens. *Trends in immunology* **25**, 601-609 (2004).

64. N. Mikami, R. Kawakami, A. Sugimoto, M. Arai, S. Sakaguchi, Generating functionally stable and antigen-specific T(reg) cells from effector T cells for cell therapy of inflammatory diseases. *Science translational medicine* **17**, eadr6049 (2025).

65. S. H. Ross, D. A. Cantrell, Signaling and Function of Interleukin-2 in T Lymphocytes. *Annual review of immunology* **36**, 411-433 (2018).

66. M. Mukai *et al.*, Conversion of pathogenic T cells into functionally stabilized T(reg) cells for antigen-specific immunosuppression in pemphigus vulgaris. *Science translational medicine* **17**, eadq9913 (2025).

67. D. Sooraj *et al.*, MED12 and BRD4 cooperate to sustain cancer growth upon loss of mediator kinase. *Mol Cell* **82**, 123-139 e127 (2022).

68. T. Smith, A. Heger, I. Sudbery, UMI-tools: modeling sequencing errors in Unique Molecular Identifiers to improve quantification accuracy. *Genome research* **27**, 491-499 (2017).

69. S. Chen, Ultrafast one-pass FASTQ data preprocessing, quality control, and deduplication using fastp. *Imeta* **2**, e107 (2023).

70. A. Dobin *et al.*, STAR: ultrafast universal RNA-seq aligner. *Bioinformatics (Oxford, England)* **29**, 15-21 (2013).

71. P. Danecek *et al.*, Twelve years of SAMtools and BCFtools. *Gigascience* **10**, (2021).

72. S. Anders, P. T. Pyl, W. Huber, HTSeq--a Python framework to work with high-throughput sequencing data. *Bioinformatics (Oxford, England)* **31**, 166-169 (2015).

73. M. I. Love, W. Huber, S. Anders, Moderated estimation of fold change and dispersion for RNA-seq data with DESeq2. *Genome biology* **15**, 550 (2014).

74. T. Wu *et al.*, clusterProfiler 4.0: A universal enrichment tool for interpreting omics data. *Innovation (Camb)* **2**, 100141 (2021).

75. S. Heinz *et al.*, Simple combinations of lineage-determining transcription factors prime cis-regulatory elements required for macrophage and B cell identities. *Mol Cell* **38**, 576-589 (2010).

76. A. A. Abdelmageed, M. C. Ferran, The Propagation, Quantification, and Storage of Vesicular Stomatitis Virus. *Current protocols in microbiology* **58**, e110 (2020).

SUPPLEMENTARY DATA FILE CAPTIONS

Data file S1. RNA-seq data of BMDMs, PMs and RAW 264.7. Cells were pretreated with SnxB or CA for 30 min and subsequently stimulated with IFNγ or LPS (BMDMs and PMs) or IFNγ only (RAW 264.7).

Data file S2. GSEA data for SnxB effects in unstimulated, IFNγ- or LPS-stimulated BMDMs.

Data file S3. Regulation of stimulus-induced genes by Mediator kinase in BMDMs and PMs. Stimulations: IFNγ, IFNβ or LPS.

Data file S4. HOMER analysis of SnxB-sensitive genes in unstimulated and stimulated BMDMs. Stimulations: IFNγ, IFNβ or LPS.

Data file S5. SnxB effects (normalized counts and Log2FC) on IFNγ-ISGs, IFNβ-ISGs and non-ISGs in unstimulated and stimulated BMDMs.

SUPPLEMENTARY FIGURES

TLR signaling switches Mediator kinase from activator to repressor of interferon-stimulated genes to dampen macrophage activation

Maurizio Forte[1,2,3], Nora Bischoff[1,2], Ronit Chakraborty[1,2,3], Jeanne Fesselet [1,2,3], Thomas Decker[1,2], Pavel Kovarik[1,2*]

[1] Max Perutz Labs, Vienna Biocenter Campus (VBC), Dr.-Bohr-Gasse 9, 1030 Vienna, Austria.
[2] University of Vienna, Max Perutz Labs, Department of Microbiology, Immunobiology and Genetics, Dr.-Bohr-Gasse 9, 1030 Vienna, Austria.
[3] Vienna Biocenter PhD Program, a Doctoral School of the University of Vienna and Medical University of Vienna, 1030 Vienna, Austria.
* correspondence pavel.kovarik@univie.ac.at

Figure S1

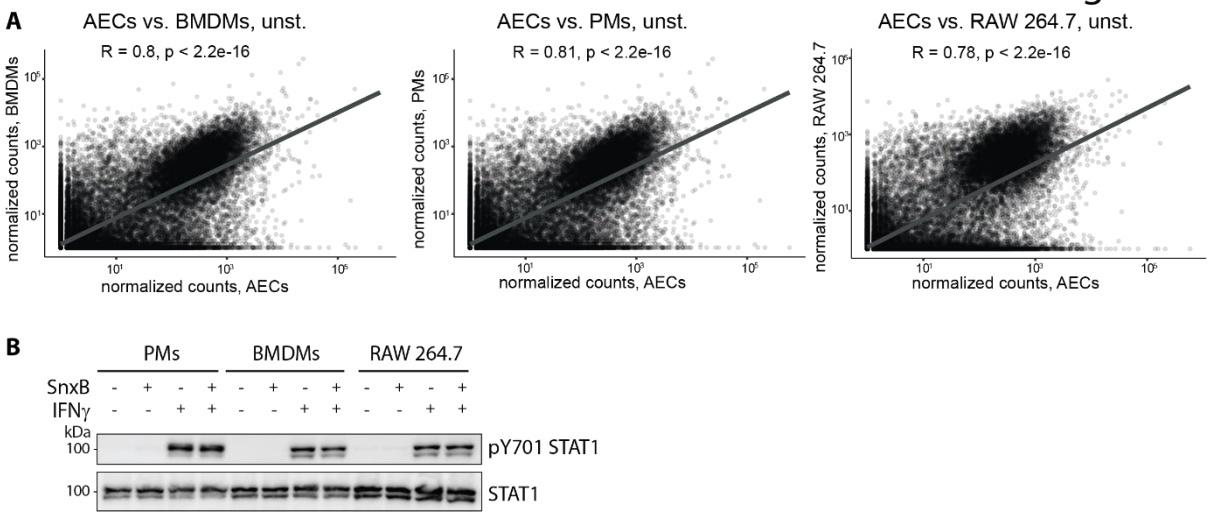

Supplementary Figure 1 (related to Figure 1). Comparisons of AECs versus macrophage transcriptomes and controls for STAT1 activation

(**A**) Comparisons of AEC transcriptome with the transcriptome of different macrophages. Mean DESeq2-normalized RNA-seq counts of BMDMs, PMs or RAW 264.7 cells were plotted against those of AECs and Pearson correlation coefficients (R) with the associated *p*-values were calculated.

(**B**) Analysis of STAT1 Y701 phosphorylation in PMs, BMDMs or RAW 264.7 cells. Cells were pretreated with SnxB (2.5 μM, 30 min) or vehicle and subsequently IFNγ was added (10 ng/mL, 45 min). Whole cell extracts were analyzed by western blotting using antibodies to pY701 STAT1 and total STAT1.

Figure S2

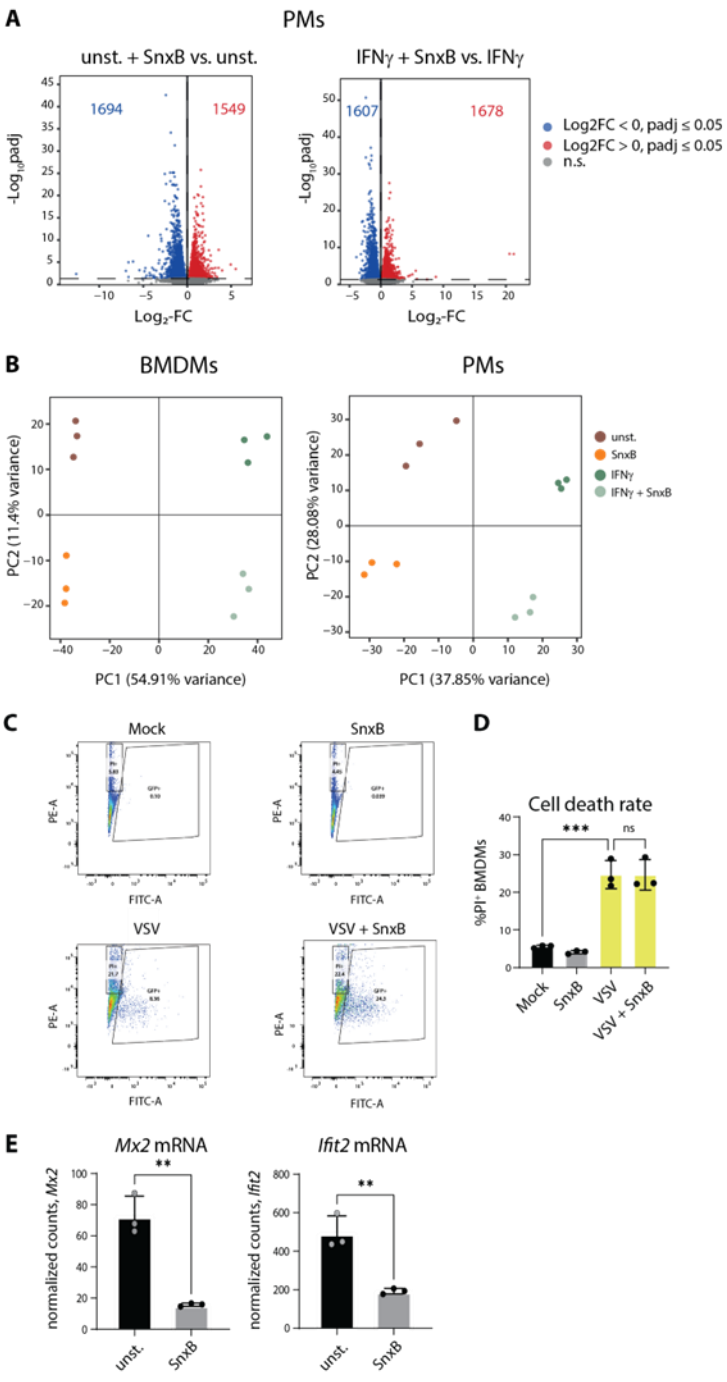

Supplementary Figure 2 (related to Figure 2). RNA-seq and VSV infection upon Mediator kinase inhibition

(**A**) Mediator kinase inhibition causes up- or down-regulation of gene expression in unstimulated and IFNγ-stimulated PMs. Unstimulated cells were pretreated with SnxB (2.5 µM) or vehicle for 4 h 30 min. IFNγ-stimulated samples are described in Figure 1B. Down-regulated genes (Log2-FC < 0; padj ≤ 0.05) shown in blue, up-regulated genes (Log2-FC > 0; padj ≤ 0.05) shown in red and non-significant genes (n.s.) in grey. (**B**) Principal component analysis (PCA) of three independent replicates of BMDMs and PMs pretreated with SnxB (2.5 µM, 30 min) or vehicle and subsequently stimulated with IFNγ (10 ng/mL, 4 h). n = 3.

(**C**) Representative flow cytometry plots of BMDMs infected with GFP-expressing VSV (MOI = 5, 24 h) after pretreatment with SnxB (2.5 µM, 30 min) or vehicle. FITC signal

corresponds to GFP and indicates infected cells, PE signal corresponds to propidium iodide (PI) and indicates dead cells.
(**D**) Percentage (%) of PI-positive cells from VSV-infected BMDMs (MOI = 5, 24 h) pretreated with SnxB (2.5 µM, 30 min) or vehicle. Mean of biological replicates ± SD; n = 3; unpaired Student´s t-test, ***p < 0.001; ns, not significant.
(**E**) Mean normalized RNA-seq counts for *Mx2* and *Ifit2* in unstimulated BMDMs pretreated with SnxB (2.5 µM, 30 min) or vehicle. Mean of biological replicates ± SD; n = 3; unpaired Student´s t-test, **p < 0.01.

Figure S3

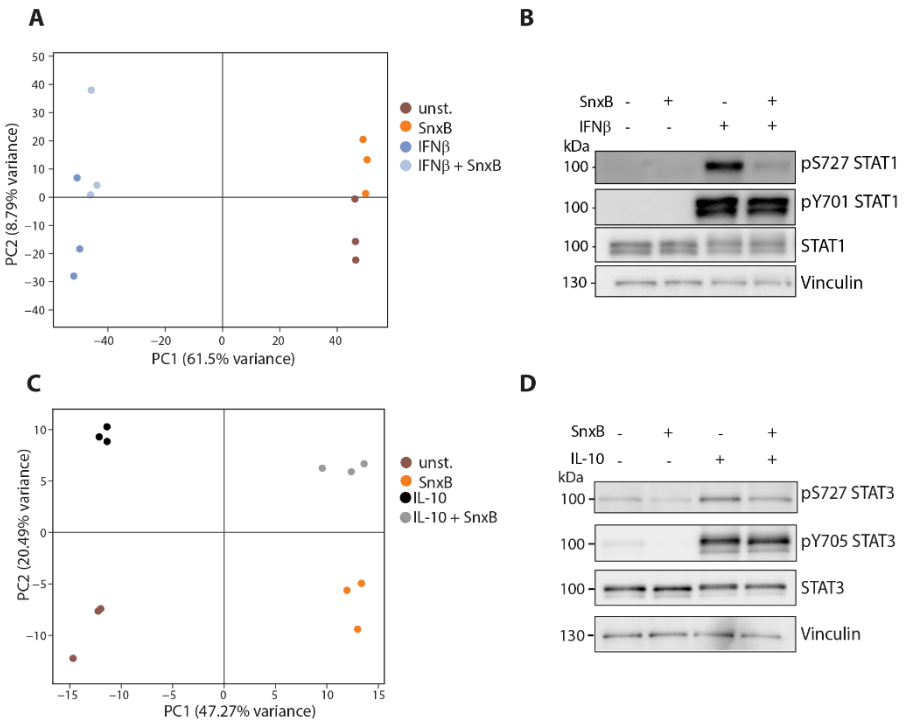

Supplementary Figure 3 (related to Figure 3). RNA-seq replicate clustering and STATs phosphorylation
(**A**) PCA of RNA-seq replicates of BMDMs pretreated with SnxB (2.5 µM, 30 min) or vehicle and stimulation with IFNβ (250 IU/mL, 4 h). n = 3.
(**B**) STAT1 phosphorylation in BMDMs pretreated with SnxB (2.5 µM, 30 min) and stimulated with IFNβ (250 IU/mL, 45 min). Whole cell extracts were analyzed by western blotting using antibodies to pS727 STAT1, pY701 STAT1 and total STAT1. Vinculin was used as a loading control.
(**C**) PCA of RNA-seq replicates of BMDMs pretreated with SnxB (2.5 µM, 30 min) or vehicle and stimulated with IL-10 (10 ng/mL, 4 h). n = 3.
(**D**) STAT3 phosphorylation in BMDMs pretreated with SnxB (2.5 µM, 30 min) and stimulated with IL-10 (10 ng/mL, 45 min). Whole cell extracts were analyzed by western blotting using antibodies to pS727 STAT3, pY705 STAT3 and total STAT3. Vinculin was used as a loading control.

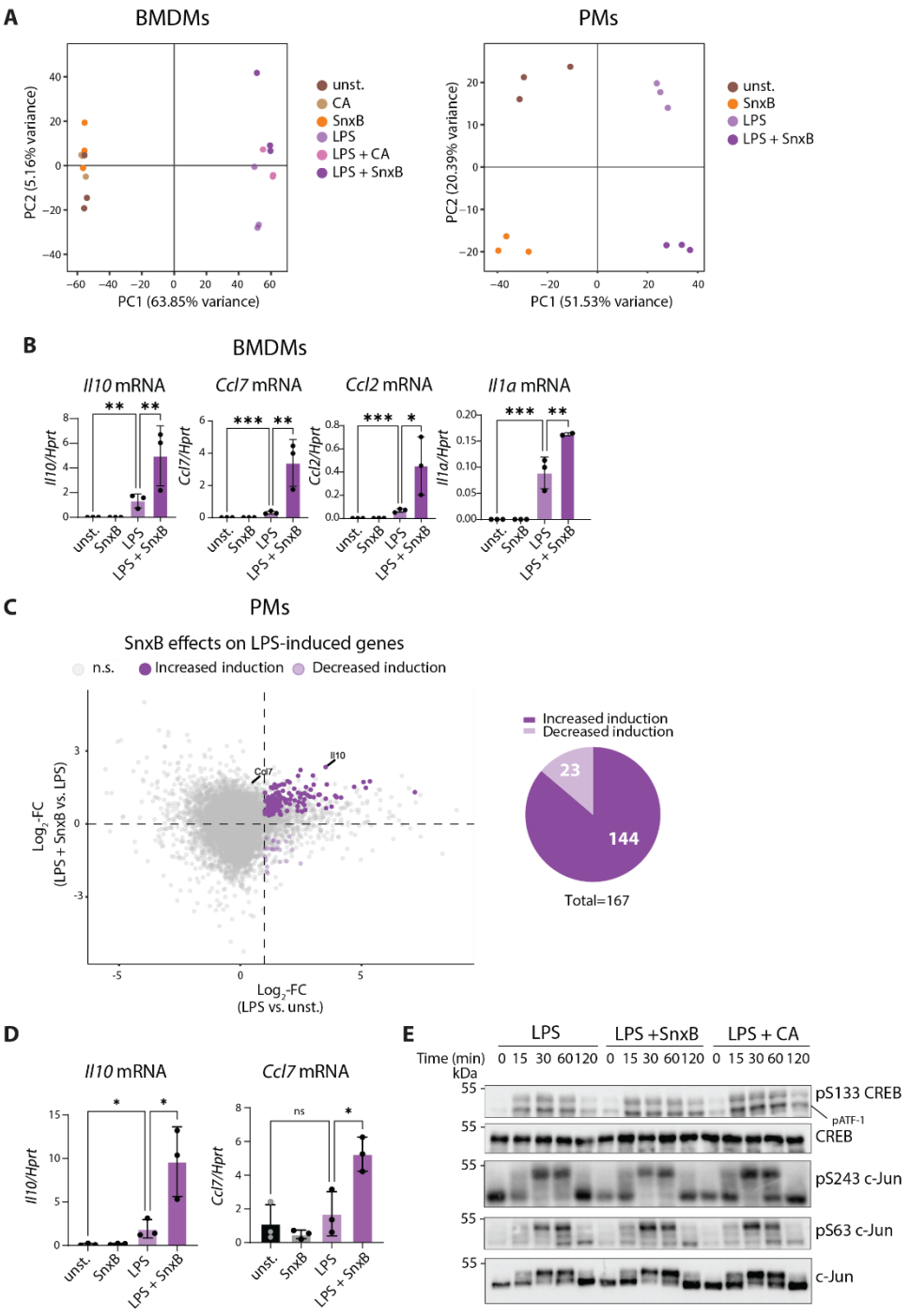

Supplementary Figure 4 (related to Figure 4). Regulation of LPS responses in BMDMs and PMs by Mediator kinase

(**A**) PCA of RNA-seq replicates of BMDMs and PMs stimulated with LPS (10 ng/mL, 4 h) after pretreatment with SnxB (2.5 µM, 30 min) or CA (0.1 µM, 30 min). n = 3.

(**B**) *Il10*, *Ccl7*, *Ccl2* and *Il1a* mRNA expression in BMDMs treated as in (A). mRNA expression was quantitated using RT-qPCR. Relative values to *Hprt* expression are shown. Mean of biological replicates ± SD; n= 3; unpaired Student´s t-test, *p < 0.05, **p < 0.01, ***p < 0.001.

(**C**) Effects of Mediator kinase inhibition on LPS-induced genes in PMs. PMs were pretreated with SnxB (2.5 µM, 30 min) or vehicle, stimulated with LPS (10 ng/mL, 4 h) and analyzed by RNA-seq. Genes induced more than 2-fold by LPS (Log2-FC > 1,

padj ≤ 0.05) showing higher induction upon SnxB treatment (Log2-FC > 0, padj ≤ 0.05) are in dark purple; genes showing decreased induction (Log2-FC < 0, padj ≤ 0.05) are in light purple. Grey, not significant. Pie chart summarizes the scatterplot results.
(**D**) *Il10* and *Ccl7* mRNA expression in PMs treated as in (B). mRNA expression was quantitated using RT-qPCR. Relative values to *Hprt* expression are shown. Mean of biological replicates ± SD; n= 3; unpaired Student´s t-test, *p < 0.05; ns, not significant.
(**E**) Phosphorylation of CREB and c-Jun TFs in BMDMs pretreated with SnxB (2.5 µM, 30 min) or CA (0.1 µM, 30 min) and stimulated with LPS (10 ng/mL) for 15 min, 30 min, 60 min or 120 min. Whole cell extracts were analyzed by western blotting using antibodies to pS133 CREB, pS243 c-Jun, pS63 c-Jun and total c-Jun and CREB.

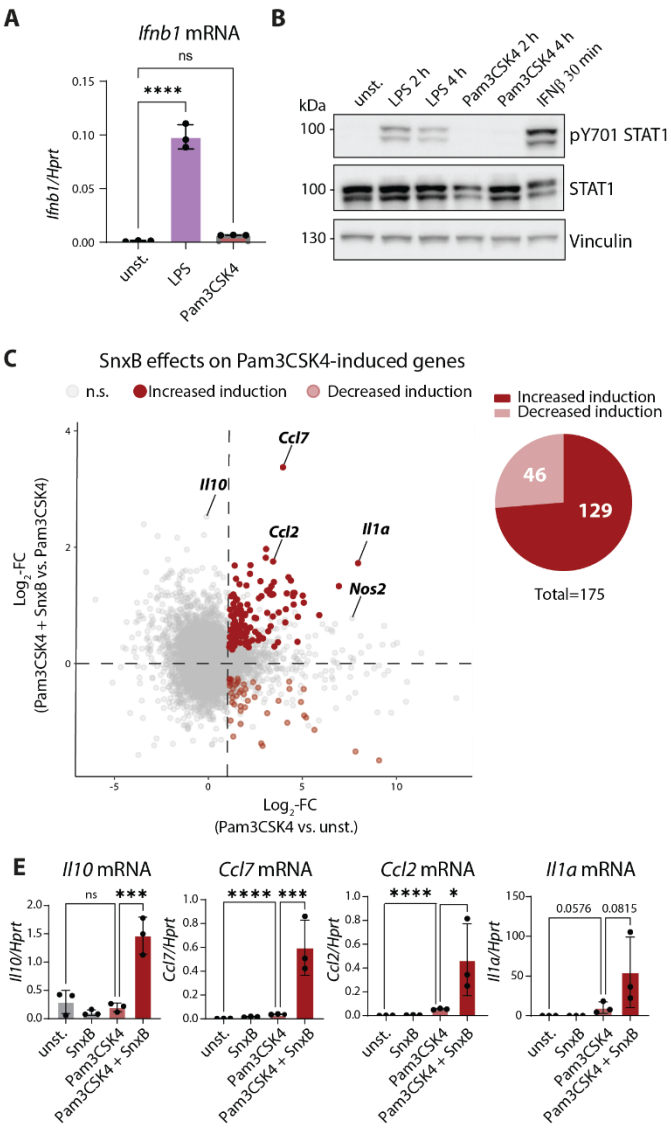

Supplementary Figure 5 (related to Figure 4). Regulation of Pam3CSK4 responses in BMDMs by Mediator kinase

(**A**) *Ifnb1* mRNA expression in BMDMs stimulated with LPS (10 ng/mL, 4 h) or Pam3SCK4 (10 ng/mL, 4 h). mRNA expression was quantitated using RT-qPCR. Relative values to *Hprt* expression are shown. Mean of biological replicates ± SD; n= 3; one-way ANOVA with Šídák's multiple comparisons test; ****p < 0.0001, ns, not significant.

(**B**) Phosphorylation of STAT1 at Y701 in BMDMs stimulated with LPS, Pam3SCK4 or IFNβ. BMDMs were stimulated with LPS (10 ng/mL) for 2 h or 4 h, Pam3SCK4 (10 ng/mL) for 2 h or 4 h, or IFNβ (250 IU/mL) for 30 min. Whole cell extracts were analyzed by western blotting using antibodies to pY701 STAT1 and total STAT1. Vinculin, loading control.

(**C**) Effects of Mediator kinase inhibition on Pam3SCK4-induced genes in BMDMs. BMDMs were pretreated with SnxB (2.5 μM, 30 min) or vehicle, stimulated with Pam3SCK4 (10 ng/mL, 4h) and analyzed by RNA-seq. Genes induced more than 2-fold by LPS (Log2-FC > 1, padj ≤ 0.05) showing higher induction upon SnxB treatment (Log2-FC > 0, padj ≤ 0.05) are in dark red; genes showing decreased induction (Log2-FC < 0, padj ≤ 0.05) are in light red. Grey, not significant. Pie chart summarizes the scatterplot results.

(**D**) *Ccl7* pre-mRNA expression in BMDMs treated as in (C). pre-mRNA expression was quantitated using RT-qPCR. Relative values to *Hprt* expression are shown. Mean of biological replicates ± SD; n= 3; unpaired Student´s t-test, **p < 0.01, ****p < 0.0001.
(**E**) *Il10*, *Ccl7*, *Ccl2* and *Il1a* mRNA expression in BMDMs treated as in (C). mRNA expression was quantitated using RT-qPCR. Relative values to *Hprt* expression are shown. Mean of biological replicates ± SD; n= 3; unpaired Student´s t-test, *p < 0.05, ***p < 0.001, ****p < 0.0001. p-values for *Il1a* are depicted. ns, not significant.

Figure S6

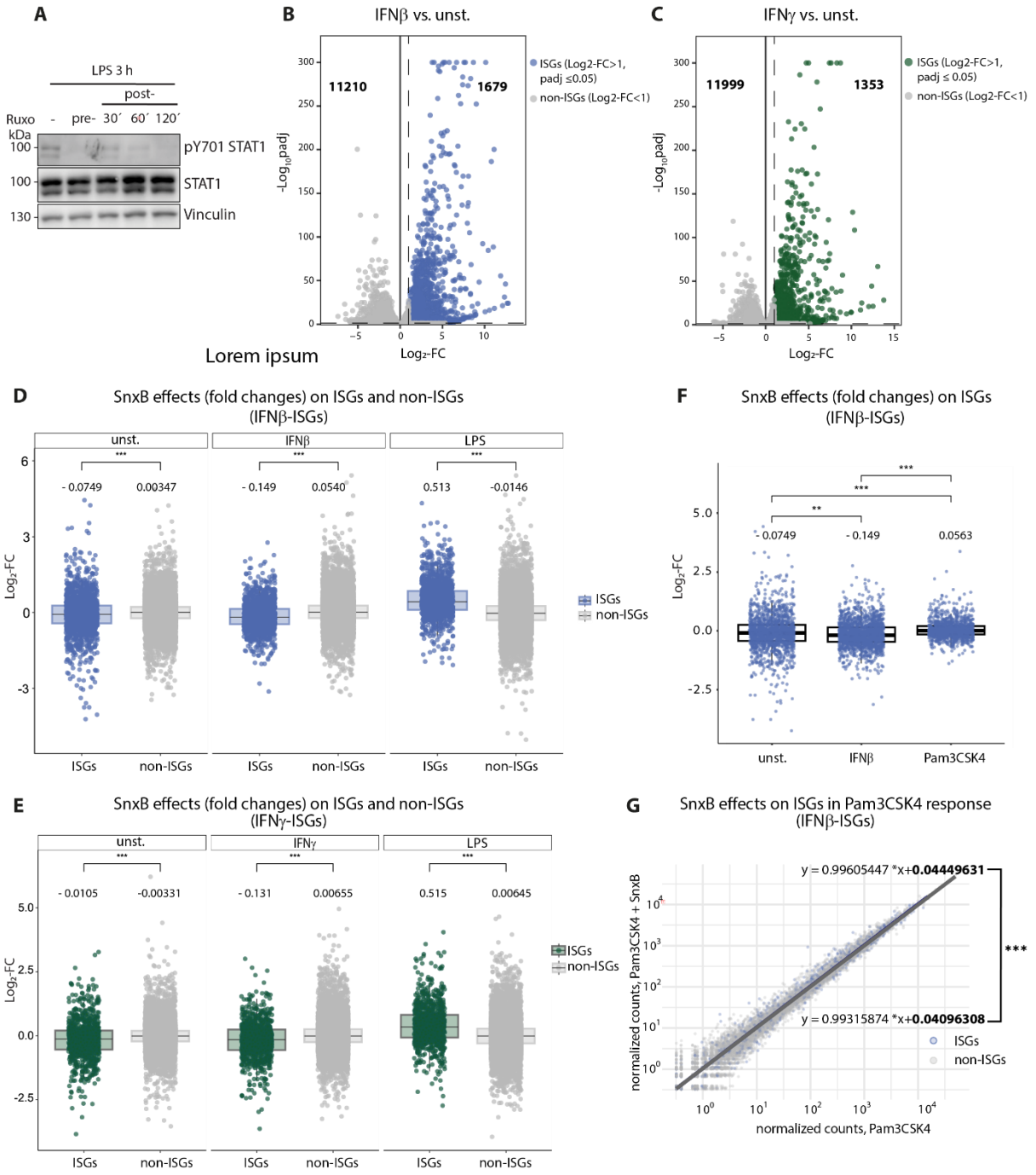

Supplementary Figure 6 (related to Figure 5). Impact of Mediator kinase inhibition on ISGs and non-ISGs in IFN, LPS and Pam3CSK4 responses

(**A**) Inhibition of LPS-induced STAT1 phosphorylation at Y701 by ruxolitinib (Ruxo). BMDMs were stimulated with LPS (10 ng/mL, 3 h) and either pretreated pretreated with Ruxo (1.5 µM) for 1 h before stimulation or treated with Ruxo 30 min, 60 min or 120 min after stimulation. Whole cell extracts were analyzed by western blotting using antibodies to pY701 STAT1 and total STAT1. Vinculin, loading control.

(**B, C**) Identification of IFNβ-induced and IFNγ-induced ISGs in BMDMs. RNA-seq data from Figures 3A and 3C were analyzed for genes induced by IFNβ (Log2-FC > 1, padj ≤ 0.05) (**B**) or IFNγ (**C**) to define IFNβ-ISGs and IFNγ-ISGs, respectively. Genes not

fulfilling the filter (Log2-FC > 1, padj ≤ 0.05) were regarded as non-ISGs. Dashed line marks the Log2-FC > 1 cutoff. Number of ISGs and non-ISGs is indicated.
(**D**) Comparison of SnxB-dependent effects (Log_2-FC) on IFNβ-ISGs versus non-ISGs under unstimulated, IFNβ- or LPS-stimulated conditions. RNA-seq data are from Figure 3C; ISGs and non ISGs are defined in (B). Mean SnxB-dependent changes across ISGs and non-ISGs are shown for each condition; differences in mean changes between ISGs versus non-ISGs were evaluated using unpaired Student´s *t*-test, ***p ≤ 0.001.
(**E**) Comparison of SnxB-dependent effects (Log_2-FC) on IFNγ-ISGs versus non-ISGs under unstimulated, IFNγ- or LPS-stimulated conditions. RNA-seq data are from Figure 3A; ISGs and non ISGs are defined in (C). Mean SnxB-dependent changes across ISGs and non-ISGs are shown for each condition; differences in mean changes between ISGs versus non-ISGs were evaluated using unpaired Student´s *t*-test, ***p ≤ 0.001.
(**F**) SnxB-dependent effects (Log_2-FC) on IFNβ-ISGs (n = 1679) under unstimulated, IFNβ- or Pam3CSK4-stimulated conditions. RNA-seq data are from Figure S5C; ISGs are defined in (B). Mean changes across ISGs are shown. The mean changes are negative under unstimulated and IFNβ-stimulated conditions but positive under Pam3CSK4-stimulated conditions. Unpaired Student´s *t*-test, ***p ≤ 0.01* ***p ≤ 0*.001.
(**G**) Comparison of normalized RNA-seq counts for ISGs and non-ISGs in SnxB-treated and Pam3CSK4-stimulated BMDMs versus Pam3CSK4-stimulated BMDMs. Means of normalized counts were plotted, and linear regression slopes and intercepts were calculated for IFNβ-ISGs and non-ISGs. ISGs and non-ISGs are defined in (B). Significance of regression intercept differences between ISGs and non-ISGs: unpaired Student's *t*-test, *** $p \leq 0.001$

Figure S7

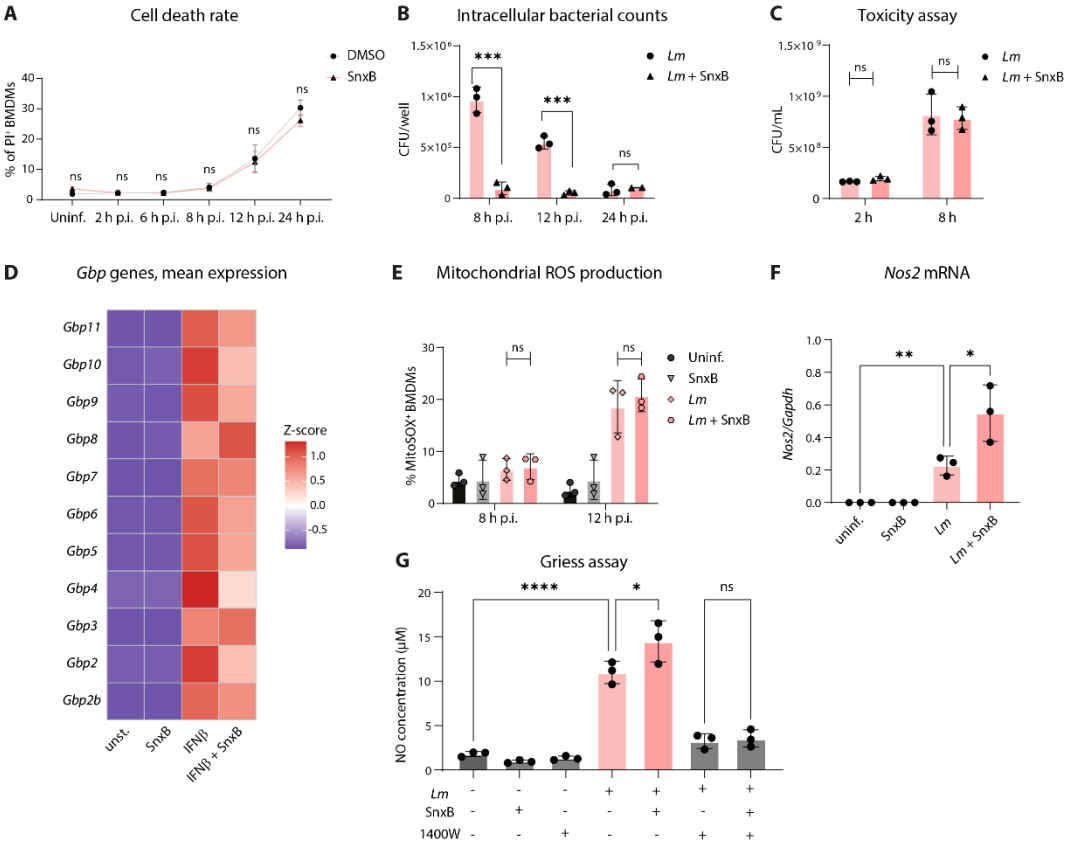

Supplementary Figure 7 (related to Figure 6). Regulation of BMDM defense against *Lm* infection by Mediator kinase

(**A**) Cell death time course during *Lm* infection. BMDMs were pretreated with SnxB (2.5 μM, 30 min) and subsequently infected with *Lm* (MOI 10) for the indicated times. Cell death was assessed using propidium iodide staining (PI; 1 μg/mL) followed by flow cytometry. Percentage of PI-positive (PI^+) cells is shown. Mean of independent biological replicates ± SD. Two-way ANOVA with Šídák's multiple comparisons test; n = 3; ns, not significant.

(**B**) Time course of intracellular bacterial load. BMDMs were pretreated with SnxB (2.5 μM, 30 min) or vehicle and infected with *Lm* at MOI 10 for the indicated times. Bacterial loads are shown as CFUs. Two-way ANOVA with Šídák's multiple comparisons test; n= 3; ***$p < 0.001$, ns, not significant

(**C**) Assessment of SnxB toxicity for *Lm*. Time course of *Lm* CFUs retrieved upon co-incubation with SnxB (2.5 μM) or vehicle. Two-way ANOVA with Šídák's multiple comparisons test; n = 3; ns, not significant.

(**D**) Regulation of *Gbp* genes by Mediator kinase in IFNβ-stimulated BMDMs. Heatmap showing Z-scores of normalized RNA-seq counts for the *Gbp* gene family in IFNβ-stimulated BMDMs pretreated with SnxB or vehicle. RNA-seq data are from Figure 3C.

(**E**) Mitochondrial ROS production in *Lm*-infected BMDMs. BMDMs were pretreated with SnxB (2.5 μM, 30 min) or vehicle and infected with *Lm* (MOI 10) for the indicated time points. Shown is the percentage of MitoSOX red^+ cells determined by flow cytometry. Two-way ANOVA with Šídák's multiple comparisons test; n = 3; ns, not significant.

(**F**) *Nos2* mRNA expression in *Lm*-infected BMDMs. BMDMs were pretreated with SnxB (2.5 µM, 30 min) or vehicle and infected with *Lm* (MOI 10) for 8 h. mRNA expression was quantitated using RT-qPCR. Relative values to *Gapdh* expression are shown. Mean of biological replicates ± SD; n= 3; unpaired Student´s t-test, *p < 0.05, **p < 0.01.
(**G**) Nitrite production by *Lm*-infected BMDMs. BMDMs were pretreated with SnxB (2.5 µM, 30 min) or vehicle and infected with *Lm* (MOI 10) for 12 h. The iNOS inhibitor 1400W (10 µM, 30 min pretreatment) was used as indicated. One-way ANOVA with Tukey`s multiple comparisons test; n = 3; *p < 0.05, ****p < 0.0001, ns, not significant.

Cytoplasmic mRNA decay controlling inflammatory gene expression is determined by pre-mRNA fate decision

Annika Bestehorn, Julius von Wire´n, Christina Zeiler, Jeanne Fesselet, Sebastian Didusch, **Maurizio Forte**, Kevin Doppelmayer, Martina Borroni, Anita Le Heron, Sara Scinicariello, WeiQiang Chen, Manuela Baccarini, Vera Pfanzagl, Gijs A. Versteeg, Markus Hartl, and Pavel Kovarik

Published in *Molecular Cell* on February 20, 2025:
DOI: 10.1016/j.molcel.2025.01.001

This study redefines the role of tristetraprolin (TTP) in inflammatory mRNA decay by uncovering a critical requirement for nuclear localization and early RNA engagement. Using RNA-binding-deficient and nuclear localization signal (NLS) mutants, we show that TTP must localize to the nucleus to recruit the mRNA decay machinery. Both mutants lost interactions with key decay factors and failed to bind canonical targets. Crosslinking and immunoprecipitation followed by sequencing (CLIP-seq) confirmed that TTP preferentially associates with pre-mRNAs rather than mRNA. These findings reveal that TTP-mediated repression begins in the nucleus, highlighting subcellular localization and RNA-binding as essential for its function in controlling inflammation.

Contribution:
In this study, I co-designed, performed, and analyzed dot-blot experiments together with Annika Bestehorn to assess the global RNA-binding activity of the TTP mutant lacking its nuclear localization signal (NLS).

Molecular Cell

Cytoplasmic mRNA decay controlling inflammatory gene expression is determined by pre-mRNA fate decision

Graphical abstract

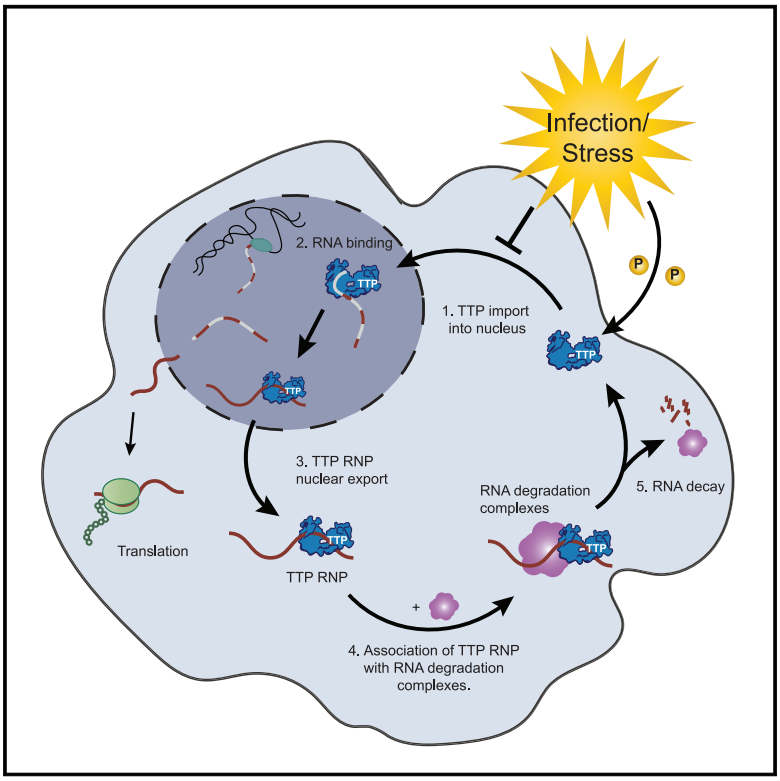

Highlights

- Cytoplasmic decay of TTP target mRNAs is licensed in the nucleus
- The main binding target of TTP is pre-mRNA, not mature mRNA
- Nucleocytoplasmic shuttling of TTP depends on its binding to RNA
- RNA binding is required for TTP to associate with mRNA degradation complexes

Authors

Annika Bestehorn, Julius von Wirén, Christina Zeiler, ..., Gijs A. Versteeg, Markus Hartl, Pavel Kovarik

Correspondence

pavel.kovarik@univie.ac.at

In brief

While mRNAs encoding inflammatory cytokines are degraded in the cytoplasm, Bestehorn et al. show that the decay of these mRNAs is licensed in the nucleus. This is achieved through binding of the RNA-destabilizing protein TTP to cytokine pre-mRNAs, ensuring their elimination before translation and thereby promoting the resolution of inflammation.

Bestehorn et al., 2025, Molecular Cell *85*, 742–755
February 20, 2025
https://doi.org/10.1016/j.molcel.2025.01.001

CellPress

CellPress
OPEN ACCESS

Molecular Cell

Article

Cytoplasmic mRNA decay controlling inflammatory gene expression is determined by pre-mRNA fate decision

Annika Bestehorn,[1,2,3] Julius von Wirén,[1,2,3,7] Christina Zeiler,[1,2,3,7] Jeanne Fesselet,[1,2,3,7] Sebastian Didusch,[1,2,3,7] Maurizio Forte,[1,2,3] Kevin Doppelmayer,[1,2] Martina Borroni,[1,2] Anita Le Heron,[1,2] Sara Scinicariello,[1,2,3] WeiQiang Chen,[4] Manuela Baccarini,[1,2] Vera Pfanzagl,[5] Gijs A. Versteeg,[1,2] Markus Hartl,[4,6] and Pavel Kovarik[1,2,8,*]

[1]Max Perutz Labs, Vienna Biocenter Campus (VBC), Dr.-Bohr-Gasse 9, 1030 Vienna, Austria
[2]University of Vienna, Max Perutz Labs, Department of Microbiology, Immunobiology and Genetics, Dr.-Bohr-Gasse 9, 1030 Vienna, Austria
[3]Vienna Biocenter PhD Program, a Doctoral School of the University of Vienna and Medical University of Vienna, 1030 Vienna, Austria
[4]Mass Spectrometry Facility, Max Perutz Labs, Vienna Biocenter Campus (VBC), Dr. Bohr-Gasse 7, 1030 Vienna, Austria
[5]University of Natural Resources and Life Sciences, Vienna, Department of Chemistry, Institute of Biochemistry, Muthgasse 18, 1190 Vienna, Austria
[6]University of Vienna, Max Perutz Labs, Department for Biochemistry and Cell Biology, Vienna Biocenter Campus (VBC), Dr. Bohr-Gasse 9, 1030 Vienna, Austria
[7]These authors contributed equally
[8]Lead contact
*Correspondence: pavel.kovarik@univie.ac.at
https://doi.org/10.1016/j.molcel.2025.01.001

SUMMARY

The fidelity of immune responses depends on timely controlled and selective mRNA degradation that is largely driven by RNA-binding proteins (RBPs). It remains unclear whether stochastic or directed processes govern the selection of an individual mRNA molecule for degradation. Using human and mouse cells, we show that tristetraprolin (TTP, also known as ZFP36), an essential anti-inflammatory RBP, destabilizes target mRNAs via a hierarchical molecular assembly. The assembly formation strictly relies on the interaction of TTP with RNA. The TTP homolog ZFP36L1 exhibits similar requirements, indicating a broader relevance of this regulatory program. Unexpectedly, the assembly of the cytoplasmic mRNA-destabilization complex is licensed in the nucleus by TTP binding to pre-mRNA, which we identify as the principal TTP target rather than mRNA. Hence, the fate of an inflammation-induced mRNA is decided concomitantly with its synthesis. This mechanism prevents the translation of excessive and potentially harmful inflammation mediators, irrespective of transcription.

INTRODUCTION

Immune responses are dependent on rapid and precisely controlled adjustments in the transcriptome and proteome to ensure protection against pathogens while minimizing damage to the host. A key safeguarding mechanism against an aggravated immune response is the selective destabilization of mRNAs coding for inflammatory mediators.[1] The major drivers of mRNA destabilization are *cis*-acting RNA-binding proteins (RBPs), which act mostly as adaptors for the RNA degradation machinery, notably the CCR4-NOT deadenylation and the DCP decapping complexes.[2–5] The selectivity in mRNA destabilization is defined by the interaction of an RBP with a sequence or structure in the target RNA. However, it remains unclear whether this interaction occurs randomly or in a defined step of the mRNA life cycle, e.g., prior to or after target mRNA translation, and what the hierarchy of RBP-driven mRNA decay is. Answering these basic questions is of key importance for understanding how biological responses to external cues, including inflammatory conditions during host defense, are efficiently controlled.

The canonical mRNA decay pathway comprises mRNA poly(A) tail shortening by deadenylation and 7-methylguanosine 5′ cap removal.[6] The unprotected mRNA is subsequently degraded in 5′–3′ direction by the XRN1 exonuclease and in 3′–5′ direction by the exosome in the cytoplasm.[7] A growing body of evidence indicates that these steps are intimately linked to the ribosome since a large portion of mRNA decay occurs co-translationally, and the deadenylation and decapping complexes associate with the ribosome.[7,8] mRNA decay mediated by RBPs is mechanistically less well characterized, and it might harbor steps distinct from the canonical mRNA decay pathway, depending on the specific RBP involved. RBPs are often involved in rapid gene expression reprogramming induced by external cues such as inflammatory

stimuli, suggesting that the RBP-mediated mRNA decay might differ from the steady-state decay pathway.

The mRNA-destabilizing RBP tristetraprolin (TTP, gene name Zfp36) is a major driver of the inflammatory gene expression control.[9] TTP deletion in mice results in multi-organ and eventually lethal inflammation caused by increased stability and expression of cytokine or chemokine mRNAs such as *Tnf*, *Il23*, *Il1a*, or *Ccl3*.[10–13] TTP binds to adenine-uridine-rich elements (AREs) in 3′ untranslated regions (UTRs) via its tandem zinc-finger (TZF) domain and destabilizes the target RNA via interactions with CCR4-NOT and DCP complexes.[14–20] Stress cues that activate the p38 MAP kinase induce TTP phosphorylation by MK2, thereby increasing TTP protein stability but inhibiting its mRNA-destabilization activity.[21,22]

Here, using proteomics, transcriptome-wide protein-RNA interaction studies, and functional approaches, we present evidence that the principal TTP target is pre-mRNA, not mature mRNA, and that the nuclear TTP-pre-mRNA interaction is a prerequisite for the formation of TTP-containing mRNA-processing ribonucleoprotein (RNP) complexes in the cytoplasm. The data reveal that the fate of TTP target RNAs is decided at the level of pre-mRNA, i.e., prior to translation, thereby ensuring efficient cessation of the inflammatory response, including cytokine production. Our results further indicate that the process is conserved in the TTP protein family.

RESULTS

RNA binding is a driver of the TTP interactome and enables the assembly of TTP-containing RNA degradation complexes

To understand the hierarchy of TTP-mediated mRNA decay, we determined molecular assemblies representing distinct steps of TTP-mediated mRNA decay using proximity-dependent labeling based on the reported engineered ascorbate peroxidase (APEX2).[23] We fused the murine wild-type (WT) TTP (GenBank: NP_035886) or an RNA-binding-deficient TZF TTP mutant (TZF^{mut}) N-terminally to APEX2 to obtain doxycycline-inducible APEX2 (APX) constructs WT-APX and TZF^{mut}-APX (Figure 1A). TZF^{mut} harbored the mutations C116R and C139R, which inactivate the zinc-coordinating properties of each of the two zinc fingers (ZFs).[24] GFP-APX was used as a background labeling control. The constructs were inducibly expressed in HEK-293 cells under steady-state and anisomycin-imposed (+aniso) stress conditions (Figure 1B). Anisomycin increases, similar to other stress cues, phosphorylation of TTP at S52 and S178, thereby reducing TTP gel mobility[25–27] (Figure 1B).

Proximity labeling with biotin-phenol (30 min) and H_2O_2 (1 min) resulted in increased levels of biotinylated proteins in lysates and streptavidin pull-down samples from WT-APX-, TZF^{mut}-APX-, or GFP-APX-expressing cells compared with samples without H_2O_2 treatment (Figure S1A). Signals in samples without H_2O_2 treatment were caused by endogenous biotinylation and biotin-dependent carboxylases. LC-MS/MS analysis of biotinylated proteins isolated by streptavidin pull-down identified similar numbers of proteins in all sample replicates and clustering of corresponding replicates (Figures 1C and S1B; Table S1). The WT-APX cluster was remarkably separated from the TZF^{mut}-APX cluster, indicating that binding of TTP to RNA was a major determinant of the TTP interactome. Surprisingly, anisomycin treatment changed the position of WT-APX and TZF^{mut}-APX samples such that both clustered in the same area (Figure 1C).

Specific interactors were defined as proteins enriched ($\log_2$FC > 1, *p*adj. $\leq$ 0.05, n = 3) over GFP-APX as determined by the amica proteomics platform.[28] WT-APX displayed 184 enriched proteins, while the number of enriched proteins was substantially lower in TZF^{mut}-APX, WT-APX+aniso, and TZF^{mut}-APX+aniso (51, 37, and 50 proteins, respectively) samples (Table S1). The WT-APX, TZF^{mut}-APX, and WT-APX+aniso interactomes showed only limited overlap (Figure 1D). However, anisomycin changed the divergent WT-APX and TZF^{mut}-APX interactomes into highly similar ones, indicating the acquisition of a uniform proximal environment by RNA-bound and RNA-unbound TTP upon stress (Figure S1C).

The WT-APX interactome comprised the XRN1 exonuclease as well as the deadenylation and decapping components CNOT1, DCP1, DCP2, and EDC3 (Figure 1E; Table S1), which were previously reported to bind to TTP.[18–20,29,30] Strikingly, the deadenylase and decapping complexes were largely missing in the TZF^{mut}-APX interactome, indicating that these interactions depend on TTP binding to RNA (Figure 1E; Table S1). This was corroborated by the interaction heat map for all detected subunits of the deadenylation and decapping complexes (Figure 1F). The preferential association of CNOT1, DCP1a, and EDC3 with WT-APX as compared with TZF^{mut}-APX was verified by western blotting (Figure S1D). Anisomycin treatment abolished WT-APX associations with the deadenylase and decapping complexes (Figure 1E; Table S1), consistent with the reported inhibition of the deadenylase binding to phosphorylated TTP.[21] The TZF^{mut}-APX+aniso interactome was devoid of the deadenylation and decapping complexes, similar to the TZF^{mut}-APX and WT-APX+aniso interactomes (Figure 1E; Table S1).

The data reveal an RNA-driven hierarchical assembly of TTP-containing mRNA-processing complexes.

RNA binding prevents continuous TTP accumulation in the nucleus

The RNA-binding-dependent and -independent TTP interactomes were further characterized by Gene Ontology (GO) analysis. Top-ranked GO terms significantly overrepresented in the WT-APX interactome, i.e., in proteins enriched in WT-APX over GFP-APX profiles, were consistent with the established TTP function and included "cytoplasmic RNP granule" and "P-body" in the category cellular compartment (CC), "posttranscriptional regulation of gene expression" and "regulation of RNA stability" in biological process (BP), and "RNA binding" in molecular function (MF) (Figure 2A). By contrast, no such terms were found in the TZF^{mut}-APX interactome, which instead comprised the CC GO terms "nucleus" and "nucleoplasm," suggesting a nuclear localization, and only one BP and no MF GO terms were identified (Figure 2A). GO terms overrepresented in the anisomycin-dependent interactomes (WT-APX+aniso and TZF^{mut}-APX+aniso) were inconsistent and hence not informative (Figure S2A). GO term comparison across all constructs and treatments highlighted the functional association of WT-APX

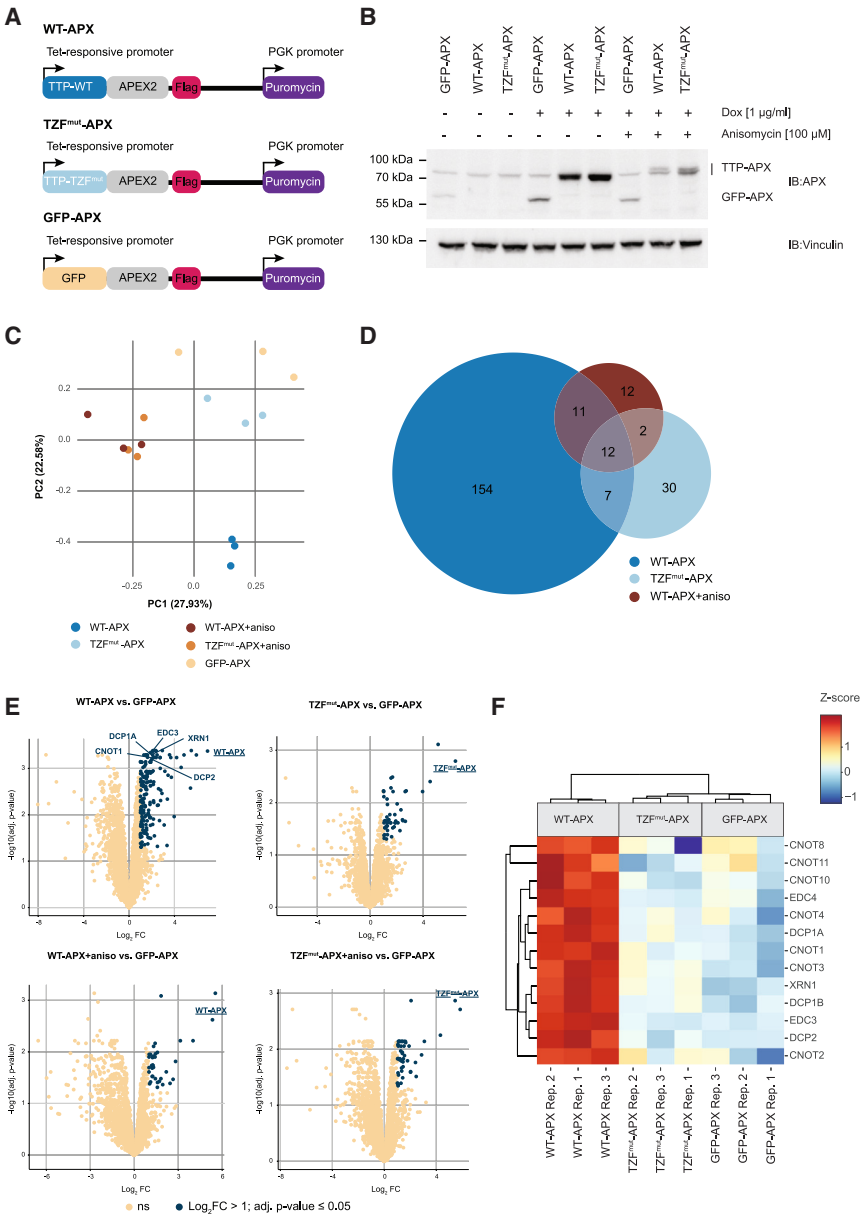

Figure 1. TTP binding to RNA is prerequisite for its association with RNA degradation complexes

(A) Schematic representation of APEX2-based proximity labeling constructs.

(B) Doxycycline-induced (1 µg/mL dox, 3.5 h) expression of WT-APX, TZF^{mut}-APX, and GFP-APX in HEK-293 cells analyzed by western blotting. Anisomycin (+aniso, 100 µM, 1.5 h) was used as indicated. Immunoblot (IB): APX and vinculin (loading control). TTP-APX and GFP-APX fusion proteins are indicated. Slower-migrating TTP-APX fusions in anisomycin samples correspond to hyperphosphorylated proteins.

(C–F) APX-based proximal TTP interactome in HEK-293 cells analyzed by LC-MS/MS. Induction of WT-APX, TZF^{mut}-APX, and GFP-APX and anisomycin treatment were as in (B). Following labeling, biotinylated proteins were enriched and analyzed by LC-MS/MS. (C) Principal-component analysis (PCA) of protein intensities visualizing replicate clusters. (D) Overlap of specific WT-APX, TZF^{mut}-APX, and WT-APX+aniso interactomes. Specific interactomes are defined as significantly enriched proteins ($\log_2$FC > 1, $p$adj. ≤ 0.05, n = 3) in differential enrichment analyses of WT-APX vs. GFP-APX (for WT-APX interactome), TZF^{mut}-APX vs. GFP-APX (TZF^{mut}-APX interactome), and WT-APX+aniso vs. GFP-APX (WT-APX+aniso interactome). (E) Differential enrichment analysis of WT-APX vs. GFP-APX, TZF^{mut}-APX vs. GFP-APX, WT-APX+aniso vs. GFP-APX, and TZF^{mut}-APX+aniso vs. GFP-APX interactomes. Significantly enriched proteins ($\log_2$FC > 1, $p$adj. ≤ 0.05, n = 3) (blue) represent specific interactomes. WT-APX, TZF^{mut}-APX, and GFP-APX fusion constructs are underlined. Subunits of deadenylation and decapping complexes known to interact with TTP are annotated, and these interactors were not significantly enriched in the TZF^{mut}-APX, WT-APX+aniso, and TZF^{mut}-APX+aniso interactomes. (F) Heatmap analysis visualizing components of the deadenylation and decapping complexes, including XRN1 nuclease, in LC-MS/MS data for WT-APX, TZF^{mut}-APX, and GFP-APX replicates.

with mRNA destabilization while TZF^{mut}-APX was linked with the nucleus (Figure 2B). Specifically, the TZF^{mut}-APX interactome was depleted of almost all "P-body" genes while it was enriched in "nucleus" genes (Figure S2B). Several "nucleus" genes were also enriched in the WT-APX interactome (Figure S2B), consistent with the reported nucleocytoplasmic shuttling of the predominantly cytoplasmic TTP protein.[26,31] The known cytoplasmic TTP binder 14-3-3 protein (gene YWHAQ)[26] interacted with WT-APX rather than with TZF^{mut}-APX ($\log_2$fold-change [FC] = 0.52, $p$adj = 0.005; Table S1). These analyses indicated that TZF^{mut}-APX was localized in the nucleus. Interestingly, none of the interactomes contained an integral ribosomal protein signature, implying that the TTP-containing pool of mRNA degradation enzymes is distinct from the ribosome-associated mRNA degradation complexes (Figure S2C).

Validation of the proximity labeling results by immunofluorescence microscopy using HEK-293 cells expressing myc-tagged TTP-WT or TTP-TZF^{mut} confirmed that TTP-WT was mostly cytoplasmic while TTP-TZF^{mut} was confined to the nucleus (Figures 2C–2E). Moreover, TTP-WT but not TTP-TZF^{mut} colocalized with DCP1a and EDC4 foci (Figures 2F and 2G), which represent cytoplasmic RNP granules possessing decapping activity.[32] Anisomycin treatment resulted in phosphorylation of both TTP-WT and TTP-TZF^{mut} proteins causing them to relocate to the cytoplasm (Figures S3A–S3D), in agreement with studies showing that p38 MAPK- and MK2-driven phosphorylation promotes nuclear export of TTP.[31] In line with the reported inhibitory effect of stress-induced DCP1a phosphorylation on P-body formation,[33] anisomycin disrupted colocalization of TTP-WT with DCP1a and EDC4 foci (Figures S3E and S3F).

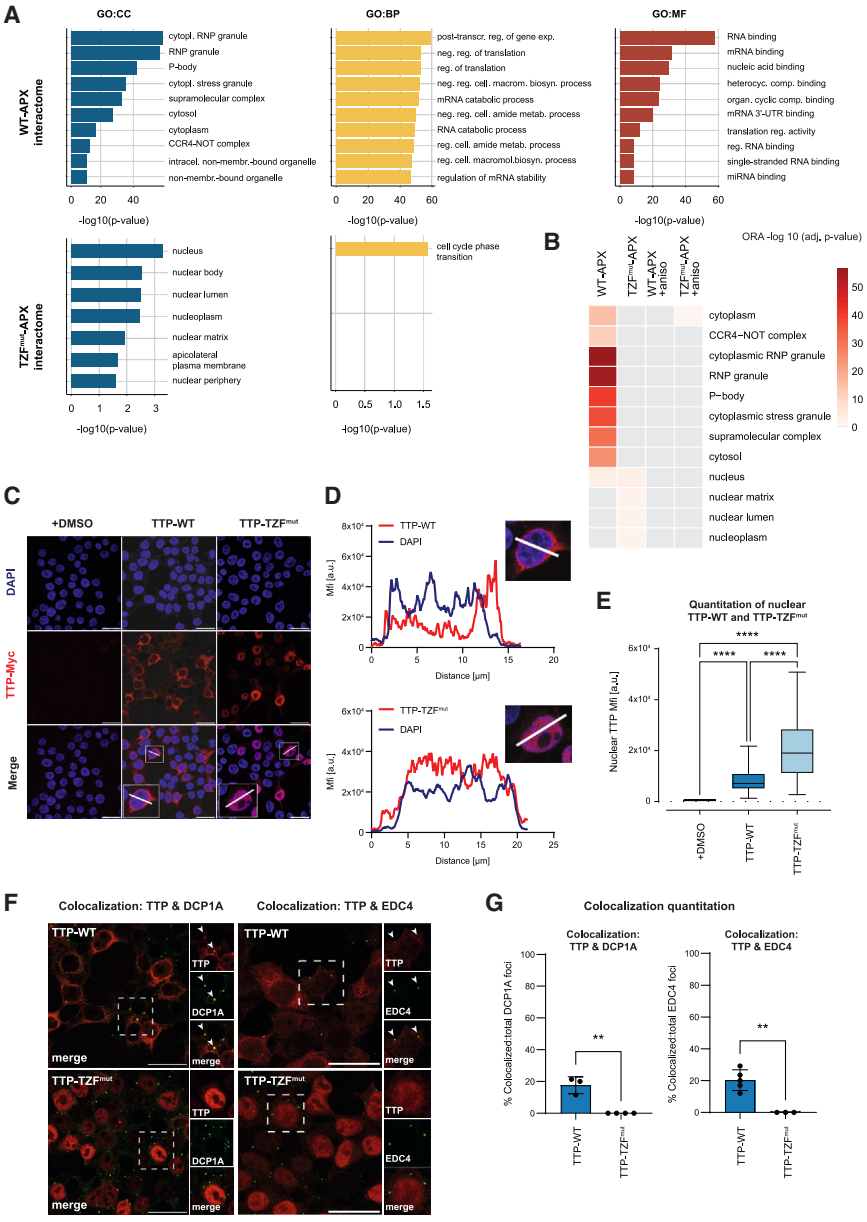

Figure 2. RNA binding prevents continuous nuclear accumulation of TTP

(A) GO term overrepresentation in WT-APX and TZF^{mut}-APX interactomes (interactomes defined in Figure 1E). Up to top 10 most significantly overrepresented terms in cellular compartment (CC), biological process (BP), and molecular function (MF) are shown. No MF terms were enriched in TZF^{mut}-APX interactome.

(B) Comparison of top 8 WT-APX and top 4 TZF^{mut}-APX terms (CC category) across all four analyzed interactomes. Top terms were selected from (A), and *p*adj. values of overrepresentation analysis (ORA) are color-coded. Gray: not significant.

(C and D) TTP-WT and TTP-TZF^{mut} localization in HEK-293 cells treated with dox (1 µg/mL, 3.5 h) to induce Myc-tagged construct expression (Myc antibody, red) or with vehicle (DMSO). Nucleus: DAPI (blue). Profile lines were drawn through representative cells (enlarged 2-fold in insets, scale bar, 25 µm) for quantitation of mean fluorescence intensity (MFI) shown in (D). TTP-TZF^{mut} and DAPI profiles were similar, implying nuclear localization of the protein.

(E) Quantitation of nuclear MFI of TTP-WT and TTP-TZF^{mut}. Masks for nuclear MFI quantitation were defined using ImageJ. Box represents interquartile range, and horizontal line in box depicts median. One-way analysis of variance (ANOVA) with Tukey's multiple comparisons test, $n = 62$, **** *p*adj. < 0.0001.

(F and G) Colocalization of TTP-WT or TTP-TZF^{mut} with endogenous DCP1A and EDC4 foci. (F) TTP-WT and TTP-TZF^{mut} (Myc antibody, red) were as in (C). Highlighted cells are shown in insets together with DCP1A or EDC4 (both green) in individual and merged channels. For EDC4 images, maximum intensity projections of Z-stacks were analyzed. Arrowheads: DCP1A or EDC4 foci colocalizing with TTP. Scale bar, 25 µm. (G) Quantitation of colocalization using Fiji Comdet. Student's t test. **padj. < 0.01, n = 60–113 cells.

Cumulatively, these results reveal that TTP binding to RNA has regulatory functions in addition to the canonical one: RNA binding is required for the maintenance of the cytoplasmic TTP pool and the association of TTP with RNA degradation complexes.

The role of RNA binding in the regulation of protein interactions and subcellular localization is conserved in TTP protein family members and across cell types

TTP is a member of a conserved family of TZF proteins that includes ZFP36L1 and ZFP36L2.[34] Sequence similarity peaks in the TZF domain with 70% identity (Figure S4A). To test whether the role of RNA binding is conserved in the TTP protein family, we determined the proximal interactomes and subcellular localization of ZFP36L1 and its RNA-binding-deficient derivative using the same strategy as for TTP. The ZFP36L1 APEX2 fusion proteins L1 WT-APX and L1 TZF^{mut}-APX were inducibly expressed in HEK-293 cells, and their labeling activity and proximal interactomes were determined (Figures S4B and S4C; Table S2).

Similar to TTP, the replicates of L1 WT-APX, L1 TZF^{mut}-APX, and GFP-APX samples clustered in separated areas (Figure S4D), and more proteins were enriched in L1 WT-APX over GFP-APX than in L1 TZF^{mut}-APX over GFP-APX (283 vs. 38) (Figure 3A; Table S2). L1 WT-APX interactome comprised subunits of the deadenylation and decapping complexes (e.g., CNOT1, CNOT4, DCP1B, EDC3, and EDC4), while these proteins were missing in L1 TZF^{mut}-APX interactome (Figures 3A and 3B). GO terms related to RNA degradation ("cytoplasmic RNP granule", "P-body", etc.) were overrepresented in proteins enriched in L1 WT-APX interactome over L1 TZF^{mut}-APX while proteins enriched in L1 TZF^{mut}-APX interactome over L1 WT-APX comprised terms related to nuclear

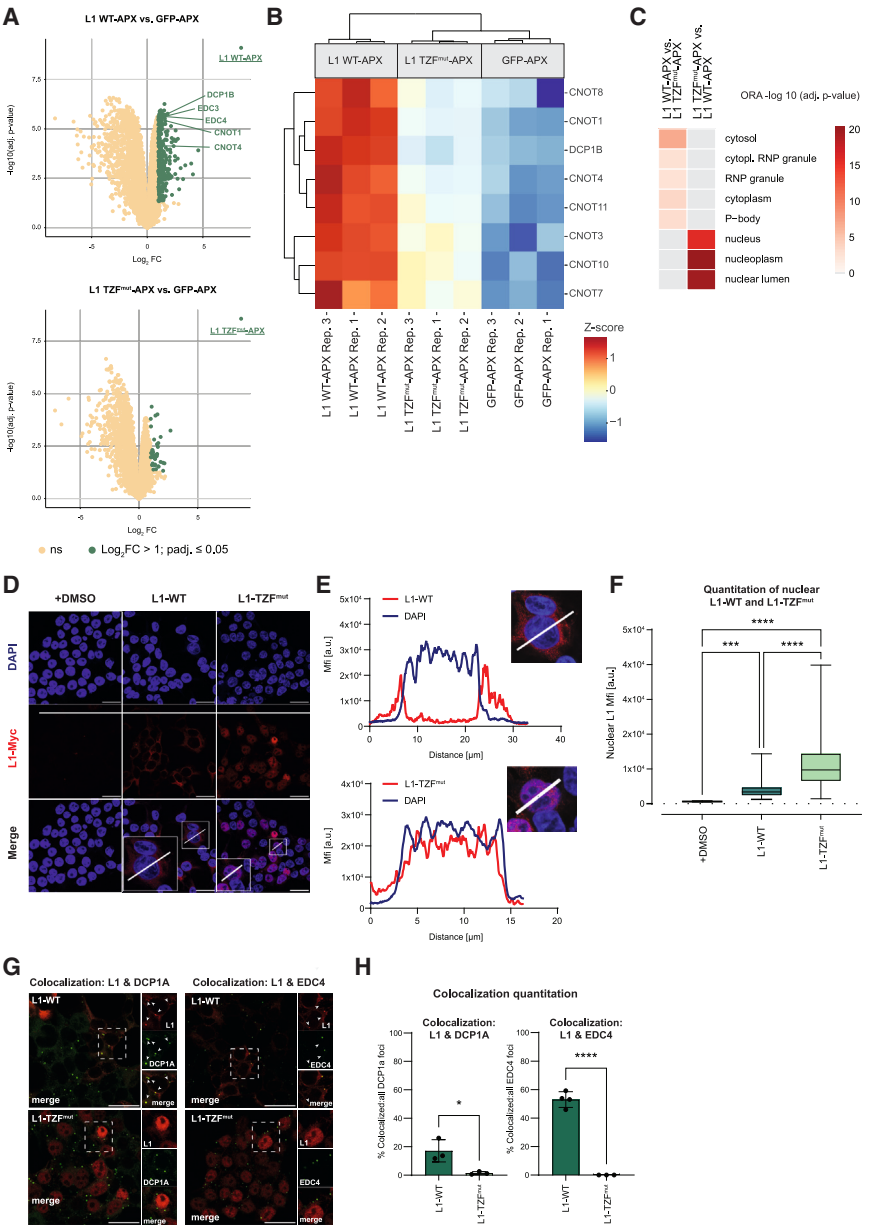

Figure 3. The regulatory function of RNA binding is conserved within the TTP protein family

(A) Differential enrichment analysis of L1 WT-APX vs. GFP-APX and L1 TZF^{mut}-APX vs. GFP-APX in HEK-293 cells. Construct expression was as in Figure 1; significantly enriched proteins ($log_2FC > 1$, $padj \leq 0.05$, $n = 3$): green; L1 WT-APX and L1 TZF^{mut}-APX constructs are underlined. Deadenylation and decapping proteins are annotated, and these interactors were not enriched in L1 TZF^{mut}-APX.

(B) Heatmap analysis visualizing components of the deadenylation and decapping complexes detected in L1 WT-APX, L1 TZF^{mut}-APX, and GFP-APX interactome replicates.

(C) GO term (CC) overrepresentation in proteins enriched ($log_2FC > 1$, $padj \leq 0.05$, $n = 3$) in L1 WT-APX vs. L1 TZF^{mut}-APX and L1 WT-APX vs. L1 TZF^{mut}-APX comparisons. ORA *p*adj. values are color-coded; gray: not significant.

(D and E) Localization of L1-WT and L1-TZF^{mut} in HEK-293 cells expressed and analyzed as in Figure 2C. Profile lines were drawn in representative cells (insets) for MFI quantitation shown in (E). Scale bar, 25 µm.

(F) Quantitation of nuclear L1-WT and L1 TZF^{mut} carried out as in Figure 2E, box represents interquartile range with median. One-way analysis of variance (ANOVA) with Tukey's multiple comparisons test. $n = 44$, ***padj. < 0.001, ****padj. < 0.0001.

(G and H) Colocalization of L1-WT or L1-TZF^{mut} with endogenous DCP1A and EDC4 foci. (G) L1-WT and L1-TZF^{mut} were as in (C). Highlighted cells are shown in insets together with DCP1A or EDC4 signals (green) in individual and merged channels. Arrowheads: DCP1A or EDC4 foci colocalizing with L1. Scale bar, 25 µm. (H) Quantitation of colocalization as in Figure 2G. Student's t test. *padj. < 0.05, ****padj. < 0.0001, n = 44–132 cells.

localization ("nuclear lumen" and "nucleus") (Figure 3C). Consistently, L1-TZF^{mut} localized in the nucleus and L1-WT was predominantly cytoplasmic (Figures 3D–3F). Furthermore, L1-WT but not L1-TZF^{mut} colocalized with DCP1a and EDC4 (Figures 3G and 3H). Thus, ZFP36L1 requires RNA binding for association with RNA processing complexes and maintenance of the cytoplasmic TTP pool.

TTP function is most evident in immune cells such as macrophages, which express physiological TTP targets, including cytokine and chemokine mRNAs.[14,35,36] We thus examined the role of RNA binding in TTP regulation using RAW 264.7 macrophages. We employed Turbo-ID (TID) proximity labeling[37] instead of APEX-based methods due to a high level of unspecific APEX2-dependent background we detected in these cells. Proximal interactomes were determined using RAW 264.7 macrophages harboring CRISPR-Cas9-mediated TTP deletion (hereafter referred to as RAW macrophages) and inducibly expressing TTP or the RNA-binding-deficient TTP mutant C-terminally fused to TID (TID-WT or TID-TZF^{mut}) (Figure S4E) or an empty TID (TID-E). The analysis revealed distinct clusters of TID-WT, TID-TZF^{mut}, and TID-E sample replicates (Figure S4F; Table S3). RNA degradation GO terms (e.g., cytoplasmic RNP granule and P-body) were enriched in the TID-WT interactome (TID-WT vs. TID-TZF^{mut} comparison, Table S3) while they were absent in the TID-TZF^{mut} interactome (Figure 4A). Instead, the TID-TZF^{mut} interactome comprised several nuclear compartment terms. The term nucleus was found also in the TID-WT interactome, in agreement with the localization of a minor TTP pool in the nucleus. GO term analysis of proteins overlapping between TID-WT interactome in RAW macrophages and TTP-APX interactome in HEK-293 contained RNA degradation

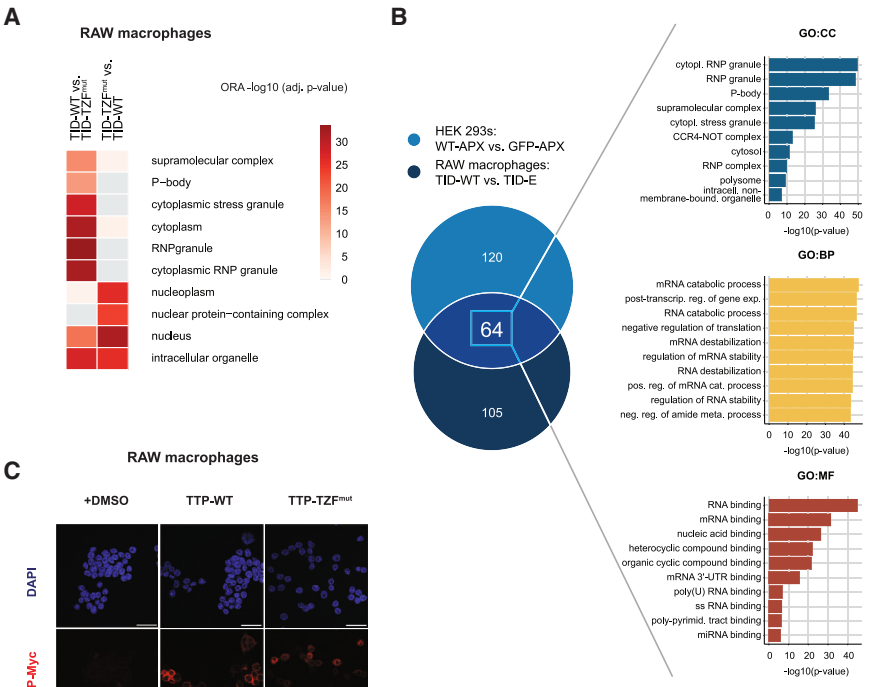

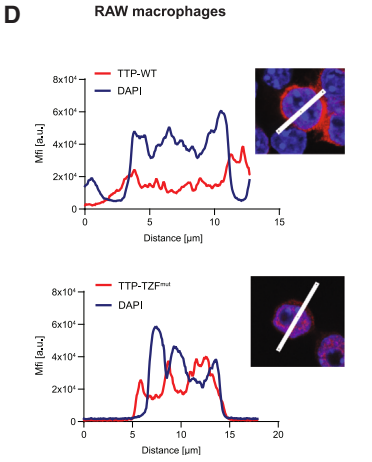

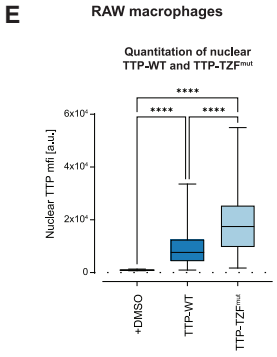

Figure 4. TTP proximal interactome in RAW macrophages

(A) GO terms overrepresented in TID-WT and TID-TZF^{mut} in RAW macrophage interactomes defined by comparisons TID-WT vs. TID-TZF^{mut} or TID-TZF^{mut} vs. TID-WT ($log_2FC > 1$, $padj \leq 0.05$, $n = 3$). Top 8 TID-WT and top 4 TID-TZF^{mut} terms (CC) are shown. ORA *p*adj. values are color-coded; gray: not significant.

(B) Overlap of TTP interactomes in HEK-293 cells (WT-APX vs. GFP-APX) and RAW macrophages (TID-WT vs. TID-E) using overrepresented GO terms (ORA, $log_2FC > 1$ and $padj. \leq 0.05$).

(C and D) Localization of TTP-WT and TTP-TZF^{mut} inducibly expressed (0.5 μg/mL dox, 24 h) in RAW macrophages. DMSO: vehicle control. TTP-WT and TTP-TZF^{mut} detection: Myc antibody (red); nucleus: DAPI (blue). Profile lines were drawn through representative cells for MFI quantitation shown in (D). Scale bar, 25 μm.

(E) Quantitation of nuclear TTP-WT and TTP-TZF^{mut} in RAW macrophages carried out as in Figure 2E. Box: interquartile range; horizontal line: median. One-way analysis of variance (ANOVA) with Tukey's multiple comparisons test, n =112, ****$padj. < 0.0001$.

signature (Figure 4B; Table S3), demonstrating the consistency of the results. Moreover, TTP-TZF^{mut} localized in the nucleus while the TTP-WT protein was mostly cytoplasmic in RAW macrophages (Figures 4C–4E), similar to HEK-293 cells.

In summary, these experiments revealed that RNA binding is required for the assembly of TTP-dependent RNA degradation complexes and the maintenance of appropriate subcellular partitioning of TTP in both immune and non-immune cells. The data further indicate that the regulatory function of RNA binding is conserved in the TTP protein family.

Assembly of TTP-containing cytoplasmic RNA degradation complexes depends on nuclear entry of TTP

The difference between the interactomes of TTP-WT, which is mostly cytoplasmic, and TTP-TZF^{mut}, which accumulates in the nucleus (Figures 1, 2, 3, and 4), might be caused, at least in part, by the distinct subcellular localizations. To test this, we generated a nuclear localization signal (NLS)-deficient TTP (TTP-NLS^{mut}) by introducing the mutations R126A and R130A (murine TTP coordinates). These residues were found essential for nuclear import of a TTP TZF peptide.[38] In agreement, TTP-NLS^{mut} was absent from the nucleus, and TTP-WT comprised minor nuclear and major cytoplasmic TTP pools (Figures 5A–5C and S5A). The proximal interactome was subsequently analyzed using an inducible NLS^{mut}-APX construct in parallel with WT-APX and GFP-APX controls (Figures S5B–S5D; Table S4). NLS^{mut}-APX interactome (defined as proteins enriched in NLS^{mut}-APX samples over GFP-APX) was distinct from WT-APX interactome and was devoid of DCP and EDC proteins (Figures 5D, 5E, and S5E and Table S4), as confirmed by missing colocalization of TTP-NLS^{mut} with the DCP1A and EDC4 decapping foci (Figures 5F and 5G). The interaction with CCR4-NOT was strongly reduced, and most subunits were not significantly enriched (*p*adj. > 0.05), such as the nuclease CNOT6 (Table S4). Interaction with the non-catalytic subunit CNOT3

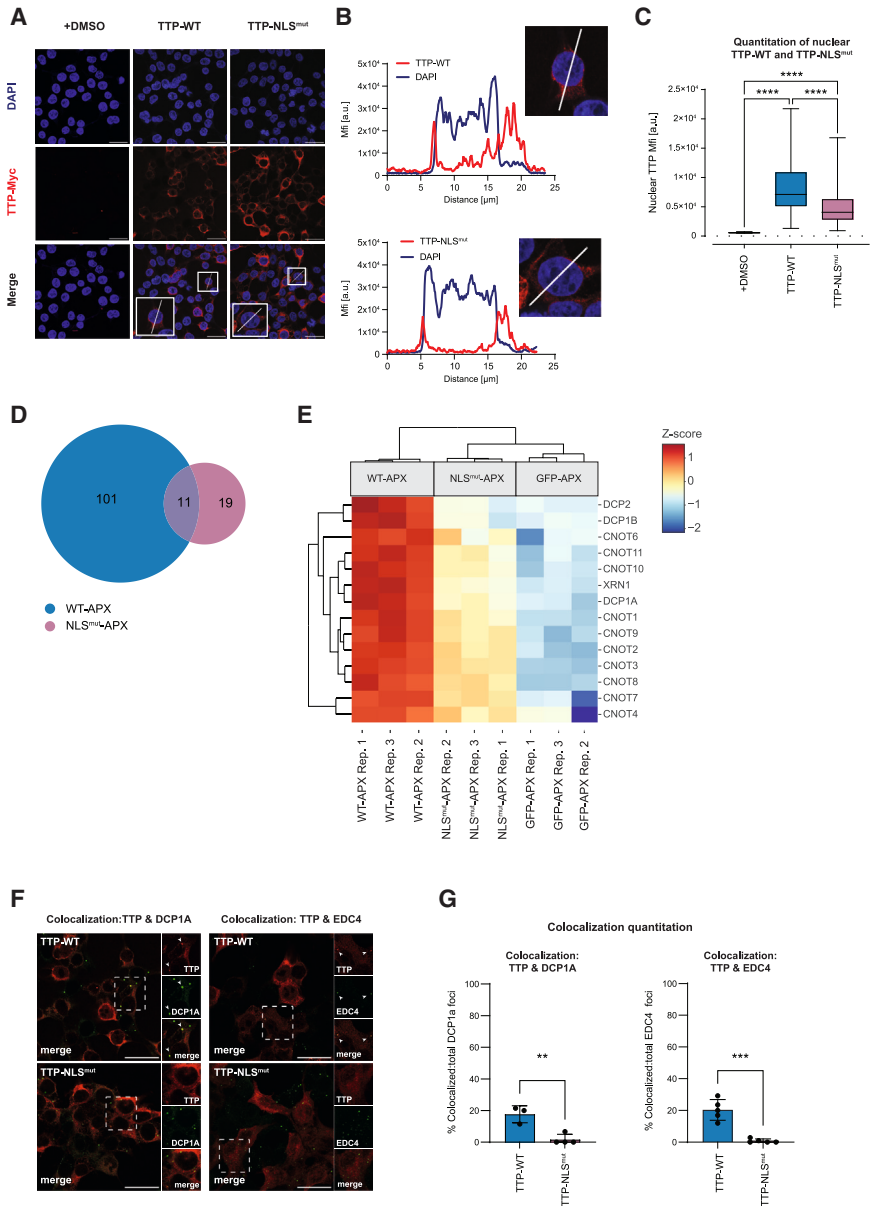

Figure 5. Nuclear import-deficient TTP fails to associate with cytoplasmic mRNA degradation complexes

(A–C) Localization of TTP-NLS^{mut} in HEK-293 cells (A) Induction of TTP-NLS^{mut} and TTP-WT was carried out as in Figure 2C. Scale bar, 25 µm. TTP-WT and TTP-NLS^{mut} detection: Myc antibody (red); nucleus: DAPI (blue).

(B) Profile lines were drawn through representative cells and MFI was quantitated.

(C) Quantitation of nuclear MFI of TTP-WT and TTP-NLS^{mut} carried out as in Figure 2E. Box represents interquartile range with median. One-way analysis of variance (ANOVA) with Tukey's multiple comparisons test, $n = 62$, ****$p$adj. < 0.0001.

(D and E) Proximal interactome of WT-APX and NLS^{mut}-APX in HEK-293 cells analyzed by LC-MS/MS. Induction of WT-APX, NLS^{mut}-APX, and GFP-APX was carried out as in Figure 1B. (D) Overlap of WT-APX and NLS^{mut}-APX interactomes. WT-APX and NLS^{mut}-APX interactomes are defined as significantly enriched proteins ($log_2FC > 1$, $p$adj. ≤ 0.05, $n = 3$) in differential enrichment analysis of WT-APX vs. GFP-APX and NLS^{mut}-APX vs. GFP-APX, respectively. (E) Heatmap visualizing components of the deadenylation and decapping complexes, including XRN1 nuclease, in WT-APX, NLS^{mut}-APX, and GFP-APX interactome replicates.

(F and G) Colocalization analysis of TTP-WT or TTP-NLS^{mut} with endogenous DCP1A and EDC4 foci in cells used in (A). (F) Colocalization of TTP-WT or TTP-NLS^{mut} (Myc tagged) with DCP1A and EDC4 (green) analyzed in individual and merged channels. Myc antibody: red. arrowheads: DCP1A or EDC4 foci colocalizing with TTP. Scale bar, 25 µm. (G) Quantitation (Fiji Comdet) of colocalization of TTP-WT or TTP-NLS^{mut} with DCP1A or EDC4 foci. Student's t test. **$p$adj. < 0.01, *** $p$adj. < 0.001, $n = 61$ and 112 cells, respectively.

was detectable by co-immunoprecipitation and sensitive to anisomycin treatment, like TTP-WT (Figure S5F). The effect of anisomycin is in line with increased phosphorylation (evidenced by lower TTP mobility, Figure S5F), which inhibits TTP binding to CCR4-NOT.[21]

Together, the data show that TTP requires nuclear entry for the complete assembly of the TTP-containing RNA degradation complexes. This was unexpected given that these complexes reside in the cytoplasm.[7,39]

Nuclear entry licenses TTP for binding to cellular target RNAs

The inability of TTP-NLS^{mut} to interact with RNA degradation enzymes is likely not caused directly by the arginine mutations since these residues are located in the linker region between the two centrally positioned ZFs (Figure S6A), while binding to RNA degradation complexes occurs via the N- and C-terminal domains.[20,29,30] We have therefore considered the possibility that the deficient interaction of NLS^{mut}-APX with the RNA processing complexes might result from impaired binding to RNA in cells, which would be consistent with the RNA-binding-deficient TZF^{mut}-APX interactome (Figures 1 and 2). We first assessed the potential of the R126A/R130A mutation to directly affect RNA binding by using structural modeling of the TZF domain. The TZF sequence and structure are conserved in the TTP protein family as evidenced by the NMR structures of the TZF of the TTP homolog ZFP36L2 in complex with RNA (PDB: 1RGO)[40] and the ZF1 of TTP (PDB: 1M9O)[41] (Figures S4A and S6B). Analysis of conformations in the ZFP36L2 TZF and TTP ZF1 NMR ensembles revealed high flexibility of the critical arginines (Figure S6B) and no direct interaction of either of the two arginines with the bound RNA molecule in the ZFP36L2 TZF–RNA complex (Figure 6A). AlphaFold2 modeling

CellPress
OPEN ACCESS

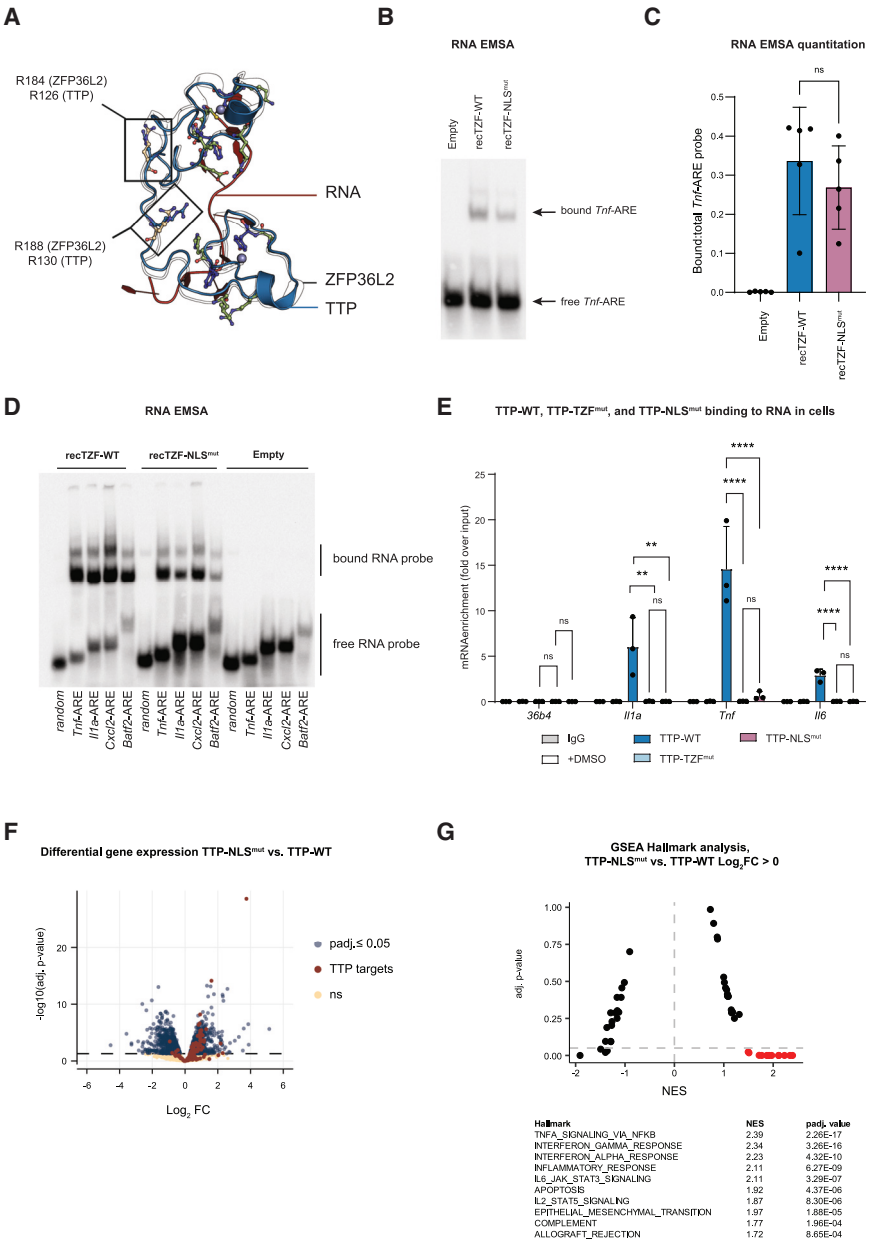

Figure 6. Nuclear entry is required for TTP to bind target RNAs and control inflammatory gene expression

(A) Superposition of ZFP36L2 TZF (black outlines)-RNA (red) complex (NMR structure; PDB: 1RGO) and AlphaFold2 TTP TZF model (blue). R184 (R126 in TTP) and R188 (R130 in TTP) (balls & sticks, yellow, in rectangles), Zn ions (gray spheres), residues involved in π- π staking with RNA (blue) and in hydrogen bonds (green) are highlighted.

(B–D) recTZF-WT and recTZF-NLS^{mut} binding to AREs. (B) Representative *Tnf*-ARE RNA EMSA of 5 independent experiments and (C) quantitation using ChemiDoc (*Znf*-ARE-bound fraction: ratio of bound vs. total *Tnf*-ARE. ANOVA, means with SDs, non-significant (ns), n = 5). (D) RNA EMSA using *Tnf*-ARE, *Il1a*-ARE, *Cxcl2*-ARE, and *Batf2*-ARE. Empty: Lysate of *E. coli* without recTZF-WT and recTZF-NLS^{mut} plasmids.

(E) Quantitation of *Il1a*, *Tnf*, and *Il6* mRNA bound to TTP-WT or TTP-NLS^{mut} in RAW macrophages. TTP-WT, TTP-NLS^{mut}, and TTP-TZF^{mut} (negative control) expression was induced (0.5 μg/mL dox, 24 h; DMSO: vehicle control) followed by treatment with 4sU (100 μM, 7 h) and LPS (10 ng/mL, 6 h, added 1 h after 4sU). Bound RNA (pull-down) and total cellular RNA (input; 10% of the amount used for pull-down) were assessed by reverse transcription quantitative PCR (RT-qPCR), and fold differences were calculated (mRNA enrichment). *36b4* mRNA: non-TTP target control. IgG: mouse isotype control. Two-way analysis of variance (ANOVA), means of RT-qPCR data with SDs, n = 3 (each in triplicates), *padj. < 0.01, ****padj. < 0.0001.

(F and G) RNA-seq of TTP-WT- or TTP-NLS^{mut}-expressing RAW macrophages. (F) TTP-WT and TTP-NLS^{mut} expression was induced as in (E) followed by LPS treatment (10 ng/mL, 6 h) and differential expression analysis. TTP targets identified by CLIP-seq[14] are shown in red. (G) GSEA Hallmark analysis for genes more highly expressed (padj. > 0.05) in TTP-NLS^{mut} vs. TTP-WT. Top-ranked gene sets (highlighted in red and listed below the plot) are related to inflammation. NES, normalized enrichment score.

predicted the TTP TZF fold to be comparable to that of the ZFP36L2 TZF (Figure 6A), indicating that interactions of the two TTP TZF arginines with RNA are unlikely. The effect of R126A/R130A mutations on the TZF fold was assessed by AlphaFold2 structure predictions using CoLabFold and comparative modeling using the Robetta server. The structural models revealed a higher root-mean-square-deviation (RMSD) between TTP-NLS^{mut} and ZFP36L2 than between TTP-WT and ZFP36L2, indicating that the mutation might increase the flexibility of the linker between ZF1 and ZF2 (Table S5). As the interaction interfaces with RNA are the ZFs, increased linker flexibility in TTP-NLS^{mut} is unlikely to significantly impact RNA binding (Figure S6C).

The potential effects of the R126A/R130A mutation on RNA binding were then assessed experimentally using recombinant WT TZF (recTZF-WT) and mutated TZF (recTZF-NLS^{mut}) domains expressed as glutathione S-transferase (GST) fusion proteins in *E. coli* (Figure S6D). RNA electrophoretic mobility shift assay (EMSA) experiments using *Tnf*-ARE as a probe showed binding of both proteins to RNA, although the binding of recTZF-NLS^{mut} was insignificantly weaker (Figures 6B and 6C). Similar results were obtained for AREs from the TTP targets *Il1a*, *Cxcl2*, and *Batf2* (Figures 6D and S6E). Titration experiments with unlabeled *Tnf*-ARE verified that the labeled *Tnf*-ARE was in excess (Figures S6F and S6G).

The structural and experimental analyses indicate that TTP-NLS^{mut} possesses biochemical RNA-binding activity. To test whether TTP-NLS^{mut} binds target RNAs in cells we employed RAW macrophages inducibly expressing TTP-WT and TTP-NLS^{mut}

which were stimulated with lipopolysaccharide (LPS) to activate expression of physiological TTP targets. A modified cross-linking and immunoprecipitation (CLIP) approach (see STAR Methods) revealed that the binding of TTP-NLS^{mut} to the *Il1a*, *Tnf*, and *Il6* cytokine mRNAs in cells was dramatically decreased, resembling the RNA-binding-deficient TTP-TZF^{mut} (Figures 6E and S6H). Moreover, no RNA binding to TTP-NLS^{mut} was detected in experiments quantitating the entire RNA (i.e., not only TTP targets) (Figure S6I). Binding of TTP-WT to RNA was abolished following anisomycin treatment (Figure S6I). Consistent with the impaired targeting of mRNA by TTP-NLS^{mut} in cells, RNA-seq and differential expression analysis revealed that the majority (148 out of 198) of mRNAs previously identified as TTP-bound targets in macrophages[14] were upregulated in TTP-NLS^{mut} cells as compared with TTP-WT controls (Figure 6F; Table S6). The genes more highly expressed in TTP-NLS^{mut} cells exhibited an inflammatory signature (Figure 6G), indicating that a functional TTP was missing. The RNA-seq results were validated by RT-qPCR for *Il1a*, *Tnf*, and *Il6* and included TTP-TZF^{mut} for comparison (Figure S6J).

Collectively, these experiments imply that the inability of the nuclear import-deficient TTP mutant (TTP-NLS^{mut}) to associate with functional deadenylation and decapping complexes is a consequence of its failure to interact with target RNA in cells despite having a functional RNA-binding domain.

The main TTP target is pre-mRNA

The failure of nuclear import-deficient TTP to bind target RNA in cells prompted us to consider that the initial TTP-RNA complex is formed in the nucleus and the assembly of TTP-containing RNA processing enzymes is completed in the cytoplasm. This idea is supported by previous CLIP-seq studies, which showed that TTP bound AREs in introns, in addition to those in 3′ UTRs.[14,36,42] Consequently, we hypothesized that the principal TTP target is pre-mRNA rather than mRNA.

If the assumption that TTP primarily targets pre-mRNA was correct, then pre-mRNA should be enriched in the TTP-bound RNA pool (Figure 7A). To test this, we isolated full-length RNA molecules bound to TTP using a modified thiouridine (4sU)-facilitated pull-down approach (see STAR Methods). RAW macrophages expressing myc-tagged TTP were stimulated with LPS (6 h) and pulsed with 4sU in the last hour of LPS stimulation prior to pull-down. RNA isolated by pull-down (pull-down samples) was analyzed by RNA-seq, together with the total cellular RNA (input samples). We first analyzed read coverage plots for *Tnf* and *Cxcl2*, as they represent TTP targets containing TTP-binding sites in the 3′ UTR (https://ttp-atlas.univie.ac.at/[14]). For these two targets, the pull-down samples contained both intronic and exonic reads (Figure 7B), indicating that TTP binds pre-mRNA of 3′ UTR targets. Next, we globally quantified pre-mRNA and mRNA by counting intronic and exonic reads separately, as described,[43] with modifications ensuring read mapping to unambiguous intronic and exonic sequences (see STAR Methods). Normalized intronic and exonic counts in pull-down and input samples were clustered according to replicates (Figure S7A). The mean counts of replicates for each gene detected in both the input and pull-down were then calculated (Table S6), and the mean intronic counts were plotted against the mean exonic counts (Figure 7C). The relationship between intronic and exonic counts was determined for both pull-down and input using linear regression analysis. The regression curve intercept was significantly higher in pull-down than in input (−1.7 vs. −2.3, respectively), demonstrating that the intronic counts were overall higher in pull-down than in input (Figure 7C). By contrast, the regression curve slopes were similar (0.774 vs. 0.778, respectively), showing that the intronic RNA enrichment in pull-down over input was independent of read counts (i.e., expression levels) for individual genes.

To exclude RNAs that might have been isolated through non-specific binding in the pull-down step, we determined the intronic RNA enrichment in pull-down fractions for high-confidence TTP targets (see STAR Methods) and calculated the intron:exon (In:Ex) ratios for pull-down and input in these targets (Table S6). The In:Ex ratios were higher in pull-down as compared with input samples (Figure 7D), as specifically reflected with the known TTP targets *Tnf* and *Cxcl2* (Figure 7E). These data supported our assumption that TTP prefers binding to pre-mRNA over mRNA, and in case of an opposite or equal binding preference, the In:Ex ratios would have been lower or same in pull-down vs. input given the much higher amounts of mRNA over pre-mRNA in cells.

Notwithstanding the preferred binding of TTP to pre-mRNA, the mean In:Ex ratio across all TTP targets was ∼0.3 in the pull-down samples (Figure 7D), indicating that a large fraction of the TTP-bound RNA was intron-free. This outcome implied that pre-mRNAs bound by TTP in 3′ UTRs were efficiently spliced to mature mRNAs, which were then isolated in the pull-down step alongside the small but significantly enriched fraction of pre-mRNAs. Consistent with this model, the In:Ex ratio was high in targets bound by TTP predominantly in introns as exemplified by *Batf2*, which was pulled down largely as an entire pre-mRNA (Figures S7B and S7C). The reported frequent binding of TTP to introns[14,36,42] correlates with the larger number of canonical TTP-binding ARE sequences occurring in introns than in exons, which is probably a consequence of a higher adenine and thymine (AT) content in introns (Figures S7D and S7E).

The preferred binding of TTP to pre-mRNA implied that the initial interaction between TTP and its target RNA occurs in the nucleus. A consequence of this implication is that continuous nucleocytoplasmic shuttling is required for TTP to couple binding to the target RNA in the nucleus with degradation of the target in the cytoplasm. This model predicts that a blockade of pre-mRNA splicing will trap TTP in the nucleus since the production of mature mRNA that could leave the nucleus together with TTP would be disrupted under these conditions. We tested this prediction by using the splicing inhibitor pladienolide B (PlaB).[44,45] Treatment of LPS-stimulated RAW macrophages expressing TTP-WT with PlaB resulted in an increase in *Tnf* and *Il1a* pre-mRNA levels while mRNA levels of these genes dropped (Figure 7F). Concomitantly, the amounts of TTP-bound *Tnf* and *Il1a* pre-mRNAs increased (Figure S7F). Importantly, PlaB treatment enhanced the nuclear accumulation of TTP-WT (Figures 7G, 7H, and S7G). TTP-NLS^{mut} remained cytoplasmic in PlaB-treated cells, confirming that the effects of PlaB on TTP localization were dependent on TTP binding to RNA in cells (Figures 7G and 7H).

Therefore, these experiments provide evidence that TTP targets initially pre-mRNA not mRNA. Moreover, the data show

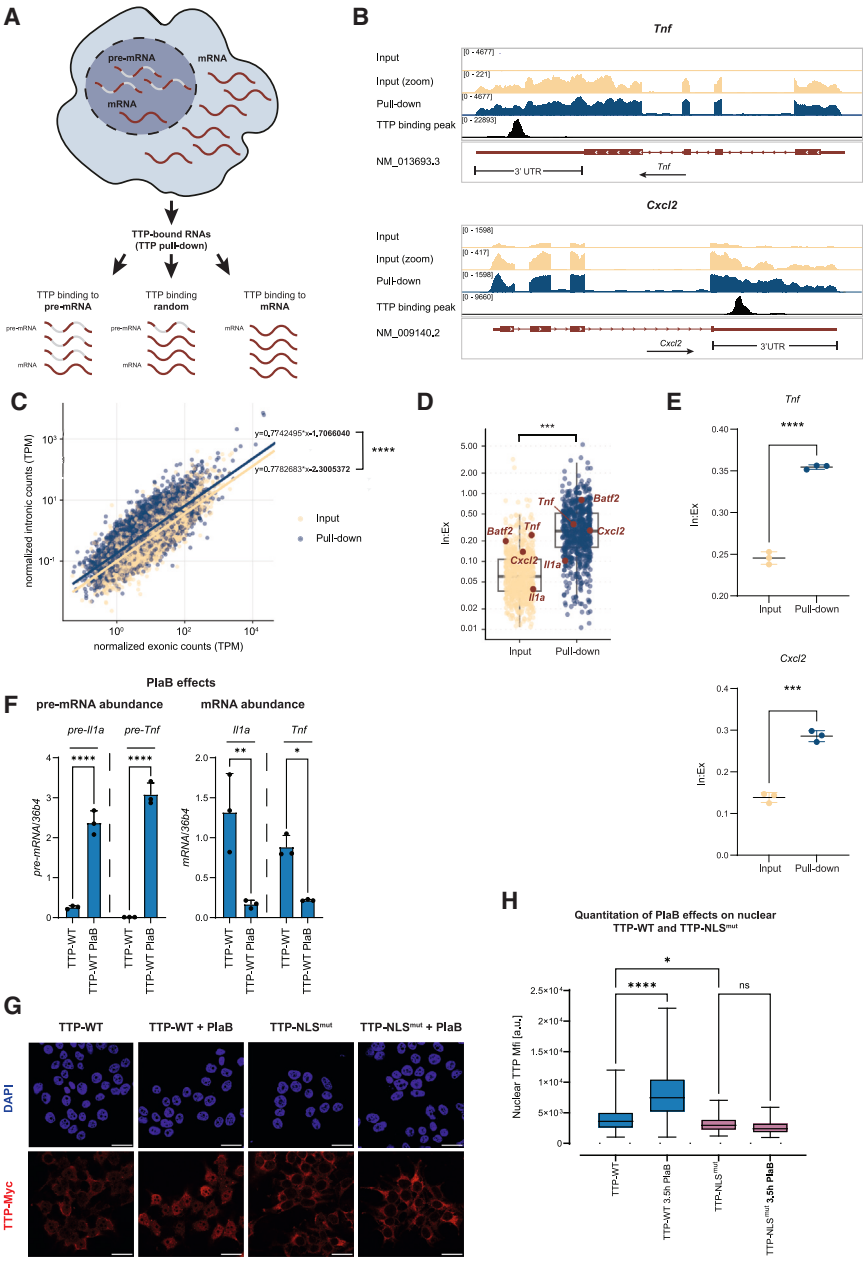

Figure 7. The principal TTP target is pre-mRNA not mRNA

(A) Scheme of analysis assessing TTP-binding preference for pre-mRNA or mRNA by using pre-mRNA:mRNA ratios in pull-down (TTP-bound RNA) vs. input. Possible outcomes are depicted.

(B) RNA-seq coverage of TTP-bound RNA (pull-down) and total RNA (input, 10% of amounts used for pull-down) for *Tnf* and *Cxcl2*. RAW macrophages were induced with dox (0.5 μg/mL, 24 h) for TTP-WT expression, stimulated with LPS (10 ng/mL, 6 h), and treated with 4sU (100 μM, last 1 h of LPS stimulation). Tracks in input, input with re-scaled y axis (zoom) for better visualization of intronic reads, and pull-down are shown. Reported TTP-binding peaks[14] are depicted.

(C) mRNA (exonic counts, x axis) and pre-mRNA (intronic counts, y axis) counts in input (yellow) and pull-down (blue). Means of normalized read counts calculated for corresponding replicates were plotted. Intercepts but not slopes of linear regression curves were significantly different input vs. pull-down. COvariance (ANCOVA), R function "Anova"- package "car," $n = 3$, ****padj. < 0.0001.

(D) Intronic:exonic count ratios (In:Ex) for TTP target genes in input and pull-down, with several TTP target genes highlighted. Input vs. pull-down difference: unpaired Student's t test, ***padj. < 0.001.

(E) In:Ex ratio in input and pull-down for TTP targets *Tnf* and *Cxcl2*; means with SD, unpaired Student's t test, ***padj. < 0.001, ****padj. < 0.0001.

(F) Effects of PlaB on amounts of *Tnf* and *Il1a* pre-mRNA and mRNA in RAW macrophages expressing TTP-WT (as in B) and treated with PlaB (500 nM, 3.5 h). mRNA and pre-mRNA were assessed (RT-qPCR) and normalized to *36b4*. Means and SDs, two-way ANOVA $n = 3$ *padj. < 0.05, **padj. < 0.01, ***padj. < 0.001, ****padj. < 0.0001.

(G and H) Subcellular localization of TTP-WT and TTP-NLS^{mut} upon PlaB treatment.

(G) TTP-WT and TTP-NLS^{mut} were induced (HEK-293 cells, 1 μg/mL dox, 16 h) followed by PlaB treatment as in (F). TTP-WT, TTP-NLS^{mut}: Myc antibody (red); nucleus: DAPI (blue). Scale bar, 25 μm.

(H) Quantitation of nuclear MFI. Box: interquartile range; horizontal line: median. One-way ANOVA with Tukey's multiple comparisons test, $n = 103$, *padj. < 0.05, ****padj. < 0.0001.

that pre-mRNA levels of TTP targets determine the amount of nuclear TTP.

DISCUSSION

Using orthogonal approaches, our study established that the principal TTP target is pre-mRNA not mature mRNA, and that RNA binding is required for association of TTP with fully functional RNA degradation enzymes in the cytoplasm. Consistent with these discoveries, nuclear entry of TTP was found to be essential for both, binding to target RNA and the assembly of TTP-containing RNA degradation complexes. Moreover, RNA binding prevents constitutive nuclear accumulation of TTP, thereby promoting its cycling between the cytoplasm and nucleus. These data support a model in which TTP binds pre-mRNA in the nucleus, and, following maturation of pre-mRNA to mRNA, the TTP-mRNA complex is exported to the cytoplasm, where it forms functional RNA degradation machinery to eliminate the bound RNA. Our results further indicate that this hierarchical process is conserved within the TTP protein family. An important implication of the study is that RBP-mediated degradation of mRNA during inflammation is dependent on a fate decision step at the level of pre-mRNA in the nucleus. This contrasts with the canonical steady-state mRNA decay, which is entirely linked to ribosomes.[7]

Earlier work suggested that TTP associates with the decapping and deadenylation enzymes irrespective of RNA binding and that RNA-unbound TTP might sequester the RNA degradation enzymes, thereby inhibiting mRNA degradation.[18–20,24] This model was later found to be inconsistent with the ZF-inactivating C116R knockin mouse model, which unequivocally excluded dominant-negative effects of an RNA-binding-deficient TTP.[46] Our work provides a mechanistic framework for the knockin mouse model by showing that TTP is incapable of interaction with complete RNA degradation enzymes in the RNA-unbound state. This conclusion derives from experiments employing an RNA-binding-deficient TTP mutant (TTP-TZF^{mut}) and a nuclear import-deficient TTP mutant (TTP-NLS^{mut}), i.e., a mutant that cannot engage pre-mRNA, which we define here as the principal TTP target. TTP-NLS^{mut} binds the non-catalytic CCR4-NOT subunits CNOT2 and CNOT3, suggesting that these two subunits are incorporated independently of the fully functional assembly. It is worth noting that CNOT2 was enriched, although not significantly, more than 2-fold also in the TTP-TZF^{mut} interactome. Both CNOT2 and CNOT3 were reported to localize in the nucleus in addition to the cytoplasm, but the nuclear function remained unresolved.[47–49]

The RNA-driven hierarchic assembly of TTP-containing RNPs is consistent with current models describing RNA-processing granules as hierarchically assembled biomolecular condensates formed upon multi-valent RNA-protein interactions.[50] These condensates often depend on intrinsically disordered regions (IDRs) in the protein subunits.[51] In support of this, TTP contains an N-terminal IDR involved in binding to DCP2.[29] The C-terminal domain involved in TTP interaction with CCR4-CNOT contains another potential IDR.[19,20,30,52] TTP interactions, such as those with CNOT1 or 14-3-3 proteins can be modulated by phosphorylation.[26,53] TTP phosphorylation also regulates nucleocytoplasmic shuttling by promoting cytoplasmic localization.[26,31,54] However, the biological significance of nucleocytoplasmic shuttling of TTP remained unclear.[26,31,39] Our study reveals that nuclear translocation is essential for TTP to interact with its primary target, which is pre-mRNA. As TTP binding to target RNA is a prerequisite for interactions with RNA degradation complexes, nuclear translocation is fundamental for the entire TTP function. Consequently, phosphorylation-enforced cytoplasmic accumulation of TTP upon p38 MAP kinase- and MK2-activating stress conditions[31] prevents both binding to RNA and to RNA degradation enzymes, thereby resolving inconsistent reports on the effects of phosphorylation.[21,36] The partitioning into a larger cytoplasmic and smaller nuclear pool under steady-state conditions depends on TTP binding to RNA, suggesting that TTP is exported from the nucleus together with the bound RNA.

Our data imply that periodic nuclear import and export are indispensable for TTP function as they continuously couple target binding, i.e., binding to pre-mRNA in the nucleus, with target degradation, which occurs in the cytoplasm. Given that pre-mRNA is short-lived, the interaction of TTP with pre-mRNA occurs probably early during the transcription process. TTP binding does not impair subsequent processing of pre-mRNA into mRNA as there is no evidence for TTP effects on splicing.[14,42] Thus, the sole role of the principal binding to pre-mRNA not mRNA is likely to be the licensing of the bound RNA for the subsequent degradation in the cytoplasm, thereby ensuring that mRNAs encoding pro-inflammatory mediators are targeted for degradation immediately after export from the nucleus and prior to the pioneering round of translation. In agreement, we did not observe a ribosomal signature in the proximal TTP interactome, which would be expected if TTP remained associated with the target mRNA during translation. The proposed model minimizes the risks of spurious inflammation-promoting translation that would occur if stochastic processes drove mRNA decay during the immune response. A key parameter of this model is the stoichiometry of nuclear TTP to pre-mRNA targets, which is determined by TTP expression, target RNA expression, and TTP phosphorylation (which causes cytoplasmic accumulation of TTP), i.e., features that are highly dynamic and characteristic for a given phase of the inflammatory response. The model reflects how TTP integrates multiple inputs and converts them into a precise control of the inflammatory response.

Limitations of the study

The results represent a snapshot under conditions defined by the experimental setup, i.e., for given TTP levels, amounts of TTP target mRNAs, and TTP phosphorylation. Detailed time course experiments monitoring these parameters and assessing the ratio of TTP-bound vs. unbound target RNA during the inflammatory response are required for deriving quantitative models. Such studies should employ unperturbed primary macrophages rather than RAW macrophages and HEK-293 cells expressing exogenous TTP as used in this work. Another limitation is the lack of structural data on full-length TTP with and without bound RNA. Such data would help understand interactions with RNA degradation enzymes and the role of RNA therein. Finally, although by including Zfp36l1 our study suggests that the model is relevant for the entire TTP protein family, specific experiments are required for the model validation also beyond the TTP paralogs.

RESOURCE AVAILABILITY

Lead contact

Requests for resources and further information should be directed to and will be fulfilled by the lead contact, Pavel Kovarik (pavel.kovarik@univie.ac.at).

Materials availability

All unique reagents generated in this study are available from the lead contact upon request.

Data and code availability

- Mass spectrometry proteomics data were deposited in the PRIDE repository with the dataset identifiers PXD046381 and PXD051662. Raw RNA-seq data were deposited at the National Center for Biotechnology Information Sequence Read Archive (SRA) database under the bioproject identifiers PRJNA1031176 and PRJNA1163675. Original images of western blots, dot blots, and RNA EMSA were deposited at Mendeley Data: https://doi.org/10.17632/ktrd3ttm36.1.
- This paper does not report original code.
- Any additional information required to reanalyze the data reported in this paper is available from the lead contact upon request.

ACKNOWLEDGMENTS

We are grateful to Kevin Eislmayr, Ronja Reinhart, Stefanie Toifl, Josef Laurin, and Thomas Peterbauer for fruitful discussions and advice; Peter Murray for critical reading of the manuscript; Nora Bischoff for technical assistance; and

Florian Ebner and Vitaly Sedlyarov for the generation of TTP-deficient RAW macrophages. All LC-MS/MS measurements were performed on instruments provided by the Vienna Biocenter Core Facilities (VBCF, www.viennabiocenter.org/facilities). We acknowledge VBCF NGS Facility for RNA sequencing advice. The study was supported by the Austrian Science Fund grants W1261, P33000-B, and P35852 to P.K.; W1261, P30231-B, and P30415-B to G.V.; W1261 to M. Baccarini; and the Max Perutz PhD fellowship to J.F.

AUTHOR CONTRIBUTIONS

A.B. and P.K. conceived the study. A.B. performed all experiments except for ZFP36L1 APEX labeling, TTP-NLS^{mut} APEX labeling, and dot-blot analysis. J.F. and J.v.W. performed ZFP36L1 and TTP-NLS^{mut} APEX labeling experiments. S.D. analyzed LC-MS/MS datasets. C.Z. analyzed RNA-seq datasets. M.F. performed dot-blot analyses. K.D., M. Borroni , A.L.H., S.S., M. Baccarini, and G.A.V. contributed reagents. V.P. performed structural modeling. W.C. and M.H. performed LC-MS/MS. A.B. and P.K. wrote the manuscript. All authors read and approved the manuscript.

DECLARATION OF INTERESTS

The authors declare no competing interests.

STAR★METHODS

Detailed methods are provided in the online version of this paper and include the following:

- KEY RESOURCES TABLE
- EXPERIMENTAL MODEL AND STUDY PARTICIPANT DETAILS
  - Cell lines
- METHOD DETAILS
  - Recombinant DNA plasmids
  - Lentiviral transduction
  - Cell lysates and western blotting
  - Coimmunoprecipitation
  - Immunofluorescence and image quantitation
  - APEX2 proximity labeling
  - Turbo-ID proximity labeling
  - Sample preparation for mass spectrometry analysis
  - Liquid chromatography-mass spectrometry analysis
  - Proteomics data analysis
  - Quantitation of TTP-bound RNA using 3′ *in vitro* labeling
  - Quantitation of TTP-bound RNA by RT-qPCR
  - Analysis of TTP-bound RNA by RNA-seq
  - RNA-seq of RAW macrophages expressing TTP-WT or TTP-NLS^{mut}
  - AT content and ARE count
  - Expression of recTZF peptides
  - RNA electrophoretic mobility shift assay
  - TZF structure prediction and modeling
- QUANTITATION AND STATISTICAL ANALYSIS

SUPPLEMENTAL INFORMATION

Supplemental information can be found online at https://doi.org/10.1016/j.molcel.2025.01.001.

Received: April 29, 2024
Revised: October 25, 2024
Accepted: January 3, 2025
Published: January 24, 2025

REFERENCES

1. Carpenter, S., Ricci, E.P., Mercier, B.C., Moore, M.J., and Fitzgerald, K.A. (2014). Post-transcriptional regulation of gene expression in innate immunity. Nat. Rev. Immunol. *14*, 361–376. https://doi.org/10.1038/nri3682.
2. Grudzien-Nogalska, E., and Kiledjian, M. (2017). New insights into decapping enzymes and selective mRNA decay. Wiley Interdiscip. Rev. RNA *8*. https://doi.org/10.1002/wrna.1379.
3. Collart, M.A. (2016). The Ccr4-Not complex is a key regulator of eukaryotic gene expression. Wiley Interdiscip. Rev. RNA *7*, 438–454. https://doi.org/10.1002/wrna.1332.
4. Turner, M., and Díaz-Muñoz, M.D. (2018). RNA-binding proteins control gene expression and cell fate in the immune system. Nat. Immunol. *19*, 120–129. https://doi.org/10.1038/s41590-017-0028-4.
5. Akira, S., and Maeda, K. (2021). Control of RNA Stability in Immunity. Annu. Rev. Immunol. *39*, 481–509. https://doi.org/10.1146/annurev-immunol-101819-075147.
6. Passmore, L.A., and Coller, J. (2022). Roles of mRNA poly(A) tails in regulation of eukaryotic gene expression. Nat. Rev. Mol. Cell Biol. *23*, 93–106. https://doi.org/10.1038/s41580-021-00417-y.
7. Heck, A.M., and Wilusz, J. (2018). The Interplay between the RNA Decay and Translation Machinery in Eukaryotes. Cold Spring Harb. Perspect. Biol. *10*, a032839. https://doi.org/10.1101/cshperspect.a032839.
8. Inada, T., and Beckmann, R. (2024). Mechanisms of Translation-coupled Quality Control. J. Mol. Biol. *436*, 168496. https://doi.org/10.1016/j.jmb.2024.168496.
9. Blackshear, P.J., and Perera, L. (2014). Phylogenetic distribution and evolution of the linked RNA-binding and NOT1-binding domains in the tristetraprolin family of tandem CCCH zinc finger proteins. J. Interferon Cytokine Res. *34*, 297–306. https://doi.org/10.1089/jir.2013.0150.
10. Molle, C., Zhang, T., Ysebrant de Lendonck, L., Gueydan, C., Andrianne, M., Sherer, F., Van Simaeys, G., Blackshear, P.J., Leo, O., and Goriely, S. (2013). Tristetraprolin regulation of interleukin 23 mRNA stability prevents a spontaneous inflammatory disease. J. Exp. Med. *210*, 1675–1684. https://doi.org/10.1084/jem.20120707.
11. Kang, J.G., Amar, M.J., Remaley, A.T., Kwon, J., Blackshear, P.J., Wang, P.Y., and Hwang, P.M. (2011). Zinc finger protein tristetraprolin interacts with CCL3 mRNA and regulates tissue inflammation. J. Immunol. *187*, 2696–2701. https://doi.org/10.4049/jimmunol.1101149.
12. Sneezum, L., Eislmayr, K., Dworak, H., Sedlyarov, V., Le Heron, A., Ebner, F., Fischer, I., Iwakura, Y., and Kovarik, P. (2020). Context-Dependent IL-1 mRNA-Destabilization by TTP Prevents Dysregulation of Immune Homeostasis Under Steady State Conditions. Front. Immunol. *11*, 1398. https://doi.org/10.3389/fimmu.2020.01398.
13. Taylor, G.A., Carballo, E., Lee, D.M., Lai, W.S., Thompson, M.J., Patel, D.D., Schenkman, D.I., Gilkeson, G.S., Broxmeyer, H.E., Haynes, B.F., and Blackshear, P.J. (1996). A pathogenetic role for TNF alpha in the syndrome of cachexia, arthritis, and autoimmunity resulting from tristetraprolin (TTP) deficiency. Immunity *4*, 445–454.
14. Sedlyarov, V., Fallmann, J., Ebner, F., Huemer, J., Sneezum, L., Ivin, M., Kreiner, K., Tanzer, A., Vogl, C., Hofacker, I., and Kovarik, P. (2016). Tristetraprolin binding site atlas in the macrophage transcriptome reveals a switch for inflammation resolution. Mol. Syst. Biol. *12*, 868. https://doi.org/10.15252/msb.20156628.
15. Stoecklin, G., Tenenbaum, S.A., Mayo, T., Chittur, S.V., George, A.D., Baroni, T.E., Blackshear, P.J., and Anderson, P. (2008). Genome-wide analysis identifies interleukin-10 mRNA as target of tristetraprolin. J. Biol. Chem. *283*, 11689–11699. https://doi.org/10.1074/jbc.M709657200.
16. Lai, W.S., Carballo, E., Thorn, J.M., Kennington, E.A., and Blackshear, P.J. (2000). Interactions of CCCH zinc finger proteins with mRNA. Binding of tristetraprolin-related zinc finger proteins to Au-rich elements and destabilization of mRNA. J. Biol. Chem. *275*, 17827–17837. https://doi.org/10.1074/jbc.M001696200.
17. Lai, W.S., Kennington, E.A., and Blackshear, P.J. (2003). Tristetraprolin and its family members can promote the cell-free deadenylation of AU-rich element-containing mRNAs by poly(A) ribonuclease. Mol. Cell. Biol. *23*, 3798–3812.

18. Lykke-Andersen, J., and Wagner, E. (2005). Recruitment and activation of mRNA decay enzymes by two ARE-mediated decay activation domains in the proteins TTP and BRF-1. Genes Dev. *19*, 351–361.

19. Sandler, H., Kreth, J., Timmers, H.T.M., and Stoecklin, G. (2011). Not1 mediates recruitment of the deadenylase Caf1 to mRNAs targeted for degradation by tristetraprolin. Nucleic Acids Res. *39*, 4373–4386. https://doi.org/10.1093/nar/gkr011.

20. Fabian, M.R., Frank, F., Rouya, C., Siddiqui, N., Lai, W.S., Karetnikov, A., Blackshear, P.J., Nagar, B., and Sonenberg, N. (2013). Structural basis for the recruitment of the human CCR4-NOT deadenylase complex by tristetraprolin. Nat. Struct. Mol. Biol. *20*, 735–739. https://doi.org/10.1038/nsmb.2572.

21. Clement, S.L., Scheckel, C., Stoecklin, G., and Lykke-Andersen, J. (2011). Phosphorylation of tristetraprolin by MK2 impairs AU-rich element mRNA decay by preventing deadenylase recruitment. Mol. Cell. Biol. *31*, 256–266. https://doi.org/10.1128/MCB.00717-10.

22. Hitti, E., Iakovleva, T., Brook, M., Deppenmeier, S., Gruber, A.D., Radzioch, D., Clark, A.R., Blackshear, P.J., Kotlyarov, A., and Gaestel, M. (2006). Mitogen-activated protein kinase-activated protein kinase 2 regulates tumor necrosis factor mRNA stability and translation mainly by altering tristetraprolin expression, stability, and binding to adenine/uridine-rich element. Mol. Cell. Biol. *26*, 2399–2407. https://doi.org/10.1128/MCB.26.6.2399-2407.2006.

23. Lam, S.S., Martell, J.D., Kamer, K.J., Deerinck, T.J., Ellisman, M.H., Mootha, V.K., and Ting, A.Y. (2015). Directed evolution of APEX2 for electron microscopy and proximity labeling. Nat. Methods *12*, 51–54. https://doi.org/10.1038/nmeth.3179.

24. Lai, W.S., Kennington, E.A., and Blackshear, P.J. (2002). Interactions of CCCH zinc finger proteins with mRNA: non-binding tristetraprolin mutants exert an inhibitory effect on degradation of AU-rich element-containing mRNAs. J. Biol. Chem. *277*, 9606–9613.

25. Schaljo, B., Kratochvill, F., Gratz, N., Sadzak, I., Sauer, I., Hammer, M., Vogl, C., Strobl, B., Müller, M., Blackshear, P.J., et al. (2009). Tristetraprolin is required for full anti-inflammatory response of murine macrophages to IL-10. J. Immunol. *183*, 1197–1206. https://doi.org/10.4049/jimmunol.0803883.

26. Stoecklin, G., Stubbs, T., Kedersha, N., Wax, S., Rigby, W.F.C., Blackwell, T.K., and Anderson, P. (2004). MK2-induced tristetraprolin:14-3-3 complexes prevent stress granule association and ARE-mRNA decay. EMBO J. *23*, 1313–1324.

27. Ross, E.A., Smallie, T., Ding, Q., O'Neil, J.D., Cunliffe, H.E., Tang, T., Rosner, D.R., Klevernic, I., Morrice, N.A., Monaco, C., et al. (2015). Dominant Suppression of Inflammation via Targeted Mutation of the mRNA Destabilizing Protein Tristetraprolin. J. Immunol. *195*, 265–276. https://doi.org/10.4049/jimmunol.1402826.

28. Didusch, S., Madern, M., Hartl, M., and Baccarini, M. (2022). amica: an interactive and user-friendly web-platform for the analysis of proteomics data. BMC Genomics *23*, 817. https://doi.org/10.1186/s12864-022-09058-7.

29. Maciej, V.D., Mateva, N., Schwarz, J., Dittmers, T., Mallick, M., Urlaub, H., and Chakrabarti, S. (2022). Intrinsically disordered regions of tristetraprolin and DCP2 directly interact to mediate decay of ARE-mRNA. Nucleic Acids Res. *50*, 10665–10679. https://doi.org/10.1093/nar/gkac797.

30. Fenger-Grøn, M., Fillman, C., Norrild, B., and Lykke-Andersen, J. (2005). Multiple processing body factors and the ARE binding protein TTP activate mRNA decapping. Mol. Cell *20*, 905–915. https://doi.org/10.1016/j.molcel.2005.10.031.

31. Johnson, B.A., Stehn, J.R., Yaffe, M.B., and Blackwell, T.K. (2002). Cytoplasmic localization of tristetraprolin involves 14-3-3-dependent and -independent mechanisms. J. Biol. Chem. *277*, 18029–18036. https://doi.org/10.1074/jbc.M110465200.

32. Youn, J.Y., Dunham, W.H., Hong, S.J., Knight, J.D.R., Bashkurov, M., Chen, G.I., Bagci, H., Rathod, B., MacLeod, G., Eng, S.W.M., et al. (2018). High-Density Proximity Mapping Reveals the Subcellular Organization of mRNA-Associated Granules and Bodies. Mol. Cell *69*, 517–532.e11. https://doi.org/10.1016/j.molcel.2017.12.020.

33. Rzeczkowski, K., Beuerlein, K., Müller, H., Dittrich-Breiholz, O., Schneider, H., Kettner-Buhrow, D., Holtmann, H., and Kracht, M. (2011). c-Jun N-terminal kinase phosphorylates DCP1a to control formation of P bodies. J. Cell Biol. *194*, 581–596. https://doi.org/10.1083/jcb.201006089.

34. Wells, M.L., Perera, L., and Blackshear, P.J. (2017). An Ancient Family of RNA-Binding Proteins: Still Important! Trends Biochem. Sci. *42*, 285–296. https://doi.org/10.1016/j.tibs.2016.12.003.

35. Carballo, E., Lai, W.S., and Blackshear, P.J. (1998). Feedback inhibition of macrophage tumor necrosis factor-alpha production by tristetraprolin. Science *281*, 1001–1005.

36. Tiedje, C., Diaz-Muñoz, M.D., Trulley, P., Ahlfors, H., Laaß, K., Blackshear, P.J., Turner, M., and Gaestel, M. (2016). The RNA-binding protein TTP is a global post-transcriptional regulator of feedback control in inflammation. Nucleic Acids Res. *44*, 7418–7440. https://doi.org/10.1093/nar/gkw474.

37. Branon, T.C., Bosch, J.A., Sanchez, A.D., Udeshi, N.D., Svinkina, T., Carr, S.A., Feldman, J.L., Perrimon, N., and Ting, A.Y. (2018). Efficient proximity labeling in living cells and organisms with TurboID. Nat. Biotechnol. *36*, 880–887. https://doi.org/10.1038/nbt.4201.

38. Murata, T., Yoshino, Y., Morita, N., and Kaneda, N. (2002). Identification of nuclear import and export signals within the structure of the zinc finger protein TIS11. Biochem. Biophys. Res. Commun. *293*, 1242–1247. https://doi.org/10.1016/S0006-291X(02)00363-7.

39. Stumpo, D.J., Lai, W.S., and Blackshear, P.J. (2010). Inflammation: cytokines and RNA-based regulation. Wiley Interdiscip. Rev. RNA *1*, 60–80. https://doi.org/10.1002/wrna.1.

40. Hudson, B.P., Martinez-Yamout, M.A., Dyson, H.J., and Wright, P.E. (2004). Recognition of the mRNA AU-rich element by the zinc finger domain of TIS11d. Nat. Struct. Mol. Biol. *11*, 257–264.

41. Amann, B.T., Worthington, M.T., and Berg, J.M. (2003). A Cys3His zinc-binding domain from Nup475/tristetraprolin: a novel fold with a disklike structure. Biochemistry *42*, 217–221. https://doi.org/10.1021/bi026988m.

42. Mukherjee, N., Jacobs, N.C., Hafner, M., Kennington, E.A., Nusbaum, J.D., Tuschl, T., Blackshear, P.J., and Ohler, U. (2014). Global target mRNA specification and regulation by the RNA-binding protein ZFP36. Genome Biol. *15*, R12. https://doi.org/10.1186/gb-2014-15-1-r12.

43. Madsen, J.G.S., Schmidt, S.F., Larsen, B.D., Loft, A., Nielsen, R., and Mandrup, S. (2015). iRNA-seq: computational method for genome-wide assessment of acute transcriptional regulation from total RNA-seq data. Nucleic Acids Res. *43*, e40. https://doi.org/10.1093/nar/gku1365.

44. Li, S., Yang, M., Shen, H., Ding, L., Lyu, X., Lin, K., Ong, J., and Du, P. (2024). Capturing totipotency in human cells through spliceosomal repression. Cell *187*, 3284–3302.e23. https://doi.org/10.1016/j.cell.2024.05.010.

45. Kotake, Y., Sagane, K., Owa, T., Mimori-Kiyosue, Y., Shimizu, H., Uesugi, M., Ishihama, Y., Iwata, M., and Mizui, Y. (2007). Splicing factor SF3b as a target of the antitumor natural product pladienolide. Nat. Chem. Biol. *3*, 570–575. https://doi.org/10.1038/nchembio.2007.16.

46. Lai, W.S., Stumpo, D.J., Qiu, L., Faccio, R., and Blackshear, P.J. (2018). A Knock-In Tristetraprolin (TTP) Zinc Finger Point Mutation in Mice: Comparison with Complete TTP Deficiency. Mol. Cell. Biol. *38*, e00488-17. https://doi.org/10.1128/MCB.00488-17.

47. Sarkar, M., Martufi, M., Roman-Trufero, M., Wang, Y.F., Whilding, C., Dormann, D., Sabbattini, P., and Dillon, N. (2021). CNOT3 interacts with the Aurora B and MAPK/ERK kinases to promote survival of differentiating mesendodermal progenitor cells. Mol. Biol. Cell *32*, ar40. https://doi.org/10.1091/mbc.E21-02-0089.

48. Boland, A., Chen, Y., Raisch, T., Jonas, S., Kuzuoğlu-Öztürk, D., Wohlbold, L., Weichenrieder, O., and Izaurralde, E. (2013). Structure and assembly of the NOT module of the human CCR4-NOT complex. Nat. Struct. Mol. Biol. *20*, 1289–1297. https://doi.org/10.1038/nsmb.2681.

49. Zwartjes, C.G.M., Jayne, S., van den Berg, D.L.C., and Timmers, H.T.M. (2004). Repression of promoter activity by CNOT2, a subunit of the

transcription regulatory Ccr4-not complex. J. Biol. Chem. *279*, 10848–10854. https://doi.org/10.1074/jbc.M311747200.

50. Ripin, N., and Parker, R. (2023). Formation, function, and pathology of RNP granules. Cell *186*, 4737–4756. https://doi.org/10.1016/j.cell.2023.09.006.
51. Youn, J.Y., Dyakov, B.J.A., Zhang, J., Knight, J.D.R., Vernon, R.M., Forman-Kay, J.D., and Gingras, A.C. (2019). Properties of Stress Granule and P-Body Proteomes. Mol. Cell *76*, 286–294. https://doi.org/10.1016/j.molcel.2019.09.014.
52. Lai, W.S., Stumpo, D.J., Wells, M.L., Gruzdev, A., Hicks, S.N., Nicholson, C.O., Yang, Z., Faccio, R., Webster, M.W., Passmore, L.A., and Blackshear, P.J. (2019). Importance of the conserved carboxyl-terminal CNOT1 binding domain to tristetraprolin (TTP) activity in vivo. Mol. Cell. Biol. *39*, e00029-19. https://doi.org/10.1128/MCB.00029-19.
53. Carreño, A., and Lykke-Andersen, J. (2022). The Conserved CNOT1 Interaction Motif of Tristetraprolin Regulates ARE-mRNA Decay Independently of the p38 MAPK-MK2 Kinase Pathway. Mol. Cell. Biol. *42*, e0005522. https://doi.org/10.1128/mcb.00055-22.
54. Phillips, R.S., Ramos, S.B.V., and Blackshear, P.J. (2002). Members of the tristetraprolin family of tandem CCCH zinc finger proteins exhibit CRM1-dependent nucleocytoplasmic shuttling. J. Biol. Chem. *277*, 11606–11613. https://doi.org/10.1074/jbc.M111457200.
55. Anders, S., Pyl, P.T., and Huber, W. (2015). HTSeq–a Python framework to work with high-throughput sequencing data. Bioinformatics Oxf. Engl. *31*, 166–169. https://doi.org/10.1093/bioinformatics/btu638.
56. Quinlan, A.R., and Hall, I.M. (2010). BEDTools: a flexible suite of utilities for comparing genomic features. Bioinformatics Oxf. Engl. *26*, 841–842. https://doi.org/10.1093/bioinformatics/btq033.
57. Smith, T., Heger, A., and Sudbery, I. (2017). UMI-tools: modeling sequencing errors in Unique Molecular Identifiers to improve quantification accuracy. Genome Res. *27*, 491–499. https://doi.org/10.1101/gr.209601.116.
58. Chen, S., Zhou, Y., Chen, Y., and Gu, J. (2018). fastp: an ultra-fast all-in-one FASTQ preprocessor. Bioinformatics Oxf. Engl. *34*, i884–i890. https://doi.org/10.1093/bioinformatics/bty560.
59. Love, M.I., Huber, W., and Anders, S. (2014). Moderated estimation of fold change and dispersion for RNA-seq data with DESeq2. Genome Biol. *15*, 550. https://doi.org/10.1186/s13059-014-0550-8.
60. Schindelin, J., Arganda-Carreras, I., Frise, E., Kaynig, V., Longair, M., Pietzsch, T., Preibisch, S., Rueden, C., Saalfeld, S., Schmid, B., et al. (2012). Fiji: an open-source platform for biological-image analysis. Nat. Methods *9*, 676–682. https://doi.org/10.1038/nmeth.2019.
61. Hung, V., Udeshi, N.D., Lam, S.S., Loh, K.H., Cox, K.J., Pedram, K., Carr, S.A., and Ting, A.Y. (2016). Spatially resolved proteomic mapping in living cells with the engineered peroxidase APEX2. Nat. Protoc. *11*, 456–475. https://doi.org/10.1038/nprot.2016.018.
62. Hollenstein, D.M., Maurer-Granofszky, M., Reiter, W., Anrather, D., Gossenreiter, T., Babic, R., Hartl, N., Kraft, C., and Hartl, M. (2023). Chemical Acetylation of Ligands and Two-Step Digestion Protocol for Reducing Codigestion in Affinity Purification-Mass Spectrometry. J. Proteome Res. *22*, 3383–3391. https://doi.org/10.1021/acs.jproteome.3c00424.
63. Rappsilber, J., Mann, M., and Ishihama, Y. (2007). Protocol for micro-purification, enrichment, pre-fractionation and storage of peptides for proteomics using StageTips. Nat. Protoc. *2*, 1896–1906. https://doi.org/10.1038/nprot.2007.261.
64. Tyanova, S., Temu, T., and Cox, J. (2016). The MaxQuant computational platform for mass spectrometry-based shotgun proteomics. Nat. Protoc. *11*, 2301–2319. https://doi.org/10.1038/nprot.2016.136.
65. Zhu, Y., Orre, L.M., Zhou Tran, Y., Mermelekas, G., Johansson, H.J., Malyutina, A., Anders, S., and Lehtiö, J. (2020). DEqMS: A Method for Accurate Variance Estimation in Differential Protein Expression Analysis. Mol. Cell. Proteomics *19*, 1047–1057. https://doi.org/10.1074/mcp.TIR119.001646.
66. Ritchie, M.E., Phipson, B., Wu, D., Hu, Y., Law, C.W., Shi, W., and Smyth, G.K. (2015). limma powers differential expression analyses for RNA-sequencing and microarray studies. Nucleic Acids Res. *43*, e47. https://doi.org/10.1093/nar/gkv007.
67. Raudvere, U., Kolberg, L., Kuzmin, I., Arak, T., Adler, P., Peterson, H., and Vilo, J. (2019). g:Profiler: a web server for functional enrichment analysis and conversions of gene lists (2019 update). Nucleic Acids Res. *47*, W191–W198. https://doi.org/10.1093/nar/gkz369.
68. Ashburner, M., Ball, C.A., Blake, J.A., Botstein, D., Butler, H., Cherry, J.M., Davis, A.P., Dolinski, K., Dwight, S.S., Eppig, J.T., et al. (2000). Gene ontology: tool for the unification of biology. The Gene Ontology Consortium. Nat. Genet. *25*, 25–29. https://doi.org/10.1038/75556.
69. Eislmayr, K., Bestehorn, A., Morelli, L., Borroni, M., Vande Walle, L.V., Lamkanfi, M., and Kovarik, P. (2022). Nonredundancy of IL-1alpha and IL-1beta is defined by distinct regulation of tissues orchestrating resistance versus tolerance to infection. Sci. Adv. *8*, eabj7293. https://doi.org/10.1126/sciadv.abj7293.
70. Blackshear, P.J., Lai, W.S., Kennington, E.A., Brewer, G., Wilson, G.M., Guan, X., and Zhou, P. (2003). Characteristics of the interaction of a synthetic human tristetraprolin tandem zinc finger peptide with AU-rich element-containing RNA substrates. J. Biol. Chem. *278*, 19947–19955.
71. Goddard, T.D., Huang, C.C., Meng, E.C., Pettersen, E.F., Couch, G.S., Morris, J.H., and Ferrin, T.E. (2018). UCSF ChimeraX: Meeting modern challenges in visualization and analysis. Protein Sci. *27*, 14–25. https://doi.org/10.1002/pro.3235.
72. Jumper, J., Evans, R., Pritzel, A., Green, T., Figurnov, M., Ronneberger, O., Tunyasuvunakool, K., Bates, R., Žídek, A., Potapenko, A., et al. (2021). Highly accurate protein structure prediction with AlphaFold. Nature *596*, 583–589. https://doi.org/10.1038/s41586-021-03819-2.
73. Mirdita, M., Schütze, K., Moriwaki, Y., Heo, L., Ovchinnikov, S., and Steinegger, M. (2022). ColabFold: making protein folding accessible to all. Nat. Methods *19*, 679–682. https://doi.org/10.1038/s41592-022-01488-1.
74. Yang, J., Anishchenko, I., Park, H., Peng, Z., Ovchinnikov, S., and Baker, D. (2020). Improved protein structure prediction using predicted interresidue orientations. Proc. Natl. Acad. Sci. USA *117*, 1496–1503. https://doi.org/10.1073/pnas.1914677117.

STAR★METHODS

KEY RESOURCES TABLE

REAGENT or RESOURCE	SOURCE	IDENTIFIER
Antibodies		
APX (APEX2)	Abcam	Cat# ab222414
Vinculin	Sigma	Cat# V9131; RRID:AB_477629
Myc-tag	Cell Signaling Technology	Cat# 2276; RRID:AB_331783
TTP	Sedlyarov et al.[14]	N/A
DCP1A	Abcam	Cat# ab183709; RRID:AB_3331658
EDC3	Cell Signaling Technology	Cat# 14495; RRID:AB_2798497
EDC4	Cell Signaling Technology	Cat# 2548; RRID:AB_10621246
GST	Laboratory E. Ogris, Max Perutz Labs	N/A
Biotin	Cell Signaling Technology	Cat# 5597; RRID:AB_10828011
CNOT1	Cell Signaling Technology	Cat# 44613; RRID:AB_2783868
CNOT3	Cell Signaling Technology	Cat# 40608; RRID:AB_2799179
Lamin A-C	Cell Signaling Technology	Cat# 2032; RRID:AB_2136278
Peroxidase-conjugated AffiniPure Goat Anti-Rabbit IgG(H+L)	Jackson Immunoresearch	Cat# 111-035-003; RRID:AB_2313567
Peroxidase-conjugated AffiniPure Goat Anti-Mouse IgG(H+L)	Jackson Immunoresearch	Cat# 115-035-003; RRID:AB_10015289
Goat anti-Rabbit IgG (H+L) Cross-Adsorbed Secondary Antibody, Alexa Fluor™ 488	Thermo Fisher Scientific	Cat# A-11008; RRID:AB_143165
Goat anti-Mouse IgG (H+L) Cross-Adsorbed Secondary Antibody, Alexa Fluor™ 594	Thermo Fisher Scientific	Cat# A-11020; RRID:AB_2534087
Chemicals, peptides, and recombinant proteins		
Acetonitrile	VWR	Cat# 83639.320
Ammonium-bicarbonate	Sigma	Cat# 09830
C18 material	Empore	Cat# 2215-C18
Dithiothreitol (DTT)	Roche	Cat# 10708984001
Iodoacetamide (IAA)	Sigma	Cat# I6125-5G
Lysyl Endopeptidase (LysC)	FUJIFILM Wako chemicals	Cat# 129-02541
Methanol	Fisher chemical	Cat# A456-212
Trifluoroacetic acid (TFA)	Thermo Scientific	Cat# 28903
Trypsin Gold Mass Spec Grade	Promega	Cat# V5280
0.1% Formic acid	Fisher chemical	Cat# LS118-500
Acetonitrile 0.1% formic acid	Fisher chemical	Cat# LS120-1
Water	Fisher chemical	Cat# W6-1
Pierce™ Streptavidin Magnetic Beads	Thermo Scientific	Cat# 88842
Pierce™ Anti-c-Myc Magnetic Beads	Thermo Scientific	Cat# 88843
Pierce™ Protein A/G Magnetic Beads	Thermo Scientific	Cat# 88803
Sulfo-NHS acetate	Thermo Scientific	Cat# 26777
Nitrocellulose blotting membrane 0.2μM NC	GE healthcare life sciences	Cat# 10600001
PageRuler Prestained Protein Ladder	Thermo Scientific	Cat# 26616
Biotin tyramide	Iris Biotech	Cat# LS-3500.1000
Biotin	Sigma	Cat# B4501
Puromycin	Sigma	Cat# P8833

(*Continued on next page*)

Continued

REAGENT or RESOURCE	SOURCE	IDENTIFIER
Poly-L-lysin	Sigma	Cat# P4832
4-thiouridin	Sigma	Cat# T4509
RNasin Ribonuclease Inhibitor	Promega	Cat# N2511
BrightStar™-Plus Positively Charged Nylon Membrane	Invitrogen	Cat# AM10102
RevertAid Reverse Transcriptase	Thermo Scientific	Cat# EP0442
IPTG, dioxane-free	Thermo Scientific	Cat# R0392
Trolox	Sigma	Cat# 238813
Proteinase K	Roche	Cat# 3115828001
DNaseI recombinant, RNAse free	Roche	Cat# 4716728001
Acid-Phenol:Chloroform, pH 4.5 (with IAA, 125:24:1)	Thermo Scientific	Cat# AM9722
FastDigest NheI	Thermo Scientific	Cat# FD0973
FastDigest BamHI	Thermo Scientific	Cat# FD0054
Random Hexamer Primers	Thermo Scientific	Cat# SO142
Pladienolide B	Santa Cruz	Cat# sc-391691
pCp-Biotin	Jena Bioscience	Cat# 17337021
T4 RNA Ligase 1 (ssRNA Ligase)	NEB	Cat# M0204S
cOmplete Protease Inhibitor Cocktail	Roche	Cat# 11836145001
Q5 High-Fidelity DNA Polymerase	NEB	Cat# M0491L
Fast Alkaline Phosphatase	Thermo Scientific	Cat# EF0651
Lipopolysaccharides from *Escherichia coli* O55:B5	Sigma	Cat# L2637
DAPI	Sigma	Cat# D9542
Doxycycline hyclate	Sigma	Cat# D9891
Anisomycin	Sigma	Cat# 176880
ProLong™ Gold Antifade Mountant	Thermo Scientific	Cat# P36934
Hydrogen peroxide solution	Sigma	Cat# H1009
Sodium-L-ascorbat	Sigma	Cat# A4034
Critical commercial assays		
NE-PER™ Nuclear and Cytoplasmic Extraction Reagents	Thermo Fisher Scientific	Cat# 78833
Pierce BCA Protein Assay Kit	Thermo Fisher Scientific	Cat# 23225
Monarch PCR & DNA Cleanup Kit (5ug)	NEB	Cat# T1030S
Monarch DNA gel extraction kit	NEB	Cat# T1020L
LightShift™ Chemiluminescent RNA EMSA Kit	Thermo Fisher Scientific	Cat# 20158
Q5 High Fidelity DNA Polymerase	NEB	Cat# M0491S
QIAGEN Plasmid Midi Kit (25)	Qiagen	Cat# 12143
T7-FlashScribe™ Transcription Kit	Tbubio	Cat# C-ASF3507
Monarch RNA Cleanup Kit (10 μg)	NEB	Cat# T2030L
Gibson Assembly Master Mix	NEB	Cat# E2611L
the NucleoSpin RNA II Kit	Macherey-Nagel	Cat# 740955
RNA 6000 Nano Assays	Agilent	Cat# 5067-1511
rRNA depletion kit Ribovanish	www.viennabiocenter.org/facilities	N/A
Ultra II Directional RNA Library Prep Kit	NEB	Cat# E7765
QuantSeq 3' mRNA-seq Library Prep Kit	Lexogen	Cat# 191
Deposited data		
Mass spectrometry data	PRIDE	PXD046381
3' mRNA -Seq	This study	SRA: PRJNA1163675

(*Continued on next page*)

Continued

REAGENT or RESOURCE	SOURCE	IDENTIFIER
CLIP full-length RNA-Seq	This study	SRA: PRJNA1031176
Raw image files - western blot, dot-blot, RNA-EMSA	This study	DOI: https://doi.org/10.17632/ktrd3ttm36.1
Mouse reference genome (GRCm39)	Genome Reference Consortium	https://www.ncbi.nlm.nih.gov/grc/mouse
Experimental models: Cell lines		
HEK-293	ATCC	Cat# CRL-1573, RRID:CVCL_0045
HEK-293: TTP-WT-APX	This study	N/A
HEK-293: TTP-TZFmut-APX	This study	N/A
HEK-293: ZFP36L1-WT-APX	This study	N/A
HEK-293: ZFP36L1-TZFmut-APX	This study	N/A
HEK-293: GFP-APX	This study	N/A
HEK-293: TTP-WT-3xMyc	This study	N/A
HEK-293: TTP-TZFmut-3xMyc	This study	N/A
HEK-293: TTP-NLSmut-3xMyc	This study	N/A
HEK-293: ZFP36L1-WT-3xMyc	This study	N/A
HEK-293: ZFP36L1-TZFmut-3xMyc	This study	N/A
RAW ΔTTP	This study	N/A
RAW ΔTTP: TID-TTP-WT	This study	N/A
RAW ΔTTP: TID-TTP-TZF^{mut}	This study	N/A
RAW ΔTTP: TID-E	This study	N/A
RAW ΔTTP: TTP-WT-3xMyc	This study	N/A
RAW ΔTTP: TTP-TZF^{mut}-3xMyc	This study	N/A
RAW ΔTTP: TTP-NLS^{mut}-3xMyc	This study	N/A
Oligonucleotides		
EMSA probes	This study	Table S7
qPCR primers	This study	Table S7
Cloning primers	This study	Table S7
Recombinant DNA		
pCW 57.1	Addgene	Cat# 41393; RRID:Addgene_41393
pEGFP-N1	Clontech	discontinued
V5-TurboID-NES_pCDNA3	Addgene	Cat# 107169; RRID:Addgene_107169
pCW 57.1-MYC-TurboID-MCS-PGK-mCherry-P2A-rtTA	Laboratory G. A. Versteeg Max Perutz Labs	N/A
pCW 57.1-TetOn-APEX2	Laboratory M. Baccarini, Max Perutz Labs	N/A
pGEX-4T-1:GST-TEV-TTP-TZD-WT	GenScript	N/A
pGEX-4T-1:GST-TEV-TTP-TZD-NLS-mut	GenScript	N/A
Software and algorithms		
SnapGene (version 7.2)	SnapGene	RRID:SCR_015052
FreeStyle (version 1.7)	Thermo Fisher Scientific	RRID:SCR_022877
MaxQuant (version 1.6.17, 2.3.1.0)	The Max Planck Institute of Biochemistry	RRID:SCR_014485
Cassiopeia_LFQ (version 4.7.0)	Max Perutz Labs	N/A
Amica (version 3.0.0)	Max Perutz Labs	N/A
Bio-Rad CFX Maestro (version 2.3)	Bio-Rad	RRID:SCR_018057
Image Lab (version 6.0.1)	Bio-Rad	RRID:SCR_014210
Gen5 Microplate Reader Software	BioTek	RRID:SCR_017317
GraphPad Prism 10	Graph Pad Software	RRID:SCR_002798
ImageJ (version 2.3.0)	National Institutes of Health	RRID:SCR_003070
Comdet ImageJ plug-in (version 0.5.5)	https://doi.org/10.5281/zenodo.4281064	https://zenodo.org/records/4281064

(*Continued on next page*)

Continued

REAGENT or RESOURCE	SOURCE	IDENTIFIER
FastQC (version 0.12.0)	https://www.bioinformatics.babraham.ac.uk/projects/fastqc/	RRID:SCR_014583
htseq-count (version 2.0.4)	Anders et al. [55]	https://pypi.python.org/pypi/HTSeq; RRID:SCR_011867
Bedtools (version 2.30.0)	Quinlan and Hall[56]	https://bedtools.readthedocs.io/en/latest/content/overview.html; RRID:SCR_006646
UMI-tools (version 1.1).5	Smith et al.[57]	https://GitHub.com/CGATOxford/UMI-tools; RRID:SCR_017048
Trim Galore (version 0.6.10)	https://usegalaxy.org/	RRID:SCR_014583
fastp (version 0.23.4)	Chen et al.[58]	https://github.com/OpenGene/fastp; RRID:SCR_016962
STAR (version 2.7.11a)	https://code.google.com/archive/p/rna-star/;	RRID:SCR_004463
SAMTOOLS (version 1.18)	https://sourceforge.net/projects/samtools/files/samtools/1.5/	RRID:SCR_002105
Deeptools bamCoverage (version 3.5.2)	Sanger Institute	https://www.htslib.org
R (version 4.4.1)	the R Core Team	https://www.r-project.org/; RRID:SCR_001905
DESeq2 (version 1.45.0)	Love et al.[59]	http://www.bioconductor.org/packages/release/bioc/html/DESeq2.html; RRID:SCR_015687
ggplot2 (version 3.5.1)	https://ggplot2.tidyverse.org/	RRID:SCR_014601
tidyverse (version 2.0.0)	https://www.tidyverse.org/packages/	RRID:SCR_019186
fgsea (version 2.73.1)	http://bioconductor.org/packages/fgsea/	RRID:SCR_020938
msigdbr (version 7.5.1)	https://igordot.github.io/msigdbr/	RRID:SCR_022870
rtracklayer (version 1.65.0)	https://www.bioconductor.org/packages/release/bioc/html/rtracklayer.html	RRID:SCR_021325
Companion on Applied Regression (Car) (version 3.1-2)	https://www.john-fox.ca/Companion	RRID:SCR_022137
Biostrings (version 2.73.1)	https://bioconductor.org/packages/Biostrings	RRID:SCR_016949
Other		
Ultimate 3000 RSLC nano-flow chromatography system	Thermo Fisher Scientific	N/A
Q Exactive HF-X Orbitrap mass spectrometer	Thermo Fisher Scientific	N/A
Exploris 480 Orbitrap mass spectrometer	Thermo Fisher Scientific	N/A
Illumina NovaSeq S1	Illumina	N/A
Illumina NovaSeqX 10B XP	Illumina	N/A

EXPERIMENTAL MODEL AND STUDY PARTICIPANT DETAILS

Cell lines

Parental cell lines used in this study were RAW264.7 (ATCC TIB-71) and HEK-293 (ATCC CRL-1573). All cell lines were cultured in DMEM (Sigma-Aldrich, D6429) containing 10% fetal bovine serum (FBS) and 1% penicillin/streptomycin at 37°C and 5% CO_2 in a humified incubator and were tested negative for mycoplasma contamination by PCR. RAW 264.7 cells used in all experiments bore a CRISPR/Cas9-generated deletion in the TTP gene and were termed RAW macrophages. The derivatives RAW macrophages and HEK-293 cells generated in this study were produced by using a lentiviral transduction.

METHOD DETAILS

Recombinant DNA plasmids

TTP, TTP C116R/C139R double point mutant (TTP-TZF^{mut}) and ZFP36L1 (from murine colon total RNA) were cloned into a modified, doxycycline hyclate (Sigma-Aldrich, D9891)-inducible lentiviral expression vector pCW 57.1 (Addgene #41393) by Gibson assembly. In brief, C-terminal 3xMyc-tag and backbone complementary overhangs for Gibson assembly were added by PCR, purified using column DNA Clean-up kit (Monarch PCR & DNA Cleanup Kit, # T1030L, NEB) and mixed with Nhe1 and BamH1 double-digested and gel-purified target pCW57.1 vector in a molecular ratio of 1:2. Gibson assembly was performed following the manufacturer's instruction (NEB, E2621S) and transformed into chemically competent DH10B E. coli. Lentiviral C-terminally 3xMyc-tagged-TTP NLS point mutant (TTP-NLS^{mut}) was generated by mutating R126 and R130 to alanine using PCR-based site-directed mutagenesis of the parental pCW57.1_tetON_TTP-3xMyc. GFP was PCR-amplified from pEGFP-N1 (Clontech) and used for Gibson cloning. APEX2 constructs were obtained by cloning of TTP-WT, TTP-TZF^{mut}, ZFP36L1-WT, ZFP36L1-TZF^{mut} and GFP into a modified pCW57.1 lentiviral expression vector containing APEX2. All expression constructs contained a puromycin resistance cassette for selection. N-terminally TurboID TTP (TID-TTP) and empty TurboID (TID-E) vectors were generated by cloning TID from V5-TurboID-NES_pCDNA3 (Addgene#107169) into a modified TurboID-containing pCW57.1 vector (pCW57.1-pCW 57.1-MYC-TurboID-MCS-PGK-mCherry-P2A-rtTA), expressing a constitutively active mCherry selection cassette. TID-TTP-TZF^{mut} was generated by exchanging TTP-WT in parental vector with TTP-TZF^{mut} by conventional restriction digest cloning. All constructs were verified by sequencing.

Lentiviral transduction

Cells were seeded 24 h before treatments which were directly added to cell culture dishes without change of the cell culture medium. Lentiviral particles were generated by co-transfecting 1.5 μg of total DNA of pMDLg/pRRE (Addgene #12251), pCMV-VSV-G (Addgene #8454), and pRSV-Rev (Addgene #12253) with modified pCW57.1 target vector in a ratio of 5: 1: 5 : 5 into HEK-293 cells using polyethyleneimine (PEI, Polysciences, 23966). Three days post-transfection, supernatants containing viral particles were harvested, passed through a 0.45 μm filter and used to infect either HEK-293 cells in a dilution of 1:5 or RAW macrophages in a dilution of 1:2 with 8 μg/ml polybrene (Sigma-Aldrich, TR1003G). Transduced cells were selected by either puromycin (Sigma-Aldrich, P8833-100MG) (3 μg/ml for HEK-293 cells or 8 μg/ml for RAW macrophages) for 1 week, or by FACS for mCherry-positive cells on day 3 post-infection.

Cell lysates and western blotting

Expression of TTP-constructs in HEK-293 cells and RAW macrophages was induced by 1 μg/μl for 3.5 h or 16 h, as indicated (HEK-293 cells) or 0.5 μg/ml for 24 h (RAW macrophages). After induction, cells were washed twice with PBS and lysed in either Frackelton buffer (10 mM Tris-HCl pH8, 30 mM $Na_4P_2O_7$, 50 mM NaCl, 50 mM NaF, 1% Triton X-100 and 1x cOmplete protease inhibitor cocktail) or RIPA buffer (50 mM Tris-HCl pH8, 150 mM NaCl, 0.1% SDS, 0.5% sodium deoxycholate, 1% NP-40, 1mM PMSF, 1x cOmplete protease inhibitor cocktail) for 5 min on ice. Lysates were cleared by centrifugation at 13200 rpm for 5 min at 4°C and supernatant was transferred into a fresh tube. To obtain nuclear and cytoplasmic cellular fractions, cells were fractionated using Thermo-Fischer NE-PER Nuclear and Cytoplasmic Extraction Reagents (Thermo-Fisher Scientific, Cat #78835) following the manufacturer's instruction, Protein concentration was determined using Pierce BCA Protein Assay Kit (Thermo-Fisher Scientific, Cat #23225). After concentration adjustment, cell lysates were mixed at a ratio of 2:1 with SDS loading dye and heated for 5 min at 95°C. Samples were loaded onto 10% SDS polyacrylamide gel for separation, followed by wet transfer onto nitrocellulose membrane (GE Healthcare) in carbonate transfer buffer (3 mM Na_2CO_3, 10 mM NaHCO3, and 20% ethanol) for 16 h at 200 mA and additional 2 h at 400 mA at 4°C. Membranes were blocked in 10% BSA in TBS-T (20 mM Tris, 150 mM NaCl, 0.5% Tween 20, pH 8.0) for 1 h at room temperature (RT) and subsequently incubated with primary antibody overnight at 4°C. Membranes were then washed three times with TBS-T for 5 min each, and incubated with HRP-conjugated secondary antibody for 1 h at RT. Chemiluminescence was detected and quantified by using a ChemiDoc Touch Imaging System (BioRad).

Coimmunoprecipitation

Cell lysate (500 μg) in Frackelton buffer was incubated 50 μl Pierce™ anti-c-Myc magnetic bead slurry (Thermo-Fisher Scientific, Cat #88843) for 3 or 16 h at 4°C while rotating. 10% of cell lysate per samples was used as input protein lysate. After immunoprecipitation, beads were washed 5x in Frackelton lysis buffer, 10% of unbound protein lysate (flow-through) was collected, and protein complexes were released by heating to 95°C for 5 min in SDS loading dye. Co-immunoprecipitated proteins were visualized by western blotting.

Immunofluorescence and image quantitation

2x10^4 HEK-293 cells, expressing C-terminally 3x Myc-tagged TTP or ZFP36L1 were seeded onto poly-lysine (Sigma-Aldrich, P4832) pretreated glass coverslips for 48 h. TTP or ZFP36L1 expression was induced by doxycycline (1 μg/ml) for 3.5 h. For anisomycin- and pladienolide B (PlaB)-treated samples, TTP expression was induced by doxycycline (1 μg/ml) for 16 h. Cells were treated with 100 μM anisomycin for 1.5 h or 500 nM PlaB 3.5 h, as indicated. Cells were then washed three times with PBS, fixed in 4% formaldehyde in PBS for 10 min at RT, washed three times with PBS, quenched with 0.1 M glycine in PBS for 10 min on RT, washed three times with

PBS and subsequently permeabilized with 0.3% Triton in 3% BSA (w/v) in PBS for 30 min on RT. Primary antibodies (Myc 1:2000, EDC4 1:500, DCP1a 1:500) were diluted in permeabilization solution and incubated for 1 h at RT. After three PBS washes, slides were incubated with secondary antibodies conjugated to Alexa Fluor 594 (for Myc) or Alexa Fluor 488 (for EDC4 and DCP1a, both 1:1000) (Thermo-Fisher Scientific, Cat # A-11005 and A-11008) for 1 h at RT. Samples were washed three times with PBS and nuclei were stained with DAPI (0.5 μg/ml, Sigma-Aldrich, D8417-10MG) for 10 min on RT. Samples were then washed twice with PBS and once with H_2O and subsequently mounted onto microscopy slides with Prolong Gold antifade reagent (Thermo-Fisher Scientific, P36934). Confocal images were captured on the Zeiss LSM 980 microscope using a 64x oil objective (Plan-Apochromat 1.4NA Oil) with a PMT detector at RT with Zeiss ZEN 3.3 software. All images were analyzed using the Fiji distribution of ImageJ.[60] Brightness and contrast were adjusted equally in all images in the same figure panel in anisomycin- and PlaB-treated samples using ImageJ. Recorded Z-stacks of Myc and EDC4 co-staining were analyzed by projecting the maximum intensity. Mean fluorescence intensity (MFI) of nuclear TTP was measured by segmenting cells using Otsu thresholding in the DAPI channel to define nuclei boundaries as regions of interest (ROI). The MFI of ROIs was then measured in the Alexa Fluor 594 (Myc) channel. Profile plots were generated with the plot profile function in Fiji by drawing a line through a cell of interest. Data generated by the plot profile function were transferred to Graphpad to obtain profile plots depicting the intensity profiles of respective channels along the line. Colocalization analysis was performed using Comdet v.0.5.5 plug-in in Fiji to detect colocalizing particles in Alexa Fluor 594 (Myc) and Alexa Fluor 488 (EDC4, DCP1a) channels. Maximum distance between colocalized spots was set to 4 pixels (~0.28 μm). In Alexa Fluor 594 (Myc) channel particles had to reach a size of 7 pixels and an intensity threshold of 50-75, in Alexa Fluor 488 channel particles had to reach a size of 10 pixels and an intensity threshold of 100-200.

APEX2 proximity labeling

APEX2 (APX) proximity labeling in HEK-293 cells was largely performed as described[61] with the following adjustments. Lentivirally transduced bait protein expression was induced in confluent 15 cm tissue culture dish by 1 μg/ml doxycycline for 3.5 h for TTP-APX experiments. For ZFP36L1 labeling experiments, bait protein expression was induced for 24 h using doxycycline at 0.02-1 μg/ml to obtain similar expression levels. Where indicated, samples were treated with 100 μM anisomycin for 1.5 h prior to labeling. Biotin-phenol was added to cells for 30 min (500 μM final concentration) prior to labeling. Labeling was induced by treating cells with 1 mM H_2O_2 for 1 min. Subsequently, cells were quenched by washing three times with quenching medium (10 mM sodium ascorbate, 5 mM Trolox and 10 mM sodium azide in PBS) and three times with PBS. Labeled cells were lysed with RIPA buffer, and protein concentration was measured using Pierce Protein Assay Kit. Prior to affinity purification, streptavidin bead slurry (Thermo-Fisher Scientific, Cat #88817) was acetylated with 5 mM sulfo-NHS acetate in 50 mM ammonium bicarbonate with 0.2% Tween at RT for 1 h, as described.[62] In brief, beads were washed three times with 50 mM HEPES, pH 7.8, 0.2% Tween on a magnetic rack, incubated with sulfo-NHS acetate while rotating for 1 h at RT, subsequently washed in 50 mM ammonium bicarbonate, 0.2% Tween, and finally stored in PBS-T (0.2% Tween), 0.02% sodium azide at 4°C until further use. Total protein lysate (1 mg) was loaded onto 150 μl acetylated streptavidin bead slurry and incubated overnight at 4°C while rotating. Samples were then washed to remove unspecific binders. Additional washes with 50 mM HEPES pH 7 (5 - 7 times) were included prior to mass spectrometry submission to remove residual detergents. For western blot analysis, 10% input sample, flow-through samples or eluted samples (pull-down) were taken. Elution of pull-down was facilitated by heating the bead slurry in 1x SDS loading dye at 95°C for 5 min.

Turbo-ID proximity labeling

Turbo-ID (TID) proximity labeling in RAW macrophages was performed similarly to APEX2-based labeling in HEK-293 cells with the following differences. Lentivirally transduced RAW macrophages were sorted for similar mCherry signal by FACS and subsequently seeded into 15 cm tissue culture dishes ($7x10^6$ cells per dish) 48 h prior to the experiment. TID-protein expression was induced the next day with 0.025 μg/ml doxycycline (TID-E) or 0.5 μg/ml doxycycline for 24 h to achieve similar expression of constructs. Labeling was performed by supplying cells with 500 μM biotin for 15 min. Afterwards, cells, were washed three times with PBS and lysed in RIPA lysis buffer (see above). Two mg of cell lysates were incubated with 100 μl acetylated streptavidin bead slurry overnight at 4°C while rotating. Washing steps and sample preparation for mass spectrometry submission as well as western blot analysis were identical to APEX2 labeling in HEK-293 cells.

Sample preparation for mass spectrometry analysis

Beads were transferred to new tubes and resuspended in 50 μl of 50 mM ammonium bicarbonate (ABC). Disulfide bonds were reduced with 10 mM dithiothreitol for 30 min at RT before adding 25 mM iodoacetamide and incubating for another 30 min at RT in the dark. The remaining iodoacetamide was quenched by adding 5 mM DTT and the proteins were digested with 150 ng LysC (mass spectrometry grade, FUJIFILM Wako chemicals) in 1.5 μl 50 mM ammonium bicarbonate at 25°C overnight. The supernatant without beads was incubated with 150 ng trypsin (Trypsin Gold, Promega) in 1.5 μl 50 mM ammonium bicarbonate at 37°C for 5 h. The digest was stopped by the addition of trifluoroacetic acid (TFA) to a final concentration of 0.5 %, and the peptides were desalted using C18 Stagetips.[63]

Liquid chromatography-mass spectrometry analysis

Peptides were separated on an Ultimate 3000 RSLC nano-flow chromatography system (Thermo-Fisher Scientific), using a pre-column for sample loading (Acclaim PepMap C18, 2 cm × 0.1 mm, 5 μm, Thermo-Fisher Scientific), and a C18 analytical column

(Acclaim PepMap C18, 50 cm × 0.75 mm, 2 μm, Thermo-Fisher Scientific), applying a segmented linear gradient from 2% to 35% and finally 80% solvent B (80 % acetonitrile, 0.1 % formic acid; solvent A 0.1 % formic acid) at a flow rate of 230 nl/min over 120 min.

In TTP-APX labeling experiment, eluted peptides were analyzed on a Q Exactive HF-X Orbitrap mass spectrometer (Thermo-Fisher Scientific), which was coupled to the column with a customized nano-spray EASY-Spray ion source (Thermo-Fisher Scientific) using coated emitter tips (New Objective). The mass spectrometer was operated in data-dependent acquisition mode (DDA), and survey scans were obtained in a mass range of 375-1500 m/z with lock mass activated, at a resolution of 120k at 200 m/z and an AGC target value of 3E6. The 25 most intense ions were selected with an isolation width of 1.4 m/z, isolation offset 0.0 m/z, fragmented in the HCD cell at 28% collision energy and the spectra recorded for max. 100 ms at a target value of 1E5 and a resolution of 30k. Peptides with a charge of +1 or >+6 were excluded from fragmentation, the peptide match feature was set to preferred, the exclude isotope feature was enabled, and selected precursors were dynamically excluded from repeated sampling for 30 seconds.

In L1-APX and TID-TTP labeling experiments, eluting peptides were analyzed on an Exploris 480 Orbitrap mass spectrometer (Thermo-Fisher Scientific) coupled to the column with a FAIMS pro ion-source (Thermo-Fisher Scientific) using coated emitter tips (PepSep, MSWil) with the following settings: The mass spectrometer was operated in DDA mode with two FAIMS compensation voltages (CV) set to -45 or -60 and 1.5 s cycle time per CV. The survey scans were obtained in a mass range of 350-1500 m/z, at a resolution of 60k at 200 m/z, and a normalized AGC target at 100%. The most intense ions were selected with an isolation width of 1.2 m/z, fragmented in the HCD cell at 28% collision energy, and the spectra recorded for max. 100 ms at a normalized AGC target of 100% and a resolution of 15k. Peptides with a charge of +2 to +6 were included for fragmentation, the peptide match feature was set to preferred, the exclude isotope feature was enabled, and selected precursors were dynamically excluded from repeated sampling for 45 seconds.

Proteomics data analysis

MS raw data split for each CV (FreeStyle 1.7, Thermo-Fisher Scientific) were analyzed using the MaxQuant[64] (version 1.6.17.0 for TTP-APX experiment and TID-TTP experiment, version 2.3.1.0 for L1-APX experiment) with the Uniprot human reference proteome (version 2020.01 for TTP-APX experiment, version 2022.05 for L1-APX experiment) and Uniprot mouse reference proteome (version 2020.01 for the TID-TTP experiment), as well as a database of most common contaminants and target protein sequences (mouse TTP in TTP-APX experiments and mouse ZFP36L1 in L1-APX experiment). The search was performed with full trypsin specificity and a maximum of two missed cleavages at a protein and peptide spectrum match false discovery rate of 1%. Carbamidomethylation of cysteine residues was set as fixed, oxidation of methionine, and N-terminal acetylation as variable modifications. For label-free quantitation the ''match between runs'' only within the sample batch and the LFQ function were activated - all other parameters were left at default.

MaxQuant output tables were further processed in R 4.2.1 (https://www.R-project.org) using amica (TTP-APX dataset).[28] Differential expression analysis was performed with DeqMS (version 1.10.0)[65] or Cassiopeia_LFQ (all other datasets) (https://github.com/maxperutzlabs-ms/Cassiopeia_LFQ). Reverse database identifications, contaminant proteins, protein groups identified only by a modified peptide, protein groups with less than two quantitative values in one experimental group, and protein groups with less than 2 razor peptides were removed for further analysis. Missing values were replaced by randomly drawing data points from a normal distribution model on the whole dataset (data mean shifted by -1.8 standard deviations, a width of the distribution of 0.3 standard deviations). Differences between groups were statistically evaluated using the LIMMA 3.52.1[66] at 5% FDR (Benjamini-Hochberg).

Output of Cassiopeia (MS reports) was further processed using amica including principal component analysis and over-representation analysis (ORA) using gprofiler2 (version 0.2.1)[67] ($log_2FC > 1$ and padj. ≤ 0.05). For ORA GO: CC, GO: MF, GO: BP of the gene ontology database[68] were used.

Quantitation of TTP-bound RNA using 3′ *in vitro* labeling

$5x10^6$ HEK-293 cells, expressing C-terminally 3x Myc-tagged TTP-WT or TTP-NLS^{mut} were seeded 24 h before the experiment. TTP expression was induced using 1 μg/ml doxycycline for 3.5 h. Cells were treated with 100 μM anisomycin for 1.5 h, as indicated. Cells were supplied with 100 μM 4-thiouridine (4sU) 1 h before harvest. After PBS washes, cells were crosslinked at 0.15 J/cm2 (wavelength: 365 nm, Stratalinker 2400), lysed in RIPA lysis buffer (50 mM Tris-HCl pH 7.4, 100 mM NaCl, 0.1% NP-40, 0.1% SDS, 0.5% sodium deoxycholate,1x cOmplete protease inhibitor cocktail) and protein concentration was estimated by Pierce BCA Protein Assay Kit (Thermo Fisher Scientific, 23225). Cell lysate (500 μg) was incubated with 50 μl Pierce anti-c-Myc magnetic bead slurry (Thermo-Fisher Scientific, Cat #88843) for 16 h at 4°C; 10 % of cell lysate were used as input. Subsequently, beads were washed in high salt buffer (50 mM Tris-HCl pH 7.4, 1 M NaCl, 1 mM EDTA, 0.1% NP-40, 0.1% SDS, 0.5% sodium deoxycholate) prior to washing in buffer as described.[14] TTP-bound RNA and input RNA were purified after proteinase K digestion by acidic phenol-chloroform extraction (Thermo Scientific) and ethanol precipitation. TTP-bound and input RNA samples were resuspended in 11 μl and 110 μl, respectively, nuclease-free water. TTP-bound RNA and input RNA (5 μl each) were 3' biotinylated using 0.15 μl pCp biotin (100 μM) (Jena Bioscience, cat#17337021), 0.5 μl T4 RNA ligase (NEB), 1.5 μl NEB ligase buffer (10x), 1.5 μl ATP (10 mM), 1.5 μl DMSO (100%) in total volume of 15 μl, at 16°C o/n. RNA was then purified using Monarch RNA Cleanup Kit (NEB, cat#T2030L) and eluted in 11 μl nuclease-free H_2O for TTP-bound samples and 110 μl volume for input samples.TTP-bound and input samples

(each 2 μl) were spotted on positively charged nylon membrane (Invitrogen, cat#AM10102). Following crosslinking with 254 nm UV light at 120 mJ/cm2, the biotin signal was detected and quantitated using a ChemiDoc Touch Imaging System (BioRad).

Quantitation of TTP-bound RNA by RT-qPCR

Metabolic labeling, crosslinking, harvesting, and immunoprecipitation of RAW macrophages for qPCR analysis was performed as described previously,[14] with modifications. Briefly, RAW macrophages (15x 106 cells) were seeded onto 15 cm tissue culture dishes 48 h prior to crosslinking and harvesting. Expression of TTP constructs was induced with 0.5 μg/μl doxycycline for 24 h in addition to a control omitting doxycycline treatment. Cells were stimulated with 10 ng/ml LPS for 6 h. In indicated experiments cells were additionally treated with PlaB (500 nM) for 3.5 h. Cells were supplied with 100 μM 4sU 7 h or 1 h (PlaB experiments) before harvest. IgG (CST, Cat #5415) bound to Protein A/G magnetic beads (Thermo-Fisher Scientific, Cat # 88802), was included as Isotype control. cDNA was produced using random hexamer primers (Mycrosynth) with recombinant M-MuLV reverse transcriptase (RevertAid, Thermo-Fisher Scientific, Cat #K1691) and used for quantitation of TTP-bound RNA and input RNA by RT-qPCR with HOT FIREPol EvaGreen qPCR Supermix (Medibena, Cat #SB_08-36-GP) on CFX Touch qPCR cyclers (Bio-Rad). Relative expression levels were calculated with the CFX Maestro Analysis software, as described previously.[69] The following primers were used for qPCR: 36B4 fw TCCTTCTTCCAGGCTTTGGG and rv GGACACCCTCCAGAAAGCGA; Il1a fw CAAACTGATGAAGCTCGTCA and rv TCTCCTTGAGCGCTCACGAA; pre-Il1a fw GGGACCACTCTCACTAAGCC and rv CTTCCCGTTGCTTGACGTTG; Il6 fw AGTTGC CTTCTTGGGACTGA and rv TTCTGCAAGTGCATCATCGT; Tnf fw GATCGGTCCCCAAAGGGATG and rv CACTTGGTGGTTT GCTACGAC; pre-Tnf fw GGCAAAGAGGAACTGTAAG and rv CCATAGAACTGATGAGAGG.

Analysis of TTP-bound RNA by RNA-seq

Metabolic labeling, crosslinking, harvesting, and immunoprecipitation of RAW macrophages for RNA-seq analysis was performed as described in the part "quantitation of TTP-bound RNA by RT-qPCR". For total RNA-seq of TTP-bound RNAs (PD) and total RNA (input), RNA quality was assessed using Agilent RNA 6000 Nano Assays (5067-1511) on an Agilent 2100 Bioanalyzer. Library preparation, quality control and sequencing were performed by the VBCF (Vienna BioCenter Core Facilities) Next Generation Sequencing (NGS) Facility (www.viennabiocenter.org/facilities). Total RNA input samples were subjected to automated ribonucleic depletion using rRNA depletion kit Ribovanish prior to library preparation. Library was prepared using Ultra II Directional RNA Library Prep Kit (NEB, Cat #E7765) for all samples. After library-quality check, samples were sequenced paired end (50 bp) on Illumina NovaSeq S1.

Annotations from Genome assembly GRCm39 were adapted by filtering for transcripts with full coverage (defined as having at least one read covering each exon as counted by htseq-count v2.0.4) at least in one of the sample replicates, followed by making intron annotations within the space between two exons of each transcript. Bedtools v2.30.0 subtract and merge were used to first remove sequences with ambiguous (i.e. introns, exons and/or more than one gene) annotations and collapse the remaining annotations to obtain unambiguous annotations for exons and introns for each gene.

Raw RNA-seq reads were adapter- and poly-A trimmed using trim-galore v0.6.10 and poly X and poly G trimmed using fastp v0.23.4, followed by alignment to the reference genome using STAR v2.7.11a. Deduplication and conversion into name-sorted bam files were performed using samtools v1.18. Deeptools bamCoverage v3.5.2 was used with a bin size of 1 and normalization using counts per million to generate stranded coverage tracks. mRNA and pre-mRNA counts were determined as described previously,[43] with the following modifications: Htseq-count v2.0.4 was used to count intronic (within intron and intron-exon boundary mapping) and exonic (within exon, exon-exon junction and exon-intron boundary mapping) fragments. Transcripts per million (TPM) values were calculated from raw exonic and intronic counts by normalizing to library size and exon or intron length determined from the collapsed unambiguous genome annotation. Regression analysis was performed comparing the slope and y-intercept for log-log linear models with exonic normalized counts as predictor and intronic normalized counts as response variable each for input and pull-down using the R functions lm, and car::Anova.

TTP target genes were defined as genes with significantly higher counts in pull-down as compared to input. Both intronic and exonic fragment counts were used. Intronic fragment counts were in general low, making them prone to inaccurate determination of significant differences in pull-down as compared to input. To minimize the risk of including potentially false-positive genes, a threshold for the lowest acceptable counts was employed. The threshold was defined as the average intronic normalized counts in pull-down samples and had the value 3.891038. Genes with normalized intronic or exonic counts (in pull-down) above the threshold were included in the enrichment analysis. Enrichment analysis was performed for intronic and exonic normalized counts separately. Both data sets were first log(ln)-transformed, tested for differences in mean normalized counts of pull-down to input (t-test, two sided) followed by p-value correction using the Benjamini-Hochberg method. Log-fold change was calculated as ln(mean pull-down)-ln(mean input). Significantly enriched genes were defined using the filters padj. $\leq$ 0.05 and log-fold change > 0. In:Ex ratios are means of the quotients of intronic and exonic normalized counts per sample.

RNA-seq of RAW macrophages expressing TTP-WT or TTP-NLS^{mut}

Raw macrophages inducibly expressing TTP-WT or TTP-NLS^{mut} (0.5 μg/ml doxycyclin, 24 h), or control cells treated with vehicle (DMSO) were stimulated with LPS (10 ng/ml) for 6 h. RNA was isolated using the NucleoSpin RNA II Kit (Macherey-Nagel, Cat# 740955). Library of RNA samples for 3' mRNA-Seq was prepared using QuantSeq 3' mRNA-seq Library Prep Kit (lexogen). After library-quality check, samples were sequenced on an Illumina NovaSeqX 10B XP flowcell SingleRead 100 platform (entire lane,

single-end read). Raw RNA-seq reads were trimmed and aligned to reference the genome as described in the previous section. De-duplication and conversion into name-sorted bam files were performed using umitools v1.15. Read counts for 3' mRNA-seq were obtained with htseq count and differential expression analysis was performed using DESeq2 v1.45.0. GSEA was performed using fgsea v1.31.0 and msigbdr v7.5.1. Significantly enriched genes in 3' mRNA-seq were defined as above (padj. $\leq$ 0.05 and log-fold change > 0). Data visualization was performed using tidyverse v2.0.0 and ggplot2 v3.5.1.

AT content and ARE count

For investigation of average AT content and TTP binding motifs, sequences of exons and introns in TTP targets were obtained from GRCm39 using rtracklayer v1.65.0 and Biostrings v2.73.1 getSeq. AT content of those sequences was then calculated for each exon or intron sequence using Biostrings letterFrequency and TTP binding motifs (TATTTAT and TTATTTATT corresponding to UAUUUAU and UUAUUUAUU in RNA sequence) occurrences were counted using Biostrings vcountPattern and normalized to 1 kb.

Expression of recTZF peptides

The TZF domain used for recombinant production in E. coli corresponded to a synthetic peptide previously used in binding studies.[70] BL21(DE3) competent cells were transformed with 50 ng of pGEX-4T-1-GST-TEV.TZF-WT or the TZF-NLS^{mut} derivative which were synthesized by Genscript. The constructs contained TTP TZF domain (amino acids 93-165, mouse coordinates) or the mutated TZF version NLS^{mut}. Untransformed BL21 was used as empty control. Over-night cultures were diluted with fresh LB medium and grown at 37°C until OD600 reached ~0.6. Expression was induced by supplementing cultures with 1 mM IPTG (Sigma), 100 μM ZnSO4 and 0.2% glucose (Sigma, Cat # G8270) for 3 h at 37°C at 165 rpm. Afterwards, cells were harvested by centrifugation and lysed by One shot cell disrupter (Constant Systems Ltd.) with a pressure of 2 kbar in lysis buffer (1 M NaCl, 25 mM HEPES pH 7.4, 0.5 mM PMSF, 1x cOmplete protease inhibitor cocktail). Subsequently, lysates were cleared by centrifugation, 6000 rpm 4°C and protein concentration was estimated by BCA protein assay kits (Thermo-Fisher Scientific, Cat #23225).

RNA electrophoretic mobility shift assay

RNA electrophoretic mobility shift assay (EMSA) was performed using LightShift Chemiluminescent RNA EMSA Kit (Thermo-Fisher Scientific, Cat #20158) according to the manufacturer's instructions. 5' biotinylated and unlabeled Tnf-ARE probes (5'-AUUAUUU AUUAUUUAUUUAUUAUUUA-3') were purchased from Microsynth. In brief, HEK-293 cells and BL21(DE3) expressing inducible TTP constructs or TZF peptide constructs, respectively, were harvested as previously described. 15 μg of HEK-293 cell extract or 100 ng of BL21(DE3) extract were incubated with 0.5 μl Poly-U RNA (100 ng/μl, Sigma, Cat# P9528) 0.25 μl of biotin 5' labeled Tnf-ARE probe (500 nM), 1x REMSA binding buffer, and 5% Glycerol for 25 min at RT. BL21 (DE3) extract was additionally incubated with biotin 5' labeled Il1a-ARE, Cxcl2-ARE, Batf2-ARE and random oligo. For titration assays, cell lysates were incubated with different ratios of unlabeled to biotinylated probe (0x, 2x, 4x, 6x, 8x, or 10x excess of unlabeled probe). Subsequently, 1X REMSA Loading Buffer was added, and the samples were run on a 6% non-reducing polyacrylamide gel for 45 min at 100 V in 0.5x TBE. After wet-blotting in 0.5X TBE for 25 min at 250 mA, the Nylon membrane was crosslinked with UV light at 120 mJ/cm2 for 60 s using a commercial UV-light crosslinking instrument equipped with 254 nm bulbs. Biotin signal was detected and quantified by chemiluminescence according to standard LightShift Chemiluminescent RNA EMSA Kit protocol using a ChemiDoc™ Touch Imaging System (BioRad).

TZF structure prediction and modeling

AlphaFold2, USFR ChimeraX and the Robetta server[71–74] were used for structure prediction of TTP TZF defined as region spanning amino acids 93 – 165 (mouse coordinates) corresponding to ZFP36L2 TZF in the PDB entry. ZFP36L2 TZF NMR entry is lacking the most N-terminal and 3 C-terminal amino acids in comparison to the TTP TZF which was kept in the same length as for RNA binding experiments in this study and as used by others previously.[70] Structure prediction using USFR ChimeraX was done without energy minimization. For structure predictions with Robetta comparative modeling PDB entry 1RGO was used as template. Hydrogen bonds were analyzed using UCSF ChimeraX with hydrogen bond parameters set to 0.4 Å distance and 30° angle deviation. Root-mean-square-deviation (RMSD) of the models to 1RGO was analyzed by PYMOLalign with cycles set to 0 for all-atom RMSD calculation. Figures were prepared with PYMOL (http://www.pymol.org/).

QUANTITATION AND STATISTICAL ANALYSIS

For all experiments, statistical tests, n, and cut-offs are listed in the figure legend. Statistical analysis was performed using GraphPad Prism v.10.0.2 software.

Molecular Cell, Volume *85*

Supplemental information

Cytoplasmic mRNA decay

controlling inflammatory gene expression

is determined by pre-mRNA fate decision

Annika Bestehorn, Julius von Wirén, Christina Zeiler, Jeanne Fesselet, Sebastian Didusch, Maurizio Forte, Kevin Doppelmayer, Martina Borroni, Anita Le Heron, Sara Scinicariello, WeiQiang Chen, Manuela Baccarini, Vera Pfanzagl, Gijs A. Versteeg, Markus Hartl, and Pavel Kovarik

Figure S1

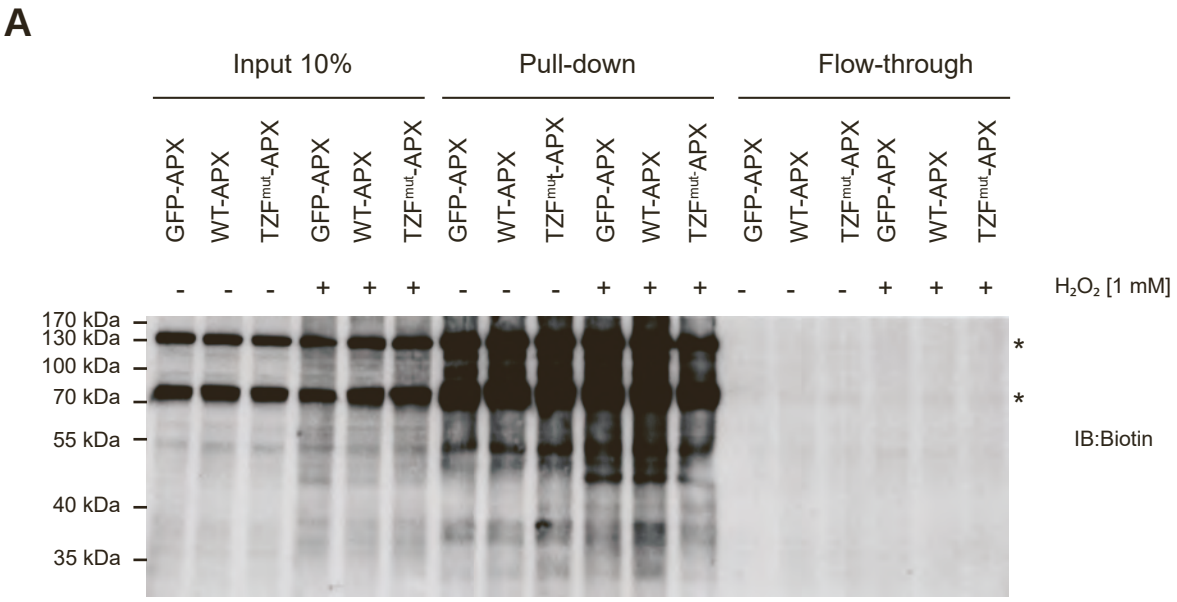
A
Input 10%
Pull-down
Flow-through
GFP-APX
WT-APX
TZFmut-APX
H2O2 [1 mM]
170 kDa
130 kDa
100 kDa
70 kDa
55 kDa
40 kDa
35 kDa
IB:Biotin

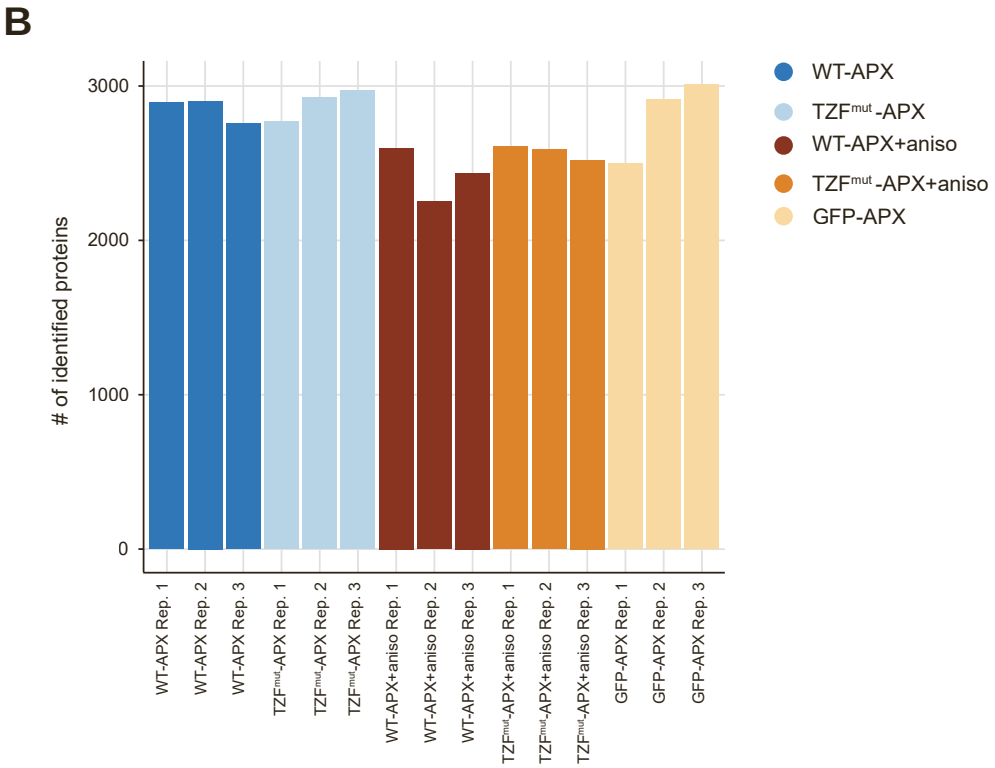
B
# of identified proteins
WT-APX
TZFmut-APX
WT-APX+aniso
TZFmut-APX+aniso
GFP-APX

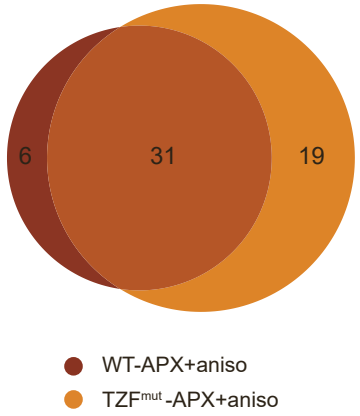
C
6
31
19
WT-APX+aniso
TZFmut-APX+aniso

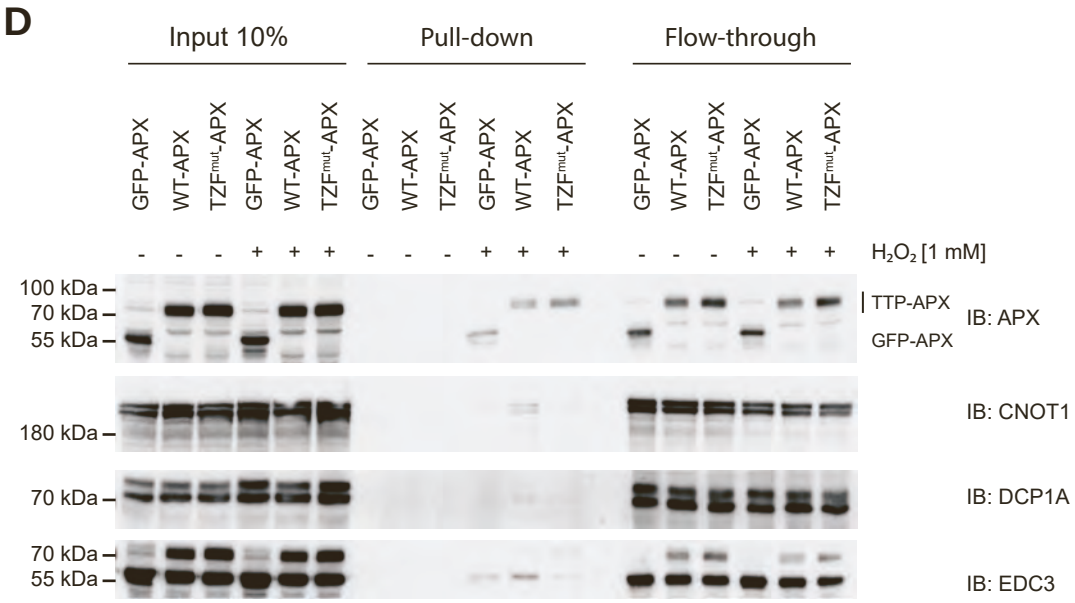
D
Input 10%
Pull-down
Flow-through
H2O2 [1 mM]
100 kDa
70 kDa
55 kDa
180 kDa
TTP-APX
GFP-APX
IB: APX
IB: CNOT1
IB: DCP1A
IB: EDC3

Figure S1. Quality control and validation of proximity labeling experiments. Related to Figure 1.
(A) Biotinylation activity of APX constructs analyzed by Western blotting. WT-APX, TZF^{mut}-APX and GFP-APX expression in HEK-293 cells was induced (1 µg/ml dox, 3.5 h) followed by the addition of biotin-phenol and H_2O_2. H_2O_2 was omitted, as indicated, to assess endogenous biotinylation. Cell lysates (Input) were subjected to streptavidin pull-down; pull-down efficiency was estimated by using the flow-through. Immunoblotting (IB): biotin antibody. The overall higher biotin signal in H_2O_2-treated input and pull-down as compared to samples without H_2O_2 confirms APX-dependent labeling. Biotin signal in samples without H_2O_2 indicates endogenous biotinylation; discrete bands (asterisks) present in input and pull-down regardless of H_2O_2 treatment show positions of biotin-dependent pyruvate carboxylase, mitochondrial (UniProt: P11498, upper band) and methylcrotonoyl-CoA carboxylase subunit alpha, mitochondrial (UniProt: Q96RQ3, lower band) (**Table S1**).
(B) Numbers of proteins identified in individual replicates by LC-MS/MS (calculated from LFQ intensities before imputation).
(C) Overlap of proteins enriched in WT-APX+aniso (WT-APX+aniso vs. GFP-APX) and TZF^{mut}-APX+aniso (TZF^{mut}-APX+aniso vs. GFP-APX) interactomes ($log_2FC > 1$, padj. ≤ 0.05, n = 3).
(D) Validation of APX-dependent interactions by Western blotting. WT-APX, TZF^{mut}-APX and GFP-APX expression in HEK-293 cells and proximity labeling was performed as in (A). H_2O_2 was omitted as indicated. Cell lysates (Input), streptavidin pull-down and flow-through samples were analyzed by immunoblotting using antibodies to APEX (APX), CNOT1, DCP1A and EDC3. Positions of TTP-APX fusion proteins (WT-APX and TZF^{mut}-APX) and the GFP-APX fusion protein are indicated. Note that the signal above the EDC3 band results from incomplete stripping of APX antibodies from the membrane.

Figure S2

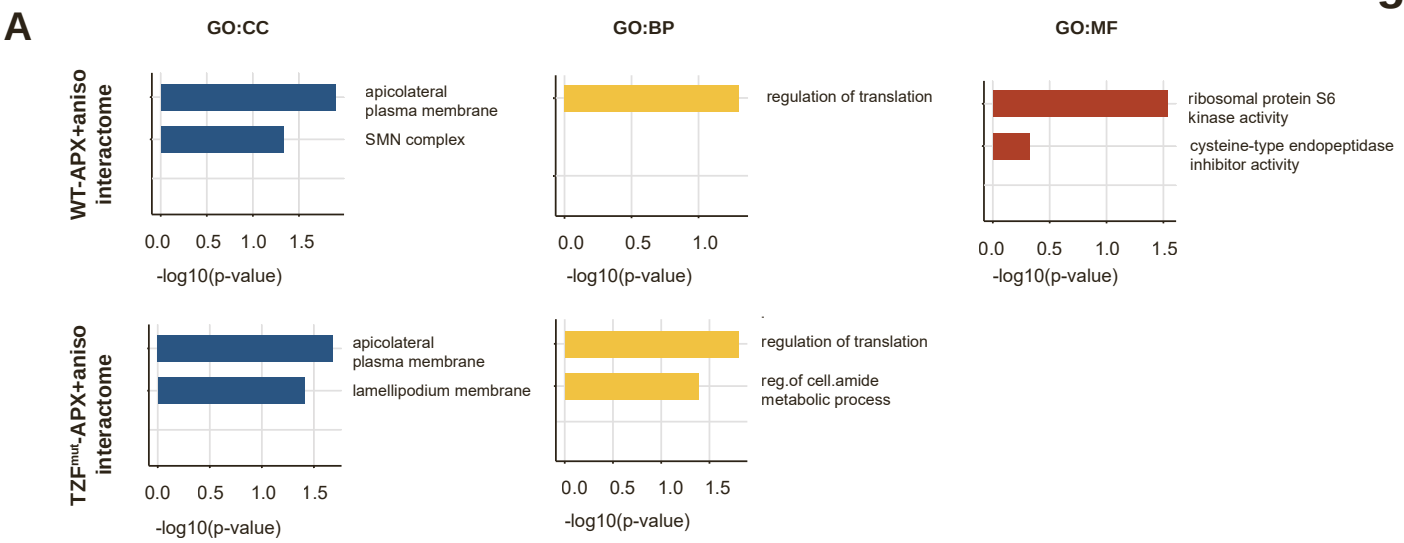
A
GO:CC
GO:BP
GO:MF
WT-APX+aniso interactome
apicolateral plasma membrane
SMN complex
regulation of translation
ribosomal protein S6 kinase activity
cysteine-type endopeptidase inhibitor activity
TZFmut-APX+aniso interactome
apicolateral plasma membrane
lamellipodium membrane
regulation of translation
reg.of cell.amide metabolic process
0.0 0.5 1.0 1.5
-log10(p-value)

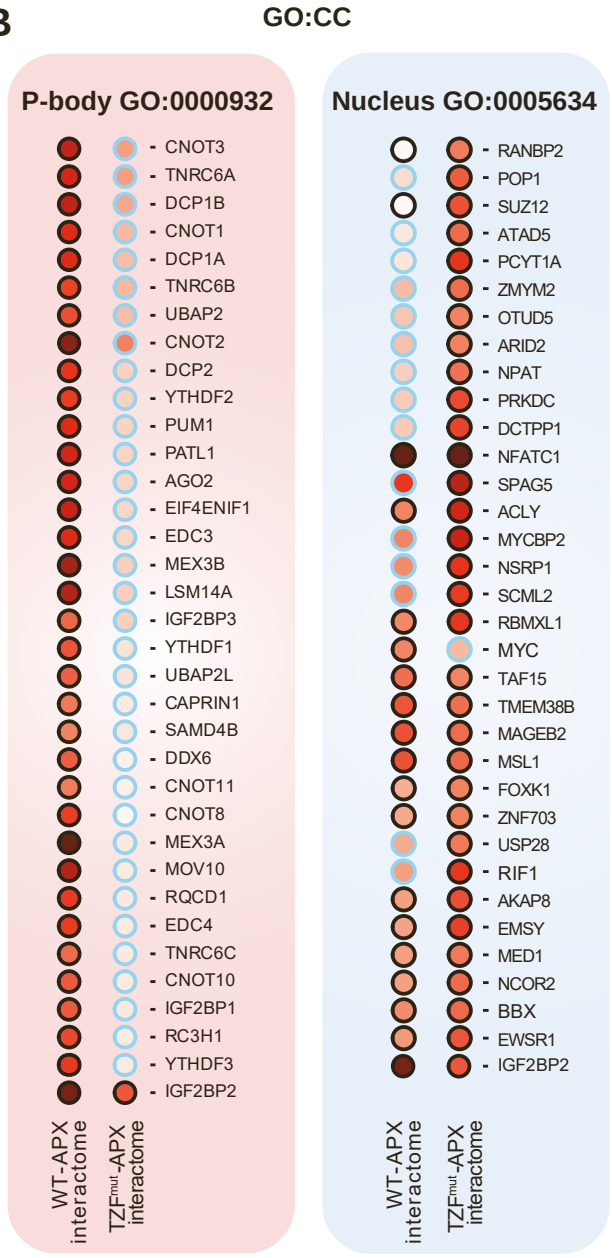
B
GO:CC
P-body GO:0000932
CNOT3
TNRC6A
DCP1B
CNOT1
DCP1A
TNRC6B
UBAP2
CNOT2
DCP2
YTHDF2
PUM1
PATL1
AGO2
EIF4ENIF1
EDC3
MEX3B
LSM14A
IGF2BP3
YTHDF1
UBAP2L
CAPRIN1
SAMD4B
DDX6
CNOT11
CNOT8
MEX3A
MOV10
RQCD1
EDC4
TNRC6C
CNOT10
IGF2BP1
RC3H1
YTHDF3
IGF2BP2
WT-APX interactome
TZFmut-APX interactome
Nucleus GO:0005634
RANBP2
POP1
SUZ12
ATAD5
PCYT1A
ZMYM2
OTUD5
ARID2
NPAT
PRKDC
DCTPP1
NFATC1
SPAG5
ACLY
MYCBP2
NSRP1
SCML2
RBMXL1
MYC
TAF15
TMEM38B
MAGEB2
MSL1
FOXK1
ZNF703
USP28
RIF1
AKAP8
EMSY
MED1
NCOR2
BBX
EWSR1
IGF2BP2
WT-APX interactome
TZFmut-APX interactome

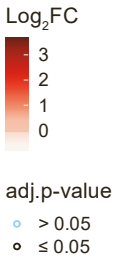
Log2FC
3
2
1
0
adj.p-value
> 0.05
≤ 0.05

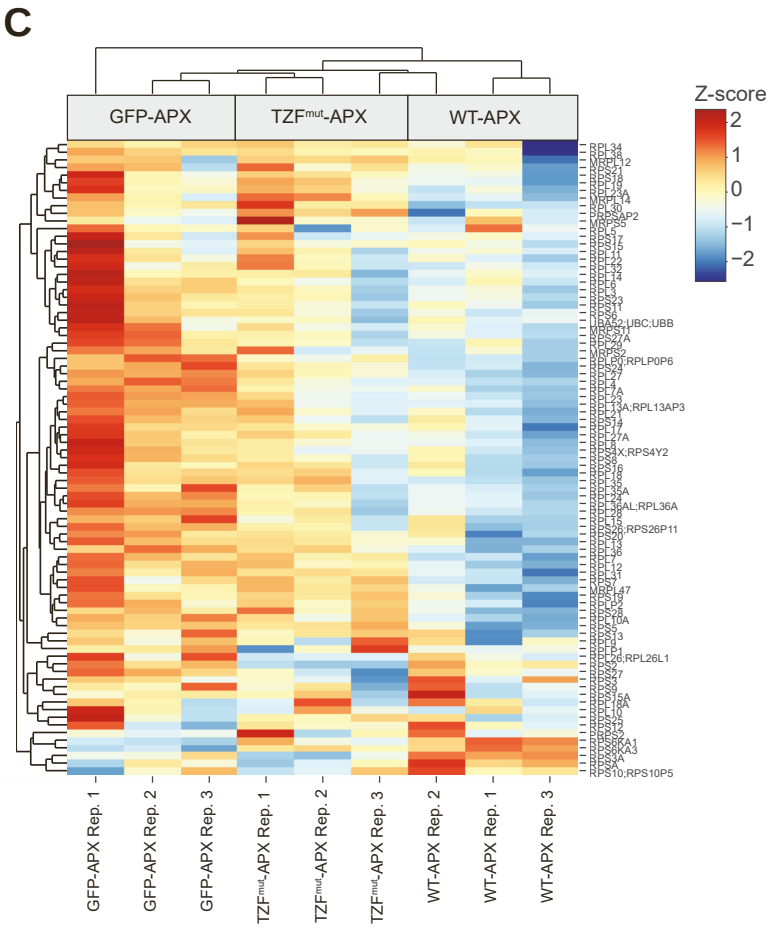
C
GFP-APX
TZFmut-APX
WT-APX
Z-score
2
1
0
−1
−2
GFP-APX Rep. 1
GFP-APX Rep. 2
GFP-APX Rep. 3
TZFmut-APX Rep. 1
TZFmut-APX Rep. 2
TZFmut-APX Rep. 3
WT-APX Rep. 2
WT-APX Rep. 1
WT-APX Rep. 3

Figure S2. WT-APX and TZF^{mut}-APX interactome analyses. Related to Figure 2.
(A) Overrepresentation of GO terms in WT-APX+aniso. and TFZ^{mut}-APX+aniso. interactomes. Interactomes were defined as proteins significantly enriched over GFP-APX background labeling control ($log_2FC \geq 1$ and padj. < 0.05, $n = 3$) in LC-MS/MS data. Bar plots depict significantly overrepresented terms in the GO categories CC, BP and MF. Note that no MF terms were enriched in TZF^{mut}-APX+aniso. interactome and are therefore not shown.
(B) Proteins from GO terms P-body (GO:000932) and Nucleus (GO: 0005634) found enriched in WT-APX or TZF^{mut}-APX interactomes. Black circles: significantly enriched proteins; blue circles: proteins not enriched. Fold-change (log_2FC) enrichment is indicated by color code.
(C) Heat map analysis visualizing integral ribosomal proteins (KEGG Ribosome 03010) in LC-MS/MS data for WT-APX, TZF^{mut}-APX and GFP-APX replicates. No enrichment of integral ribosomal proteins in WT-APX and TZF^{mut}-APX interactomes as compared to GFP-APX interactome is detectable.

Figure S3

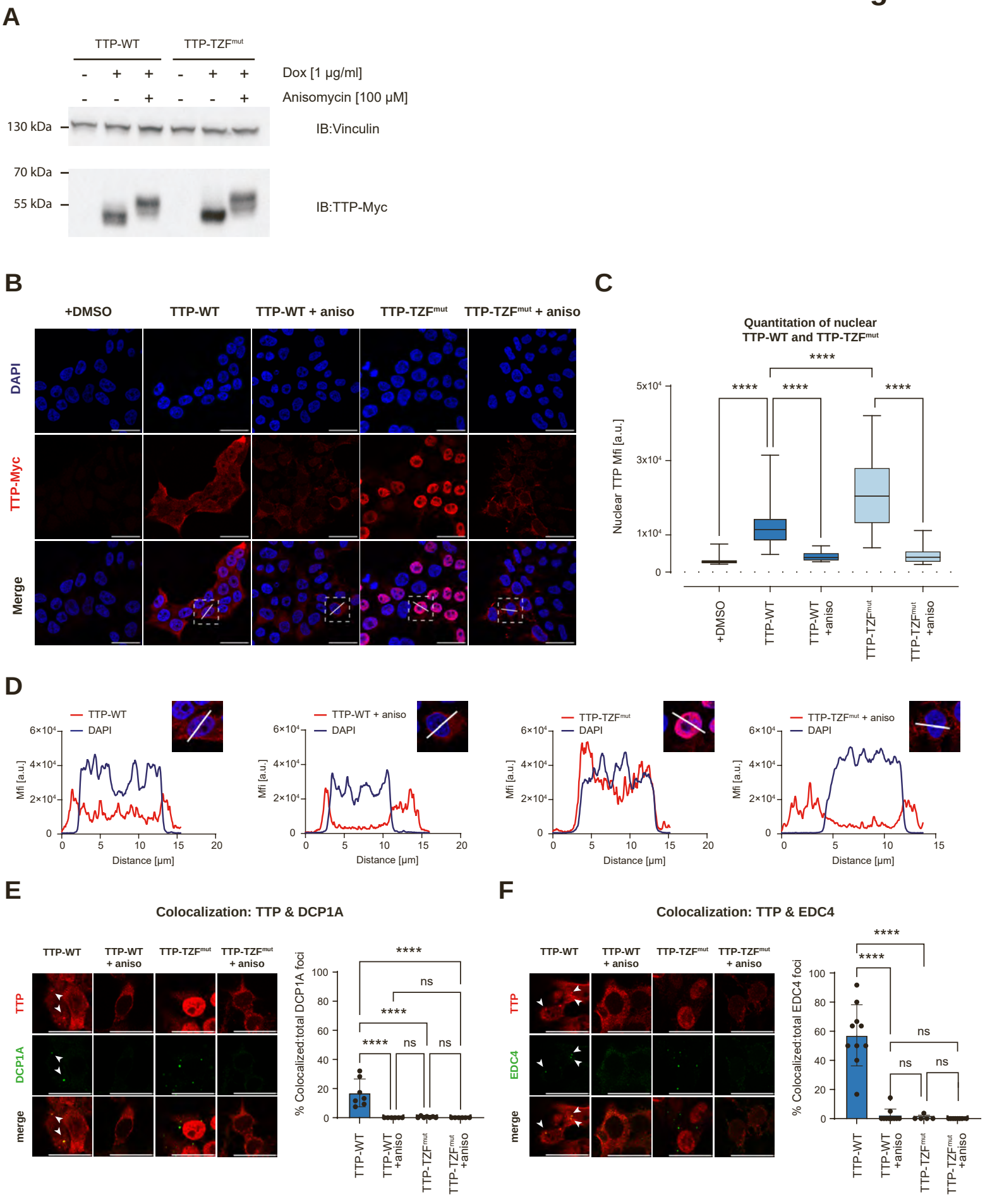
A
TTP-WT
TTP-TZF^mut
Dox [1 µg/ml]
Anisomycin [100 µM]
130 kDa
IB:Vinculin
70 kDa
55 kDa
IB:TTP-Myc
B
+DMSO
TTP-WT
TTP-WT + aniso
TTP-TZF^mut
TTP-TZF^mut + aniso
DAPI
TTP-Myc
Merge
C
Quantitation of nuclear TTP-WT and TTP-TZF^mut
Nuclear TTP Mfi [a.u.]
D
TTP-WT
TTP-WT + aniso
TTP-TZF^mut
TTP-TZF^mut + aniso
DAPI
Mfi [a.u.]
Distance [µm]
E
Colocalization: TTP & DCP1A
TTP
DCP1A
merge
% Colocalized:total DCP1A foci
F
Colocalization: TTP & EDC4
EDC4
% Colocalized:total EDC4 foci
ns

Figure S3. Anisomycin regulates subcellular localization of TTP independent of RNA binding. Related to Figure 2.
(A) Phosphorylation of TTP-WT and TTP-TZF^{mut} upon anisomycin treatment (100 µM, 1.5 h) in HEK-293 cells visualized by Western blotting. TTP-WT and TTP-TZF^{mut} expression was induced (1 µg/ml dox, 16 h). Immunoblot (IB): Myc (myc tagged TTP), and vinculin (loading control).
(B - D) TTP-WT and TTP-TZF^{mut} localization in HEK-293 cells upon anisomycin-induced stress. (**B**) Representative immunofluorescence images of inducibly expressed (1 µg/ml dox, 16 h) TTP-WT and TTP-TZF^{mut} in HEK-293 cells. Control cells were treated with vehicle (DMSO). Brightness and contrast of Myc channel were adjusted equally in all images of the panel using ImageJ. TTP-WT and TTP-NLS^{mut} detection: Myc antibody (red); nucleus: DAPI (blue). Profile lines were drawn through representative cells (enlarged 2-fold in insets) for quantitation of mean fluorescence intensity (MFI) in (D). Scale bar = 25 µm. **(C)** Quantitation of nuclear MFI of TTP-WT and TTP-TZF^{mut}. Masks for quantitation of nuclear MFI were computationally defined by using ImageJ. Box represents interquartile range, horizontal line in box depicts median. One-way analysis of variance (ANOVA) with Tukey's multiple comparisons test, n = 105, ****padj. < 0.0001. (**D**) MFI quantitation along profile lines drawn in (B). TTP-TZF^{mut} and DAPI profiles were similar, implying nuclear localization.
(E and F) Anisomycin effects on colocalization of TTP-WT or TTP-TZF^{mut} (Myc antibody, red) with endogenous DCP1A **(E)** and EDC4 **(F)** foci (green). TTP-WT and TTP-TZF^{mut} expression and anisomycin treatment were as in (B). Individual cells are shown in insets together with DCP1A or EDC4 (both green) in individual and merged channels (left). Arrowheads: DCP1A or EDC4 foci colocalizing with TTP. Scale bar = 25 µm. Quantitation (Fiji Comdet) of colocalization of TTP-WT or TTP-TZF^{mut} with DCP1A or EDC4 foci (right). Student's t test. ****padj. < 0.0001, n = 105-152 cells.

A

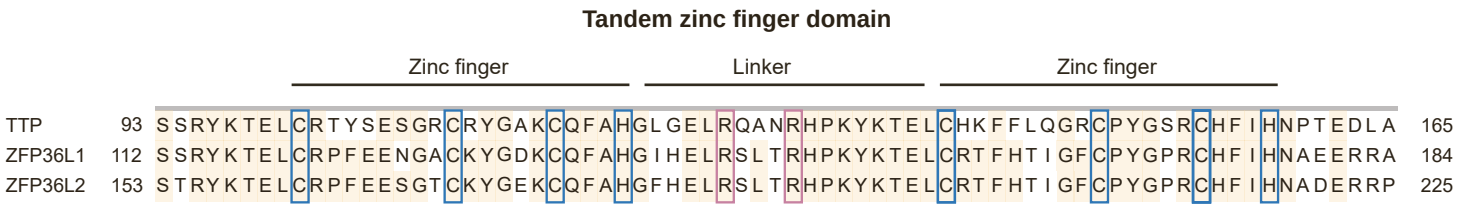
Tandem zinc finger domain
Zinc finger
Linker
Zinc finger
TTP 93 SSRYKTELCRTYSESGRCRYGAKCQFAHGLGELRQANRHPKYKTELCHKFFLQGRCPYGSRCHFIHNPTEDLA 165
ZFP36L1 112 SSRYKTELCRPFEENGACKYGDKCQFAHGIHELRSLTRHPKYKTELCRTFHTIGFCPYGPRCHFIHNAEERRA 184
ZFP36L2 153 STRYKTELCRPFEESGTCKYGEKCQFAHGFHELRSLTRHPKYKTELCRTFHTIGFCPYGPRCHFIHNADERRP 225

B

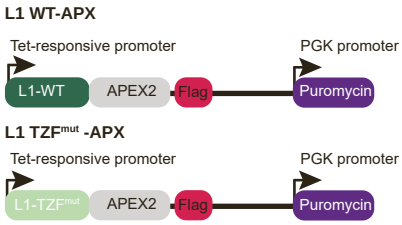
L1 WT-APX
Tet-responsive promoter
PGK promoter
L1-WT
APEX2
Flag
Puromycin
L1 TZFmut -APX
Tet-responsive promoter
PGK promoter
L1-TZFmut
APEX2
Flag
Puromycin

C

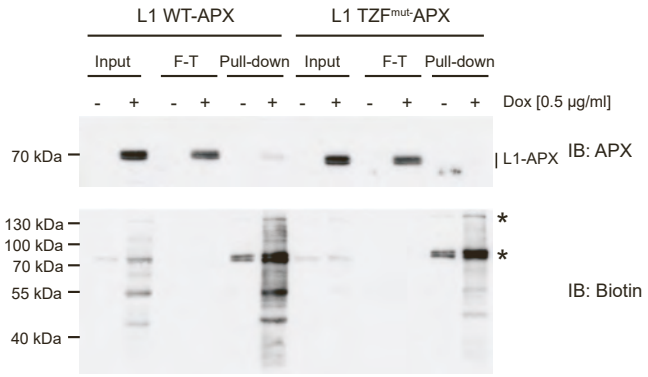
L1 WT-APX
L1 TZFmut-APX
Input
F-T
Pull-down
Input
F-T
Pull-down
- + - + - + - + - + - +
Dox [0.5 µg/ml]
70 kDa
L1-APX
IB: APX
130 kDa
100 kDa
70 kDa
55 kDa
40 kDa
*
*
IB: Biotin

D

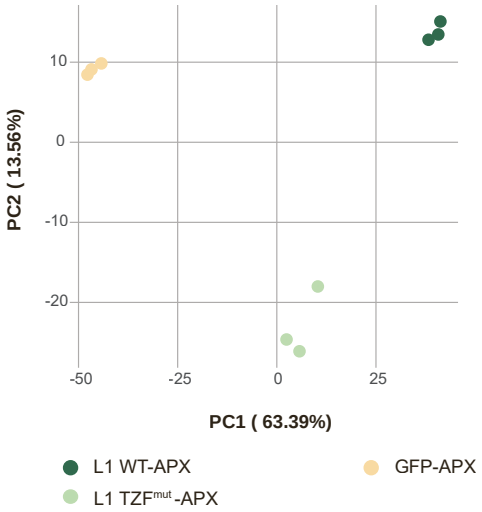
10
0
-10
-20
PC2 (13.56%)
-50
-25
0
25
PC1 (63.39%)
L1 WT-APX
GFP-APX
L1 TZFmut -APX

E

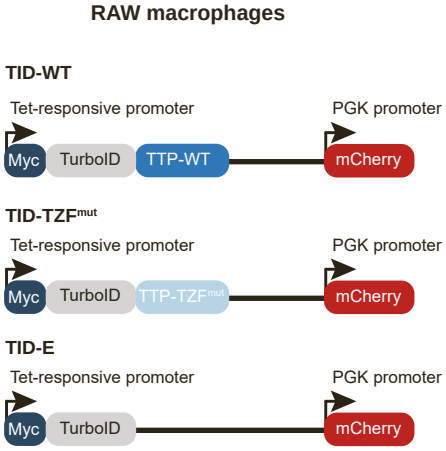
RAW macrophages
TID-WT
Tet-responsive promoter
PGK promoter
Myc
TurboID
TTP-WT
mCherry
TID-TZFmut
Tet-responsive promoter
PGK promoter
Myc
TurboID
TTP-TZFmut
mCherry
TID-E
Tet-responsive promoter
PGK promoter
Myc
TurboID
mCherry

F

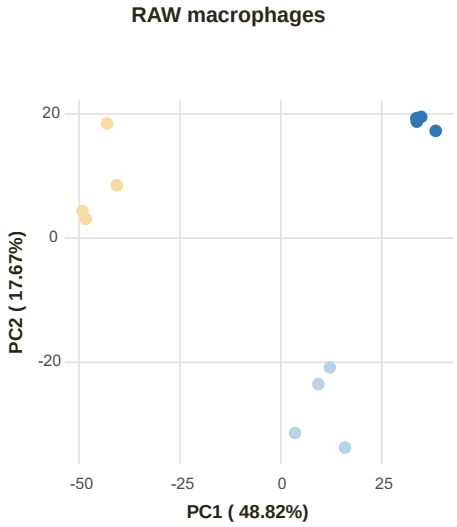
RAW macrophages
20
0
-20
PC2 (17.67%)
-50
-25
0
25
PC1 (48.82%)

Figure S4. Impact of RNA binding on the interactome and subcellular localization of ZFP36L1 in HEK-293 and TTP in RAW macrophages. Related to Figures 3 and 4.

(A) Multiple sequence alignment of TZF domains of murine TTP (NP_035886), ZFP36L1 (NP_031590) and ZFP36L2 (NP_001001806). TZF domain is defined as a 73 amino acid long region comprising ZF1, ZF2, linker between ZFs, conserved N-terminal leader sequence and seven C-terminal amino acids. ZF cysteines and histidines are in blue, arginines relevant for the nuclear localization are in lilac.

(B Scheme of ZFP36L1 WT and TZF^{mut} fused N-terminally to APEX2 (L1 WT-APX and L1 TZF^{mut}-APX) downstream of a tetracycline-responsive promoter. All constructs contained a C-terminal Flag tag. Puromycin was used for selection following lentivirus-mediated transduction of HEK-293 cells.

(C) Biotinylation activity of L1 WT-APX and L1 TZF^{mut}-APX analyzed by Western blotting. L1 WT-APX and L1 TZF^{mut}-APX expression in HEK-293 cells was induced (0.5 µg/ml dox, 16 h) followed by the addition of biotin-phenol and H_2O_2. Controls without doxycycline treatment were included. Cell lysates (Input) were subjected to streptavidin pull-down (Pull-down); pull-down efficiency was estimated using the flow-through (F-T). Immunoblotting (IB): biotin antibody. Discrete bands (asterisks) present in input and pull-down samples regardless of H_2O_2 treatment show positions of biotin-dependent pyruvate carboxylase, mitochondrial (UniProt: P11498, upper band) and methylcrotonoyl-CoA carboxylase subunit alpha, mitochondrial (UniProt: Q96RQ3, lower band) (**Table S2**).

(D) PCA of protein intensities of L1 WT-APX, L1 TZF^{mut}-APX and GFP-APX replicates.

(E) Scheme of TTP WT and TTP TZF^{mut} C-terminally fused to TurboID (TID-WT and TID-TZF^{mut}) for doxycycline-inducible expression in RAW macrophages. TID-empty (TID-E) was included as a background labeling control. All constructs were N-terminally Myc tagged. mCherry was used for selection by flow cytometry.

(F) PCA of protein intensities visualizing clustering of four biological replicates of TID-WT, TID-TZF^{mut} and TID-E. TID-WT and TID-TZF^{mut} expression was induced with doxycycline (0.5 µg/ml, 24 h).

Figure S5

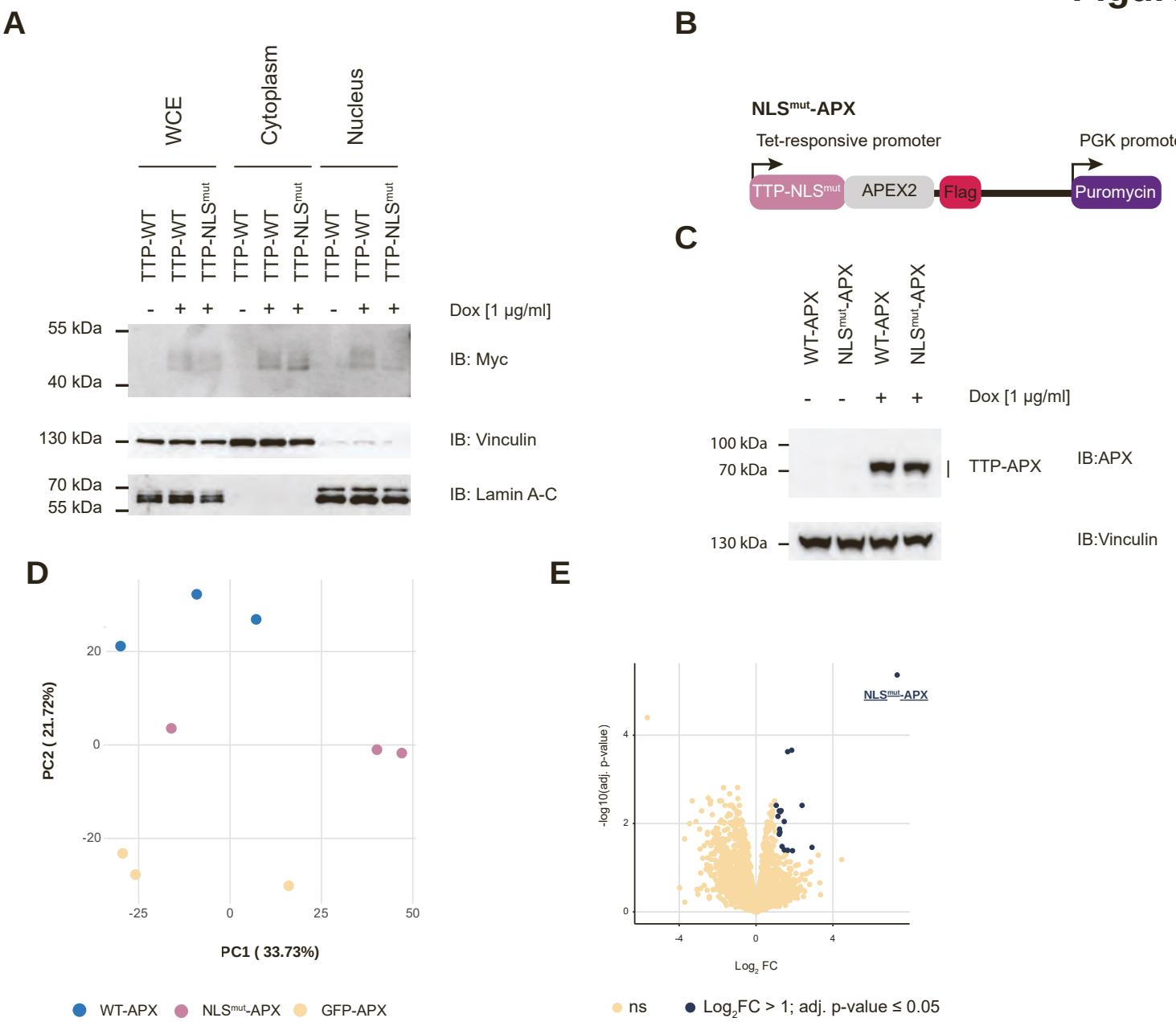
A
WCE
Cytoplasm
Nucleus
TTP-WT
TTP-NLSmut
Dox [1 µg/ml]
55 kDa
40 kDa
IB: Myc
130 kDa
IB: Vinculin
70 kDa
55 kDa
IB: Lamin A-C
B
NLSmut-APX
Tet-responsive promoter
PGK promoter
TTP-NLSmut
APEX2
Flag
Puromycin
C
WT-APX
NLSmut-APX
Dox [1 µg/ml]
100 kDa
70 kDa
TTP-APX
IB:APX
130 kDa
IB:Vinculin
D
PC2 (21.72%)
PC1 (33.73%)
WT-APX
NLSmut-APX
GFP-APX
E
NLSmut-APX
-log10(adj. p-value)
Log2 FC
ns
Log2FC > 1; adj. p-value ≤ 0.05
F
Input 10%
Pull-down
Flow-through
Dox [1 µg/ml]
Anisomycin [100 µM]
130 kDa
IB:CNOT3
IB:CNOT3 (overexposed)
55 kDa
IB:TTP
IB:TTP (overexposed)

Figure S5. Nuclear import-deficient TTP interactome. Related to Figure 5.
(A) Subcellular localization of inducibly expressed (1 µg/ml dox, 3.5 h) TTP-WT and TTP-NLS^{mut} in HEK-293 cells analyzed by fractionation and Western blotting. (-dox) was used as negative control. Anisomycin (+aniso, 1.5 h) was used as indicated. Whole-cell extract (WCE), cytoplasmic (Cytoplasm) and nuclear (Nucleus) fractions were analyzed. Immunoblot (IB): Myc (myc-tagged TTP), vinculin (cytoplasmic loading control), lamin A-C (nuclear loading control).
(B) Scheme of NLS^{mut}-APX construct used for proximity-dependent labeling.
(C) Inducible expression of WT-APX and NLS^{mut}-APX in HEK-293 cells used for subsequent proximity labeling experiments.
(D) PCA of protein intensities visualizing replicate clusters of WT-APX, NLS^{mut}-APX and GFP-APX interactomes in HEK-293 analyzed by LC-MS/MS. Induction of WT-APX, NLS^{mut}-APX and GFP-APX were carried out as in Figure 1B.
(**E**) Differential enrichment analysis of NLS^{mut}-APX vs. GFP-APX interactomes. Significantly enriched proteins ($log_2FC > 1$, padj. ≤ 0.05, n = 3) are highlighted (blue).
(**F**) Co-immunoprecipitation experiments for the analysis of interactions between TTP-WT or TTP-NLS^{mut} with CNOT3. Lysates (Input) from doxycycline (1 µg/ml, 3.5 h) or vehicle (DMSO)-treated HEK-293 cells expressing inducible TTP-WT or TTP-NLS^{mut} constructs were subjected to Myc pull-down followed by immunoblotting (IB) using CNOT3 and Myc antibodies. Anisomycin (+aniso, 1.5 h) was used as indicated. Pull-down efficiency was estimated by the analysis of the flow-through fractions.

Figure S6

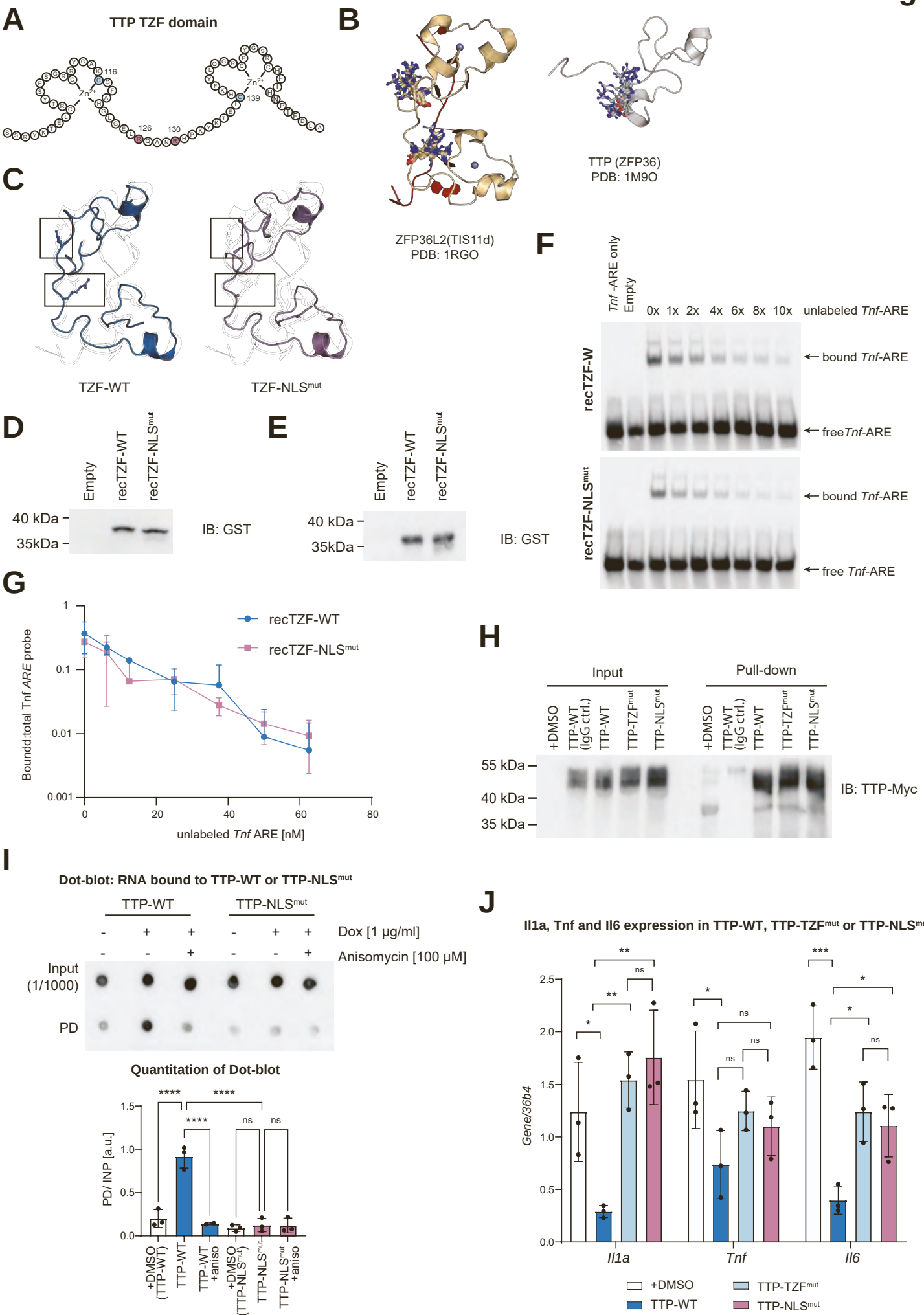
A
TTP TZF domain
116
126
130
139
B
ZFP36L2(TIS11d)
PDB: 1RGO
TTP (ZFP36)
PDB: 1M9O
C
TZF-WT
TZF-NLSmut
D
Empty
recTZF-WT
recTZF-NLSmut
40 kDa
35kDa
IB: GST
E
Empty
recTZF-WT
recTZF-NLSmut
40 kDa
35kDa
IB: GST
F
Tnf -ARE only
Empty
0x 1x 2x 4x 6x 8x 10x unlabeled Tnf-ARE
recTZF-W
bound Tnf-ARE
freeTnf-ARE
recTZF-NLSmut
bound Tnf-ARE
free Tnf-ARE
G
recTZF-WT
recTZF-NLSmut
Boundd:total Tnf ARE probe
unlabeled Tnf ARE [nM]
H
Input
Pull-down
+DMSO
TTP-WT (IgG ctrl.)
TTP-WT
TTP-TZFmut
TTP-NLSmut
55 kDa
40 kDa
35 kDa
IB: TTP-Myc
I
Dot-blot: RNA bound to TTP-WT or TTP-NLSmut
TTP-WT
TTP-NLSmut
Dox [1 µg/ml]
Anisomycin [100 µM]
Input (1/1000)
PD
Quantitation of Dot-blot
PD/ INP [a.u.]
+DMSO (TTP-WT)
TTP-WT
TTP-WT +aniso
+DMSO (TTP-NLSmut)
TTP-NLSmut
TTP-NLSmut +aniso
J
Il1a, Tnf and Il6 expression in TTP-WT, TTP-TZFmut or TTP-NLSmut cells
Gene/36b4
Il1a
Tnf
Il6
+DMSO
TTP-WT
TTP-TZFmut
TTP-NLSmut

Figure S6. Analysis of nuclear import-deficient TTP mutant. Related to Figure 6.
(A) Murine TTP TZF domain. R126 and R130 (lilac) mutated in TTP-NLS^{mut}, and C116 and C139 (blue) mutated in TTP-TZF^{mut} are highlighted.
(B) NMR ensemble conformations of arginine residues critical for functional NLS in ZFP36L2 and TTP. Reported NMR structure of RNA-bound ZFP36L2 TZF (PDB: 1RGO) and all conformations (20 states in NMR ensemble) of R184 and R188 (full length coordinates) shown on left. Reported NMR structure of TTP ZF1 (PDB: 1M9O) and all conformations (23 states in NMR ensemble) of R126 (full length coordinate) shown on the right. Only R126 is comprised in the available TTP ZF1 structure. Relevant arginines shown as balls and sticks, protein backbone structures shown as cartoon.
(C) Superposition of TTP TZF-WT (left, blue) and TTP TZF-NLS^{mut} (right, lilac) AlphaFold2 models with NMR structure of ZFP36L2 TZF (1RGO, state 11, black outline). Protein backbones shown as cartoons, relevant arginines shown as balls & sticks and highlighted in rectangles. Mutations of R to A in TTP TZF-NLS^{mut} (right, lilac) are highlighted in rectangles and visible against R residues in ZFP36L2 background (black outline).
(D and E) Expression of recTZF-WT and recTZF-NLS^{mut} used in Figure 6B and 6D. IB: GST antibody.
(F and G) Binding of recombinant TZF-WT and TZF-NLS^{mut} GST fusion proteins (recTZF-WT and recTZF-NLS^{mut}) to *Tnf*-ARE assessed by RNA EMSA upon different excess (0x, 1x, 2x, 4x, 6x, 8x or 10x) of unlabeled *Tnf*-ARE. Control (Empty): *E. coli* without expression constructs. (**F**) Images representative of three independent experiments. (**G**) Quantitation (ChemiDoc) of RNA EMSA: *Tnf*-ARE-bound fraction was determined as ratio of bound versus total labeled *Tnf*-ARE and depicted as means and SDs (n = 3), in $\log_{10}$ scale.
(H) Inducible expression of TTP-WT, TTP-NLS^{mut}, and TTP-TZF^{mut} in RAW macrophages. Construct expression was induced with doxycycline (0.5 µg/ml, 24 h); DMSO was used as vehicle control. Cell lysates (Input) were subjected to Myc antibody-mediated pull-down followed by Western blotting using TTP antibodies. Isotype IgG was used as negative control.
(I) Dot blot analysis of RNA bound by TTP-WT or TTP-NLS^{mut} in HEK-293 cells. TTP-WT and TTP-NLS^{mut} were induced (dox 1 µg/ml, 3.5 h) followed by 4sU treatment (100 µM, added 1 h prior to harvest). Anisomycin treatment (100 µM, 1.5 h) as indicated. Cells were crosslinked and subsequently subjected to Myc antibody-mediated pull-down followed by RNA isolation, in vitro 3' RNA biotin ligation and dot-blotting with a streptavidin-HRP conjugate (top). Quantitation of representative dot-blot from 3 independent experiments (bottom). One-way ANOVA n = 3, ****padj. < 0.0001.
(J) *Il1a, Tnf* and *Il6* mRNA levels in RAW macrophages expressing TTP-WT, TTP-NLS^{mut}, and TTP-TZF^{mut} assessed by qRT-PCR analysis. Cells were treated with doxycycline (0.5 µg/ml, 24 h, DMSO as negative control) to induce TTP construct expression followed by LPS stimulation (10 ng/ml, 6 h). *36b4* was used for normalization. Means and SDs, with all data points shown. Two-way ANOVA n = 3, *padj. < 0.05, **padj. < 0.01, ***padj. < 0.001.

Figure S7

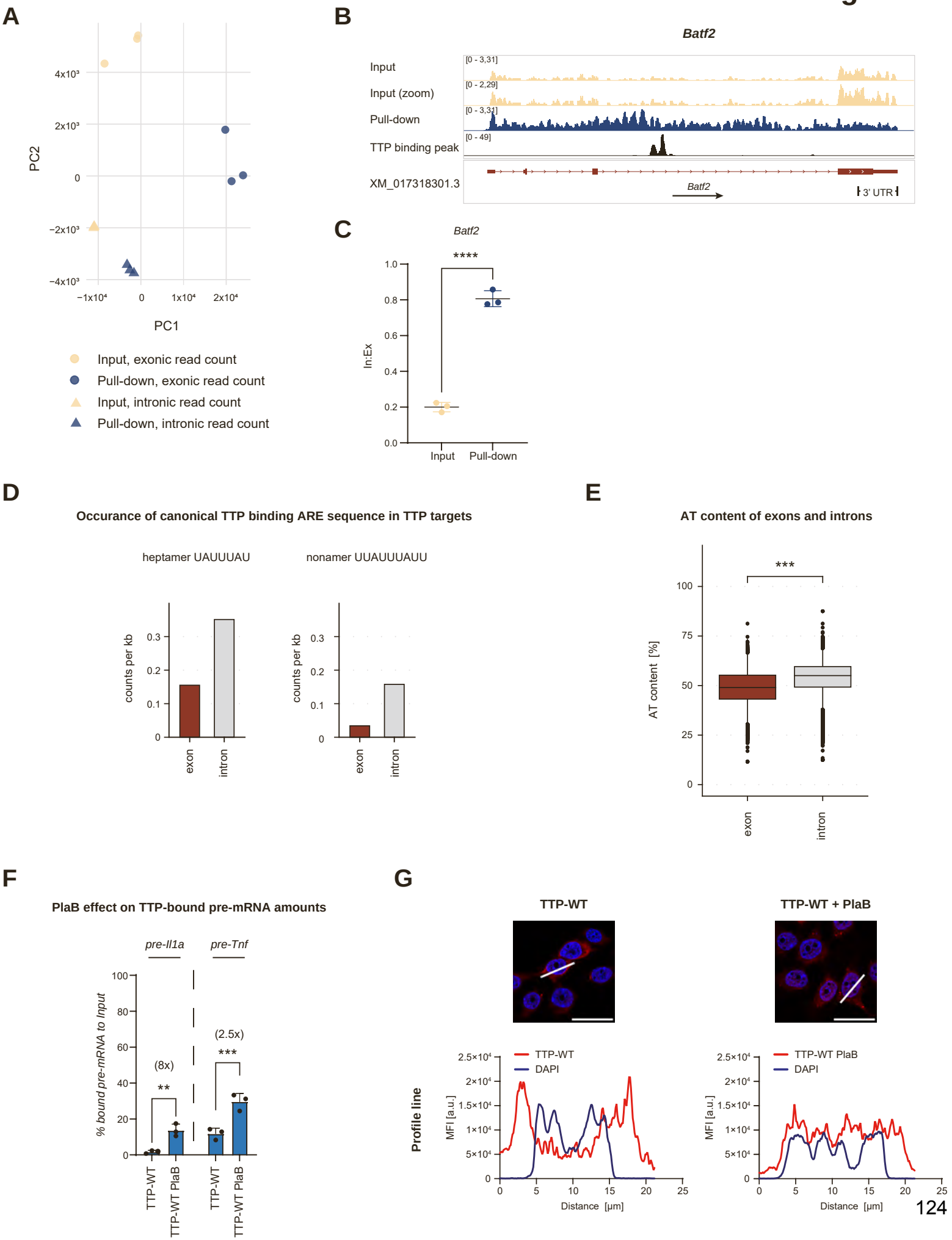
A
PC2
PC1
Input, exonic read count
Pull-down, exonic read count
Input, intronic read count
Pull-down, intronic read count
B
Batf2
Input
Input (zoom)
Pull-down
TTP binding peak
XM_017318301.3
3' UTR
C
Batf2
In:Ex
Input
Pull-down
D
Occurance of canonical TTP binding ARE sequence in TTP targets
heptamer UAUUUAU
nonamer UUAUUUAUU
counts per kb
exon
intron
E
AT content of exons and introns
AT content [%]
F
PlaB effect on TTP-bound pre-mRNA amounts
pre-Il1a
pre-Tnf
% bound pre-mRNA to Input
(8x)
(2.5x)
TTP-WT
TTP-WT PlaB
G
TTP-WT
TTP-WT + PlaB
Profile line
MFI [a.u.]
Distance [µm]
DAPI

Figure S7. Differential enrichment of pre-mRNA versus mRNA in TTP-bound RNA in RAW macrophages. Related to Figure 7.
(A) Intronic and exonic RNA-seq read counts of TTP-bound RNA (pull-down) and of total cellular RNA (input) visualized by PCA. RAW macrophage treatment and RNA isolation were as described in Figure 7. Exonic and intronic reads were annotated and separately counted. Replicates of individual samples are indicated.
(B) Representative tracks for TTP target *Batf2* in input and pull-down samples. Data generation and visualization as described in Figure 7.
(C) In:Ex ratio in input and pull-down for TTP target *Batf2* means with SD, unpaired Student's t test, ****padj. < 0.0001.
(D) Occurrence of canonical TTP binding ARE heptamer UAUUUAU or nonamer UUAUUUAUU in exons and introns of high confidence TTP targets (defined in Figure 7D). ARE counts were normalized to sequence length (kb).
(E) Global assessment of AT-content [%] in exon and intron reads from Pull-down RNA seq data set (Figure 7). Box represents interquartile range, and horizontal line in box depicts median, unpaired Student's t test, ***padj. < 0.001.
(F) Quantitation of pre-mRNAs bound to TTP-WT in RAW macrophages upon PlaB treatment (500 nM, 3.5 h), assessed by RT-qPCR. Cells were stimulated and processed as in Figure 6F. Enrichment of pre-Il1a and pre-Tnf mRNA in pull-down is shown as percentage of pull-down to input RNA. Two-way analysis of variance (ANOVA), means of RT-qPCR data with SDs, n = 3, **padj. < 0.01, ***padj. < 0.001.
(G) Quantitation of PlaB effect on nuclear localization of TTP-WT in HEK-293 cells. Induction of TTP-WT was carried out as in Figure 7G. Profile lines were drawn through representative cells (top) and MFI was quantitated across the line (bottom). Scale bar = 25 µm. TTP-WT detection: Myc antibody (red); nucleus: DAPI (blue).

Discussion

Mediator kinase activity, conferred by CDK8 and its paralog CDK19, has emerged as a critical regulator of transcriptional responses to cytokine signaling, most notably in the IFN pathway. Previous work from our lab has elucidated the role of Mediator kinase in supporting IFNγ-induced gene expression via phosphorylation of STAT1 at S727 and promotion of RNA pol II pause release, establishing Mediator kinase as a positive regulator of JAK-STAT signaling.[134-135] However, whether these activating functions extend beyond IFN signaling, and how they intersect with other inflammatory pathways such as TLR signaling, remained largely unexplored. In the main part of this thesis, we employed selective Mediator kinase inhibitors to uncover a previously unappreciated context-dependent role for Mediator kinase in macrophages: while promoting STAT-dependent transcription in response to IFNs and IL-10, Mediator kinase unexpectedly represses TLR-induced transcriptional programs downstream of LPS and Pam3CSK4. To our knowledge, this study provides the first systematic characterization of Mediator kinase function across multiple innate immune pathways within the same physiologically relevant immune cell type, namely macrophages.

By performing RNA-seq in different macrophage types, we found that primary murine macrophages, exhibited a robust transcriptional response to Mediator kinase inhibition in the context of IFNγ stimulation. In contrast, the RAW264.7 macrophage cell line showed only marginal sensitivity. The limited response in RAW264.7 cells may derive from their proliferative state, as opposed to terminally differentiated primary macrophages. Given that transcriptional CDKs are often modulated by the cell cycle[348], it is plausible that Mediator kinase–dependent regulation is similarly affected. Furthermore, RAW264.7 cells exhibit a different transcriptome and proteome compared to primary macrophages[349-350], likely impacting their capacity to model inflammatory signaling. Overall, Mediator kinase inhibition in macrophages produced one of the most pronounced effects on IFNγ responses reported to date, in comparison with previous studies investigating Mediator kinase function in other immortalized cell types.[134-135] These findings highlight the importance of using physiologically relevant immune cells to uncover context-specific regulatory functions of Mediator kinase.

Even though Mediator kinase inhibition in PMs led to a higher perturbation of the transcriptome, especially at ground state, we focused our investigation on BMDMs due to practical and technical considerations (e.g. PMs impaired IFNγ signaling). We found that Mediator kinase activity promotes basal expression of ISGs. Our transcriptomic analysis of unstimulated BMDMs showed that inhibition of Mediator kinase led to a broad downregulation of ISGs. Gene Set Enrichment Analysis (GSEA) consistently identified interferon-related gene sets, particularly the IFN-α and IFN-γ response hallmarks, as the most significantly suppressed pathways upon kinase inhibition. These findings suggest that Mediator kinase activity supports a tonic IFN signaling program in macrophages, potentially maintaining an immunoregulatory state under homeostatic conditions. While tonic IFN signaling is often described in vivo[351], its presence in vitro, especially in primary macrophages and DCs, has been shown to sustain basal ISG expression and ensure rapid responsiveness to subsequent immune activation. Our finding that Mediator kinase inhibition suppresses basal ISG expression

in unstimulated BMDMs raises the intriguing possibility that Mediator kinase supports U-STAT-dependent transcription. Previous studies have established that even in the absence of IFN signaling or during its prolonged activation, unphosphorylated STAT1 and STAT2 (U-STATs), in complex with IRF9, sustain tonic ISG expression critical for immune homeostasis.[89-102] The strong enrichment of IFNα and IFNγ hallmark gene sets among downregulated DEGs upon Mediator kinase inhibition suggests that Mediator kinase activity may be required for the transcriptional function of U-STATs. We speculate that Mediator kinase may facilitate U-STAT-driven gene expression partially via phosphorylation of STAT1 S727 residue. Future work, such as assessing U-ISGF3 occupancy and Pol II dynamics at ISG loci upon Mediator kinase inhibition, will help clarify this link. Mediator kinase inhibition impaired macrophage protection against VSV infection and reduced induction of antiviral ISGs, which levels were reduced even in unstimulated cells. Since baseline ISG expression is critical for antiviral immunity[351], our data reveal a functional link between Mediator kinase activity at steady state and the antiviral capacity of macrophages.

Our study expands the understanding of Mediator kinase function by demonstrating that its activity supports not only IFNγ-induced gene expression, but also transcriptional responses downstream of IFNβ and IL-10 in macrophages. These pathways converge on JAK-STAT signaling, with IFNγ and IFNβ primarily engaging STAT1, and IL-10 engaging STAT3. Inhibition of Mediator kinase consistently reduced expression of IL-10 target genes, such as *Socs3*, and dampened STAT3-dependent gene programs in macrophages. This is in stark contrast with studies performed in IL-6 stimulated T cells where Mediator kinase was found to restrict STAT3 residency at target gene loci.[308] The difference between our studies could be explained by the different kinetic of IL-6 and IL-10 signaling in different cell types, even though they both signal through STAT3. Mechanistically, the JAK-STAT-dependent activation may relate to the role of Mediator kinase in regulating Pol II pause release, a process we previously demonstrated to be critical for IFNγ-induced gene expression in MEFs.[135] Many stimuli-induced genes exhibit promoter-proximal paused Pol II prior to stimulation, which permits rapid and robust induction upon signaling through efficient pause release.[352] While genome-wide studies tracking Pol II have demonstrated heterogeneity among ISGs in terms of Pol II pausing[353-354], with majority of ISGs recruiting Pol II de novo after stimulation, this mechanism is especially relevant for a subset of ISGs in macrophages, particularly in response to IFNβ .[91-353-354] In macrophages, Mediator kinase likely contributes to this process by enabling productive elongation downstream of STAT binding, thereby amplifying cytokine-driven transcriptional programs. Together, our data position Mediator kinase as an important positive regulator of JAK-STAT–dependent transcription in innate immune cells, independently of the pro- or anti-inflammatory nature of the genes being induced.

In addition to its activating role in JAK-STAT signaling, our study uncovered a surprising repressive function of Mediator kinase in TLR-induced gene expression. This effect was evident not only at the transcriptional level, but also at the protein level for selected cytokines and chemokines. Although Mediator kinase is canonically associated with gene activation, recent studies have also highlighted its context-

dependent repressive functions, especially in genes rapidly induced by external cues. In line with our findings, Mediator kinase was identified as a negative regulator of IL-10 expression in macrophages using a chemogenomic screen, providing evidence that Mediator kinase dampens anti-inflammatory responses in myeloid cells.[305] Similarly, usage of Mediator kinase inhibitors promoted IL-10 expression and suppressed colitis *in vivo*.[307] Repressive effects of Mediator kinase have also been observed in T cells. Inhibition of Mediator kinase was shown to convert effector/memory T cells into Foxp3+ Tregs, in part through derepression of Treg-associated gene programs.[309] In line with this, Mediator kinase inhibition promoted Treg differentiation and ameliorated autoimmunity.[310] Conversely, in anti-tumor settings, Mediator kinase inhibition enhanced T cell effector functions and cytokine production[311], underscoring the context-specific outcomes of Mediator kinase activity across cell types. In contrast, two recent studies from the Roninson group have reported that Mediator kinase positively regulates NF-κB–mediated transcription in HEK293 cells. However, these findings were obtained in non-immune epithelial cells, which show limited responsiveness to innate immune stimuli, for instance only ~10 ISGs are induced in these systems. This highlights the importance of cellular context: while Mediator kinase may enhance transcription in some settings (like HEK293 cells), it can function as a transcriptional brake in primary immune cells such as macrophages and T cells. This highlights that Mediator kinase function is highly context-dependent, requiring investigation in relevant immune cell types for accurate interpretation. In macrophages, this includes limiting both pro-and anti-inflammatory mediators, suggesting that Mediator kinase modulates the magnitude of the TLR response rather than promoting a particular polarization state.

To gain deeper insights into the transcriptional regulatory logic behind the repressive effects of Mediator kinase, we performed HOMER motif enrichment analysis on the differentially expressed genes upon Mediator kinase inhibition. This revealed a striking condition-specific enrichment of the ISRE motif. In unstimulated, IFNγ- and IFNβ-stimulated BMDMs, ISRE-containing genes were significantly enriched among genes showing decreased induction following Mediator kinase inhibition. Notably, the GAS motif was not significantly enriched in any condition. This suggests that the dominant transcriptional changes upon Mediator kinase inhibition occur at ISRE-driven genes, even in response to IFNγ, which is canonically associated with STAT1 homodimer binding to GAS elements. The absence of significant GAS enrichment may reflect both technical and biological aspects. Biologically, many ISGs induced by IFNs, including our model genes *Gbp4* and *Cxcl9*, are in fact regulated through ISRE-containing promoters, often via indirect activation of ISGF3 components (STAT1/STAT2/IRF9). Additionally, GAS-only genes tend to be fewer in number, exhibit lower fold changes and have early expression kinetics compared to ISRE-driven ISGs, making them less prominent in enrichment analyses. From a technical perspective, HOMER identifies motifs that are overrepresented in DEG sets compared to a genomic background[355]; thus, even if GAS-driven genes are induced, they may not rise to statistical significance unless they form a dominant regulatory signature in the dataset. By contrast, in LPS-stimulated BMDMs, we observed an unexpected upregulation of

ISRE-containing genes. Accordingly, the TLR-induced repressive activity of Mediator kinase appears to act through the IFN/JAK–STAT signaling, as evidenced by its sensitivity to the JAK1/JAK2 inhibitor ruxolitinib. Pam3CSK4-stimulated macrophages were not included in the Homer analysis as Pam3CSK4 does not trigger secondary type I IFN responses, which we confirmed by looking at tyrosine phosphorylation of STAT1 in these cells. To complement the motif analysis, we assessed ISG expression across these conditions. Upon Mediator kinase inhibition the mean log□ fold change (Log□FC) of ISG expression increased significantly in the context of TLR stimulation (LPS and Pam3CSK4), but decreased in unstimulated, IFNγ-, or IFNβ-treated cells. This differential regulation of ISGs by Mediator kinase was further supported by regression analysis of gene expression data, in which ISGs and non-ISGs displayed significantly different slopes but not intercepts in their normalized expression profiles in LPS- and Pam3CSK4-stimulated macrophages. These results indicate that both induced and basal IFN signaling are reversed upon Mediator kinase inhibition, independently of ISG expression levels. These findings emphasize a dual role of Mediator kinase, promoting ISGs expression downstream of IFN-JAK-STAT signaling, while repressing it downstream to TLR signals. One possible explanation for this duality lies in the interplay between TF networks. Several studies have emphasized that ISG regulation is not exclusively dependent on the canonical IFN-JAK-STAT pathway. For instance, Farlik et al. showed that Nos2 expression requires noncanonical transcription factor assemblies involving STAT1 and NF-κB[147], while Boccuni et al. provided compelling evidence that stress signaling via p38 MAPK enhances ISG transcription by reshaping the transcriptional complex at ISRE-containing promoters.[90] The latter study revealed that stress-activated TFs, particularly CREB and members of the AP-1 complex, such as c-Jun, can co-occupy ISG promoters alongside canonical ISGF3 components, under conditions of co-stimulation with IFNs and stress cues (e.g., anisomycin). In contrast, our HOMER motif enrichment analysis in LPS-stimulated BMDMs did not reveal preferential enrichment of a specific TLR-induced transcription factor motif upon Mediator kinase inhibition; instead, all major TF motifs, NF-κB, AP-1, CREB, were comparably ranked and broadly represented, with a preference observed only for IRF motifs. This suggests that TF identity alone is insufficient to explain the selective derepression of ISGs, pointing instead to Mediator kinase-dependent mechanisms that may involve chromatin accessibility, cofactor dynamics, or promoter/enhancer architecture. These data highlight the layered regulation of ISG promoters and suggest that Mediator kinase modulates ISRE activation in a context-dependent manner, limiting antiviral gene induction during TLR stimulation to maintain the balance between inflammatory and antiviral programs in macrophages.

In mammals, most of the mechanistic aspects about Mediator kinase function are on its role as transcriptional activator, mostly through promotion of Pol II pause release and productive elongation[135-288-289], as well as phosphorylation of stimulus-dependent TFs[134-286-287]. However, the repressive function remains underexplored. Phosphoproteomic profiling by Poss et al. identified numerous Mediator kinase substrates involved in chromatin regulation and transcriptional repression, suggesting a broader role for Mediator kinase beyond direct activation of TFs.[296] In our system,

we did not detect significant changes in the phosphorylation of canonical TLR-induced TFs upon Mediator kinase inhibition in macrophages, indicating that the observed transcriptional repression is unlikely to result from altered TF activation. Instead, the repressive effect may arise from local actions of Mediator kinase at specific promoters or enhancers, possibly through modulation of chromatin accessibility, recruitment of corepressors, or inhibition of coactivator assembly. Mediator kinase may contribute to maintaining a repressive chromatin environment at target gene loci, for example by influencing nucleosome positioning or modulating histone modifications that limit transcriptional accessibility. One possibility is that Mediator kinase facilitates the recruitment or activation of chromatin remodelers or histone-modifying enzymes that reinforce a repressive chromatin state, for example through the maintenance of H3K27me3 or inhibition of H3K27ac deposition. Mediator kinase may exert repressive control over multiple stages of the Pol II transcription cycle by limiting re-initiation, impairing productive elongation, or promoting premature transcription termination. Alternatively, Mediator kinase may modulate enhancer-promoter communication by limiting looping interactions required for robust transcriptional activation of ISGs in response to TLR signaling. These mechanisms are not mutually exclusive and may together establish a checkpoint that prevents inappropriate activation of inflammatory gene programs during innate immune responses. Chromatin-centric approaches such as CUT&RUN or ChIP for CDK8/19, Pol II, histone marks, and key TFs, as well as 3D chromatin conformation assays, will be essential to elucidate how Mediator kinase exerts this transcriptional repression.

Building on our transcriptional findings, we explored whether Mediator kinase inhibition enhances the capacity of macrophages to control intracellular bacterial infection. *Listeria monocytogenes* is a Gram-positive, facultative intracellular bacterium widely used as a model organism for investigating host-pathogen interactions and innate immune defense mechanisms. Its ability to infect and replicate within macrophages provides a robust tool for dissecting antimicrobial pathways, including those mediated by IFNs and nitric oxide (NO). In *Listeria*-infected BMDMs, Mediator kinase inhibition significantly reduced bacterial burden, indicating that Mediator kinase activity limits the full antimicrobial potential of macrophages. Since pathogen uptake and bacteria viability remained unaffected, we reasoned that this improved control was likely driven by enhanced effector responses rather than altered entry or survival. One prominent antimicrobial mechanism in macrophages involves the production of NO by inducible nitric oxide synthase (iNOS), which exerts cytotoxic effects on intracellular pathogens.[356] Since its discovery as a key effector, the role of NO in *Listeria* infection has been debated, with reports suggesting both protective and detrimental outcomes. On the protective side, seminal *in vivo* studies showed that pharmacological inhibition of NO synthesis in *Listeria*-infected mice led to higher bacterial burdens, worsened clinical signs, and impaired clearance, demonstrating NO's importance in host defense.[357] *In vitro*, IFNγ-activated macrophages limit *Listeria* replication through NO and reactive oxygen species generation[358], and nitrosative stress targets bacterial virulence factors such as listeriolysin O, further restricting infection.[359] Conversely, other studies revealed that in TLR-activated macrophages, NO can paradoxically

promote *Listeria* cell-to-cell spread by increasing bacterial escape from secondary vacuoles and delaying phagosomal maturation.[360] Thus, the overall impact of NO during *Listeria* infection likely depends on its timing, localization, and magnitude: early controlled NO production supports bacterial clearance, whereas excessive or dysregulated NO can enhance bacterial spread or suppress host immunity. Consistent with a protective role, we observed a temporally coordinated increase in NO levels upon Mediator kinase inhibition: *Nos2* expression was induced early, followed by enhanced NO release. This progressive activation reflects a sustained shift towards a bactericidal state. In contrast, Wienerroither et al. reported that the Mediator kinase module is required for activation of the *Nos2* gene in BMDMs co-stimulated with heat-killed *Listeria* and IFNβ.[361] The discrepancy with our findings may derive from key experimental differences: their study relied on partial genetic depletion rather than acute pharmacological inhibition of kinase activity, and used a non-infectious model involving heat-killed bacteria and IFNβ costimulation instead of live *Listeria* infection.

In our infection model, Mediator kinase inhibition led to elevated ROS levels. Given the lack of a mitochondrial signature, these reactive species likely originate from the phagosomal NADPH oxidase complex (NOX2). Both ROS and NO are well-established effectors of cell-intrinsic resistance to *Listeria*, as demonstrated by the profound susceptibility of double-deficient mouse models lacking both iNOS and NOX2.[362] Surprisingly, we did not observe transcriptional upregulation of phagocyte oxidase complex subunits in our LPS-stimulated dataset upon Mediator kinase inhibition, suggesting that the observed increase in ROS may result from post-translational modifications or increased complex assembly.

While we did not comprehensively profile ISG expression during *Listeria* infection, we speculate that the pattern of gene regulation observed in TLR-stimulated BMDMs, particularly the derepression of ISGs upon Mediator kinase inhibition, could similarly apply in this context. In support of this, *Listeria* is known to activate multiple innate sensing pathways, including TLRs, and elicit limited type I IFN responses[151], which may be amplified when Mediator kinase activity is blocked. If so, this would imply that Mediator kinase inhibition lifts a transcriptional brake not only on classical antimicrobial genes like *Nos2* but also on selected ISGs that contribute to intracellular pathogen control. A growing body of literature demonstrates that ISGs and IFN-inducible factors also contribute to host defense, and, in certain scenarios, to bacterial pathogenesis, during Listeria infection. Large-scale cell-based screens have systematically identified ISGs showing that they can both restrict or promote *Listeria* replication.[153] In other studies, ISG15 was shown to counteract *Listeria in vitro* and *in vivo*[363], and ISGylome profiling during infection revealed a network of metabolic and autophagy-linked pathways regulated by ISG15 conjugation[364]. Interestingly, certain ISGs may be hijacked by *Listeria*, as in the case of IFITM3, which the pathogen exploits to suppress the bactericidal response of phagocytes.[365] This illustrates the paradoxical roles of ISG products in bacterial infection *in vitro*, echoing findings *in vivo*.[81-83-167-366] An interesting subset of ISGs is represented by the *Gbp* family. GBPs constitute a group of proteins that promote microbial killing through various mechanisms, including the enhancement of NADPH-dependent reactive oxygen species (ROS) production[367],

thereby providing a potential functional link to the elevated ROS signature observed upon Mediator kinase inhibition during *Listeria* infection. Several members of the *Gbp* gene cluster (11 genes in mice) showed increased expression in Mediator kinase–inhibited, LPS-stimulated macrophages, including *Gbp10*, which was also upregulated in the context of *Listeria* infection. Notably, *Gbp10*, together with three other *Gbps*, has been reported to severely restrict *Listeria* by preventing phagosomal escape[368]. Finally, in addition to the modulation of ISGs, our transcriptomic data also revealed that Mediator kinase inhibition in LPS-stimulated macrophages broadly enhances the expression of key pro-inflammatory cytokines and chemokines, such as CCL7 (MCP-3), CCL2 (MCP-1) and IL-1α, which may further contribute to improved bacterial clearance.

To disentangle the protective versus detrimental roles of ISG programs under different infectious contexts, future studies could compare the effects of Mediator kinase inhibition on ISG induction and antimicrobial activity in both bacterial and viral infection models. Given that *Listeria* is a Gram-positive bacterium and LPS is a Gram-negative bacterial product, which engages TLR4, studies incorporating additional Gram-negative pathogens that activate TLR4 could help validate and extend the generability of Mediator kinase's role in modulating bacterial infections. In addition, viral systems offer well-characterized ISGs antiviral activities, with outcomes sensitive to ISG induction levels. Given the distinct regulatory outcomes observed in macrophages compared to non-immune cells, conducting functional studies directly in macrophages, or other immune cells, would be essential to accurately capture cell type–specific mechanisms governing ISG induction and antimicrobial activity. This approach will provide more physiologically relevant insights into how Mediator kinase modulates innate immunity in myeloid cells, ultimately informing targeted therapeutic strategies against diverse pathogens.

Collectively, our findings underscore a dual role for Mediator kinase in innate immunity: it acts as an amplifier of JAK-STAT–driven transcription while serving as a context-dependent repressor downstream of TLR signaling. This finely tuned regulatory balance is likely critical for tailoring macrophage responses to distinct inflammatory versus infectious stimuli, further highlighting Mediator kinase as a pivotal regulator of innate immune transcription.

In the second project of this dissertation, entitled "Cytoplasmic mRNA decay controlling inflammatory gene expression is determined by pre-mRNA fate decision", we investigated the role of RNA-binding activity in TTP-mediate mRNA decay. Using proximity-based labeling coupled with mass spectrometry, we compared wild-type TTP (TTP-WT) to an RNA-binding-deficient mutant (TZF^{mut}). The TTP TZF^{mut} showed marked loss of several known TTP interactors, including the deadenylation and decapping components such as CNOT1, DCP1, DCP2, and EDC3, suggesting that RNA-binding is essential for recruiting the mRNA decay machinery.

Over-representation analysis (ORA) of TZF^{mut} interactors revealed enrichment for nuclear localization terms, in contrast to TTP-WT, which was associated with RNA-protein (RNP) granules and P-bodies, cytoplasmic compartments involved in mRNA

storage and decay.[369] A similar shift was observed for the homolog ZFP36L1, suggesting a conserved mechanism across TTP family members.

To further examine the role of nuclear localization, we generated a mutant lacking its nuclear localization signal (NLS^{mut}). Despite being restricted to the cytoplasm, the NLS^{mut} phenocopied the RNA-binding mutant, showing impaired interaction with decay machinery and loss of target binding, as confirmed by CLIP-qPCR and electrophoretic-mobility shift assays (EMSAs). Most critically, a modified CLIP-seq approach demonstrated that TTP preferentially binds pre-mRNAs rather than mature mRNAs, validating and extending previous findings from our lab.[330]

Our findings re-define the original view of TTP as a cytoplasmic decay factor by revealing that its mRNA-destabilizing function depends on early, nuclear engagement with pre-mRNA. By engaging pre-mRNAs in the nucleus, TTP ensures timely repression of inflammatory transcripts, providing an additional layer of post-transcriptional control critical for immune homeostasis.

References

1. Wynn, T. A., Chawla, A., & Pollard, J. W. (2013). Macrophage biology in development, homeostasis and disease. *Nature*, *496*(7446), 445-455. https://doi.org/10.1038/nature12034

2. Ginhoux, F., & Guilliams, M. (2016). Tissue-Resident Macrophage Ontogeny and Homeostasis. *Immunity*, *44*(3), 439-449. https://doi.org/10.1016/j.immuni.2016.02.024

3. Mantovani, A., Sica, A., Sozzani, S., Allavena, P., Vecchi, A., & Locati, M. (2004). The chemokine system in diverse forms of macrophage activation and polarization. *Trends Immunol*, *25*(12), 677-686. https://doi.org/10.1016/j.it.2004.09.015

4. Xue, J., Schmidt, S. V., Sander, J., Draffehn, A., Krebs, W., Quester, I., De Nardo, D., Gohel, T. D., Emde, M., Schmidleithner, L., Ganesan, H., Nino-Castro, A., Mallmann, M. R., Labzin, L., Theis, H., Kraut, M., Beyer, M., Latz, E., Freeman, T. C., . . . Schultze, J. L. (2014). Transcriptome-based network analysis reveals a spectrum model of human macrophage activation. *Immunity*, *40*(2), 274-288. https://doi.org/10.1016/j.immuni.2014.01.006

5. Locati, M., Curtale, G., & Mantovani, A. (2020). Diversity, Mechanisms, and Significance of Macrophage Plasticity. *Annu Rev Pathol*, *15*, 123-147. https://doi.org/10.1146/annurev-pathmechdis-012418-012718

6. Gordon, S. (2016). Phagocytosis: An Immunobiologic Process. *Immunity*, *44*(3), 463-475. https://doi.org/10.1016/j.immuni.2016.02.026

7. Sweet, M. J., Ramnath, D., Singhal, A., & Kapetanovic, R. (2025). Inducible antibacterial responses in macrophages. *Nat Rev Immunol*, *25*(2), 92-107. https://doi.org/10.1038/s41577-024-01080-y

8. Sheu, K. M., & Hoffmann, A. (2022). Functional Hallmarks of Healthy Macrophage Responses: Their Regulatory Basis and Disease Relevance. *Annu Rev Immunol*, *40*, 295-321. https://doi.org/10.1146/annurev-immunol-101320-031555

9. Muntjewerff, E. M., Meesters, L. D., & van den Bogaart, G. (2020). Antigen Cross-Presentation by Macrophages. *Front Immunol*, *11*, 1276. https://doi.org/10.3389/fimmu.2020.01276

10. Janeway, C. A., Jr. (1989). Approaching the asymptote? Evolution and revolution in immunology. *Cold Spring Harb Symp Quant Biol*, *54 Pt 1*, 1-13. https://doi.org/10.1101/sqb.1989.054.01.003

11. Ashida, M., Ishizaki, Y., & Iwahana, H. (1983). Activation of pro-phenoloxidase by bacterial cell walls or beta-1,3-glucans in plasma of the silkworm, Bombyx mori. *Biochem Biophys Res Commun*, *113*(2), 562-568. https://doi.org/10.1016/0006-291x(83)91762-x

12. Kawabata, S., & Muta, T. (2010). Sadaaki Iwanaga: Discovery of the lipopolysaccharide- and beta-1,3-D-glucan-mediated proteolytic cascade and unique proteins in invertebrate immunity. *J Biochem*, *147*(5), 611-618. https://doi.org/10.1093/jb/mvq026

13. Matzinger, P. (2002). The danger model: a renewed sense of self. *Science*, *296*(5566), 301-305. https://doi.org/10.1126/science.1071059

14. Lemaitre, B., Nicolas, E., Michaut, L., Reichhart, J. M., & Hoffmann, J. A. (1996). The dorsoventral regulatory gene cassette spätzle/Toll/cactus controls the potent antifungal response in Drosophila adults. *Cell*, *86*(6), 973-983. https://doi.org/10.1016/s0092-8674(00)80172-5

15. Medzhitov, R., Preston-Hurlburt, P., & Janeway, C. A., Jr. (1997). A human homologue of the Drosophila Toll protein signals activation of adaptive immunity. *Nature*, *388*(6640), 394-397. https://doi.org/10.1038/41131

16. Akira, S., Uematsu, S., & Takeuchi, O. (2006). Pathogen recognition and innate immunity. *Cell*, *124*(4), 783-801. https://doi.org/10.1016/j.cell.2006.02.015

17. Park, B. S., Song, D. H., Kim, H. M., Choi, B. S., Lee, H., & Lee, J. O. (2009). The structural basis of lipopolysaccharide recognition by the TLR4-MD-2 complex. *Nature*, *458*(7242), 1191-1195. https://doi.org/10.1038/nature07830

18. Tobias, P. S., Mathison, J. C., & Ulevitch, R. J. (1988). A family of lipopolysaccharide binding proteins involved in responses to gram-negative sepsis. *J Biol Chem*, *263*(27), 13479-13481.

19. Jiang, Z., Georgel, P., Du, X., Shamel, L., Sovath, S., Mudd, S., Huber, M., Kalis, C., Keck, S., Galanos, C., Freudenberg, M., & Beutler, B. (2005). CD14 is required for MyD88-independent LPS signaling. *Nat Immunol*, *6*(6), 565-570. https://doi.org/10.1038/ni1207

20. Gioannini, T. L., Teghanemt, A., Zhang, D., Coussens, N. P., Dockstader, W., Ramaswamy, S., & Weiss, J. P. (2004). Isolation of an endotoxin-MD-2 complex that produces Toll-like receptor 4-dependent cell activation at picomolar concentrations. *Proc Natl Acad Sci U S A*, *101*(12), 4186-4191. https://doi.org/10.1073/pnas.0306906101

21. Nagai, Y., Akashi, S., Nagafuku, M., Ogata, M., Iwakura, Y., Akira, S., Kitamura, T., Kosugi, A., Kimoto, M., & Miyake, K. (2002). Essential role of MD-2 in LPS responsiveness and TLR4 distribution. *Nat Immunol*, *3*(7), 667-672. https://doi.org/10.1038/ni809

22. Poltorak, A., He, X., Smirnova, I., Liu, M. Y., Van Huffel, C., Du, X., Birdwell, D., Alejos, E., Silva, M., Galanos, C., Freudenberg, M., Ricciardi-Castagnoli, P., Layton, B., & Beutler, B. (1998). Defective LPS signaling in C3H/HeJ and C57BL/10ScCr mice: mutations in Tlr4 gene. *Science*, *282*(5396), 2085-2088. https://doi.org/10.1126/science.282.5396.2085

23. Hoshino, K., Takeuchi, O., Kawai, T., Sanjo, H., Ogawa, T., Takeda, Y., Takeda, K., & Akira, S. (1999). Cutting edge: Toll-like receptor 4 (TLR4)-deficient mice are hyporesponsive to lipopolysaccharide: evidence for TLR4 as the Lps gene product. *J Immunol*, *162*(7), 3749-3752.

24. Watanabe, S., Zenke, K., & Muroi, M. (2023). Lipoteichoic Acid Inhibits Lipopolysaccharide-Induced TLR4 Signaling by Forming an Inactive TLR4/MD-2 Complex Dimer. *J Immunol*, *210*(9), 1386-1395. https://doi.org/10.4049/jimmunol.2200872

25. Hodgkinson, C. P., Patel, K., & Ye, S. (2008). Functional Toll-like receptor 4 mutations modulate the response to fibrinogen. *Thromb Haemost*, *100*(2), 301-307.

26. Sahasrabudhe, N. M., Dokter-Fokkens, J., & de Vos, P. (2016). Particulate β-glucans synergistically activate TLR4 and Dectin-1 in human dendritic cells. *Mol Nutr Food Res*, *60*(11), 2514-2522. https://doi.org/10.1002/mnfr.201600356

27. Tada, H., Nemoto, E., Shimauchi, H., Watanabe, T., Mikami, T., Matsumoto, T., Ohno, N., Tamura, H., Shibata, K., Akashi, S., Miyake, K., Sugawara, S., & Takada, H. (2002). Saccharomyces cerevisiae- and Candida albicans-derived mannan induced production of tumor necrosis factor alpha by human monocytes in a CD14- and Toll-like receptor 4-dependent manner. *Microbiol Immunol*, *46*(7), 503-512. https://doi.org/10.1111/j.1348-0421.2002.tb02727.x

28. Shoham, S., Huang, C., Chen, J. M., Golenbock, D. T., & Levitz, S. M. (2001). Toll-like receptor 4 mediates intracellular signaling without TNF-alpha release in response to Cryptococcus neoformans polysaccharide capsule. *J Immunol*, *166*(7), 4620-4626. https://doi.org/10.4049/jimmunol.166.7.4620

29. Trompette, A., Divanovic, S., Visintin, A., Blanchard, C., Hegde, R. S., Madan, R., Thorne, P. S., Wills-Karp, M., Gioannini, T. L., Weiss, J. P., & Karp, C. L. (2009).

Allergenicity resulting from functional mimicry of a Toll-like receptor complex protein. *Nature*, *457*(7229), 585-588. https://doi.org/10.1038/nature07548

30. Takeuchi, O., Kaufmann, A., Grote, K., Kawai, T., Hoshino, K., Morr, M., Mühlradt, P. F., & Akira, S. (2000). Cutting edge: preferentially the R-stereoisomer of the mycoplasmal lipopeptide macrophage-activating lipopeptide-2 activates immune cells through a toll-like receptor 2- and MyD88-dependent signaling pathway. *J Immunol*, *164*(2), 554-557. https://doi.org/10.4049/jimmunol.164.2.554
31. Ozinsky, A., Underhill, D. M., Fontenot, J. D., Hajjar, A. M., Smith, K. D., Wilson, C. B., Schroeder, L., & Aderem, A. (2000). The repertoire for pattern recognition of pathogens by the innate immune system is defined by cooperation between toll-like receptors. *Proc Natl Acad Sci U S A*, *97*(25), 13766-13771. https://doi.org/10.1073/pnas.250476497
32. Hajjar, A. M., O'Mahony, D. S., Ozinsky, A., Underhill, D. M., Aderem, A., Klebanoff, S. J., & Wilson, C. B. (2001). Cutting edge: functional interactions between toll-like receptor (TLR) 2 and TLR1 or TLR6 in response to phenol-soluble modulin. *J Immunol*, *166*(1), 15-19. https://doi.org/10.4049/jimmunol.166.1.15
33. Takeuchi, O., Sato, S., Horiuchi, T., Hoshino, K., Takeda, K., Dong, Z., Modlin, R. L., & Akira, S. (2002). Cutting edge: role of Toll-like receptor 1 in mediating immune response to microbial lipoproteins. *J Immunol*, *169*(1), 10-14. https://doi.org/10.4049/jimmunol.169.1.10
34. Takeuchi, O., Kawai, T., Mühlradt, P. F., Morr, M., Radolf, J. D., Zychlinsky, A., Takeda, K., & Akira, S. (2001). Discrimination of bacterial lipoproteins by Toll-like receptor 6. *Int Immunol*, *13*(7), 933-940. https://doi.org/10.1093/intimm/13.7.933
35. Jin, M. S., Kim, S. E., Heo, J. Y., Lee, M. E., Kim, H. M., Paik, S. G., Lee, H., & Lee, J. O. (2007). Crystal structure of the TLR1-TLR2 heterodimer induced by binding of a tri-acylated lipopeptide. *Cell*, *130*(6), 1071-1082. https://doi.org/10.1016/j.cell.2007.09.008
36. Kang, J. Y., Nan, X., Jin, M. S., Youn, S. J., Ryu, Y. H., Mah, S., Han, S. H., Lee, H., Paik, S. G., & Lee, J. O. (2009). Recognition of lipopeptide patterns by Toll-like receptor 2-Toll-like receptor 6 heterodimer. *Immunity*, *31*(6), 873-884. https://doi.org/10.1016/j.immuni.2009.09.018
37. Hayashi, F., Smith, K. D., Ozinsky, A., Hawn, T. R., Yi, E. C., Goodlett, D. R., Eng, J. K., Akira, S., Underhill, D. M., & Aderem, A. (2001). The innate immune response to bacterial flagellin is mediated by Toll-like receptor 5. *Nature*, *410*(6832), 1099-1103. https://doi.org/10.1038/35074106
38. Andersen-Nissen, E., Hawn, T. R., Smith, K. D., Nachman, A., Lampano, A. E., Uematsu, S., Akira, S., & Aderem, A. (2007). Cutting edge: Tlr5-/- mice are more susceptible to Escherichia coli urinary tract infection. *J Immunol*, *178*(8), 4717-4720. https://doi.org/10.4049/jimmunol.178.8.4717
39. Feuillet, V., Medjane, S., Mondor, I., Demaria, O., Pagni, P. P., Galán, J. E., Flavell, R. A., & Alexopoulou, L. (2006). Involvement of Toll-like receptor 5 in the recognition of flagellated bacteria. *Proc Natl Acad Sci U S A*, *103*(33), 12487-12492. https://doi.org/10.1073/pnas.0605200103
40. Zhang, D., Zhang, G., Hayden, M. S., Greenblatt, M. B., Bussey, C., Flavell, R. A., & Ghosh, S. (2004). A toll-like receptor that prevents infection by uropathogenic bacteria. *Science*, *303*(5663), 1522-1526. https://doi.org/10.1126/science.1094351
41. Yarovinsky, F., Zhang, D., Andersen, J. F., Bannenberg, G. L., Serhan, C. N., Hayden, M. S., Hieny, S., Sutterwala, F. S., Flavell, R. A., Ghosh, S., & Sher, A. (2005). TLR11 activation of dendritic cells by a protozoan profilin-like protein. *Science*, *308*(5728), 1626-1629. https://doi.org/10.1126/science.1109893

42. Koblansky, A. A., Jankovic, D., Oh, H., Hieny, S., Sungnak, W., Mathur, R., Hayden, M. S., Akira, S., Sher, A., & Ghosh, S. (2013). Recognition of profilin by Toll-like receptor 12 is critical for host resistance to Toxoplasma gondii. *Immunity*, *38*(1), 119-130. https://doi.org/10.1016/j.immuni.2012.09.016

43. Alexopoulou, L., Holt, A. C., Medzhitov, R., & Flavell, R. A. (2001). Recognition of double-stranded RNA and activation of NF-kappaB by Toll-like receptor 3. *Nature*, *413*(6857), 732-738. https://doi.org/10.1038/35099560

44. Plociennikowska, A., Frankish, J., Moraes, T., Del Prete, D., Kahnt, F., Acuna, C., Slezak, M., Binder, M., & Bartenschlager, R. (2021). TLR3 activation by Zika virus stimulates inflammatory cytokine production which dampens the antiviral response induced by RIG-I-like receptors. *J Virol*, *95*(10). https://doi.org/10.1128/jvi.01050-20

45. Sato, R., Kato, A., Chimura, T., Saitoh, S. I., Shibata, T., Murakami, Y., Fukui, R., Liu, K., Zhang, Y., Arii, J., Sun-Wada, G. H., Wada, Y., Ikenoue, T., Barber, G. N., Manabe, T., Kawaguchi, Y., & Miyake, K. (2018). Combating herpesvirus encephalitis by potentiating a TLR3-mTORC2 axis. *Nat Immunol*, *19*(10), 1071-1082. https://doi.org/10.1038/s41590-018-0203-2

46. Lund, J. M., Alexopoulou, L., Sato, A., Karow, M., Adams, N. C., Gale, N. W., Iwasaki, A., & Flavell, R. A. (2004). Recognition of single-stranded RNA viruses by Toll-like receptor 7. *Proc Natl Acad Sci U S A*, *101*(15), 5598-5603. https://doi.org/10.1073/pnas.0400937101

47. Tanji, H., Ohto, U., Shibata, T., Taoka, M., Yamauchi, Y., Isobe, T., Miyake, K., & Shimizu, T. (2015). Toll-like receptor 8 senses degradation products of single-stranded RNA. *Nat Struct Mol Biol*, *22*(2), 109-115. https://doi.org/10.1038/nsmb.2943

48. Wang, J. P., Bowen, G. N., Padden, C., Cerny, A., Finberg, R. W., Newburger, P. E., & Kurt-Jones, E. A. (2008). Toll-like receptor-mediated activation of neutrophils by influenza A virus. *Blood*, *112*(5), 2028-2034. https://doi.org/10.1182/blood-2008-01-132860

49. Heil, F., Hemmi, H., Hochrein, H., Ampenberger, F., Kirschning, C., Akira, S., Lipford, G., Wagner, H., & Bauer, S. (2004). Species-specific recognition of single-stranded RNA via toll-like receptor 7 and 8. *Science*, *303*(5663), 1526-1529. https://doi.org/10.1126/science.1093620

50. Laurent, P., Yang, C., Rendeiro, A. F., Nilsson-Payant, B. E., Carrau, L., Chandar, V., Bram, Y., tenOever, B. R., Elemento, O., Ivashkiv, L. B., Schwartz, R. E., & Barrat, F. J. (2022). Sensing of SARS-CoV-2 by pDCs and their subsequent production of IFN-I contribute to macrophage-induced cytokine storm during COVID-19. *Sci Immunol*, *7*(75), eadd4906. https://doi.org/10.1126/sciimmunol.add4906

51. Hemmi, H., Takeuchi, O., Kawai, T., Kaisho, T., Sato, S., Sanjo, H., Matsumoto, M., Hoshino, K., Wagner, H., Takeda, K., & Akira, S. (2000). A Toll-like receptor recognizes bacterial DNA. *Nature*, *408*(6813), 740-745. https://doi.org/10.1038/35047123

52. Haas, T., Metzger, J., Schmitz, F., Heit, A., Müller, T., Latz, E., & Wagner, H. (2008). The DNA sugar backbone 2' deoxyribose determines toll-like receptor 9 activation. *Immunity*, *28*(3), 315-323. https://doi.org/10.1016/j.immuni.2008.01.013

53. Sabatel, C., Radermecker, C., Fievez, L., Paulissen, G., Chakarov, S., Fernandes, C., Olivier, S., Toussaint, M., Pirottin, D., Xiao, X., Quatresooz, P., Sirard, J. C., Cataldo, D., Gillet, L., Bouabe, H., Desmet, C. J., Ginhoux, F., Marichal, T., & Bureau, F. (2017). Exposure to Bacterial CpG DNA Protects from Airway Allergic Inflammation by Expanding Regulatory Lung Interstitial Macrophages. *Immunity*, *46*(3), 457-473. https://doi.org/10.1016/j.immuni.2017.02.016

54. Li, X. D., & Chen, Z. J. (2012). Sequence specific detection of bacterial 23S ribosomal RNA by TLR13. *Elife*, *1*, e00102. https://doi.org/10.7554/eLife.00102

55. Oldenburg, M., Krüger, A., Ferstl, R., Kaufmann, A., Nees, G., Sigmund, A., Bathke, B., Lauterbach, H., Suter, M., Dreher, S., Koedel, U., Akira, S., Kawai, T., Buer, J., Wagner, H., Bauer, S., Hochrein, H., & Kirschning, C. J. (2012). TLR13 recognizes bacterial 23S rRNA devoid of erythromycin resistance-forming modification. *Science*, *337*(6098), 1111-1115. https://doi.org/10.1126/science.1220363

56. Lee, S. M., Yip, T. F., Yan, S., Jin, D. Y., Wei, H. L., Guo, R. T., & Peiris, J. S. M. (2018). Recognition of Double-Stranded RNA and Regulation of Interferon Pathway by Toll-Like Receptor 10. *Front Immunol*, *9*, 516. https://doi.org/10.3389/fimmu.2018.00516

57. Lee, S. M., Kok, K. H., Jaume, M., Cheung, T. K., Yip, T. F., Lai, J. C., Guan, Y., Webster, R. G., Jin, D. Y., & Peiris, J. S. (2014). Toll-like receptor 10 is involved in induction of innate immune responses to influenza virus infection. *Proc Natl Acad Sci U S A*, *111*(10), 3793-3798. https://doi.org/10.1073/pnas.1324266111

58. Henrick, B. M., Yao, X. D., Zahoor, M. A., Abimiku, A., Osawe, S., & Rosenthal, K. L. (2019). TLR10 Senses HIV-1 Proteins and Significantly Enhances HIV-1 Infection. *Front Immunol*, *10*, 482. https://doi.org/10.3389/fimmu.2019.00482

59. Kagan, J. C., Magupalli, V. G., & Wu, H. (2014). SMOCs: supramolecular organizing centres that control innate immunity. *Nat Rev Immunol*, *14*(12), 821-826. https://doi.org/10.1038/nri3757

60. Lin, S. C., Lo, Y. C., & Wu, H. (2010). Helical assembly in the MyD88-IRAK4-IRAK2 complex in TLR/IL-1R signalling. *Nature*, *465*(7300), 885-890. https://doi.org/10.1038/nature09121

61. Motshwene, P. G., Moncrieffe, M. C., Grossmann, J. G., Kao, C., Ayaluru, M., Sandercock, A. M., Robinson, C. V., Latz, E., & Gay, N. J. (2009). An oligomeric signaling platform formed by the Toll-like receptor signal transducers MyD88 and IRAK-4. *J Biol Chem*, *284*(37), 25404-25411. https://doi.org/10.1074/jbc.M109.022392

62. Fitzgerald, K. A., & Kagan, J. C. (2020). Toll-like Receptors and the Control of Immunity. *Cell*, *180*(6), 1044-1066. https://doi.org/10.1016/j.cell.2020.02.041

63. Sun, J., Li, N., Oh, K. S., Dutta, B., Vayttaden, S. J., Lin, B., Ebert, T. S., De Nardo, D., Davis, J., Bagirzadeh, R., Lounsbury, N. W., Pasare, C., Latz, E., Hornung, V., & Fraser, I. D. (2016). Comprehensive RNAi-based screening of human and mouse TLR pathways identifies species-specific preferences in signaling protein use. *Sci Signal*, *9*(409), ra3. https://doi.org/10.1126/scisignal.aab2191

64. Everts, B., Amiel, E., Huang, S. C., Smith, A. M., Chang, C. H., Lam, W. Y., Redmann, V., Freitas, T. C., Blagih, J., van der Windt, G. J., Artyomov, M. N., Jones, R. G., Pearce, E. L., & Pearce, E. J. (2014). TLR-driven early glycolytic reprogramming via the kinases TBK1-IKKε supports the anabolic demands of dendritic cell activation. *Nat Immunol*, *15*(4), 323-332. https://doi.org/10.1038/ni.2833

65. Hinz, M., & Scheidereit, C. (2014). The IκB kinase complex in NF-κB regulation and beyond. *EMBO Rep*, *15*(1), 46-61. https://doi.org/10.1002/embr.201337983

66. Kawai, T., Takeuchi, O., Fujita, T., Inoue, J., Mühlradt, P. F., Sato, S., Hoshino, K., & Akira, S. (2001). Lipopolysaccharide stimulates the MyD88-independent pathway and results in activation of IFN-regulatory factor 3 and the expression of a subset of lipopolysaccharide-inducible genes. *J Immunol*, *167*(10), 5887-5894. https://doi.org/10.4049/jimmunol.167.10.5887

67. Toshchakov, V., Jones, B. W., Perera, P. Y., Thomas, K., Cody, M. J., Zhang, S., Williams, B. R., Major, J., Hamilton, T. A., Fenton, M. J., & Vogel, S. N. (2002). TLR4, but not TLR2, mediates IFN-beta-induced STAT1alpha/beta-dependent gene expression in macrophages. *Nat Immunol*, *3*(4), 392-398. https://doi.org/10.1038/ni774

68. Doyle, S., Vaidya, S., O'Connell, R., Dadgostar, H., Dempsey, P., Wu, T., Rao, G., Sun, R., Haberland, M., Modlin, R., & Cheng, G. (2002). IRF3 mediates a TLR3/TLR4-

specific antiviral gene program. *Immunity*, *17*(3), 251-263. https://doi.org/10.1016/s1074-7613(02)00390-4

69. Kagan, J. C., Su, T., Horng, T., Chow, A., Akira, S., & Medzhitov, R. (2008). TRAM couples endocytosis of Toll-like receptor 4 to the induction of interferon-beta. *Nat Immunol*, *9*(4), 361-368. https://doi.org/10.1038/ni1569
70. Sharma, S., tenOever, B. R., Grandvaux, N., Zhou, G. P., Lin, R., & Hiscott, J. (2003). Triggering the interferon antiviral response through an IKK-related pathway. *Science*, *300*(5622), 1148-1151. https://doi.org/10.1126/science.1081315
71. Fitzgerald, K. A., McWhirter, S. M., Faia, K. L., Rowe, D. C., Latz, E., Golenbock, D. T., Coyle, A. J., Liao, S. M., & Maniatis, T. (2003). IKKepsilon and TBK1 are essential components of the IRF3 signaling pathway. *Nat Immunol*, *4*(5), 491-496. https://doi.org/10.1038/ni921
72. McWhirter, S. M., Fitzgerald, K. A., Rosains, J., Rowe, D. C., Golenbock, D. T., & Maniatis, T. (2004). IFN-regulatory factor 3-dependent gene expression is defective in Tbk1-deficient mouse embryonic fibroblasts. *Proc Natl Acad Sci U S A*, *101*(1), 233-238. https://doi.org/10.1073/pnas.2237236100
73. Isaacs, A., Lindenmann, J., & Valentine, R. C. (1957). Virus interference. II. Some properties of interferon. *Proc R Soc Lond B Biol Sci*, *147*(927), 268-273. https://doi.org/10.1098/rspb.1957.0049
74. Levy, D., Larner, A., Chaudhuri, A., Babiss, L. E., & Darnell, J. E., Jr. (1986). Interferon-stimulated transcription: isolation of an inducible gene and identification of its regulatory region. *Proc Natl Acad Sci U S A*, *83*(23), 8929-8933. https://doi.org/10.1073/pnas.83.23.8929
75. Velazquez, L., Fellous, M., Stark, G. R., & Pellegrini, S. (1992). A protein tyrosine kinase in the interferon alpha/beta signaling pathway. *Cell*, *70*(2), 313-322. https://doi.org/10.1016/0092-8674(92)90105-l
76. Wilks, A. F., Harpur, A. G., Kurban, R. R., Ralph, S. J., Zürcher, G., & Ziemiecki, A. (1991). Two novel protein-tyrosine kinases, each with a second phosphotransferase-related catalytic domain, define a new class of protein kinase. *Mol Cell Biol*, *11*(4), 2057-2065. https://doi.org/10.1128/mcb.11.4.2057-2065.1991
77. Stark, G. R., & Darnell, J. E., Jr. (2012). The JAK-STAT pathway at twenty. *Immunity*, *36*(4), 503-514. https://doi.org/10.1016/j.immuni.2012.03.013
78. Renauld, J. C. (2003). Class II cytokine receptors and their ligands: key antiviral and inflammatory modulators. *Nat Rev Immunol*, *3*(8), 667-676. https://doi.org/10.1038/nri1153
79. Trinchieri, G. (2010). Type I interferon: friend or foe? *J Exp Med*, *207*(10), 2053-2063. https://doi.org/10.1084/jem.20101664
80. Müller, U., Steinhoff, U., Reis, L. F., Hemmi, S., Pavlovic, J., Zinkernagel, R. M., & Aguet, M. (1994). Functional role of type I and type II interferons in antiviral defense. *Science*, *264*(5167), 1918-1921. https://doi.org/10.1126/science.8009221
81. Kovarik, P., Castiglia, V., Ivin, M., & Ebner, F. (2016). Type I Interferons in Bacterial Infections: A Balancing Act. *Front Immunol*, *7*, 652. https://doi.org/10.3389/fimmu.2016.00652
82. Castiglia, V., Piersigilli, A., Ebner, F., Janos, M., Goldmann, O., Damböck, U., Kröger, A., Weiss, S., Knapp, S., Jamieson, A. M., Kirschning, C., Kalinke, U., Strobl, B., Müller, M., Stoiber, D., Lienenklaus, S., & Kovarik, P. (2016). Type I Interferon Signaling Prevents IL-1β-Driven Lethal Systemic Hyperinflammation during Invasive Bacterial Infection of Soft Tissue. *Cell Host Microbe*, *19*(3), 375-387. https://doi.org/10.1016/j.chom.2016.02.003

83. Demiroz, D., Platanitis, E., Bryant, M., Fischer, P., Prchal-Murphy, M., Lercher, A., Lassnig, C., Baccarini, M., Müller, M., Bergthaler, A., Sexl, V., Dolezal, M., & Decker, T. (2021). Listeria monocytogenes infection rewires host metabolism with regulatory input from type I interferons. *PLoS Pathog*, *17*(7), e1009697. https://doi.org/10.1371/journal.ppat.1009697

84. Pestka, S., Krause, C. D., & Walter, M. R. (2004). Interferons, interferon-like cytokines, and their receptors. *Immunol Rev*, *202*, 8-32. https://doi.org/10.1111/j.0105-2896.2004.00204.x

85. Levy, D. E., Kessler, D. S., Pine, R., Reich, N., & Darnell, J. E., Jr. (1988). Interferon-induced nuclear factors that bind a shared promoter element correlate with positive and negative transcriptional control. *Genes Dev*, *2*(4), 383-393. https://doi.org/10.1101/gad.2.4.383

86. Reich, N., Evans, B., Levy, D., Fahey, D., Knight, E., Jr., & Darnell, J. E., Jr. (1987). Interferon-induced transcription of a gene encoding a 15-kDa protein depends on an upstream enhancer element. *Proc Natl Acad Sci U S A*, *84*(18), 6394-6398. https://doi.org/10.1073/pnas.84.18.6394

87. Decker, T., Lew, D. J., Mirkovitch, J., & Darnell, J. E., Jr. (1991). Cytoplasmic activation of GAF, an IFN-gamma-regulated DNA-binding factor. *Embo j*, *10*(4), 927-932. https://doi.org/10.1002/j.1460-2075.1991.tb08026.x

88. Babadei, O., Strobl, B., Müller, M., & Decker, T. (2024). Transcriptional control of interferon-stimulated genes. *J Biol Chem*, *300*(10), 107771. https://doi.org/10.1016/j.jbc.2024.107771

89. Platanitis, E., Demiroz, D., Schneller, A., Fischer, K., Capelle, C., Hartl, M., Gossenreiter, T., Müller, M., Novatchkova, M., & Decker, T. (2019). A molecular switch from STAT2-IRF9 to ISGF3 underlies interferon-induced gene transcription. *Nat Commun*, *10*(1), 2921. https://doi.org/10.1038/s41467-019-10970-y

90. Boccuni, L., Podgorschek, E., Schmiedeberg, M., Platanitis, E., Traxler, P., Fischer, P., Schirripa, A., Novoszel, P., Nebreda, A. R., Arthur, J. S. C., Fortelny, N., Farlik, M., Sexl, V., Bock, C., Sibilia, M., Kovarik, P., Müller, M., & Decker, T. (2022). Stress signaling boosts interferon-induced gene transcription in macrophages. *Sci Signal*, *15*(764), eabq5389. https://doi.org/10.1126/scisignal.abq5389

91. Ravi Sundar Jose Geetha, A., Fischer, K., Babadei, O., Smesnik, G., Vogt, A., Platanitis, E., Müller, M., Farlik, M., & Decker, T. (2024). Dynamic control of gene expression by ISGF3 and IRF1 during IFNβ and IFNγ signaling. *Embo j*, *43*(11), 2233-2263. https://doi.org/10.1038/s44318-024-00092-7

92. Huang, S., Hendriks, W., Althage, A., Hemmi, S., Bluethmann, H., Kamijo, R., Vilcek, J., Zinkernagel, R. M., & Aguet, M. (1993). Immune response in mice that lack the interferon-gamma receptor. *Science*, *259*(5102), 1742-1745. https://doi.org/10.1126/science.8456301

93. Lazear, H. M., Schoggins, J. W., & Diamond, M. S. (2019). Shared and Distinct Functions of Type I and Type III Interferons. *Immunity*, *50*(4), 907-923. https://doi.org/10.1016/j.immuni.2019.03.025

94. Wang, Y., & Levy, D. E. (2012). Comparative evolutionary genomics of the STAT family of transcription factors. *Jakstat*, *1*(1), 23-33. https://doi.org/10.4161/jkst.19418

95. Murakami, M., Narazaki, M., Hibi, M., Yawata, H., Yasukawa, K., Hamaguchi, M., Taga, T., & Kishimoto, T. (1991). Critical cytoplasmic region of the interleukin 6 signal transducer gp130 is conserved in the cytokine receptor family. *Proc Natl Acad Sci U S A*, *88*(24), 11349-11353. https://doi.org/10.1073/pnas.88.24.11349

96. Glassman, C. R., Tsutsumi, N., Saxton, R. A., Lupardus, P. J., Jude, K. M., & Garcia, K. C. (2022). Structure of a Janus kinase cytokine receptor complex reveals the basis for

dimeric activation. *Science*, *376*(6589), 163-169. https://doi.org/10.1126/science.abn8933

97. Decker, T., & Kovarik, P. (2000). Serine phosphorylation of STATs. *Oncogene*, *19*(21), 2628-2637. https://doi.org/10.1038/sj.onc.1203481

98. Begitt, A., Droescher, M., Meyer, T., Schmid, C. D., Baker, M., Antunes, F., Knobeloch, K. P., Owen, M. R., Naumann, R., Decker, T., & Vinkemeier, U. (2014). STAT1-cooperative DNA binding distinguishes type 1 from type 2 interferon signaling. *Nat Immunol*, *15*(2), 168-176. https://doi.org/10.1038/ni.2794

99. Zhang, X., & Darnell, J. E., Jr. (2001). Functional importance of Stat3 tetramerization in activation of the alpha 2-macroglobulin gene. *J Biol Chem*, *276*(36), 33576-33581. https://doi.org/10.1074/jbc.M104978200

100. Yang, J., Liao, X., Agarwal, M. K., Barnes, L., Auron, P. E., & Stark, G. R. (2007). Unphosphorylated STAT3 accumulates in response to IL-6 and activates transcription by binding to NFkappaB. *Genes Dev*, *21*(11), 1396-1408. https://doi.org/10.1101/gad.1553707

101. Cheon, H., & Stark, G. R. (2009). Unphosphorylated STAT1 prolongs the expression of interferon-induced immune regulatory genes. *Proc Natl Acad Sci U S A*, *106*(23), 9373-9378. https://doi.org/10.1073/pnas.0903487106

102. Cheon, H., Holvey-Bates, E. G., Schoggins, J. W., Forster, S., Hertzog, P., Imanaka, N., Rice, C. M., Jackson, M. W., Junk, D. J., & Stark, G. R. (2013). IFNβ-dependent increases in STAT1, STAT2, and IRF9 mediate resistance to viruses and DNA damage. *Embo j*, *32*(20), 2751-2763. https://doi.org/10.1038/emboj.2013.203

103. Yan, S. J., Lim, S. J., Shi, S., Dutta, P., & Li, W. X. (2011). Unphosphorylated STAT and heterochromatin protect genome stability. *Faseb j*, *25*(1), 232-241. https://doi.org/10.1096/fj.10-169367

104. Hu, X., Dutta, P., Tsurumi, A., Li, J., Wang, J., Land, H., & Li, W. X. (2013). Unphosphorylated STAT5A stabilizes heterochromatin and suppresses tumor growth. *Proc Natl Acad Sci U S A*, *110*(25), 10213-10218. https://doi.org/10.1073/pnas.1221243110

105. Gough, D. J., Corlett, A., Schlessinger, K., Wegrzyn, J., Larner, A. C., & Levy, D. E. (2009). Mitochondrial STAT3 supports Ras-dependent oncogenic transformation. *Science*, *324*(5935), 1713-1716. https://doi.org/10.1126/science.1171721

106. Hilton, D. J., Richardson, R. T., Alexander, W. S., Viney, E. M., Willson, T. A., Sprigg, N. S., Starr, R., Nicholson, S. E., Metcalf, D., & Nicola, N. A. (1998). Twenty proteins containing a C-terminal SOCS box form five structural classes. *Proc Natl Acad Sci U S A*, *95*(1), 114-119. https://doi.org/10.1073/pnas.95.1.114

107. Kile, B. T., Schulman, B. A., Alexander, W. S., Nicola, N. A., Martin, H. M., & Hilton, D. J. (2002). The SOCS box: a tale of destruction and degradation. *Trends Biochem Sci*, *27*(5), 235-241. https://doi.org/10.1016/s0968-0004(02)02085-6

108. Endo, T. A., Masuhara, M., Yokouchi, M., Suzuki, R., Sakamoto, H., Mitsui, K., Matsumoto, A., Tanimura, S., Ohtsubo, M., Misawa, H., Miyazaki, T., Leonor, N., Taniguchi, T., Fujita, T., Kanakura, Y., Komiya, S., & Yoshimura, A. (1997). A new protein containing an SH2 domain that inhibits JAK kinases. *Nature*, *387*(6636), 921-924. https://doi.org/10.1038/43213

109. Nicholson, S. E., Willson, T. A., Farley, A., Starr, R., Zhang, J. G., Baca, M., Alexander, W. S., Metcalf, D., Hilton, D. J., & Nicola, N. A. (1999). Mutational analyses of the SOCS proteins suggest a dual domain requirement but distinct mechanisms for inhibition of LIF and IL-6 signal transduction. *Embo j*, *18*(2), 375-385. https://doi.org/10.1093/emboj/18.2.375

110. Sasaki, A., Yasukawa, H., Shouda, T., Kitamura, T., Dikic, I., & Yoshimura, A. (2000). CIS3/SOCS-3 suppresses erythropoietin (EPO) signaling by binding the EPO

receptor and JAK2. *J Biol Chem*, *275*(38), 29338-29347. https://doi.org/10.1074/jbc.M003456200

111. Yoshimura, A. (1998). The CIS family: negative regulators of JAK-STAT signaling. *Cytokine Growth Factor Rev*, *9*(3-4), 197-204. https://doi.org/10.1016/s1359-6101(98)00019-7

112. Kamura, T., Sato, S., Haque, D., Liu, L., Kaelin, W. G., Jr., Conaway, R. C., & Conaway, J. W. (1998). The Elongin BC complex interacts with the conserved SOCS-box motif present in members of the SOCS, ras, WD-40 repeat, and ankyrin repeat families. *Genes Dev*, *12*(24), 3872-3881. https://doi.org/10.1101/gad.12.24.3872

113. Zhang, J. G., Farley, A., Nicholson, S. E., Willson, T. A., Zugaro, L. M., Simpson, R. J., Moritz, R. L., Cary, D., Richardson, R., Hausmann, G., Kile, B. T., Kent, S. B., Alexander, W. S., Metcalf, D., Hilton, D. J., Nicola, N. A., & Baca, M. (1999). The conserved SOCS box motif in suppressors of cytokine signaling binds to elongins B and C and may couple bound proteins to proteasomal degradation. *Proc Natl Acad Sci U S A*, *96*(5), 2071-2076. https://doi.org/10.1073/pnas.96.5.2071

114. Alexander, W. S., Starr, R., Fenner, J. E., Scott, C. L., Handman, E., Sprigg, N. S., Corbin, J. E., Cornish, A. L., Darwiche, R., Owczarek, C. M., Kay, T. W., Nicola, N. A., Hertzog, P. J., Metcalf, D., & Hilton, D. J. (1999). SOCS1 is a critical inhibitor of interferon gamma signaling and prevents the potentially fatal neonatal actions of this cytokine. *Cell*, *98*(5), 597-608. https://doi.org/10.1016/s0092-8674(00)80047-1

115. Marine, J. C., Topham, D. J., McKay, C., Wang, D., Parganas, E., Stravopodis, D., Yoshimura, A., & Ihle, J. N. (1999). SOCS1 deficiency causes a lymphocyte-dependent perinatal lethality. *Cell*, *98*(5), 609-616. https://doi.org/10.1016/s0092-8674(00)80048-3

116. Roberts, A. W., Robb, L., Rakar, S., Hartley, L., Cluse, L., Nicola, N. A., Metcalf, D., Hilton, D. J., & Alexander, W. S. (2001). Placental defects and embryonic lethality in mice lacking suppressor of cytokine signaling 3. *Proc Natl Acad Sci U S A*, *98*(16), 9324-9329. https://doi.org/10.1073/pnas.161271798

117. Marine, J. C., McKay, C., Wang, D., Topham, D. J., Parganas, E., Nakajima, H., Pendeville, H., Yasukawa, H., Sasaki, A., Yoshimura, A., & Ihle, J. N. (1999). SOCS3 is essential in the regulation of fetal liver erythropoiesis. *Cell*, *98*(5), 617-627. https://doi.org/10.1016/s0092-8674(00)80049-5

118. Böhmer, F. D., & Friedrich, K. (2014). Protein tyrosine phosphatases as wardens of STAT signaling. *Jakstat*, *3*(1), e28087. https://doi.org/10.4161/jkst.28087

119. Kim, T. K., & Maniatis, T. (1996). Regulation of interferon-gamma-activated STAT1 by the ubiquitin-proteasome pathway. *Science*, *273*(5282), 1717-1719. https://doi.org/10.1126/science.273.5282.1717

120. Tanaka, T., Soriano, M. A., & Grusby, M. J. (2005). SLIM is a nuclear ubiquitin E3 ligase that negatively regulates STAT signaling. *Immunity*, *22*(6), 729-736. https://doi.org/10.1016/j.immuni.2005.04.008

121. Yuan, C., Qi, J., Zhao, X., & Gao, C. (2012). Smurf1 protein negatively regulates interferon-γ signaling through promoting STAT1 protein ubiquitination and degradation. *J Biol Chem*, *287*(21), 17006-17015. https://doi.org/10.1074/jbc.M112.341198

122. Shuai, K., & Liu, B. (2005). Regulation of gene-activation pathways by PIAS proteins in the immune system. *Nat Rev Immunol*, *5*(8), 593-605. https://doi.org/10.1038/nri1667

123. Liu, B., Liao, J., Rao, X., Kushner, S. A., Chung, C. D., Chang, D. D., & Shuai, K. (1998). Inhibition of Stat1-mediated gene activation by PIAS1. *Proc Natl Acad Sci U S A*, *95*(18), 10626-10631. https://doi.org/10.1073/pnas.95.18.10626

124. Chung, C. D., Liao, J., Liu, B., Rao, X., Jay, P., Berta, P., & Shuai, K. (1997). Specific inhibition of Stat3 signal transduction by PIAS3. *Science*, *278*(5344), 1803-1805. https://doi.org/10.1126/science.278.5344.1803

125. Arora, T., Liu, B., He, H., Kim, J., Murphy, T. L., Murphy, K. M., Modlin, R. L., & Shuai, K. (2003). PIASx is a transcriptional co-repressor of signal transducer and activator of transcription 4. *J Biol Chem*, *278*(24), 21327-21330. https://doi.org/10.1074/jbc.C300119200

126. Liu, B., Gross, M., ten Hoeve, J., & Shuai, K. (2001). A transcriptional corepressor of Stat1 with an essential LXXLL signature motif. *Proc Natl Acad Sci U S A*, *98*(6), 3203-3207. https://doi.org/10.1073/pnas.051489598

127. Flotho, A., & Melchior, F. (2013). Sumoylation: a regulatory protein modification in health and disease. *Annu Rev Biochem*, *82*, 357-385. https://doi.org/10.1146/annurev-biochem-061909-093311

128. Ungureanu, D., Vanhatupa, S., Kotaja, N., Yang, J., Aittomaki, S., Jänne, O. A., Palvimo, J. J., & Silvennoinen, O. (2003). PIAS proteins promote SUMO-1 conjugation to STAT1. *Blood*, *102*(9), 3311-3313. https://doi.org/10.1182/blood-2002-12-3816

129. McBride, K. M., Banninger, G., McDonald, C., & Reich, N. C. (2002). Regulated nuclear import of the STAT1 transcription factor by direct binding of importin-alpha. *Embo j*, *21*(7), 1754-1763. https://doi.org/10.1093/emboj/21.7.1754

130. Müller, M., Laxton, C., Briscoe, J., Schindler, C., Improta, T., Darnell, J. E., Jr., Stark, G. R., & Kerr, I. M. (1993). Complementation of a mutant cell line: central role of the 91 kDa polypeptide of ISGF3 in the interferon-alpha and -gamma signal transduction pathways. *Embo j*, *12*(11), 4221-4228. https://doi.org/10.1002/j.1460-2075.1993.tb06106.x

131. Bromberg, J. F., Horvath, C. M., Wen, Z., Schreiber, R. D., & Darnell, J. E., Jr. (1996). Transcriptionally active Stat1 is required for the antiproliferative effects of both interferon alpha and interferon gamma. *Proc Natl Acad Sci U S A*, *93*(15), 7673-7678. https://doi.org/10.1073/pnas.93.15.7673

132. Sadzak, I., Schiff, M., Gattermeier, I., Glinitzer, R., Sauer, I., Saalmüller, A., Yang, E., Schaljo, B., & Kovarik, P. (2008). Recruitment of Stat1 to chromatin is required for interferon-induced serine phosphorylation of Stat1 transactivation domain. *Proc Natl Acad Sci U S A*, *105*(26), 8944-8949. https://doi.org/10.1073/pnas.0801794105

133. Wen, Z., Zhong, Z., & Darnell, J. E., Jr. (1995). Maximal activation of transcription by Stat1 and Stat3 requires both tyrosine and serine phosphorylation. *Cell*, *82*(2), 241-250. https://doi.org/10.1016/0092-8674(95)90311-9

134. Bancerek, J., Poss, Z. C., Steinparzer, I., Sedlyarov, V., Pfaffenwimmer, T., Mikulic, I., Dölken, L., Strobl, B., Müller, M., Taatjes, D. J., & Kovarik, P. (2013). CDK8 kinase phosphorylates transcription factor STAT1 to selectively regulate the interferon response. *Immunity*, *38*(2), 250-262. https://doi.org/10.1016/j.immuni.2012.10.017

135. Steinparzer, I., Sedlyarov, V., Rubin, J. D., Eislmayr, K., Galbraith, M. D., Levandowski, C. B., Vcelkova, T., Sneezum, L., Wascher, F., Amman, F., Kleinova, R., Bender, H., Andrysik, Z., Espinosa, J. M., Superti-Furga, G., Dowell, R. D., Taatjes, D. J., & Kovarik, P. (2019). Transcriptional Responses to IFN-γ Require Mediator Kinase-Dependent Pause Release and Mechanistically Distinct CDK8 and CDK19 Functions. *Mol Cell*, *76*(3), 485-499.e488. https://doi.org/10.1016/j.molcel.2019.07.034

136. Tenoever, B. R., Ng, S. L., Chua, M. A., McWhirter, S. M., García-Sastre, A., & Maniatis, T. (2007). Multiple functions of the IKK-related kinase IKKepsilon in interferon-mediated antiviral immunity. *Science*, *315*(5816), 1274-1278. https://doi.org/10.1126/science.1136567

137. Ng, S. L., Friedman, B. A., Schmid, S., Gertz, J., Myers, R. M., Tenoever, B. R., & Maniatis, T. (2011). IκB kinase epsilon (IKK(epsilon)) regulates the balance between

type I and type II interferon responses. *Proc Natl Acad Sci U S A*, *108*(52), 21170-21175. https://doi.org/10.1073/pnas.1119137109

138. Perwitasari, O., Cho, H., Diamond, M. S., & Gale, M., Jr. (2011). Inhibitor of κB kinase epsilon (IKK(epsilon)), STAT1, and IFIT2 proteins define novel innate immune effector pathway against West Nile virus infection. *J Biol Chem*, *286*(52), 44412-44423. https://doi.org/10.1074/jbc.M111.285205

139. Meissner, T., Krause, E., Lödige, I., & Vinkemeier, U. (2004). Arginine methylation of STAT1: a reassessment. *Cell*, *119*(5), 587-589; discussion 589-590. https://doi.org/10.1016/j.cell.2004.11.024

140. Komyod, W., Bauer, U. M., Heinrich, P. C., Haan, S., & Behrmann, I. (2005). Are STATS arginine-methylated? *J Biol Chem*, *280*(23), 21700-21705. https://doi.org/10.1074/jbc.C400606200

141. Iwasaki, H., Kovacic, J. C., Olive, M., Beers, J. K., Yoshimoto, T., Crook, M. F., Tonelli, L. H., & Nabel, E. G. (2010). Disruption of protein arginine N-methyltransferase 2 regulates leptin signaling and produces leanness in vivo through loss of STAT3 methylation. *Circ Res*, *107*(8), 992-1001. https://doi.org/10.1161/circresaha.110.225326

142. Yuan, Z. L., Guan, Y. J., Chatterjee, D., & Chin, Y. E. (2005). Stat3 dimerization regulated by reversible acetylation of a single lysine residue. *Science*, *307*(5707), 269-273. https://doi.org/10.1126/science.1105166

143. Lee, J. L., Wang, M. J., & Chen, J. Y. (2009). Acetylation and activation of STAT3 mediated by nuclear translocation of CD44. *J Cell Biol*, *185*(6), 949-957. https://doi.org/10.1083/jcb.200812060

144. Nie, Y., Erion, D. M., Yuan, Z., Dietrich, M., Shulman, G. I., Horvath, T. L., & Gao, Q. (2009). STAT3 inhibition of gluconeogenesis is downregulated by SirT1. *Nat Cell Biol*, *11*(4), 492-500. https://doi.org/10.1038/ncb1857

145. Sestito, R., Madonna, S., Scarponi, C., Cianfarani, F., Failla, C. M., Cavani, A., Girolomoni, G., & Albanesi, C. (2011). STAT3-dependent effects of IL-22 in human keratinocytes are counterregulated by sirtuin 1 through a direct inhibition of STAT3 acetylation. *Faseb j*, *25*(3), 916-927. https://doi.org/10.1096/fj.10-172288

146. Hu, X., Chen, J., Wang, L., & Ivashkiv, L. B. (2007). Crosstalk among Jak-STAT, Toll-like receptor, and ITAM-dependent pathways in macrophage activation. *J Leukoc Biol*, *82*(2), 237-243. https://doi.org/10.1189/jlb.1206763

147. Farlik, M., Reutterer, B., Schindler, C., Greten, F., Vogl, C., Müller, M., & Decker, T. (2010). Nonconventional initiation complex assembly by STAT and NF-kappaB transcription factors regulates nitric oxide synthase expression. *Immunity*, *33*(1), 25-34. https://doi.org/10.1016/j.immuni.2010.07.001

148. Czimmerer, Z., Halasz, L., Daniel, B., Varga, Z., Bene, K., Domokos, A., Hoeksema, M., Shen, Z., Berger, W. K., Cseh, T., Jambrovics, K., Kolostyak, Z., Fenyvesi, F., Varadi, J., Poliska, S., Hajas, G., Szatmari, I., Glass, C. K., Bacsi, A., & Nagy, L. (2022). The epigenetic state of IL-4-polarized macrophages enables inflammatory cistromic expansion and extended synergistic response to TLR ligands. *Immunity*, *55*(11), 2006-2026.e2006. https://doi.org/10.1016/j.immuni.2022.10.004

149. Zhao, M., Jankovic, D., Link, V. M., Souza, C. O. S., Hornick, K. M., Oyesola, O., Belkaid, Y., Lack, J., & Loke, P. (2025). Genetic variation in IL-4 activated tissue resident macrophages determines strain-specific synergistic responses to LPS epigenetically. *Nat Commun*, *16*(1), 1030. https://doi.org/10.1038/s41467-025-56379-8

150. Hoeksema, M. A., Shen, Z., Holtman, I. R., Zheng, A., Spann, N. J., Cobo, I., Gymrek, M., & Glass, C. K. (2021). Mechanisms underlying divergent responses of genetically distinct macrophages to IL-4. *Sci Adv*, *7*(25). https://doi.org/10.1126/sciadv.abf9808

151. Radoshevich, L., & Cossart, P. (2018). Listeria monocytogenes: towards a complete picture of its physiology and pathogenesis. *Nat Rev Microbiol*, *16*(1), 32-46. https://doi.org/10.1038/nrmicro.2017.126

152. Cossart, P., & Helenius, A. (2014). Endocytosis of viruses and bacteria. *Cold Spring Harb Perspect Biol*, *6*(8). https://doi.org/10.1101/cshperspect.a016972

153. Perelman, S. S., Abrams, M. E., Eitson, J. L., Chen, D., Jimenez, A., Mettlen, M., Schoggins, J. W., & Alto, N. M. (2016). Cell-Based Screen Identifies Human Interferon-Stimulated Regulators of Listeria monocytogenes Infection. *PLoS Pathog*, *12*(12), e1006102. https://doi.org/10.1371/journal.ppat.1006102

154. Hamon, M. A., Ribet, D., Stavru, F., & Cossart, P. (2012). Listeriolysin O: the Swiss army knife of Listeria. *Trends Microbiol*, *20*(8), 360-368. https://doi.org/10.1016/j.tim.2012.04.006

155. Stavru, F., Bouillaud, F., Sartori, A., Ricquier, D., & Cossart, P. (2011). Listeria monocytogenes transiently alters mitochondrial dynamics during infection. *Proc Natl Acad Sci U S A*, *108*(9), 3612-3617. https://doi.org/10.1073/pnas.1100126108

156. Pillich, H., Loose, M., Zimmer, K. P., & Chakraborty, T. (2012). Activation of the unfolded protein response by Listeria monocytogenes. *Cell Microbiol*, *14*(6), 949-964. https://doi.org/10.1111/j.1462-5822.2012.01769.x

157. Malet, J. K., Cossart, P., & Ribet, D. (2017). Alteration of epithelial cell lysosomal integrity induced by bacterial cholesterol-dependent cytolysins. *Cell Microbiol*, *19*(4). https://doi.org/10.1111/cmi.12682

158. Bierne, H., & Cossart, P. (2012). When bacteria target the nucleus: the emerging family of nucleomodulins. *Cell Microbiol*, *14*(5), 622-633. https://doi.org/10.1111/j.1462-5822.2012.01758.x

159. Lebreton, A., Lakisic, G., Job, V., Fritsch, L., Tham, T. N., Camejo, A., Matteï, P. J., Regnault, B., Nahori, M. A., Cabanes, D., Gautreau, A., Ait-Si-Ali, S., Dessen, A., Cossart, P., & Bierne, H. (2011). A bacterial protein targets the BAHD1 chromatin complex to stimulate type III interferon response. *Science*, *331*(6022), 1319-1321. https://doi.org/10.1126/science.1200120

160. Woodward, J. J., Iavarone, A. T., & Portnoy, D. A. (2010). c-di-AMP secreted by intracellular Listeria monocytogenes activates a host type I interferon response. *Science*, *328*(5986), 1703-1705. https://doi.org/10.1126/science.1189801

161. Burdette, D. L., Monroe, K. M., Sotelo-Troha, K., Iwig, J. S., Eckert, B., Hyodo, M., Hayakawa, Y., & Vance, R. E. (2011). STING is a direct innate immune sensor of cyclic di-GMP. *Nature*, *478*(7370), 515-518. https://doi.org/10.1038/nature10429

162. Abdullah, Z., Schlee, M., Roth, S., Mraheil, M. A., Barchet, W., Böttcher, J., Hain, T., Geiger, S., Hayakawa, Y., Fritz, J. H., Civril, F., Hopfner, K. P., Kurts, C., Ruland, J., Hartmann, G., Chakraborty, T., & Knolle, P. A. (2012). RIG-I detects infection with live Listeria by sensing secreted bacterial nucleic acids. *Embo j*, *31*(21), 4153-4164. https://doi.org/10.1038/emboj.2012.274

163. Ishikawa, H., Ma, Z., & Barber, G. N. (2009). STING regulates intracellular DNA-mediated, type I interferon-dependent innate immunity. *Nature*, *461*(7265), 788-792. https://doi.org/10.1038/nature08476

164. Sauer, J. D., Witte, C. E., Zemansky, J., Hanson, B., Lauer, P., & Portnoy, D. A. (2010). Listeria monocytogenes triggers AIM2-mediated pyroptosis upon infrequent bacteriolysis in the macrophage cytosol. *Cell Host Microbe*, *7*(5), 412-419. https://doi.org/10.1016/j.chom.2010.04.004

165. Kim, S., Bauernfeind, F., Ablasser, A., Hartmann, G., Fitzgerald, K. A., Latz, E., & Hornung, V. (2010). Listeria monocytogenes is sensed by the NLRP3 and AIM2 inflammasome. *Eur J Immunol*, *40*(6), 1545-1551. https://doi.org/10.1002/eji.201040425

166. Latz, E., Xiao, T. S., & Stutz, A. (2013). Activation and regulation of the inflammasomes. *Nat Rev Immunol*, *13*(6), 397-411. https://doi.org/10.1038/nri3452

167. O'Connell, R. M., Saha, S. K., Vaidya, S. A., Bruhn, K. W., Miranda, G. A., Zarnegar, B., Perry, A. K., Nguyen, B. O., Lane, T. F., Taniguchi, T., Miller, J. F., & Cheng, G. (2004). Type I interferon production enhances susceptibility to Listeria monocytogenes infection. *J Exp Med*, *200*(4), 437-445. https://doi.org/10.1084/jem.20040712

168. Carrero, J. A., Calderon, B., & Unanue, E. R. (2004). Type I interferon sensitizes lymphocytes to apoptosis and reduces resistance to Listeria infection. *J Exp Med*, *200*(4), 535-540. https://doi.org/10.1084/jem.20040769

169. Boxx, G. M., & Cheng, G. (2016). The Roles of Type I Interferon in Bacterial Infection. *Cell Host Microbe*, *19*(6), 760-769. https://doi.org/10.1016/j.chom.2016.05.016

170. Gupta, M., Shin, D. M., Ramakrishna, L., Goussetis, D. J., Platanias, L. C., Xiong, H., Morse, H. C., 3rd, & Ozato, K. (2015). IRF8 directs stress-induced autophagy in macrophages and promotes clearance of Listeria monocytogenes. *Nat Commun*, *6*, 6379. https://doi.org/10.1038/ncomms7379

171. Mitchell, G., Cheng, M. I., Chen, C., Nguyen, B. N., Whiteley, A. T., Kianian, S., Cox, J. S., Green, D. R., McDonald, K. L., & Portnoy, D. A. (2018). Listeria monocytogenes triggers noncanonical autophagy upon phagocytosis, but avoids subsequent growth-restricting xenophagy. *Proc Natl Acad Sci U S A*, *115*(2), E210-e217. https://doi.org/10.1073/pnas.1716055115

172. Girbig, M., Misiaszek, A. D., & Müller, C. W. (2022). Structural insights into nuclear transcription by eukaryotic DNA-dependent RNA polymerases. *Nat Rev Mol Cell Biol*, *23*(9), 603-622. https://doi.org/10.1038/s41580-022-00476-9

173. West, M. L., & Corden, J. L. (1995). Construction and analysis of yeast RNA polymerase II CTD deletion and substitution mutations. *Genetics*, *140*(4), 1223-1233. https://doi.org/10.1093/genetics/140.4.1223

174. Morrill, S. A., Exner, A. E., Babokhov, M., Reinfeld, B. I., & Fuchs, S. M. (2016). DNA Instability Maintains the Repeat Length of the Yeast RNA Polymerase II C-terminal Domain. *J Biol Chem*, *291*(22), 11540-11550. https://doi.org/10.1074/jbc.M115.696252

175. Sawicka, A., Villamil, G., Lidschreiber, M., Darzacq, X., Dugast-Darzacq, C., Schwalb, B., & Cramer, P. (2021). Transcription activation depends on the length of the RNA polymerase II C-terminal domain. *Embo j*, *40*(9), e107015. https://doi.org/10.15252/embj.2020107015

176. Kwon, I., Kato, M., Xiang, S., Wu, L., Theodoropoulos, P., Mirzaei, H., Han, T., Xie, S., Corden, J. L., & McKnight, S. L. (2013). Phosphorylation-regulated binding of RNA polymerase II to fibrous polymers of low-complexity domains. *Cell*, *155*(5), 1049-1060. https://doi.org/10.1016/j.cell.2013.10.033

177. Burke, K. A., Janke, A. M., Rhine, C. L., & Fawzi, N. L. (2015). Residue-by-Residue View of In Vitro FUS Granules that Bind the C-Terminal Domain of RNA Polymerase II. *Mol Cell*, *60*(2), 231-241. https://doi.org/10.1016/j.molcel.2015.09.006

178. Lu, H., Flores, O., Weinmann, R., & Reinberg, D. (1991). The nonphosphorylated form of RNA polymerase II preferentially associates with the preinitiation complex. *Proc Natl Acad Sci U S A*, *88*(22), 10004-10008. https://doi.org/10.1073/pnas.88.22.10004

179. Robinson, P. J., Trnka, M. J., Bushnell, D. A., Davis, R. E., Mattei, P. J., Burlingame, A. L., & Kornberg, R. D. (2016). Structure of a Complete Mediator-RNA Polymerase II Pre-Initiation Complex. *Cell*, *166*(6), 1411-1422.e1416. https://doi.org/10.1016/j.cell.2016.08.050

180. Komarnitsky, P., Cho, E. J., & Buratowski, S. (2000). Different phosphorylated forms of RNA polymerase II and associated mRNA processing factors during transcription. *Genes Dev*, *14*(19), 2452-2460. https://doi.org/10.1101/gad.824700

181. Harlen, K. M., & Churchman, L. S. (2017). The code and beyond: transcription regulation by the RNA polymerase II carboxy-terminal domain. *Nat Rev Mol Cell Biol*, *18*(4), 263-273. https://doi.org/10.1038/nrm.2017.10

182. Collin, P., Jeronimo, C., Poitras, C., & Robert, F. (2019). RNA Polymerase II CTD Tyrosine 1 Is Required for Efficient Termination by the Nrd1-Nab3-Sen1 Pathway. *Mol Cell*, *73*(4), 655-669.e657. https://doi.org/10.1016/j.molcel.2018.12.002

183. Descostes, N., Heidemann, M., Spinelli, L., Schüller, R., Maqbool, M. A., Fenouil, R., Koch, F., Innocenti, C., Gut, M., Gut, I., Eick, D., & Andrau, J. C. (2014). Tyrosine phosphorylation of RNA polymerase II CTD is associated with antisense promoter transcription and active enhancers in mammalian cells. *Elife*, *3*, e02105. https://doi.org/10.7554/eLife.02105

184. Hsin, J. P., Li, W., Hoque, M., Tian, B., & Manley, J. L. (2014). RNAP II CTD tyrosine 1 performs diverse functions in vertebrate cells. *Elife*, *3*, e02112. https://doi.org/10.7554/eLife.02112

185. Egloff, S., O'Reilly, D., Chapman, R. D., Taylor, A., Tanzhaus, K., Pitts, L., Eick, D., & Murphy, S. (2007). Serine-7 of the RNA polymerase II CTD is specifically required for snRNA gene expression. *Science*, *318*(5857), 1777-1779. https://doi.org/10.1126/science.1145989

186. Egloff, S. (2012). Role of Ser7 phosphorylation of the CTD during transcription of snRNA genes. *RNA Biol*, *9*(8), 1033-1038. https://doi.org/10.4161/rna.21166

187. Hsin, J. P., Sheth, A., & Manley, J. L. (2011). RNAP II CTD phosphorylated on threonine-4 is required for histone mRNA 3' end processing. *Science*, *334*(6056), 683-686. https://doi.org/10.1126/science.1206034

188. Moreno, R. Y., Panina, S. B., Irani, S., Hardtke, H. A., Stephenson, R., Floyd, B. M., Marcotte, E. M., Zhang, Q., & Zhang, Y. J. (2024). Thr(4) phosphorylation on RNA Pol II occurs at early transcription regulating 3'-end processing. *Sci Adv*, *10*(36), eadq0350. https://doi.org/10.1126/sciadv.adq0350

189. Heidemann, M., Hintermair, C., Voß, K., & Eick, D. (2013). Dynamic phosphorylation patterns of RNA polymerase II CTD during transcription. *Biochim Biophys Acta*, *1829*(1), 55-62. https://doi.org/10.1016/j.bbagrm.2012.08.013

190. Roeder, R. G. (1996). The role of general initiation factors in transcription by RNA polymerase II. *Trends Biochem Sci*, *21*(9), 327-335.

191. Haberle, V., & Stark, A. (2018). Eukaryotic core promoters and the functional basis of transcription initiation. *Nat Rev Mol Cell Biol*, *19*(10), 621-637. https://doi.org/10.1038/s41580-018-0028-8

192. Martinez, E., Chiang, C. M., Ge, H., & Roeder, R. G. (1994). TATA-binding protein-associated factor(s) in TFIID function through the initiator to direct basal transcription from a TATA-less class II promoter. *Embo j*, *13*(13), 3115-3126. https://doi.org/10.1002/j.1460-2075.1994.tb06610.x

193. Burley, S. K., & Roeder, R. G. (1996). Biochemistry and structural biology of transcription factor IID (TFIID). *Annu Rev Biochem*, *65*, 769-799. https://doi.org/10.1146/annurev.bi.65.070196.004005

194. Tan, S., Hunziker, Y., Sargent, D. F., & Richmond, T. J. (1996). Crystal structure of a yeast TFIIA/TBP/DNA complex. *Nature*, *381*(6578), 127-151. https://doi.org/10.1038/381127a0

195. Nikolov, D. B., Chen, H., Halay, E. D., Usheva, A. A., Hisatake, K., Lee, D. K., Roeder, R. G., & Burley, S. K. (1995). Crystal structure of a TFIIB-TBP-TATA-element ternary complex. *Nature*, *377*(6545), 119-128. https://doi.org/10.1038/377119a0

196. Zawel, L., Kumar, K. P., & Reinberg, D. (1995). Recycling of the general transcription factors during RNA polymerase II transcription. *Genes Dev*, *9*(12), 1479-1490. https://doi.org/10.1101/gad.9.12.1479

197. Leuther, K. K., Bushnell, D. A., & Kornberg, R. D. (1996). Two-dimensional crystallography of TFIIB- and IIE-RNA polymerase II complexes: implications for start site selection and initiation complex formation. *Cell*, *85*(5), 773-779. https://doi.org/10.1016/s0092-8674(00)81242-8

198. Maxon, M. E., Goodrich, J. A., & Tjian, R. (1994). Transcription factor IIE binds preferentially to RNA polymerase IIa and recruits TFIIH: a model for promoter clearance. *Genes Dev*, *8*(5), 515-524. https://doi.org/10.1101/gad.8.5.515

199. Tirode, F., Busso, D., Coin, F., & Egly, J. M. (1999). Reconstitution of the transcription factor TFIIH: assignment of functions for the three enzymatic subunits, XPB, XPD, and cdk7. *Mol Cell*, *3*(1), 87-95. https://doi.org/10.1016/s1097-2765(00)80177-x

200. Akhtar, M. S., Heidemann, M., Tietjen, J. R., Zhang, D. W., Chapman, R. D., Eick, D., & Ansari, A. Z. (2009). TFIIH kinase places bivalent marks on the carboxy-terminal domain of RNA polymerase II. *Mol Cell*, *34*(3), 387-393. https://doi.org/10.1016/j.molcel.2009.04.016

201. Kim, M., Suh, H., Cho, E. J., & Buratowski, S. (2009). Phosphorylation of the yeast Rpb1 C-terminal domain at serines 2, 5, and 7. *J Biol Chem*, *284*(39), 26421-26426. https://doi.org/10.1074/jbc.M109.028993

202. Gilmour, D. S., & Lis, J. T. (1986). RNA polymerase II interacts with the promoter region of the noninduced hsp70 gene in Drosophila melanogaster cells. *Mol Cell Biol*, *6*(11), 3984-3989. https://doi.org/10.1128/mcb.6.11.3984-3989.1986

203. Rougvie, A. E., & Lis, J. T. (1988). The RNA polymerase II molecule at the 5' end of the uninduced hsp70 gene of D. melanogaster is transcriptionally engaged. *Cell*, *54*(6), 795-804. https://doi.org/10.1016/s0092-8674(88)91087-2

204. Gariglio, P., Bellard, M., & Chambon, P. (1981). Clustering of RNA polymerase B molecules in the 5' moiety of the adult beta-globin gene of hen erythrocytes. *Nucleic Acids Res*, *9*(11), 2589-2598. https://doi.org/10.1093/nar/9.11.2589

205. Krumm, A., Meulia, T., Brunvand, M., & Groudine, M. (1992). The block to transcriptional elongation within the human c-myc gene is determined in the promoter-proximal region. *Genes Dev*, *6*(11), 2201-2213. https://doi.org/10.1101/gad.6.11.2201

206. Plet, A., Eick, D., & Blanchard, J. M. (1995). Elongation and premature termination of transcripts initiated from c-fos and c-myc promoters show dissimilar patterns. *Oncogene*, *10*(2), 319-328.

207. Kim, T. H., Barrera, L. O., Zheng, M., Qu, C., Singer, M. A., Richmond, T. A., Wu, Y., Green, R. D., & Ren, B. (2005). A high-resolution map of active promoters in the human genome. *Nature*, *436*(7052), 876-880. https://doi.org/10.1038/nature03877

208. Guenther, M. G., Levine, S. S., Boyer, L. A., Jaenisch, R., & Young, R. A. (2007). A chromatin landmark and transcription initiation at most promoters in human cells. *Cell*, *130*(1), 77-88. https://doi.org/10.1016/j.cell.2007.05.042

209. Muse, G. W., Gilchrist, D. A., Nechaev, S., Shah, R., Parker, J. S., Grissom, S. F., Zeitlinger, J., & Adelman, K. (2007). RNA polymerase is poised for activation across the genome. *Nat Genet*, *39*(12), 1507-1511. https://doi.org/10.1038/ng.2007.21

210. Zeitlinger, J., Stark, A., Kellis, M., Hong, J. W., Nechaev, S., Adelman, K., Levine, M., & Young, R. A. (2007). RNA polymerase stalling at developmental control genes in the Drosophila melanogaster embryo. *Nat Genet*, *39*(12), 1512-1516. https://doi.org/10.1038/ng.2007.26

211. Bernecky, C., Plitzko, J. M., & Cramer, P. (2017). Structure of a transcribing RNA polymerase II-DSIF complex reveals a multidentate DNA-RNA clamp. *Nat Struct Mol Biol*, *24*(10), 809-815. https://doi.org/10.1038/nsmb.3465

212. Vos, S. M., Farnung, L., Boehning, M., Wigge, C., Linden, A., Urlaub, H., & Cramer, P. (2018). Structure of activated transcription complex Pol II-DSIF-PAF-SPT6. *Nature*, *560*(7720), 607-612. https://doi.org/10.1038/s41586-018-0440-4

213. Wen, Y., & Shatkin, A. J. (1999). Transcription elongation factor hSPT5 stimulates mRNA capping. *Genes Dev*, *13*(14), 1774-1779. https://doi.org/10.1101/gad.13.14.1774

214. Pei, Y., & Shuman, S. (2002). Interactions between fission yeast mRNA capping enzymes and elongation factor Spt5. *J Biol Chem*, *277*(22), 19639-19648. https://doi.org/10.1074/jbc.M200015200

215. Cheng, B., & Price, D. H. (2007). Properties of RNA polymerase II elongation complexes before and after the P-TEFb-mediated transition into productive elongation. *J Biol Chem*, *282*(30), 21901-21912. https://doi.org/10.1074/jbc.M702936200

216. Yamaguchi, Y., Inukai, N., Narita, T., Wada, T., & Handa, H. (2002). Evidence that negative elongation factor represses transcription elongation through binding to a DRB sensitivity-inducing factor/RNA polymerase II complex and RNA. *Mol Cell Biol*, *22*(9), 2918-2927. https://doi.org/10.1128/mcb.22.9.2918-2927.2002

217. Aiyar, S. E., Sun, J. L., Blair, A. L., Moskaluk, C. A., Lu, Y. Z., Ye, Q. N., Yamaguchi, Y., Mukherjee, A., Ren, D. M., Handa, H., & Li, R. (2004). Attenuation of estrogen receptor alpha-mediated transcription through estrogen-stimulated recruitment of a negative elongation factor. *Genes Dev*, *18*(17), 2134-2146. https://doi.org/10.1101/gad.1214104

218. Rao, J. N., Neumann, L., Wenzel, S., Schweimer, K., Rösch, P., & Wöhrl, B. M. (2006). Structural studies on the RNA-recognition motif of NELF E, a cellular negative transcription elongation factor involved in the regulation of HIV transcription. *Biochem J*, *400*(3), 449-456. https://doi.org/10.1042/bj20060421

219. Amleh, A., Nair, S. J., Sun, J., Sutherland, A., Hasty, P., & Li, R. (2009). Mouse cofactor of BRCA1 (Cobra1) is required for early embryogenesis. *PLoS One*, *4*(4), e5034. https://doi.org/10.1371/journal.pone.0005034

220. Adelman, K., Kennedy, M. A., Nechaev, S., Gilchrist, D. A., Muse, G. W., Chinenov, Y., & Rogatsky, I. (2009). Immediate mediators of the inflammatory response are poised for gene activation through RNA polymerase II stalling. *Proc Natl Acad Sci U S A*, *106*(43), 18207-18212. https://doi.org/10.1073/pnas.0910177106

221. Yu, L., Zhang, B., Deochand, D., Sacta, M. A., Coppo, M., Shang, Y., Guo, Z., Zeng, X., Rollins, D. A., Tharmalingam, B., Li, R., Chinenov, Y., Rogatsky, I., & Hu, X. (2020). Negative elongation factor complex enables macrophage inflammatory responses by controlling anti-inflammatory gene expression. *Nat Commun*, *11*(1), 2286. https://doi.org/10.1038/s41467-020-16209-5

222. Aoi, Y., Smith, E. R., Shah, A. P., Rendleman, E. J., Marshall, S. A., Woodfin, A. R., Chen, F. X., Shiekhattar, R., & Shilatifard, A. (2020). NELF Regulates a Promoter-Proximal Step Distinct from RNA Pol II Pause-Release. *Mol Cell*, *78*(2), 261-274.e265. https://doi.org/10.1016/j.molcel.2020.02.014

223. Kuś, K., Carrique, L., Kecman, T., Fournier, M., Hassanein, S. S., Aydin, E., Kilchert, C., Grimes, J. M., & Vasiljeva, L. (2025). DSIF factor Spt5 coordinates transcription, maturation and exoribonucleolysis of RNA polymerase II transcripts. *Nat Commun*, *16*(1), 10. https://doi.org/10.1038/s41467-024-55063-7

224. Wada, T., Takagi, T., Yamaguchi, Y., Ferdous, A., Imai, T., Hirose, S., Sugimoto, S., Yano, K., Hartzog, G. A., Winston, F., Buratowski, S., & Handa, H. (1998). DSIF, a

novel transcription elongation factor that regulates RNA polymerase II processivity, is composed of human Spt4 and Spt5 homologs. *Genes Dev*, *12*(3), 343-356. https://doi.org/10.1101/gad.12.3.343

225. Fujinaga, K., Huang, F., & Peterlin, B. M. (2023). P-TEFb: The master regulator of transcription elongation. *Mol Cell*, *83*(3), 393-403. https://doi.org/10.1016/j.molcel.2022.12.006

226. Bartkowiak, B., Liu, P., Phatnani, H. P., Fuda, N. J., Cooper, J. J., Price, D. H., Adelman, K., Lis, J. T., & Greenleaf, A. L. (2010). CDK12 is a transcription elongation-associated CTD kinase, the metazoan ortholog of yeast Ctk1. *Genes Dev*, *24*(20), 2303-2316. https://doi.org/10.1101/gad.1968210

227. Blazek, D., Kohoutek, J., Bartholomeeusen, K., Johansen, E., Hulinkova, P., Luo, Z., Cimermancic, P., Ule, J., & Peterlin, B. M. (2011). The Cyclin K/Cdk12 complex maintains genomic stability via regulation of expression of DNA damage response genes. *Genes Dev*, *25*(20), 2158-2172. https://doi.org/10.1101/gad.16962311

228. Chao, S. H., & Price, D. H. (2001). Flavopiridol inactivates P-TEFb and blocks most RNA polymerase II transcription in vivo. *J Biol Chem*, *276*(34), 31793-31799. https://doi.org/10.1074/jbc.M102306200

229. Henriques, T., Gilchrist, D. A., Nechaev, S., Bern, M., Muse, G. W., Burkholder, A., Fargo, D. C., & Adelman, K. (2013). Stable pausing by RNA polymerase II provides an opportunity to target and integrate regulatory signals. *Mol Cell*, *52*(4), 517-528. https://doi.org/10.1016/j.molcel.2013.10.001

230. AJ, C. Q., Bugai, A., & Barboric, M. (2016). Cracking the control of RNA polymerase II elongation by 7SK snRNP and P-TEFb. *Nucleic Acids Res*, *44*(16), 7527-7539. https://doi.org/10.1093/nar/gkw585

231. Barboric, M., Yik, J. H., Czudnochowski, N., Yang, Z., Chen, R., Contreras, X., Geyer, M., Matija Peterlin, B., & Zhou, Q. (2007). Tat competes with HEXIM1 to increase the active pool of P-TEFb for HIV-1 transcription. *Nucleic Acids Res*, *35*(6), 2003-2012. https://doi.org/10.1093/nar/gkm063

232. Schröder, S., Cho, S., Zeng, L., Zhang, Q., Kaehlcke, K., Mak, L., Lau, J., Bisgrove, D., Schnölzer, M., Verdin, E., Zhou, M. M., & Ott, M. (2012). Two-pronged binding with bromodomain-containing protein 4 liberates positive transcription elongation factor b from inactive ribonucleoprotein complexes. *J Biol Chem*, *287*(2), 1090-1099. https://doi.org/10.1074/jbc.M111.282855

233. Luo, Z., Lin, C., & Shilatifard, A. (2012). The super elongation complex (SEC) family in transcriptional control. *Nat Rev Mol Cell Biol*, *13*(9), 543-547. https://doi.org/10.1038/nrm3417

234. Orphanides, G., LeRoy, G., Chang, C. H., Luse, D. S., & Reinberg, D. (1998). FACT, a factor that facilitates transcript elongation through nucleosomes. *Cell*, *92*(1), 105-116. https://doi.org/10.1016/s0092-8674(00)80903-4

235. Saunders, A., Werner, J., Andrulis, E. D., Nakayama, T., Hirose, S., Reinberg, D., & Lis, J. T. (2003). Tracking FACT and the RNA polymerase II elongation complex through chromatin in vivo. *Science*, *301*(5636), 1094-1096. https://doi.org/10.1126/science.1085712

236. Bondarenko, V. A., Steele, L. M., Ujvári, A., Gaykalova, D. A., Kulaeva, O. I., Polikanov, Y. S., Luse, D. S., & Studitsky, V. M. (2006). Nucleosomes can form a polar barrier to transcript elongation by RNA polymerase II. *Mol Cell*, *24*(3), 469-479. https://doi.org/10.1016/j.molcel.2006.09.009

237. Vakoc, C. R., Sachdeva, M. M., Wang, H., & Blobel, G. A. (2006). Profile of histone lysine methylation across transcribed mammalian chromatin. *Mol Cell Biol*, *26*(24), 9185-9195. https://doi.org/10.1128/mcb.01529-06

238. Fuchs, G., Hollander, D., Voichek, Y., Ast, G., & Oren, M. (2014). Cotranscriptional histone H2B monoubiquitylation is tightly coupled with RNA polymerase II elongation rate. *Genome Res*, *24*(10), 1572-1583. https://doi.org/10.1101/gr.176487.114

239. Carrozza, M. J., Li, B., Florens, L., Suganuma, T., Swanson, S. K., Lee, K. K., Shia, W. J., Anderson, S., Yates, J., Washburn, M. P., & Workman, J. L. (2005). Histone H3 methylation by Set2 directs deacetylation of coding regions by Rpd3S to suppress spurious intragenic transcription. *Cell*, *123*(4), 581-592. https://doi.org/10.1016/j.cell.2005.10.023

240. Smolle, M., Venkatesh, S., Gogol, M. M., Li, H., Zhang, Y., Florens, L., Washburn, M. P., & Workman, J. L. (2012). Chromatin remodelers Isw1 and Chd1 maintain chromatin structure during transcription by preventing histone exchange. *Nat Struct Mol Biol*, *19*(9), 884-892. https://doi.org/10.1038/nsmb.2312

241. Chen, F. X., Smith, E. R., & Shilatifard, A. (2018). Born to run: control of transcription elongation by RNA polymerase II. *Nat Rev Mol Cell Biol*, *19*(7), 464-478. https://doi.org/10.1038/s41580-018-0010-5

242. Sun, Y., Hamilton, K., & Tong, L. (2020). Recent molecular insights into canonical pre-mRNA 3'-end processing. *Transcription*, *11*(2), 83-96. https://doi.org/10.1080/21541264.2020.1777047

243. Zhao, J., Hyman, L., & Moore, C. (1999). Formation of mRNA 3' ends in eukaryotes: mechanism, regulation, and interrelationships with other steps in mRNA synthesis. *Microbiol Mol Biol Rev*, *63*(2), 405-445. https://doi.org/10.1128/mmbr.63.2.405-445.1999

244. Mandel, C. R., Kaneko, S., Zhang, H., Gebauer, D., Vethantham, V., Manley, J. L., & Tong, L. (2006). Polyadenylation factor CPSF-73 is the pre-mRNA 3'-end-processing endonuclease. *Nature*, *444*(7121), 953-956. https://doi.org/10.1038/nature05363

245. Proudfoot, N. J. (1989). How RNA polymerase II terminates transcription in higher eukaryotes. *Trends Biochem Sci*, *14*(3), 105-110. https://doi.org/10.1016/0968-0004(89)90132-1

246. Connelly, S., & Manley, J. L. (1988). A functional mRNA polyadenylation signal is required for transcription termination by RNA polymerase II. *Genes Dev*, *2*(4), 440-452. https://doi.org/10.1101/gad.2.4.440

247. Shi, Y., Di Giammartino, D. C., Taylor, D., Sarkeshik, A., Rice, W. J., Yates, J. R., 3rd, Frank, J., & Manley, J. L. (2009). Molecular architecture of the human pre-mRNA 3' processing complex. *Mol Cell*, *33*(3), 365-376. https://doi.org/10.1016/j.molcel.2008.12.028

248. Cortazar, M. A., Sheridan, R. M., Erickson, B., Fong, N., Glover-Cutter, K., Brannan, K., & Bentley, D. L. (2019). Control of RNA Pol II Speed by PNUTS-PP1 and Spt5 Dephosphorylation Facilitates Termination by a "Sitting Duck Torpedo" Mechanism. *Mol Cell*, *76*(6), 896-908.e894. https://doi.org/10.1016/j.molcel.2019.09.031

249. Wagner, E. J., Tong, L., & Adelman, K. (2023). Integrator is a global promoter-proximal termination complex. *Mol Cell*, *83*(3), 416-427. https://doi.org/10.1016/j.molcel.2022.11.012

250. Huang, K. L., Jee, D., Stein, C. B., Elrod, N. D., Henriques, T., Mascibroda, L. G., Baillat, D., Russell, W. K., Adelman, K., & Wagner, E. J. (2020). Integrator Recruits Protein Phosphatase 2A to Prevent Pause Release and Facilitate Transcription Termination. *Mol Cell*, *80*(2), 345-358.e349. https://doi.org/10.1016/j.molcel.2020.08.016

251. Fong, N., Brannan, K., Erickson, B., Kim, H., Cortazar, M. A., Sheridan, R. M., Nguyen, T., Karp, S., & Bentley, D. L. (2015). Effects of Transcription Elongation Rate and Xrn2 Exonuclease Activity on RNA Polymerase II Termination Suggest Widespread

Kinetic Competition. *Mol Cell*, *60*(2), 256-267. https://doi.org/10.1016/j.molcel.2015.09.026

252. Flanagan, P. M., Kelleher, R. J., 3rd, Sayre, M. H., Tschochner, H., & Kornberg, R. D. (1991). A mediator required for activation of RNA polymerase II transcription in vitro. *Nature*, *350*(6317), 436-438. https://doi.org/10.1038/350436a0

253. Richter, W. F., Nayak, S., Iwasa, J., & Taatjes, D. J. (2022). The Mediator complex as a master regulator of transcription by RNA polymerase II. *Nat Rev Mol Cell Biol*, *23*(11), 732-749. https://doi.org/10.1038/s41580-022-00498-3

254. Chen, X., Yin, X., Li, J., Wu, Z., Qi, Y., Wang, X., Liu, W., & Xu, Y. (2021). Structures of the human Mediator and Mediator-bound preinitiation complex. *Science*, *372*(6546). https://doi.org/10.1126/science.abg0635

255. Abdella, R., Talyzina, A., Chen, S., Inouye, C. J., Tjian, R., & He, Y. (2021). Structure of the human Mediator-bound transcription preinitiation complex. *Science*, *372*(6537), 52-56. https://doi.org/10.1126/science.abg3074

256. Rengachari, S., Schilbach, S., Aibara, S., Dienemann, C., & Cramer, P. (2021). Structure of the human Mediator-RNA polymerase II pre-initiation complex. *Nature*, *594*(7861), 129-133. https://doi.org/10.1038/s41586-021-03555-7

257. Knuesel, M. T., Meyer, K. D., Donner, A. J., Espinosa, J. M., & Taatjes, D. J. (2009). The human CDK8 subcomplex is a histone kinase that requires Med12 for activity and can function independently of mediator. *Mol Cell Biol*, *29*(3), 650-661. https://doi.org/10.1128/mcb.00993-08

258. Sato, S., Tomomori-Sato, C., Parmely, T. J., Florens, L., Zybailov, B., Swanson, S. K., Banks, C. A., Jin, J., Cai, Y., Washburn, M. P., Conaway, J. W., & Conaway, R. C. (2004). A set of consensus mammalian mediator subunits identified by multidimensional protein identification technology. *Mol Cell*, *14*(5), 685-691. https://doi.org/10.1016/j.molcel.2004.05.006

259. Paoletti, A. C., Parmely, T. J., Tomomori-Sato, C., Sato, S., Zhu, D., Conaway, R. C., Conaway, J. W., Florens, L., & Washburn, M. P. (2006). Quantitative proteomic analysis of distinct mammalian Mediator complexes using normalized spectral abundance factors. *Proc Natl Acad Sci U S A*, *103*(50), 18928-18933. https://doi.org/10.1073/pnas.0606379103

260. Yudkovsky, N., Ranish, J. A., & Hahn, S. (2000). A transcription reinitiation intermediate that is stabilized by activator. *Nature*, *408*(6809), 225-229. https://doi.org/10.1038/35041603

261. Smith, E. R., Lin, C., Garrett, A. S., Thornton, J., Mohaghegh, N., Hu, D., Jackson, J., Saraf, A., Swanson, S. K., Seidel, C., Florens, L., Washburn, M. P., Eissenberg, J. C., & Shilatifard, A. (2011). The little elongation complex regulates small nuclear RNA transcription. *Mol Cell*, *44*(6), 954-965. https://doi.org/10.1016/j.molcel.2011.12.008

262. Takahashi, H., Parmely, T. J., Sato, S., Tomomori-Sato, C., Banks, C. A., Kong, S. E., Szutorisz, H., Swanson, S. K., Martin-Brown, S., Washburn, M. P., Florens, L., Seidel, C. W., Lin, C., Smith, E. R., Shilatifard, A., Conaway, R. C., & Conaway, J. W. (2011). Human mediator subunit MED26 functions as a docking site for transcription elongation factors. *Cell*, *146*(1), 92-104. https://doi.org/10.1016/j.cell.2011.06.005

263. Takahashi, H., Takigawa, I., Watanabe, M., Anwar, D., Shibata, M., Tomomori-Sato, C., Sato, S., Ranjan, A., Seidel, C. W., Tsukiyama, T., Mizushima, W., Hayashi, M., Ohkawa, Y., Conaway, J. W., Conaway, R. C., & Hatakeyama, S. (2015). MED26 regulates the transcription of snRNA genes through the recruitment of little elongation complex. *Nat Commun*, *6*, 5941. https://doi.org/10.1038/ncomms6941

264. Takahashi, H., Ranjan, A., Chen, S., Suzuki, H., Shibata, M., Hirose, T., Hirose, H., Sasaki, K., Abe, R., Chen, K., He, Y., Zhang, Y., Takigawa, I., Tsukiyama, T., Watanabe, M., Fujii, S., Iida, M., Yamamoto, J., Yamaguchi, Y., . . . Hatakeyama, S.

(2020). The role of Mediator and Little Elongation Complex in transcription termination. *Nat Commun*, *11*(1), 1063. https://doi.org/10.1038/s41467-020-14849-1

265. Lu, C., Bai, X., Zhang, H., Zhang, Y., Yang, M., Zheng, Y., Jin, Z., Yang, W., Guo, G., Huang, Q., Huang, Y., Wu, L., Fu, X. D., Zhang, Z., & Wang, G. (2025). Mediator regulates transcriptional termination through crosstalk with pre-mRNA 3' end processing factors. *Mol Cell*, *85*(11), 2147-2164.e2110. https://doi.org/10.1016/j.molcel.2025.05.006

266. Russo, M., Gualdrini, F., Vallelonga, V., Prosperini, E., Noberini, R., Pedretti, S., Borriero, C., Di Chiaro, P., Polletti, S., Imperato, G., Marenda, M., Ghirardi, C., Bedin, F., Cuomo, A., Rodighiero, S., Bonaldi, T., Mitro, N., Ghisletti, S., & Natoli, G. (2024). Acetyl-CoA production by Mediator-bound 2-ketoacid dehydrogenases boosts de novo histone acetylation and is regulated by nitric oxide. *Mol Cell*, *84*(5), 967-980.e910. https://doi.org/10.1016/j.molcel.2023.12.033

267. Malumbres, M. (2014). Cyclin-dependent kinases. *Genome Biol*, *15*(6), 122. https://doi.org/10.1186/gb4184

268. Leclerc, V., Tassan, J. P., O'Farrell, P. H., Nigg, E. A., & Léopold, P. (1996). Drosophila Cdk8, a kinase partner of cyclin C that interacts with the large subunit of RNA polymerase II. *Mol Biol Cell*, *7*(4), 505-513. https://doi.org/10.1091/mbc.7.4.505

269. Li, Y. C., Chao, T. C., Kim, H. J., Cholko, T., Chen, S. F., Li, G., Snyder, L., Nakanishi, K., Chang, C. E., Murakami, K., Garcia, B. A., Boyer, T. G., & Tsai, K. L. (2021). Structure and noncanonical Cdk8 activation mechanism within an Argonaute-containing Mediator kinase module. *Sci Adv*, *7*(3). https://doi.org/10.1126/sciadv.abd4484

270. Chao, T. C., Chen, S. F., Kim, H. J., Tang, H. C., Tseng, H. C., Xu, A., Palao, L., 3rd, Khadka, S., Li, T., Huang, M. F., Lee, D. F., Murakami, K., Boyer, T. G., & Tsai, K. L. (2024). Structural basis of the human transcriptional Mediator regulated by its dissociable kinase module. *Mol Cell*, *84*(20), 3932-3949.e3910. https://doi.org/10.1016/j.molcel.2024.09.001

271. Osman, S., Mohammad, E., Lidschreiber, M., Stuetzer, A., Bazsó, F. L., Maier, K. C., Urlaub, H., & Cramer, P. (2021). The Cdk8 kinase module regulates interaction of the mediator complex with RNA polymerase II. *J Biol Chem*, *296*, 100734. https://doi.org/10.1016/j.jbc.2021.100734

272. Ren, S., & Rollins, B. J. (2004). Cyclin C/cdk3 promotes Rb-dependent G0 exit. *Cell*, *117*(2), 239-251. https://doi.org/10.1016/s0092-8674(04)00300-9

273. Clark, A. D., Oldenbroek, M., & Boyer, T. G. (2015). Mediator kinase module and human tumorigenesis. *Crit Rev Biochem Mol Biol*, *50*(5), 393-426. https://doi.org/10.3109/10409238.2015.1064854

274. Plassche, S. V., & Brouwer, A. P. (2021). MED12-Related (Neuro)Developmental Disorders: A Question of Causality. *Genes (Basel)*, *12*(5). https://doi.org/10.3390/genes12050663

275. Chi, Y., Huddleston, M. J., Zhang, X., Young, R. A., Annan, R. S., Carr, S. A., & Deshaies, R. J. (2001). Negative regulation of Gcn4 and Msn2 transcription factors by Srb10 cyclin-dependent kinase. *Genes Dev*, *15*(9), 1078-1092. https://doi.org/10.1101/gad.867501

276. Nelson, C., Goto, S., Lund, K., Hung, W., & Sadowski, I. (2003). Srb10/Cdk8 regulates yeast filamentous growth by phosphorylating the transcription factor Ste12. *Nature*, *421*(6919), 187-190. https://doi.org/10.1038/nature01243

277. Akoulitchev, S., Chuikov, S., & Reinberg, D. (2000). TFIIH is negatively regulated by cdk8-containing mediator complexes. *Nature*, *407*(6800), 102-106. https://doi.org/10.1038/35024111

278. Taatjes, D. J., Näär, A. M., Andel, F., 3rd, Nogales, E., & Tjian, R. (2002). Structure, function, and activator-induced conformations of the CRSP coactivator. *Science*, *295*(5557), 1058-1062. https://doi.org/10.1126/science.1065249

279. Näär, A. M., Taatjes, D. J., Zhai, W., Nogales, E., & Tjian, R. (2002). Human CRSP interacts with RNA polymerase II CTD and adopts a specific CTD-bound conformation. *Genes Dev*, *16*(11), 1339-1344. https://doi.org/10.1101/gad.987602

280. Elmlund, H., Baraznenok, V., Lindahl, M., Samuelsen, C. O., Koeck, P. J., Holmberg, S., Hebert, H., & Gustafsson, C. M. (2006). The cyclin-dependent kinase 8 module sterically blocks Mediator interactions with RNA polymerase II. *Proc Natl Acad Sci U S A*, *103*(43), 15788-15793. https://doi.org/10.1073/pnas.0607483103

281. Tsai, K. L., Sato, S., Tomomori-Sato, C., Conaway, R. C., Conaway, J. W., & Asturias, F. J. (2013). A conserved Mediator-CDK8 kinase module association regulates Mediator-RNA polymerase II interaction. *Nat Struct Mol Biol*, *20*(5), 611-619. https://doi.org/10.1038/nsmb.2549

282. Mo, X., Kowenz-Leutz, E., Xu, H., & Leutz, A. (2004). Ras induces mediator complex exchange on C/EBP beta. *Mol Cell*, *13*(2), 241-250. https://doi.org/10.1016/s1097-2765(03)00521-5

283. Pavri, R., Lewis, B., Kim, T. K., Dilworth, F. J., Erdjument-Bromage, H., Tempst, P., de Murcia, G., Evans, R., Chambon, P., & Reinberg, D. (2005). PARP-1 determines specificity in a retinoid signaling pathway via direct modulation of mediator. *Mol Cell*, *18*(1), 83-96. https://doi.org/10.1016/j.molcel.2005.02.034

284. van de Peppel, J., Kettelarij, N., van Bakel, H., Kockelkorn, T. T., van Leenen, D., & Holstege, F. C. (2005). Mediator expression profiling epistasis reveals a signal transduction pathway with antagonistic submodules and highly specific downstream targets. *Mol Cell*, *19*(4), 511-522. https://doi.org/10.1016/j.molcel.2005.06.033

285. Kim, Y. K., Bourgeois, C. F., Pearson, R., Tyagi, M., West, M. J., Wong, J., Wu, S. Y., Chiang, C. M., & Karn, J. (2006). Recruitment of TFIIH to the HIV LTR is a rate-limiting step in the emergence of HIV from latency. *Embo j*, *25*(15), 3596-3604. https://doi.org/10.1038/sj.emboj.7601248

286. Fryer, C. J., White, J. B., & Jones, K. A. (2004). Mastermind recruits CycC:CDK8 to phosphorylate the Notch ICD and coordinate activation with turnover. *Mol Cell*, *16*(4), 509-520. https://doi.org/10.1016/j.molcel.2004.10.014

287. Alarcón, C., Zaromytidou, A. I., Xi, Q., Gao, S., Yu, J., Fujisawa, S., Barlas, A., Miller, A. N., Manova-Todorova, K., Macias, M. J., Sapkota, G., Pan, D., & Massagué, J. (2009). Nuclear CDKs drive Smad transcriptional activation and turnover in BMP and TGF-beta pathways. *Cell*, *139*(4), 757-769. https://doi.org/10.1016/j.cell.2009.09.035

288. Donner, A. J., Szostek, S., Hoover, J. M., & Espinosa, J. M. (2007). CDK8 is a stimulus-specific positive coregulator of p53 target genes. *Mol Cell*, *27*(1), 121-133. https://doi.org/10.1016/j.molcel.2007.05.026

289. Donner, A. J., Ebmeier, C. C., Taatjes, D. J., & Espinosa, J. M. (2010). CDK8 is a positive regulator of transcriptional elongation within the serum response network. *Nat Struct Mol Biol*, *17*(2), 194-201. https://doi.org/10.1038/nsmb.1752

290. Galbraith, M. D., Allen, M. A., Bensard, C. L., Wang, X., Schwinn, M. K., Qin, B., Long, H. W., Daniels, D. L., Hahn, W. C., Dowell, R. D., & Espinosa, J. M. (2013). HIF1A employs CDK8-mediator to stimulate RNAPII elongation in response to hypoxia. *Cell*, *153*(6), 1327-1339. https://doi.org/10.1016/j.cell.2013.04.048

291. Galbraith, M. D., Andrysik, Z., Pandey, A., Hoh, M., Bonner, E. A., Hill, A. A., Sullivan, K. D., & Espinosa, J. M. (2017). CDK8 Kinase Activity Promotes Glycolysis. *Cell Rep*, *21*(6), 1495-1506. https://doi.org/10.1016/j.celrep.2017.10.058

292. Porter, D. C., Farmaki, E., Altilia, S., Schools, G. P., West, D. K., Chen, M., Chang, B. D., Puzyrev, A. T., Lim, C. U., Rokow-Kittell, R., Friedhoff, L. T., Papavassiliou, A. G.,

Kalurupalle, S., Hurteau, G., Shi, J., Baran, P. S., Gyorffy, B., Wentland, M. P., Broude, E. V., . . . Roninson, I. B. (2012). Cyclin-dependent kinase 8 mediates chemotherapy-induced tumor-promoting paracrine activities. *Proc Natl Acad Sci U S A*, *109*(34), 13799-13804. https://doi.org/10.1073/pnas.1206906109

293. Hnisz, D., Abraham, B. J., Lee, T. I., Lau, A., Saint-André, V., Sigova, A. A., Hoke, H. A., & Young, R. A. (2013). Super-enhancers in the control of cell identity and disease. *Cell*, *155*(4), 934-947. https://doi.org/10.1016/j.cell.2013.09.053

294. Pelish, H. E., Liau, B. B., Nitulescu, II, Tangpeerachaikul, A., Poss, Z. C., Da Silva, D. H., Caruso, B. T., Arefolov, A., Fadeyi, O., Christie, A. L., Du, K., Banka, D., Schneider, E. V., Jestel, A., Zou, G., Si, C., Ebmeier, C. C., Bronson, R. T., Krivtsov, A. V., . . . Shair, M. D. (2015). Mediator kinase inhibition further activates super-enhancer-associated genes in AML. *Nature*, *526*(7572), 273-276. https://doi.org/10.1038/nature14904

295. Lynch, C. J., Bernad, R., Martínez-Val, A., Shahbazi, M. N., Nóbrega-Pereira, S., Calvo, I., Blanco-Aparicio, C., Tarantino, C., Garreta, E., Richart-Ginés, L., Alcazar, N., Graña-Castro, O., Gómez-Lopez, G., Aksoy, I., Muñoz-Martín, M., Martinez, S., Ortega, S., Prieto, S., Simboeck, E., . . . Serrano, M. (2020). Global hyperactivation of enhancers stabilizes human and mouse naive pluripotency through inhibition of CDK8/19 Mediator kinases. *Nat Cell Biol*, *22*(10), 1223-1238. https://doi.org/10.1038/s41556-020-0573-1

296. Poss, Z. C., Ebmeier, C. C., Odell, A. T., Tangpeerachaikul, A., Lee, T., Pelish, H. E., Shair, M. D., Dowell, R. D., Old, W. M., & Taatjes, D. J. (2016). Identification of Mediator Kinase Substrates in Human Cells using Cortistatin A and Quantitative Phosphoproteomics. *Cell Rep*, *15*(2), 436-450. https://doi.org/10.1016/j.celrep.2016.03.030

297. Chen, M., Li, J., Zhang, L., Wang, L., Cheng, C., Ji, H., Altilia, S., Ding, X., Cai, G., Altomare, D., Shtutman, M., Byrum, S. D., Mackintosh, S. G., Feoktistov, A., Soshnikova, N., Mogila, V. A., Tatarskiy, V., Erokhin, M., Chetverina, D., . . . Roninson, I. B. (2023). CDK8 and CDK19: positive regulators of signal-induced transcription and negative regulators of Mediator complex proteins. *Nucleic Acids Res*, *51*(14), 7288-7313. https://doi.org/10.1093/nar/gkad538

298. Audetat, K. A., Galbraith, M. D., Odell, A. T., Lee, T., Pandey, A., Espinosa, J. M., Dowell, R. D., & Taatjes, D. J. (2017). A Kinase-Independent Role for Cyclin-Dependent Kinase 19 in p53 Response. *Mol Cell Biol*, *37*(13). https://doi.org/10.1128/mcb.00626-16

299. Menzl, I., Zhang, T., Berger-Becvar, A., Grausenburger, R., Heller, G., Prchal-Murphy, M., Edlinger, L., Knab, V. M., Uras, I. Z., Grundschober, E., Bauer, K., Roth, M., Skucha, A., Liu, Y., Hatcher, J. M., Liang, Y., Kwiatkowski, N. P., Fux, D., Hoelbl-Kovacic, A., . . . Sexl, V. (2019). A kinase-independent role for CDK8 in BCR-ABL1(+) leukemia. *Nat Commun*, *10*(1), 4741. https://doi.org/10.1038/s41467-019-12656-x

300. Dannappel, M. V., Zhu, D., Sun, X., Chua, H. K., Poppelaars, M., Suehiro, M., Khadka, S., Lim Kam Sian, T. C., Sooraj, D., Loi, M., Gao, H., Croagh, D., Daly, R. J., Faridi, P., Boyer, T. G., & Firestein, R. (2022). CDK8 and CDK19 regulate intestinal differentiation and homeostasis via the chromatin remodeling complex SWI/SNF. *J Clin Invest*, *132*(20). https://doi.org/10.1172/jci158593

301. Prieto, S., Dubra, G., Camasses, A., Aznar, A. B., Begon-Pescia, C., Simboeck, E., Pirot, N., Gerbe, F., Angevin, L., Jay, P., Krasinska, L., & Fisher, D. (2023). CDK8 and CDK19 act redundantly to control the CFTR pathway in the intestinal epithelium. *EMBO Rep*, *24*(2), e54261. https://doi.org/10.15252/embr.202154261

302. Chen, M., Liang, J., Ji, H., Yang, Z., Altilia, S., Hu, B., Schronce, A., McDermott, M. S. J., Schools, G. P., Lim, C. U., Oliver, D., Shtutman, M. S., Lu, T., Stark, G. R., Porter, D. C., Broude, E. V., & Roninson, I. B. (2017). CDK8/19 Mediator kinases potentiate

induction of transcription by NFκB. *Proc Natl Acad Sci U S A*, *114*(38), 10208-10213. https://doi.org/10.1073/pnas.1710467114

303. Philip, S., Kumarasiri, M., Teo, T., Yu, M., & Wang, S. (2018). Cyclin-Dependent Kinase 8: A New Hope in Targeted Cancer Therapy? *J Med Chem*, *61*(12), 5073-5092. https://doi.org/10.1021/acs.jmedchem.7b00901

304. Cozzolino, K. A., Sanford, L., Hunter, S., Molison, K., Erickson, B., Courvan, M. C. S., Jones, T., Ajit, D., Galbraith, M. D., Espinosa, J. M., Bentley, D., Allen, M. A., Dowell, R. D., & Taatjes, D. J. (2025). Mediator kinase inhibition suppresses hyperactive interferon signaling in Down syndrome. *Elife*, *13*. https://doi.org/10.7554/eLife.100197

305. Johannessen, L., Sundberg, T. B., O'Connell, D. J., Kolde, R., Berstler, J., Billings, K. J., Khor, B., Seashore-Ludlow, B., Fassl, A., Russell, C. N., Latorre, I. J., Jiang, B., Graham, D. B., Perez, J. R., Sicinski, P., Phillips, A. J., Schreiber, S. L., Gray, N. S., Shamji, A. F., & Xavier, R. J. (2017). Small-molecule studies identify CDK8 as a regulator of IL-10 in myeloid cells. *Nat Chem Biol*, *13*(10), 1102-1108. https://doi.org/10.1038/nchembio.2458

306. Mizuno, N., Shiga, S., Tanaka, Y., Kimura, T., & Yanagawa, Y. (2024). CDK8/19 inhibitor enhances arginase-1 expression in macrophages via STAT6 and p38 MAPK activation. *Eur J Pharmacol*, *979*, 176852. https://doi.org/10.1016/j.ejphar.2024.176852

307. Yan, Y., Xing, C., Xiao, Y., Shen, X., Zhang, Z., He, C., Shi, J. B., Liu, M., & Liu, X. (2022). Discovery and Anti-Inflammatory Activity Evaluation of a Novel CDK8 Inhibitor through Upregulation of IL-10 for the Treatment of Inflammatory Bowel Disease In Vivo. *J Med Chem*, *65*(10), 7334-7362. https://doi.org/10.1021/acs.jmedchem.2c00356

308. Martinez-Fabregas, J., Wang, L., Pohler, E., Cozzani, A., Wilmes, S., Kazemian, M., Mitra, S., & Moraga, I. (2020). CDK8 Fine-Tunes IL-6 Transcriptional Activities by Limiting STAT3 Resident Time at the Gene Loci. *Cell Rep*, *33*(12), 108545. https://doi.org/10.1016/j.celrep.2020.108545

309. Akamatsu, M., Mikami, N., Ohkura, N., Kawakami, R., Kitagawa, Y., Sugimoto, A., Hirota, K., Nakamura, N., Ujihara, S., Kurosaki, T., Hamaguchi, H., Harada, H., Xia, G., Morita, Y., Aramori, I., Narumiya, S., & Sakaguchi, S. (2019). Conversion of antigen-specific effector/memory T cells into Foxp3-expressing T(reg) cells by inhibition of CDK8/19. *Sci Immunol*, *4*(40). https://doi.org/10.1126/sciimmunol.aaw2707

310. Guo, Z., Wang, G., Lv, Y., Wan, Y. Y., & Zheng, J. (2019). Inhibition of Cdk8/Cdk19 Activity Promotes Treg Cell Differentiation and Suppresses Autoimmune Diseases. *Front Immunol*, *10*, 1988. https://doi.org/10.3389/fimmu.2019.01988

311. Freitas, K. A., Belk, J. A., Sotillo, E., Quinn, P. J., Ramello, M. C., Malipatlolla, M., Daniel, B., Sandor, K., Klysz, D., Bjelajac, J., Xu, P., Burdsall, K. A., Tieu, V., Duong, V. T., Donovan, M. G., Weber, E. W., Chang, H. Y., Majzner, R. G., Espinosa, J. M., . . . Mackall, C. L. (2022). Enhanced T cell effector activity by targeting the Mediator kinase module. *Science*, *378*(6620), eabn5647. https://doi.org/10.1126/science.abn5647

312. Butler, M., Chotiwan, N., Brewster, C. D., DiLisio, J. E., Ackart, D. F., Podell, B. K., Basaraba, R. J., Perera, R., Quackenbush, S. L., & Rovnak, J. (2020). Cyclin-Dependent Kinases 8 and 19 Regulate Host Cell Metabolism during Dengue Virus Serotype 2 Infection. *Viruses*, *12*(6). https://doi.org/10.3390/v12060654

313. Kokinos, E. K., Tsymbal, S. A., Galochkina, A. V., Bezlepkina, S. A., Nikolaeva, J. V., Vershinina, S. O., Shtro, A. A., Tatarskiy, V. V., Shtil, A. A., Broude, E. V., Roninson, I. B., & Dukhinova, M. (2023). Inhibition of Cyclin-Dependent Kinases 8/19 Restricts Bacterial and Virus-Induced Inflammatory Responses in Monocytes. *Viruses*, *15*(6). https://doi.org/10.3390/v15061292

314. Obergfäll, D., Wild, M., Sommerer, M., Barillas Dahm, M., Kicuntod, J., Tillmanns, J., Kögler, M., Lösing, J., Dhotre, K., Müller, R., Wangen, C., Wagner, S., Phan, Q. V., Wiebusch, L., Briestenská, K., Mistríková, J., Kerr-Jones, L., Stanton, R. J., Voigt, S., . . . Marschall, M. (2024). Cyclin-Dependent Kinase 8 Represents a Positive Regulator of Cytomegalovirus Replication and a Novel Host Target for Antiviral Strategies. *Pharmaceutics*, *16*(9). https://doi.org/10.3390/pharmaceutics16091238

315. Turner, M., & Díaz-Muñoz, M. D. (2018). RNA-binding proteins control gene expression and cell fate in the immune system. *Nat Immunol*, *19*(2), 120-129. https://doi.org/10.1038/s41590-017-0028-4

316. Schoenberg, D. R., & Maquat, L. E. (2012). Regulation of cytoplasmic mRNA decay. *Nat Rev Genet*, *13*(4), 246-259. https://doi.org/10.1038/nrg3160

317. Stumpo, D. J., Byrd, N. A., Phillips, R. S., Ghosh, S., Maronpot, R. R., Castranio, T., Meyers, E. N., Mishina, Y., & Blackshear, P. J. (2004). Chorioallantoic fusion defects and embryonic lethality resulting from disruption of Zfp36L1, a gene encoding a CCCH tandem zinc finger protein of the Tristetraprolin family. *Mol Cell Biol*, *24*(14), 6445-6455. https://doi.org/10.1128/mcb.24.14.6445-6455.2004

318. Stumpo, D. J., Broxmeyer, H. E., Ward, T., Cooper, S., Hangoc, G., Chung, Y. J., Shelley, W. C., Richfield, E. K., Ray, M. K., Yoder, M. C., Aplan, P. D., & Blackshear, P. J. (2009). Targeted disruption of Zfp36l2, encoding a CCCH tandem zinc finger RNA-binding protein, results in defective hematopoiesis. *Blood*, *114*(12), 2401-2410. https://doi.org/10.1182/blood-2009-04-214619

319. Carballo, E., Lai, W. S., & Blackshear, P. J. (1998). Feedback inhibition of macrophage tumor necrosis factor-alpha production by tristetraprolin. *Science*, *281*(5379), 1001-1005. https://doi.org/10.1126/science.281.5379.1001

320. Taylor, G. A., Carballo, E., Lee, D. M., Lai, W. S., Thompson, M. J., Patel, D. D., Schenkman, D. I., Gilkeson, G. S., Broxmeyer, H. E., Haynes, B. F., & Blackshear, P. J. (1996). A pathogenetic role for TNF alpha in the syndrome of cachexia, arthritis, and autoimmunity resulting from tristetraprolin (TTP) deficiency. *Immunity*, *4*(5), 445-454. https://doi.org/10.1016/s1074-7613(00)80411-2

321. Kang, J. G., Amar, M. J., Remaley, A. T., Kwon, J., Blackshear, P. J., Wang, P. Y., & Hwang, P. M. (2011). Zinc finger protein tristetraprolin interacts with CCL3 mRNA and regulates tissue inflammation. *J Immunol*, *187*(5), 2696-2701. https://doi.org/10.4049/jimmunol.1101149

322. Molle, C., Zhang, T., Ysebrant de Lendonck, L., Gueydan, C., Andrianne, M., Sherer, F., Van Simaeys, G., Blackshear, P. J., Leo, O., & Goriely, S. (2013). Tristetraprolin regulation of interleukin 23 mRNA stability prevents a spontaneous inflammatory disease. *J Exp Med*, *210*(9), 1675-1684. https://doi.org/10.1084/jem.20120707

323. Qiu, L. Q., Stumpo, D. J., & Blackshear, P. J. (2012). Myeloid-specific tristetraprolin deficiency in mice results in extreme lipopolysaccharide sensitivity in an otherwise minimal phenotype. *J Immunol*, *188*(10), 5150-5159. https://doi.org/10.4049/jimmunol.1103700

324. Sneezum, L., Eislmayr, K., Dworak, H., Sedlyarov, V., Le Heron, A., Ebner, F., Fischer, I., Iwakura, Y., & Kovarik, P. (2020). Context-Dependent IL-1 mRNA-Destabilization by TTP Prevents Dysregulation of Immune Homeostasis Under Steady State Conditions. *Front Immunol*, *11*, 1398. https://doi.org/10.3389/fimmu.2020.01398

325. Lai, W. S., Kennington, E. A., & Blackshear, P. J. (2002). Interactions of CCCH zinc finger proteins with mRNA: non-binding tristetraprolin mutants exert an inhibitory effect on degradation of AU-rich element-containing mRNAs. *J Biol Chem*, *277*(11), 9606-9613. https://doi.org/10.1074/jbc.M110395200

326. Lykke-Andersen, J., & Wagner, E. (2005). Recruitment and activation of mRNA decay enzymes by two ARE-mediated decay activation domains in the proteins TTP and BRF-1. *Genes Dev*, *19*(3), 351-361. https://doi.org/10.1101/gad.1282305

327. Fabian, M. R., Frank, F., Rouya, C., Siddiqui, N., Lai, W. S., Karetnikov, A., Blackshear, P. J., Nagar, B., & Sonenberg, N. (2013). Structural basis for the recruitment of the human CCR4-NOT deadenylase complex by tristetraprolin. *Nat Struct Mol Biol*, *20*(6), 735-739. https://doi.org/10.1038/nsmb.2572

328. Heck, A. M., & Wilusz, J. (2018). The Interplay between the RNA Decay and Translation Machinery in Eukaryotes. *Cold Spring Harb Perspect Biol*, *10*(5). https://doi.org/10.1101/cshperspect.a032839

329. Lai, W. S., Stumpo, D. J., Qiu, L., Faccio, R., & Blackshear, P. J. (2018). A Knock-In Tristetraprolin (TTP) Zinc Finger Point Mutation in Mice: Comparison with Complete TTP Deficiency. *Mol Cell Biol*, *38*(4). https://doi.org/10.1128/mcb.00488-17

330. Sedlyarov, V., Fallmann, J., Ebner, F., Huemer, J., Sneezum, L., Ivin, M., Kreiner, K., Tanzer, A., Vogl, C., Hofacker, I., & Kovarik, P. (2016). Tristetraprolin binding site atlas in the macrophage transcriptome reveals a switch for inflammation resolution. *Mol Syst Biol*, *12*(5), 868. https://doi.org/10.15252/msb.20156628

331. Tiedje, C., Diaz-Muñoz, M. D., Trulley, P., Ahlfors, H., Laaß, K., Blackshear, P. J., Turner, M., & Gaestel, M. (2016). The RNA-binding protein TTP is a global post-transcriptional regulator of feedback control in inflammation. *Nucleic Acids Res*, *44*(15), 7418-7440. https://doi.org/10.1093/nar/gkw474

332. Moore, M. J., Blachere, N. E., Fak, J. J., Park, C. Y., Sawicka, K., Parveen, S., Zucker-Scharff, I., Moltedo, B., Rudensky, A. Y., & Darnell, R. B. (2018). ZFP36 RNA-binding proteins restrain T cell activation and anti-viral immunity. *Elife*, *7*. https://doi.org/10.7554/eLife.33057

333. Zhang, X., Chen, X., Liu, Q., Zhang, S., & Hu, W. (2017). Translation repression via modulation of the cytoplasmic poly(A)-binding protein in the inflammatory response. *Elife*, *6*. https://doi.org/10.7554/eLife.27786

334. Tchen, C. R., Brook, M., Saklatvala, J., & Clark, A. R. (2004). The stability of tristetraprolin mRNA is regulated by mitogen-activated protein kinase p38 and by tristetraprolin itself. *J Biol Chem*, *279*(31), 32393-32400. https://doi.org/10.1074/jbc.M402059200

335. Suzuki, K., Nakajima, H., Ikeda, K., Maezawa, Y., Suto, A., Takatori, H., Saito, Y., & Iwamoto, I. (2003). IL-4-Stat6 signaling induces tristetraprolin expression and inhibits TNF-alpha production in mast cells. *J Exp Med*, *198*(11), 1717-1727. https://doi.org/10.1084/jem.20031701

336. Schaljo, B., Kratochvill, F., Gratz, N., Sadzak, I., Sauer, I., Hammer, M., Vogl, C., Strobl, B., Müller, M., Blackshear, P. J., Poli, V., Lang, R., Murray, P. J., & Kovarik, P. (2009). Tristetraprolin is required for full anti-inflammatory response of murine macrophages to IL-10. *J Immunol*, *183*(2), 1197-1206. https://doi.org/10.4049/jimmunol.0803883

337. Sauer, I., Schaljo, B., Vogl, C., Gattermeier, I., Kolbe, T., Müller, M., Blackshear, P. J., & Kovarik, P. (2006). Interferons limit inflammatory responses by induction of tristetraprolin. *Blood*, *107*(12), 4790-4797. https://doi.org/10.1182/blood-2005-07-3058

338. Chen, Y. L., Jiang, Y. W., Su, Y. L., Lee, S. C., Chang, M. S., & Chang, C. J. (2013). Transcriptional regulation of tristetraprolin by NF-κB signaling in LPS-stimulated macrophages. *Mol Biol Rep*, *40*(4), 2867-2877. https://doi.org/10.1007/s11033-012-2302-8

339. Clark, A. R., & Dean, J. L. (2016). The control of inflammation via the phosphorylation and dephosphorylation of tristetraprolin: a tale of two phosphatases. *Biochem Soc Trans*, *44*(5), 1321-1337. https://doi.org/10.1042/bst20160166

340. Mahtani, K. R., Brook, M., Dean, J. L., Sully, G., Saklatvala, J., & Clark, A. R. (2001). Mitogen-activated protein kinase p38 controls the expression and posttranslational modification of tristetraprolin, a regulator of tumor necrosis factor alpha mRNA stability. *Mol Cell Biol*, *21*(19), 6461-6469. https://doi.org/10.1128/mcb.21.9.6461-6469.2001

341. Brook, M., Tchen, C. R., Santalucia, T., McIlrath, J., Arthur, J. S., Saklatvala, J., & Clark, A. R. (2006). Posttranslational regulation of tristetraprolin subcellular localization and protein stability by p38 mitogen-activated protein kinase and extracellular signal-regulated kinase pathways. *Mol Cell Biol*, *26*(6), 2408-2418. https://doi.org/10.1128/mcb.26.6.2408-2418.2006

342. Hitti, E., Iakovleva, T., Brook, M., Deppenmeier, S., Gruber, A. D., Radzioch, D., Clark, A. R., Blackshear, P. J., Kotlyarov, A., & Gaestel, M. (2006). Mitogen-activated protein kinase-activated protein kinase 2 regulates tumor necrosis factor mRNA stability and translation mainly by altering tristetraprolin expression, stability, and binding to adenine/uridine-rich element. *Mol Cell Biol*, *26*(6), 2399-2407. https://doi.org/10.1128/mcb.26.6.2399-2407.2006

343. Clement, S. L., Scheckel, C., Stoecklin, G., & Lykke-Andersen, J. (2011). Phosphorylation of tristetraprolin by MK2 impairs AU-rich element mRNA decay by preventing deadenylase recruitment. *Mol Cell Biol*, *31*(2), 256-266. https://doi.org/10.1128/mcb.00717-10

344. Stoecklin, G., Stubbs, T., Kedersha, N., Wax, S., Rigby, W. F., Blackwell, T. K., & Anderson, P. (2004). MK2-induced tristetraprolin:14-3-3 complexes prevent stress granule association and ARE-mRNA decay. *Embo j*, *23*(6), 1313-1324. https://doi.org/10.1038/sj.emboj.7600163

345. Tiedje, C., Ronkina, N., Tehrani, M., Dhamija, S., Laass, K., Holtmann, H., Kotlyarov, A., & Gaestel, M. (2012). The p38/MK2-driven exchange between tristetraprolin and HuR regulates AU-rich element-dependent translation. *PLoS Genet*, *8*(9), e1002977. https://doi.org/10.1371/journal.pgen.1002977

346. Ross, E. A., Smallie, T., Ding, Q., O'Neil, J. D., Cunliffe, H. E., Tang, T., Rosner, D. R., Klevernic, I., Morrice, N. A., Monaco, C., Cunningham, A. F., Buckley, C. D., Saklatvala, J., Dean, J. L., & Clark, A. R. (2015). Dominant Suppression of Inflammation via Targeted Mutation of the mRNA Destabilizing Protein Tristetraprolin. *J Immunol*, *195*(1), 265-276. https://doi.org/10.4049/jimmunol.1402826

347. Scinicariello, S., Soderholm, A., Schäfer, M., Shulkina, A., Schwartz, I., Hacker, K., Gogova, R., Kalis, R., Froussios, K., Budroni, V., Bestehorn, A., Clausen, T., Kovarik, P., Zuber, J., & Versteeg, G. A. (2023). HUWE1 controls tristetraprolin proteasomal degradation by regulating its phosphorylation. *Elife*, *12*. https://doi.org/10.7554/eLife.83159

348. Jones, T., Feng, J., Luyties, O., Cozzolino, K., Sanford, L., Rimel, J. K., Ebmeier, C. C., Shelby, G. S., Watts, L. P., Rodino, J., Rajagopal, N., Hu, S., Brennan, F., Maas, Z. L., Alnemy, S., Richter, W. F., Koh, A. F., Cronin, N. B., Madduri, A., . . . Taatjes, D. J. (2025). TFIIH kinase CDK7 drives cell proliferation through a common core transcription factor network. *Sci Adv*, *11*(9), eadr9660. https://doi.org/10.1126/sciadv.adr9660

349. Das, A., Yang, C. S., Arifuzzaman, S., Kim, S., Kim, S. Y., Jung, K. H., Lee, Y. S., & Chai, Y. G. (2018). High-Resolution Mapping and Dynamics of the Transcriptome, Transcription Factors, and Transcription Co-Factor Networks in Classically and Alternatively Activated Macrophages. *Front Immunol*, *9*, 22. https://doi.org/10.3389/fimmu.2018.00022

350. Gudgeon, J., Dannoura, A., Chatterjee, R., Sidgwick, F., Raymond, B. B., Frey, A. M., Marin-Rubio, J. L., & Trost, M. (2025). Mass spectrometry-based proteomic

exploration of diverse murine macrophage cellular models. *Life Sci Alliance*, *8*(1). https://doi.org/10.26508/lsa.202402760

351. Gough, D. J., Messina, N. L., Clarke, C. J., Johnstone, R. W., & Levy, D. E. (2012). Constitutive type I interferon modulates homeostatic balance through tonic signaling. *Immunity*, *36*(2), 166-174. https://doi.org/10.1016/j.immuni.2012.01.011

352. Core, L., & Adelman, K. (2019). Promoter-proximal pausing of RNA polymerase II: a nexus of gene regulation. *Genes Dev*, *33*(15-16), 960-982. https://doi.org/10.1101/gad.325142.119

353. Kamada, R., Yang, W., Zhang, Y., Patel, M. C., Yang, Y., Ouda, R., Dey, A., Wakabayashi, Y., Sakaguchi, K., Fujita, T., Tamura, T., Zhu, J., & Ozato, K. (2018). Interferon stimulation creates chromatin marks and establishes transcriptional memory. *Proc Natl Acad Sci U S A*, *115*(39), E9162-e9171. https://doi.org/10.1073/pnas.1720930115

354. Mostafavi, S., Yoshida, H., Moodley, D., LeBoité, H., Rothamel, K., Raj, T., Ye, C. J., Chevrier, N., Zhang, S. Y., Feng, T., Lee, M., Casanova, J. L., Clark, J. D., Hegen, M., Telliez, J. B., Hacohen, N., De Jager, P. L., Regev, A., Mathis, D., & Benoist, C. (2016). Parsing the Interferon Transcriptional Network and Its Disease Associations. *Cell*, *164*(3), 564-578. https://doi.org/10.1016/j.cell.2015.12.032

355. Heinz, S., Benner, C., Spann, N., Bertolino, E., Lin, Y. C., Laslo, P., Cheng, J. X., Murre, C., Singh, H., & Glass, C. K. (2010). Simple combinations of lineage-determining transcription factors prime cis-regulatory elements required for macrophage and B cell identities. *Mol Cell*, *38*(4), 576-589. https://doi.org/10.1016/j.molcel.2010.05.004

356. MacMicking, J., Xie, Q. W., & Nathan, C. (1997). Nitric oxide and macrophage function. *Annu Rev Immunol*, *15*, 323-350. https://doi.org/10.1146/annurev.immunol.15.1.323

357. Boockvar, K. S., Granger, D. L., Poston, R. M., Maybodi, M., Washington, M. K., Hibbs, J. B., Jr., & Kurlander, R. L. (1994). Nitric oxide produced during murine listeriosis is protective. *Infect Immun*, *62*(3), 1089-1100. https://doi.org/10.1128/iai.62.3.1089-1100.1994

358. Bermudez, L. E. (1993). Differential mechanisms of intracellular killing of Mycobacterium avium and Listeria monocytogenes by activated human and murine macrophages. The role of nitric oxide. *Clin Exp Immunol*, *91*(2), 277-281. https://doi.org/10.1111/j.1365-2249.1993.tb05895.x

359. Ogawa, R., Pacelli, R., Espey, M. G., Miranda, K. M., Friedman, N., Kim, S. M., Cox, G., Mitchell, J. B., Wink, D. A., & Russo, A. (2001). Comparison of control of Listeria by nitric oxide redox chemistry from murine macrophages and NO donors: insights into listeriocidal activity of oxidative and nitrosative stress. *Free Radic Biol Med*, *30*(3), 268-276. https://doi.org/10.1016/s0891-5849(00)00470-6

360. Cole, C., Thomas, S., Filak, H., Henson, P. M., & Lenz, L. L. (2012). Nitric oxide increases susceptibility of Toll-like receptor-activated macrophages to spreading Listeria monocytogenes. *Immunity*, *36*(5), 807-820. https://doi.org/10.1016/j.immuni.2012.03.011

361. Wienerroither, S., Shukla, P., Farlik, M., Majoros, A., Stych, B., Vogl, C., Cheon, H., Stark, G. R., Strobl, B., Müller, M., & Decker, T. (2015). Cooperative Transcriptional Activation of Antimicrobial Genes by STAT and NF-κB Pathways by Concerted Recruitment of the Mediator Complex. *Cell Rep*, *12*(2), 300-312. https://doi.org/10.1016/j.celrep.2015.06.021

362. Shiloh, M. U., MacMicking, J. D., Nicholson, S., Brause, J. E., Potter, S., Marino, M., Fang, F., Dinauer, M., & Nathan, C. (1999). Phenotype of mice and macrophages deficient in both phagocyte oxidase and inducible nitric oxide synthase. *Immunity*, *10*(1), 29-38. https://doi.org/10.1016/s1074-7613(00)80004-7

363. Radoshevich, L., Impens, F., Ribet, D., Quereda, J. J., Nam Tham, T., Nahori, M. A., Bierne, H., Dussurget, O., Pizarro-Cerdá, J., Knobeloch, K. P., & Cossart, P. (2015). ISG15 counteracts Listeria monocytogenes infection. *Elife*, *4*. https://doi.org/10.7554/eLife.06848

364. Zhang, Y., Thery, F., Wu, N. C., Luhmann, E. K., Dussurget, O., Foecke, M., Bredow, C., Jiménez-Fernández, D., Leandro, K., Beling, A., Knobeloch, K. P., Impens, F., Cossart, P., & Radoshevich, L. (2019). The in vivo ISGylome links ISG15 to metabolic pathways and autophagy upon Listeria monocytogenes infection. *Nat Commun*, *10*(1), 5383. https://doi.org/10.1038/s41467-019-13393-x

365. Tan, J. M. J., Garner, M. E., Regeimbal, J. M., Greene, C. J., Márquez, J. D. R., Ammendolia, D. A., McCluggage, A. R. R., Li, T., Wu, K. J., Cemma, M., Ostrowski, P. P., Raught, B., Diamond, M. S., Grinstein, S., Yates, R. M., Higgins, D. E., & Brumell, J. H. (2021). Listeria exploits IFITM3 to suppress antibacterial activity in phagocytes. *Nat Commun*, *12*(1), 4999. https://doi.org/10.1038/s41467-021-24982-0

366. Dussurget, O., Bierne, H., & Cossart, P. (2014). The bacterial pathogen Listeria monocytogenes and the interferon family: type I, type II and type III interferons. *Front Cell Infect Microbiol*, *4*, 50. https://doi.org/10.3389/fcimb.2014.00050

367. MacMicking, J. D. (2012). Interferon-inducible effector mechanisms in cell-autonomous immunity. *Nat Rev Immunol*, *12*(5), 367-382. https://doi.org/10.1038/nri3210

368. Kim, B. H., Shenoy, A. R., Kumar, P., Das, R., Tiwari, S., & MacMicking, J. D. (2011). A family of IFN-γ-inducible 65-kD GTPases protects against bacterial infection. *Science*, *332*(6030), 717-721. https://doi.org/10.1126/science.1201711

369. Standart, N., & Weil, D. (2018). P-Bodies: Cytosolic Droplets for Coordinated mRNA Storage. *Trends Genet*, *34*(8), 612-626. https://doi.org/10.1016/j.tig.2018.05.005

Zusammenfassung

Das angeborene Immunsystem wird auf mehreren Ebenen streng reguliert, um eine schnelle und dennoch ausgewogene Reaktion auf externe Reize zu gewährleisten. Diese Arbeit untersucht die Regulation durch transkriptionelle und teilweise auch durch posttranskriptionelle Mechanismen, wobei der Schwerpunkt auf Makrophagen als wichtige Effektorzellen der angeborenen Immunität liegt.

Der erste Teil dieser Arbeit beschreibt das Hauprojekt, dass sich auf die Mediator-Kinase konzentriert, die eine zentrale regulatorische Komponente des Transkriptionsapparats darstellt. Die enzymatisch aktiven Untereinheiten der Mediator-Kinase sind die paraloge Proteine CDK8 und CDK19. Als Teil des Mediator-Komplexes moduliert die Mediator-Kinase die signalinduzierte Transkription und wirkt dabei entweder als Aktivator oder als Repressor. Die Dissertation untersucht, wie die Mediator-Kinase die Reaktionen von Makrophagen auf verschiedene Immunreize beeinflusst, wobei der Fokus auf Toll-like-Rezeptoren (TLR)- und JAK-STAT-Signalwegen liegt.

Unter Verwendung selektiver niedermolekularer Inhibitoren von Mediator-Kinase in Kombination mit Transkriptom-Profiling, Transkriptionsfaktor-Aktivitätsinferenz und funktionellen Infektionsassays konnte eine starke Regulation von primären Makrophagen durch Mediator-Kinase nachgewiesen werden. Im Gegensatz dazu war die Abhängigkeit in immortalisierten Zelllinien nur schwach ausgeprägt. Die Mediator-Kinase steigerte die JAK-STAT-abhängige Transkription nach Stimulation mit Zytokinen, einschließlich Interferonen (IFNs), unterdrückte jedoch die TLR-induzierte Genexpression. Viele IFN-stimulierte Gene (ISGs) zeigten bei einer Inhibition der Mediator-Kinase eine erhöhte Induktion nach TLR-Stimulation. Motif-Anreicherungsanalysen identifizierten das IFN-stimulierte Response-Element (ISRE) als ein wichtiges regulatorisches Motiv. Dieses Ergebnis deutete darauf hin, dass die TLR-Signalübertragung die ISRE-gesteuerte Transkription auf eine stimulus-spezifische Weise unterdrückt. Die Hemmung der Mediator-Kinase hob diese Unterdrückung auf und verstärkte die Clearance von Listeria monocytogenes, das sowohl den TLR- als auch den JAK-STAT-Signalweg aktiviert.

Das zweite Projekt dieser Arbeit untersucht die Hierarchie der Zielerkennung durch das mRNA-destabilisierende Protein Tristetraprolin (TTP) und zeigt, dass das Schicksal der mRNA durch die Bindung im Zellkern vorbestimmt werden kann.